# SOUTH CHINA KARST II

Editors: Martin Knez, Hong Liu, Tadej Slabe

**Series**
**CARSOLOGICA**
**SOUTH CHINA KARST II**

# SOUTH CHINA KARST II

**Editors: Martin Knez, Hong Liu, Tadej Slabe**

# FOREWORD

THE EDITORS

The exceptional features of the diverse Yunnan karst, from the tropical cone karst in the south and the stone forests in the center to the mountain karst and high plateau karst of Tibet in the north, are a magnet that has always drawn karstologists. Their distinctiveness offers a revelation of the basic characteristics of how karst is formed. The relatively dense settlement of the region, the corresponding great need for clean water, and growing tourism offer opportunities for research and even demand that karstologists study the modern human impact on this vulnerable karst region.

The long-term cooperation between karstologists from the Yunnan Institute of Geography of the University of Yunnan and the Karst Research Institute of the Scientific Research Center of the Slovenian Academy of Sciences and Arts, which has grown into personal friendship, has brought numerous fruits to international karstology. Before you is our second book about the karst of southern China in which we assemble the results of research in the Yunnan karst on stone forests and other types of karst surfaces, soil erosion, the formation of tufa, vegetation, the development, age, and sediments of karst caves, karst waters, epikarst fauna, and the protection of the natural heritage.

Our cooperation continues in full swing and we hope that we will soon succeed in realizing our long-term desire to establish an international laboratory in Kunming for studying karst waters.

For fifteen years, our work in China has been supported by Slovenia's Ministry of Higher Education, Science, and Technology, the Slovenian Research Agency, and China's Ministry of Science.

For many years we have cooperated successfully as the first non-Chinese in the Shilin Research Foundation.

The research was also included in UNESCO IGCP projects 379, 448, and 513.

We thank Professor David C. Culver (American University, Washington, D. C., USA) for his help with the biological part of the manuscript.

# CONTENTS

# THE SHAPE AND ROCK RELIEF OF PILLARS IN THE NAIGU STONE FOREST

MARTIN KNEZ, TADEJ SLABE

Naigu stone forest (1) lies 20 km east of the Central Lunan stone forest and is an important tourist attraction. Pillars including 20–30 m tall tower-like rock masses and smaller pillars stand side by side or separately. Their shapes reflect lithological properties of the rock and their evolution. Mushroom shaped pillars are the most frequent. The tops of the pillars merged into more extensive towers are located at a uniform level and have several short, conical peaks.



**1**  *Naigu* stone forest.

Rock teeth are either rounded or pointed and often dissected by subsoil channels. The diverse rock has little influence on their shape.

Underneath the forest there is the Baiyun tourist cave whose rock relief, sediments and flowstone make it possible to discern many periods in its development (*Kogovšek et al.*, 1999, 239).

The stone forest stretches along two slightly uplifted tectonic ridges. Faults bordering the fault zone are very strong, and intermediate faults, mostly running in the northwest-southeast direction, are several kilometres in length and very deep. The pillars formed in more than 100 m thick beds of Lower Permian carbonate stone of the Qixia formation that is strongly reflected in their shape and rock relief. In places, limestone is micritic and thinly laminated, elsewhere it is microsparitic and partly porous, and in some places late diagenetically dolomitized.

Naigu stone forest is composed of carbonates of the Lower Permian Qixia formation. This is one of the more important base formations on which numerous stone forests in the southern Yunnan province of Lunan stand. Important characteristics of the Qixia formation include primarily a strong diagenetic change in the basic rock, dolomitization, and in certain places considerable secondary porosity, and a high percentage of carbonate (*Knez*, 1997; 1998). The geological profile of rock properties indicates great diversity, and from the morphogenetic aspect we divided segments of the beds into three groups, A, B, and C (2). We traced changes in colour, bedding, porosity, inclusions, and other characteristics. The beds of Group A are composed of homogeneous carbonates that are the most resistant; the beds of Group B are less resistant to erosion, porous, and heavily dolomitized in some places; and the beds of Group C are composed of characteristically striped dolomitized massive limestone (3).

**2** Cross-section of the *Naigu* stone forest with a lithological column.
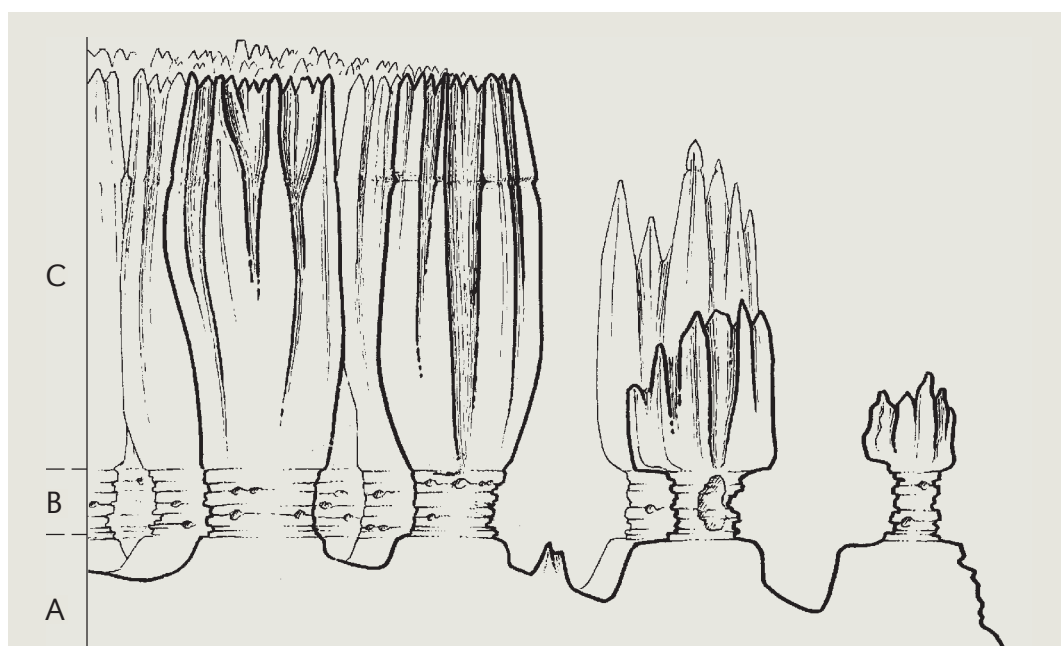


**3** Upper part of the stone forest (beds of groups B and C).



10
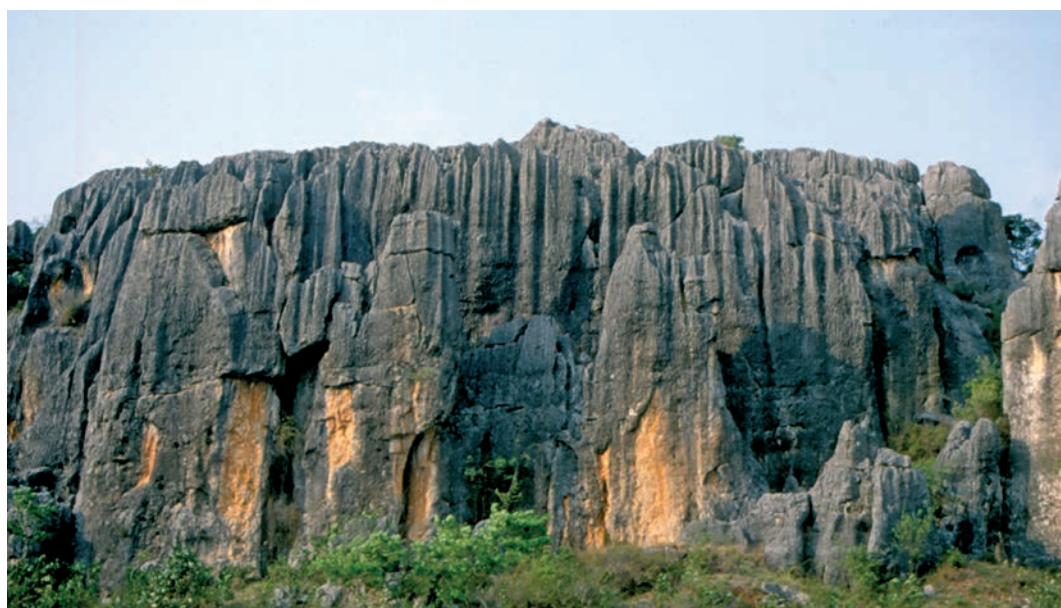
The feet of the lowest exposed part of the Naigu stone forest (the beds of Group A) are composed of light brown and orange to light grey massive and homogeneous carbonate in which the largest, Baiyun karst cave is also located. In it we distinguished three textural variations. We perceived smaller dolomite sections ranging from a few to several dozen cm² in size in the lowest part, alternating dolomite and limestone seams in the middle, and thin lamination in the upper part. We observed neither calcite veins nor secondary porosity in the rock. The rock with such properties enables development of subsoil rock forms as well as rock forms carved by rainwater.

Rocks that are less resistant to corrosion and erosion (the beds of Group B) follow in the geological profile. They form the narrower part of the pillars below the wider and consequently considerably more resistant upper part. In this part, primary limestone is heavily late diagenetically dolomitized. In some places the density of the dolomitized sections changes laterally as well as vertically. Due to the mostly idiomorphic grains of dolomite, the rock can be labelled the grainstone type of dolosparite. The grains of dolomite are poorly cemented and the erosion process easily washes them from overhanging and vertical walls. The secondary intergranular porosity can change laterally but in general it is estimated to be at 5–10 %. The possibility of subsoil corrosion of the rock is great, mostly due to the considerable porosity and poorly cemented dolomite crystals.

The border of the Group C beds with the middle section (the beds of Group B) is macroscopically sharp but not identical with any of the bedding planes or the change in sedimentation. The outer side of the massive dolomitized limestone typical of the upper part is characteristically rough and striped with protrusions of dolomite sections. Due to their convex shape on the surface of the rock, more pronounced roughness and consequently heavier lichen cover, the dolomite sections are of a dark grey colour which on the surface of the rock appears as dark grey to black stripes on a light coloured base. In the major part of the Group C beds, the percentage of the surface of non-dolomitized limestone equals the percentage of dolomitized sections. In spite of the fact that relative to the surrounding rock, the proportion of dolomitized sections is not equally distributed, it never completely disappears throughout the studied area.

According to the shape, size, mutual contact, and other factors, dolomite crystals in dolomite sections are of a late diagenetic origin.

## 1.2    THE SHAPE OF ROCK PILLARS

The size of pillars is mainly the consequence of faults and fissures that vertically crisscross the beds and the effectiveness of subsoil dissolution of the rock along them. The network is diverse and the stone forest is thus composed of larger rock masses as well as smaller pillars that stand either close to one another or separately (4, 5). The shape of rock pillars is dictated primarily by diverse beds of rock and their development from subsoil karren.

The pillars developed at different levels of the described beds of rock, which is reflected in their shape. The most characteristic are mushroom-shaped pillars and distinctive notches have developed along the beds of Group B rock (3). This is the consequence of more rapid subsoil corrosion and hollowing of this part of rock, which is the most porous and decomposes fastest on the surface. Along the beds of rock we marked as B, pillars are therefore narrower. The mushroom shape characteristic of the larger pillars that developed in the beds of A, B, and C rock groups is naturally less distinct than that of the narrower pillars. Most often, the lower lying pillars whose lower upper part devel-

**4** The edge of the stone forest with separate stone pillars.



**5** Separate stone pillars.

oped from the beds of rock marked as Group C have the most distinct mushroom shape (6), especially distinct when the beds are criss-crossed by larger subsoil pipes. The pillars in Group C located above the beds of rock of Group B are overhanging, with traces of water creeping down from their tops. The pillars whose tops are located in the beds of Group B are narrower and in general lack the characteristic regular shapes dictated by subsoil factors and rainwater. The beds of Group A often form the wider bases of the pillars belonging to the beds of groups B and C.

Wide pillars whose tops are of the rock of the beds from groups C or A also have wide peaks dissected by funnel-shaped notches and smaller conical peaks created by subsoil shaping of the rock. Water percolates through soil in a dispersed fashion, dissolving the upper part of the rock most distinctly. This has been demonstrated by experiments with plaster subsoil karren. Rainwater further sharpens the peaks. The upper parts of 15-m pillars on the beds of rock of groups C and A tend to narrow from the bottom upwards. Funnel-shaped notches whose mouths are surrounded by blade-shaped and conical peaks originated from subsoil channels and recesses.

In most cases, the shape of subsoil teeth does not distinctly reflect the varied composition of the rock.

## 1.3  ROCK RELIEF OF THE NAIGU STONE FOREST

The rock forms on the pillars of the stone forest can be divided into subsoil relief forms, relief forms carved by rainwater, and composite relief forms, i.e. subsoil relief forms or those reshaped by rainwater (*Slabe*, 1998, 51).

### 1.3.1  *Subsoil rock forms*

Such forms are divided into those formed under sediments and soil due to percolation of water along the contact between them and the rock, those due to percolation of water through soil that only partly covers the rock, and rock forms that occur at the level of soil or sediments surrounding the rock (*Slabe*, 1999). Most of these relief forms can be observed on the pillars of the Naigu stone forest as well, except for subsoil scallops representing the traces of percolation of water along the permeable contact between rock

6  A mushroom stone pillar.

and sediment, which were not evident. It appears that in the upper, higher part of the pillars they have been transformed by rainwater and that they never occurred on the lower parts of the pillars on the beds of Group B.

Large subsoil channels occurred due to percolation of water at the contact of the wall and sediment covering the rock and filling up crevices along vertical fissures. The largest channels are several metres across. Many of them run from the top to the bottom of the pillars and are dozens of metres long. Their lower parts often widen to bell-like forms. Their upper parts are either reshaped by smaller channels that lead from subsoil channels and subsoil cups or dissected by smaller channels carved by rainwater trickling down the walls. Subsoil teeth are in most cases dissected by large vertical channels or their starting mouths.

The relatively flat tops of the larger pillars and teeth are dissected by medium-sized and smaller subsoil channels (*Slabe*, 1999, 259) that developed where soil only partly covered the rock due to percolation of water through soil and its flowing along the contact with the rock. Their cross-sections are characteristically semi-circular or in the shape of an inverted letter omega and thus wider at the bottom, and their diameters can reach up to one metre. At their bends, especially at the edges of the tops, they are narrower and deeper. Often they have semi-circular mouths. In most cases they are linked in a branched network. Above larger channels, the walls are often dissected by smaller vertical subsoil channels where water runs under soil and accumulates in a larger channel. Several stories high subsoil channels testify to the gradual denudation of rock teeth. The surface of recently denuded channels is smooth while the surface of long denuded channels is rough. The ridges between the long denuded channels as well as their walls are covered with flutes carved by rainwater.

Subsoil cups (*Slabe*, 1999, 263) are semi-circular hollows with diameters from a few centimetres to one metre or more. They occur on the largest tops of rock pillars and on the walls below them, i.e. at the bottom of funnel-shaped notches. After denudation they can transform into open solution pans and eventually be reshaped once more into subsoil cups; at the bottom of the funnel-shaped notches they can also wedge out.

The beds of rock classified in Group B are relatively densely hollowed by subsoil cavities whose diameters measure from a few centimetres to several metres. Rock relief is visible on their edges as well. They are composed of above-sediment channels, the consequence of water flowing over sediment when the cavities were filled, and floor channels that developed when the cavities were emptying and the level of sediment surrounding the pillars lowered.

### 1.3.2   *Rock forms carved by rainwater*

Rock forms carved by rainwater, which naturally are the most distinct on the tops and the upper parts of the walls of stone pillars, include flutes, channels and solution pans. They often develop on old subsoil rock relief forms, reshaping them in the process, or combine with other factors that shape subsoil relief forms to create composite relief forms.

Flutes are a less distinct rock relief form found on the tops of the pillars. Their average diameter is 2.42 cm (the largest flute is 5 cm and the smallest one 1.5 cm wide). We measured them on the surface inclined from 25° to 80°, and the largest flutes were found at the steepest inclination. Most of the flutes are short, a result especially of the previous dissection of the rock by subsoil rock relief forms. They are found on wider tops in

particular and rarely occur on conical tops. We find them on bulges where they radiate from the highest point as well as on the walls of subsoil channels and denuded karren. Below, there are larger channels which additionally deepen older subsoil channels. Flutes are connected on both sides of a ridge, while subsoil channels lie side by side. At the edges of the wide tops or in some places on the conical tops, flutes merge downwards into channels. Flutes are of relatively irregular shape. Their ridges are jagged and meandering and they are wavy, which is usually characteristic of flutes on surfaces with steep inclinations. Their network is interrupted by dolomite protrusions 1–5 cm in size and their surface is rough. The tops of short flutes often occur on more slowly soluble parts of the rock and not on individual sections where the rock surface is the roughest. In some places we can only observe their beginnings, i.e. individual parts of networks of mature flutes. Their occurrence and shape are thus influenced in particular by characteristically dolomitized rock.

Channels dissect the tops of the rock pillars more distinctly (7, 8). They are 0.50 m in diameter, up to 5 m long and relatively shallow, particularly when compared with those connected with the original subsoil formation of the rock. We must distinguish them from the above-mentioned channels with subsoil origins and those that are still connected with development of subsoil rock relief forms. They are a sign of the activity of rainwater and often begin on the relatively sharp tops. Over time these channels also develop originally less distinct funnel-shaped mouths. Smaller channels of this type can be connected into a large channel.

Solution pans occur on the wider tops of the rock pillars. Smaller solution pans, 10–20 cm in diameter, are shallow, usually having irregular circular shapes with meandering edges. Larger solution pans that formed from subsoil cups and have a semi-circular form



*The shape and rock relief of pillars in the Naigu stone forest*

**7** The top of a stone pillar with funnel-shaped notches and channels.

are often open with a discharge channel and flutes on the edges. Their diameters can exceed one metre. They also occur at the bottom of funnel-shaped notches which also formed from subsoil cups.

### 1.3.3 Composite rock forms

One of the most distinctive composite rock forms on the rock pillars are medium-sized channels on the upper part of the pillar walls (3). They occurred due to discharge of water from the subsoil channels and cups located on the top of the pillars or leading from the funnel-shaped notches. Subsoil cups are found or used to exist at their bottom. The diameter of the channels measures from 10 cm to 1 m and therefore they are cut relatively deep into the rock; in the higher part of the rock pillars they reach all the way to the beds of the rock classified as Group B, but only the largest channels cut into these as well. The edges of their tops therefore have larger or smaller funnel-shaped mouths that in most cases have been reshaped by rainwater. Often their surface is rough, the consequence of the rock composition. Vertical channels running from subsoil cups are smaller and have a similar origin.



**8**  A mushroom stone pillar with distinctive traces of water.

In particular, rainwater reshapes and deepens also the subsoil channels that criss-cross the wider tops.

#### CONCLUSION

Like other Lunan stone forests, the Naigu stone forest also formed from subsoil karren. Its unique shape was determined primarily by a degree of tectonic bed deformation and composition at different levels of diverse beds of rock on which the stone forest developed. The size of pillars is dictated by faults and fissures vertically criss-crossing the rock beds. It is also influenced by efficiency of subsoil dissolution of the rock. The stone forest is composed of larger rock masses and smaller pillars that stand side by side or separately. The shape of the pillars, which are often undercut, and their rock relief clearly indicate the importance of their subsoil formation. Rainwater is slowly reshaping the pillars from the top downwards.

The rock changes considerably through the geological profile. The Naigu stone forest is characterized by mostly micritic and thinly laminated limestone in the lower part (the beds of Group A), prevalent microsparitic and considerable secondary porosity and in some places heavily late diagenetically dolomitized limestone in the middle part (the

beds of Group B), and a thicker block of massive, striped dolomitized limestone in the upper part (the beds of Group C). The type of the rock has a direct and key influence on selective corrosion and erosion and thus on morphological appearance of individual rock pillars and rock blocks of various heights.

The pillars developed at different levels of the described beds of rock, that reflects in their shape. Mushroom-shaped pillars are the most characteristic, and distinctive notches have developed in the beds of Group B. This is the consequence of more rapid subsoil corrosion and hollowing of the most porous part of the rock that disintegrates relatively fast when it appears on the surface. The pillars whose tops are located in the beds of Group B are narrower and in most cases without characteristic regular shapes, dictated by the factors of their development. The beds of Group A are often wider plinths of the pillars belonging to the beds of groups B and C.

The shape of subsoil teeth as a rule does not distinctly reflect the varied composition of the rock.

Subsoil and composite rock relief forms are the most distinct. Subsoil rock relief forms include large channels, overhanging undercuts of the pillars, and subsoil channels on the wider tops. The channels running from subsoil channels or subsoil cups are composite rock relief forms. The deepening of subsoil cups and the discharge of water down the channels are caused by the dissection of the tops of the pillars, especially the larger ones, into cones with funnel-shaped notches between them.

Subsoil rock relief forms that as a rule are larger develop on all types of the rock in the Naigu stone forest. The rock influences their shape, especially the shape of the smallest relief forms that frequently have jagged edges on dolomitized rock. Flutes carved by rainwater are a less distinct rock relief form in Naigu. Their occurrence and development is influenced primarily by the composition of the rock and less by the recently exposed rock. Rock relief forms have developed on the majority of the beds of diverse rock but are almost non-existent on the beds of Group B where subsoil pipes developed in them. Where these beds of rock are located at the tops of the pillars, smaller rock relief forms carved by rainwater practically do not occur. In some places there are only solution pans or rainwater reshapes larger subsoil rock forms. The rock relief therefore developed relative to the position of these beds in the pillars.

The traces of the development of the Baiyun Cave in the central part of the stone forest testify to the forest's gradual and diverse development which naturally is linked to the development of the caves underneath it. The cave's sediments and its rock relief reveal many periods in the development of the cave in the epiphreatic part of the aquifer as well as the rapid lowering of the level of ground-water, which probably caused the faster 'growth' of the stone forest.

# LITHOLOGICAL AND MORPHOLOGICAL CHARACTERISTICS AND ROCK RELIEF OF THE LAO HEI GIN STONE FOREST

2

MARTIN KNEZ, TADEJ SLABE

Stone forests developed from subcutaneous karren where thick layers of sediments and soil covered the carbonate rock. They are composed of stone pillars and stone teeth (*Song*, 1986) and formed on various horizontal and mildly inclined rock beds (5–15°) cut by vertical faults and cracks (*Ford et al.*, 1996).

The central part of the Lunan stone forest covers over 80 ha, while larger and smaller stone forests spread over 350 km². Unique among the stone forests is Lao Hei Gin. The forest is composed of pillars, standing in groups or individually, that can reach up to 20 m in height. Most are lower, however, up to about 10 m. The dominant and most characteristic form of the pillars is a mushroom-like shape. Watercourses run through caves that occur some 20–30 m deep below the forests.

We have presented our research of the Lunan stone forests in more detail in descriptions and collected notes published in the book South China Karst 1 (*Chen et al.,* 1998) and elsewhere (e.g. *Knez* and *Slabe*, 2001a; 2001b; 2002). In this article we are adding the results of our exploration of yet another stone forest, unique in its formation.

The Lao Hei Gin stone forest (1, 2, 3) lies 20 km north of Shilin (Major stone forest). Individual stone pillars and larger rock blocks shaped by corrosion and erosion cover only about 2 km². Morphologically, the pillars are similar to those in the Naigu stone forest.



**1** *Lao Hei Gin* stone forest.

**2** *Lao Hei Gin* stone forest. View from the top.

## 2.1 LITHOLOGICAL CHARACTERISTICS OF THE STONE FOREST

The geological column is divided into five lithologically and morphologically diverse sequences: A, B, C, D, and E (3, 4, 5). Sequence A is built mostly of low-porous and grained late diagenetic dolomite, Sequence B of highly porous late diagenetic grained dolomite, Sequence C of slightly dolomitic limestone, Sequence D of low-porous grained late diagenetic dolomite, and Sequence E of compact speckled dolomitic limestone. The total thickness of the researched geological profile (stone pillar) is 26 m.

**3** Cross-section of the *Lao Hei Gin* stone forest.
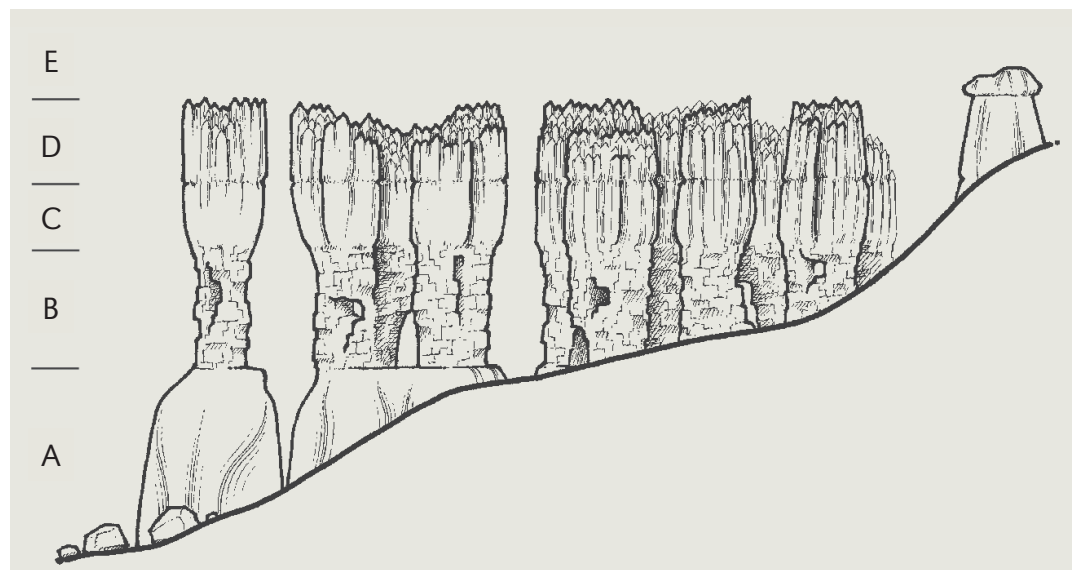
### 2.1.1 Sequence A

This sequence is 7 m thick. The lower part of the stone pillar is formed from highly recrystalized dolosparite to dolomicrosparite of a grainstone type. The primary limestone had been highly diagenetically transformed – under the microscope we can observe subhedral to euhedral dolomite grains which form a hipidiotopic to idiotopic structure. The dolomite grains are up to one-third of a millimetre in size. In diffused light they mostly have a slightly brown hue, whereas individual larger grains are exceptionally clean and almost totally translucent. Autogenous overgrowth is clearly visible in a small percentage of the dolomite crystals. The rock also contains a certain percentage of calcite. Secondary porosity is substantial.

### 2.1.2 Sequence B

Sequence B is 8 m thick and does not mineralogically differ much from Sequence A; on average, however, the rock contains twice as much calcite as the rock from Sequence A. The rock in this sequence is a grainstone-type dolosparite to dolomicrosparite. Grainstone-type dolomite (dolomicrosparite to dolosparite) consists of subhedral to euhedral dolomite grains that form a hipidiotopic to idiotopic structure. The essential difference of the rock from both sequences is that the rock in Sequence B shows substantially more secondary porosity than the rock in Sequence A. On average, the dolomite crystals are smaller than the crystals in Sequence A – in the upper part of the sequence even less than one tenth of a millimetre – and less pure.

### 2.1.3 Sequence C

Sequence C is 4 m thick. Here the rock is mostly limestone with no more than 10 % dolomite crystals. The boundary between sequences B and C is sharp and immediately transforms into biopelintramicrite to biopelmicrosparite in the vertical direction. The

**4** Single mushroom-like stone pillars.
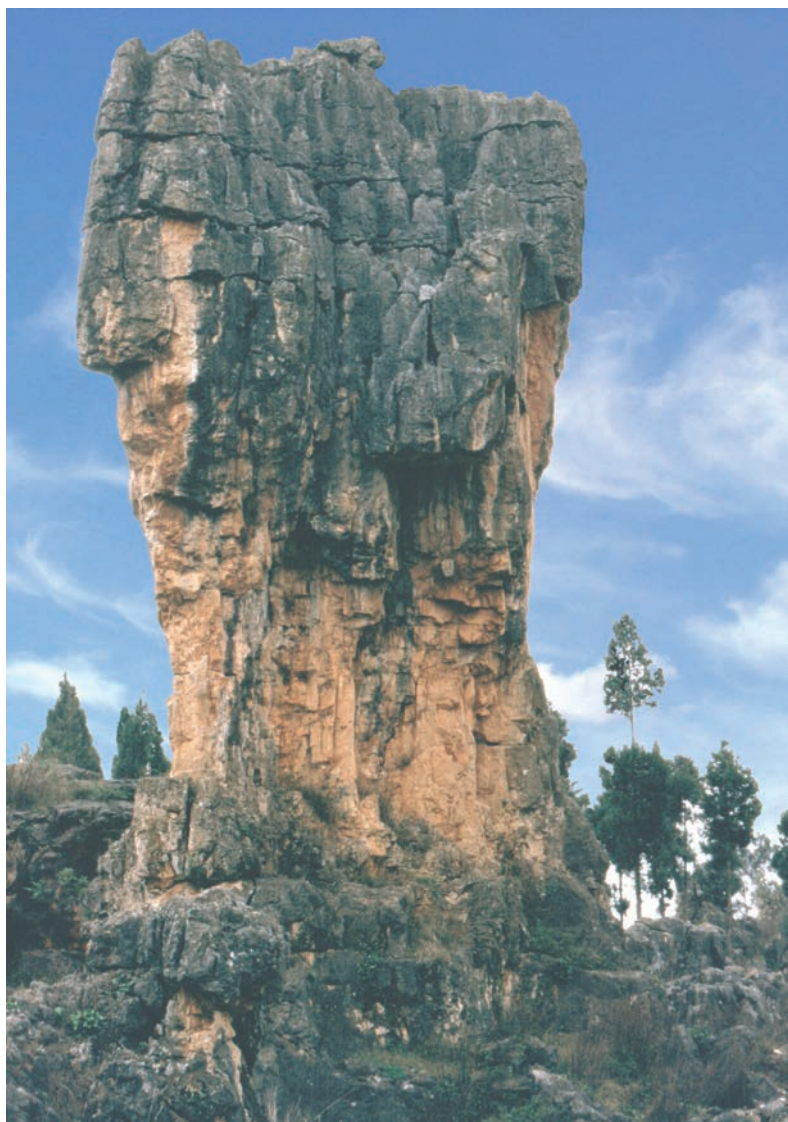
fossil remains are generally less preserved; only occasionally some foraminiferas and thick-shelled gastropods have better undergone the diagenetic processes. Secondary porosity is barely present.

### 2.1.4  *Sequence D*

The thickness of Sequence D is 5 m. The upper part of the pillars forms a highly recrystalized and grained dolosparite to dolomicrosparite. The boundary between sequences C and D is often blurred and difficult to determine visually and macroscopically. The primary limestone was highly diagenetically altered. Under the microscope we can observe subhedral to euhedral dolomite grains which form a hipidiotopic to idiotopic structure of the rock. The dolomite grains in this sequence are also about one-third of a millimetre in size. In diffused light the dolomite grains mostly have a slightly brown hue.

### 2.1.5  *Sequence E*

Sequence E is up to 2 m thick. Massive dolomitic limestone is characteristic for the upper part which we found only on some pillars. On the outside it has a coarse and speckled appearance, characteristic of a large part of the Naigu stone forest (*Knez* and *Slabe*, 2001a). Because of the bulginess on the rock surface, coarseness and subsequent algae overgrowth, the dolomite fields are dark grey. On the rock surface we can see them as dark grey to black spots, which gradate into lighter limestone fields in all directions. In most parts of the sequence, a percentage of the surface, as well as the volume, of non-dolomitic limestone and dolomitic zones are equal.

## 2.2  THE SHAPE OF THE STONE FOREST

The larger groups of stone pillars consist of several tens of pillars (1, 2, 3, 4). Between them are corroded fissures or narrow passages. The smaller groups of pillars, composed of ten or less pillars, are most often cut only by cracks and corroded fissures. Over a relatively large area of the stone forest we find only individual pillars and stone teeth. Individual pillars are relatively large, broad and high, or else they are low and wide.

The bedding is reflected in the form of the pillars mainly because of the diverse composition of the rock. Below the soil, as well as on the surface, the beds of Sequence B decay and decompose faster, and subsequently the individual thinner and tall pillars



**5**  A stone pillar whose shape is dictated by the rock.

are unstable. The tall pillars are generally mushroom-shaped. The beds of sequences A, C and D are more resistant and extensive. In some areas the upper parts of the pillars have disappeared, and only low pillars formed in rock sequence A are preserved. Subcutaneous tubes transformed by rainfall dripping down the pillars frequently hollow the porous rock of the beds in Sequence B. The rare pillar tops that form in such rock are often diversely shaped.

## 2.3   ROCK RELIEF OF THE STONE FOREST

We find three distinct types of rock forms on the pillars: subcutaneous forms, forms created by rainfall and combined rock forms. The creation of these rock forms and their uniqueness are defined mainly by the rock itself, especially where it is exposed. The subcutaneous forms are less explicitly defined by the rock.

### 2.3.1   *Subcutaneous rock forms*

These forms are divided into those that were formed below deposits and soil as the result of water flowing at the contact of the rock and soil, forms created by water percolation through the soil that only partially covers the rock, and forms at the level of the soil or deposits that surround the rock (*Slabe*, 1999).

The first group of subcutaneous rock forms are subcutaneous channels of various sizes that were formed by continuous water-flow at the contact of the rock and deposits that covered the rock and filled fissures in vertical cracks. The diameter of the larger channels can reach up to several metres (6). They dissect all different rock sequences. At the tops of the higher pillars they were transformed by rainfall, while the B beds decom-

**6**   Subcutaneously shaped stone teeth.

pose too quickly for the channels to remain preserved on them for a longer period. They are therefore mainly a characteristic of the lower parts of the pillars and stone teeth. Subcutaneous scallops that form on the relatively permeable contact area of the rock and deposits are preserved mostly in the beds of sequences A, C and D or on the beds of Sequence B that had been exposed for only a shorter period. Also the walls of the largest subcutaneous channels could be dissected by them.

The more extensive pillar tops and teeth are segmented by mid-sized and smaller subcutaneous channels and subcutaneous cups (*Slabe*, 1999) that were formed under the soil that partially covered the rock, therefore as the result of water percolation through the soil and its flow along the area where it touches the rock.

They have characteristic semi-circular cross-sections or cross-sections in the shape of the upturned letter omega. They are wider at the lower part and their diameters can reach up to 1 m. They are usually linked into a branched network. The subcutaneous cups (*Slabe*, 1999) are of various sizes and diameters, from a few centimetres to a metre or more. They occur on the tops of the large pillars and on the bottoms of the funnelled notches in the walls below them. The most porous strata are fairly densely perforated by subcutaneous tubes of diameters ranging between a few centimetres and a metre or two.

The pillars in the beds of Sequence B are generally distinctly undercut below the ground which is visible from the overhanging lower parts of the pillars that have developed on these rock strata.

### 2.3.2 *Rock formations carved by rainfall*

**7** The top of a stone pillar carved by rainfall.

These types of rock formations, especially the smallest flutes and cups, do not occur on this type of the rock. The exceptions are the more limited highest zones of the stone

forest where the teeth tops are created in the dolomitic limestone of the E beds. Segmentation of most of the tops is therefore defined by composition and diversification of the rock (7). The rock exposed to rainfall is coarse and contains only rock forms that do not exceed the size of the individual segmentation of the coarse surface. The solution pans with a distinctly segmented and coarse surface are developing from subcutaneous cups; only the bottom of solution pans covered by thin-layered deposits and overgrown remain even and relatively smooth.

On the steep walls the segments resemble channels, usually very narrow but relatively deep and angulated, which are 2–3 m long with diameters measuring 1–10 cm.

At the highest section of the stone forest we find dolomitic limestone on the pillar tops with flutes carved in them (8). Smaller channels with a diameter of 1–2 cm appear on the limestone where there are fields of dolomite in the limestone which generally protrude a centimetre or two from the wall and do not exhibit other rock formations.

### 2.3.3 *Combined rock forms*

These are the larger channels in the upper parts of the pillar walls. They develop as the result of water flowing from the subcutaneous channels which appear on the larger pillar tops or by water dripping from the funnelled notches. Subcutaneous cups occur at the bottom of the latter or else were once present there. They thus have larger or smaller funnel-shaped outlets at the edges of the tops which have in most cases been transformed by rainfall. They are especially noticeable in the beds of the A, C and D sequences or, if the top is in the beds of Sequence D, they reach the beds of Sequence B. Their distribution and shapes, relatively narrow and deep, are defined by how crushed the rock is, how serrated the rims of the rock are, and also by the composition of the rock.

25

Rainfall transforms, mainly deepens, the former subcutaneous channels and cups that criss-cross the wider tops. Such rock formations therefore exhibit traces of subcutaneous dissolution of the rock and of rainwater which can gradually, with denudation of the rock, completely take over. Below the soil the channels and cups are relatively evenly shaped with smooth walls, but as they become exposed, their shapes become distinctively uneven with many branches and segmented rims.

Half-bells are formed on the more durable levels of the soil and deposits that surround the pillars (*Slabe*, 1999).

## CONCLUSION

The stone pillars in the forest are either solitary or in groups within which there are only cracks and fissures. They were formed at various levels on nearly horizontal rock beds and in corresponding shapes. The exposed lower part of the geological profile or stone pillar is composed of fully dolomitized limestone, the middle part (Sequence B) is composed of porous dolomite and the upper parts of the stone pillars are composed of more durable limestone and dolomitic limestone, resistant to erosion. Sequence B rock beds decay and decompose faster, below as well as above the ground, and since they are generally covered by more durable strata, the pillars form characteristic mushroom-like shapes. The pillars are wider below the narrower parts if the lower dolomite strata are exposed.

The rock relief consists of various groups of rock forms: subcutaneous, those carved by rainfall and combined forms – their characteristics are defined by the composition of various rock beds. The tops are sharp and well segmented around the cracks. Such are all the forms carved by rainfall – these are channeled rock forms and solution pans. Their surface is notably coarse. On the limestone beds that occur only in some of the highest lying parts of the stone forest, the flutes and small channels are evenly shaped. On the porous and faster-disintegrating beds there are no distinct rock formations carved by rainfall, except at the beginning on exposed rock covered by more rounded parts of the subcutaneous rock relief. These are distinctly formed on all different types of the rock beds. Only their surface is mildly coarse.

In our research we have observed (*Knez*, 1998; *Slabe*, 1998; *Knez* and *Slabe*, 2001a; 2001b) that the lithological composition and tectonic properties of the rock play a decisive role corresponding to the morphological picture of the stone pillars and that they are essentially important in selective corrosion and erosion.

# LITHOLOGY, THE SHAPE AND ROCK RELIEF OF PILLARS IN THE PU CHAO CHUN STONE FOREST

**3**

MARTIN KNEZ, TADEJ SLABE

Pu Chao Chun is a minor stone forest 15 km south of the central Lunan stone forest (1). Rock pillars are situated on a ridge where their configuration is the densest and on the slope below it. The pillars in the upper part of the stone forest can be divided into two types, the high and the low ones. The latter are often lower than 5 m and could be called rock teeth were it not for their development – they are the remains of pillars and can be clearly distinguished from the real rock teeth which are conical and protrude up from the earth. They are wide, rather than high, and they stand close to one another. Their tops are relatively flat and at an equal level. The higher pillars reach up to 10 m. They stand alone or in groups of two or three and their cross-sections are usually quadrangular and only slightly tapered at the top. Their rims are toothed, a result of various cracks between relatively thin rock strata. They are often broader in the direction of the ridge and distributed in parallel rows which is a characteristic of this type of the crushed rock zone. In the lower part of the stone forest the pillars are larger and fairly evenly conical.

The pillars are bare, due to the removal of vegetation from them, and at many locations the tops are missing. The local population collect soil at the feet of the pillars.

**1** *Pu Chao Chun* stone forest – the upper part.

The development of the rock pillars on the various rock beds indirectly determined the relief which clearly indicates their evolution from underground limestone karren into a stone forest.

The basic characteristics of the Lunan stone forests were presented in the book South China Karst 1 (*Chen et al.*, 1998). These are, however, diverse, largely as a result of the rock on which they developed. This chapter explains the differences in more detail. We have already described the characteristics of the Naigu stone forest and Lao Hei Gin stone forest; here we add our discoveries concerning the particular shape of the Pu Chao Chun stone forest.

### 3.1 CHARACTERISTICS OF THE ROCK FROM WHICH THE STONE FOREST DEVELOPED

The Pu Chao Chun stone forest consists of Lower Permian carbonates of the Maokou formation (*Huang* and *Liu*, 1998). The formation is one of the more important base formations from which numerous stone forests in the Lunan region of southern Yunnan develop. The main characteristics of the Maokou formation are roughly similar to the Qixia formation, except that in the Maokou carbonates there are no major traces of dolomitization. There are considerable diagenetic changes in the basic rock, undoubtedly a result of the intense volcanic activity (basalt lava) during the period between the Palaeozoic and the Mesozoic (*Knez*, 1998); the rock is homogeneous and slightly cracked, there is practically no secondary porosity, and the carbonate content is exceptionally high.

Limestone dominates in the older part of the formation, altering with dolomites and dolomitic limestone. In the upper part it is possible to trace the sequence of limestone that is in some places thin-bedded and elsewhere forms strata several metres thick, and massive limestone which in individual horizons contains chert nodules up to several decimetres in diameter.

We have divided the rock sequences in Pu Chao Chun from the lithostratigraphic and morphostructural aspects into two parts, the lower and the upper one (2). The lower



**2** Cross-section of the *Pu Chao Chun* stone forest.

part consists of light grey to white thick-bedded to massive limestone, while the upper part consists of the beds of almost completely white limestone several tens of centimetres thick (3). Both are tectonically deformed with numerous sub-vertical faults running in various directions. Lithostratigraphically, they are genetically connected, with no stratigraphic gaps between them. They also indicate a similar depositional environment. The diagenetic influences through their geological history are evenly expressed across the entire profile.

In the lower part of the profile we can trace only a single textural variant. The limestone contains numerous bioclasts, some reaching several centimetres in diameter, and pellets. According to texture, limestone is micritic to microsparitic, most often biopelmicrosparitic. Only exceptionally are there calcite veins in the rock. There is no trace of secondary porosity. The rock of such characteristics allows the development of subcutaneous rock forms as well as features carved by rainfall.

In the geological profile the beds of the upper part follow in succession. The layers are 10–50 cm thick (only the lowest bed of the upper part exceeds 1 m). The latter shows a kind of logical depositional transition between the massive lower part and the more thin-layered limestone of the upper part. All the nine beds are equally resistant to corrosion and erosion. They form the narrower part of the pillar above the wider and much more resistant part.

Limestone in all the beds contains numerous bioclasts and pellets. Often the bioclasts account for up to 80 % of the volume. The basic rock varies between micritic and sparitic – the microsparitic dominates – and the limestone of the upper part can thus be called biosparitic and biomicritic, the biomicrosparitic type dominating. Neither dolomitization nor secondary porosity are expressed in the limestone. In some places there are stylolites with non-soluble residue alongside them.

**3** The lower part of the *Pu Chao Chun* stone forest consists of light grey to white thick-bedded to massive limestone. The upper part consists of the beds of almost completely white limestone up to some tens of centimetres thick.

In terms of the shape the rock pillars can be divided into two types, defined mainly by stratification of the rock from which they formed. In the upper part of the stone forest the characteristic shape of the pillars is a result of the thin rock beds (4). The upper parts of the pillars (1, 2) are relatively narrow; the largest consist of nine relatively thin beds of rock. Well expressed notches and subcutaneous holes have formed in the contact zone. The lower parts of the pillars are stout and made from a single thick rock bed. The narrower rock pillars are narrowest where the strata are thinnest. The pillars are oblong, due to the cracked rock. The tips of the pillars are relatively level where the top beds of the rock were thin and swiftly disintegrated. Only the thicker beds of rock have become tapered and are marked by funnels and rock formations carved out by rainwater. More or less distinctly shaped subcutaneous rock features are dominant in the first type. Most often only small and sharp rocks remain as the tips.

In the lower part of the stone forest which developed in the thick rock beds, the rock pillars are of a more even shape: stout at the bottom if they were not thinned by the subcutaneous action and tapered towards the top, with relatively sharp tips. Distinct subcutaneous features, holes as well as features on the rock surface have also formed between the beds of this type. The transition between the various different stone forests is gradual, depending on the position of the rock pillars and the rock beds (3).

### 3.3 THE ROCK RELIEF OF THE STONE FORESTS

The rock features of the stone forest pillars can be divided into subcutaneous forms, rock features carved by rainwater and combined rock features, formed by subcutaneous

**4** The top of a pillar in thin-bedded rock.

factors as well as rainwater (*Slabe*, 1998, 51). This particular, specifically shaped stone forest also has its characteristic rock relief.

### 3.3.1   *Subcutaneous rock forms*

The subcutaneous rock features below deposits and soil are divided into those that formed because of water flowing along the contact surface between them and the rock, then those that formed because of water permeating into soil that only partially covers the rock, and those that formed at the level of deposit or soil enveloping the rock (*Slabe*, 1999).

Large subcutaneous channels (3) formed as a result of water flowing along the contact surface between the rock and deposits that covered the rock and filled vertical cracks. The diameter of the largest exceeds one metre. They cannot be recognized on the upper parts of the larger pillars because these were reshaped by later processes. Their features are more expressed on the lower part, on the thicker rock bed which has not been exposed for as long. In some cases three quarters of the channel is cut into the rock face. It then continues under the current ground level. Only narrow edges have remained between them. The rock teeth are also most often partitioned by subcutaneous channels and their beginnings – mouths.

Subcutaneous notches have formed where more long-lasting soil enveloped the rock face. Under the ground their rims are broken up by semi-circular indentations – scallops where water percolated evenly. Sometimes channels lead to the upper indentations; these are larger. The rock is hollowed out under the overhanging edges of the largest notches.

The other type of subcutaneous channels (5) are the horizontal ones, having been formed under soil and overgrowing vegetation which only partially covered the rock. The mesh of subcutaneous channels can cover the entire horizontal tip of a pillar. These

**5**   The flat top of a rock pillar with subcutaneous channels and flutes and remains of the sharp pillar tip.

*Lithology, the
shape and rock
relief of pillars in
the Pu Chao Chun
stone forest*

are semi-circular and at the bottom often wider than at the opening. Their diameter can reach up to 1 metre. Individual channels can be narrowly deepened where the soil covers only their bottoms. The deeper channels have minor subcutaneous channels along their walls. Funnel shaped notches form at the ends of the channels situated on the rims of the tops. Water drains through them down the face, and the above-described vertical subcutaneous channels, especially under the largest ones, are located where it reaches the earth. These often develop from subcutaneous holes that were exposed when the upper layers disintegrated. They are formed as subcutaneous channels from the point where the level of the soil enveloping the pillars is lower than the channels, therefore also while they are still in the middle of the rock pillars. After they are exposed and there is no more soil in them they are directly eroded by rain.

The cups are of a similar origin. Subcutaneous channels lead from the largest, while the smaller ones might deepen the bottoms of the large subcutaneous channels. The cups closer the rims of the pillar tops can develop with the direct action of rainwater into funnel shaped notches.



**6**  The net of flutes and channels, carved by rainwater.

Networks of minor subcutaneous holes (6) develop along the bedding-planes and also along the cracks.

### 3.3.2 Rock formations carved by rainfall

The relatively homogeneous structure of the rock allows the formation of smaller rock features, directly carved by rainwater – rain pits, flutes and individual channels (1, 6).

The average diameter of the flutes is 2.5 cm; the largest reach 5.5 cm in width and the smallest ones 1.2 cm. They are measured on the surface inclined at angles of between 25° and 80°. The larger flutes are mainly those with greater inclinations and are the most expressed rock features on the rock tops. The largest flutes formed on the upper parts of the steep rock faces and on the beds that protrude from the faces. They are no less expressed, but usually shorter, on the rock surface with reshaped subcutaneous rock features. On the lesser inclinations of the larger rock tops individual channels have formed in the bottom of the notches between the protruding edges with flutes. Several such channels can cause the formation of minor funnel shaped notches on the rims, with steep sides separated by relatively shallow channels with less expressed edges. Rain pits are formed on the more level sections and rain scallops on the overhanging walls by water dripping down the rough rock surface. Kamenitzas are in most cases formed on the bases of the exposed subcutaneous rock features.

### 3.3.3 Combined rock forms

A significant part of the rock relief consists of combined rock features (5, 6). They are divided into those which were formed by a direct interaction of underground factors and rainwater and those that acquired their particular shapes through changes to their subcutaneous features caused by rainwater.

The water that drains from subcutaneous channels at the tops of the lower pillars also carves pillars on the vertical rock. Their diameter rarely reaches 20 cm. Funnel shaped mouths are formed at the rims. The funnel shape and the sharp edges are direct results of the rainwater acting on the rock. Such channels also lead from the dense mesh of holes that were formed along the bedding-planes and are now situated higher on the rock pillar. There are many holes and channels on the rock face running close to each other, while the funnel shaped notches at their mouths are less expressed since rainwater reaches them directly only when they are situated on the rock strata which protrude from the walls. Rainwater has substantially reshaped the large even tops of the pillars criss-crossed by exposed subcutaneous channels and holes. It sharpened the edges between them, their walls became covered by smaller rain pits and flutes, and the subcutaneous channels are often deepened by a narrower channel down which the rainwater drains. On the sharpened tips the remains of the subcutaneous features are the larger funnel shaped notches and, indirectly, also the channels below them.

### CONCLUSION

Pu Chao Chun stone forest, as other Lunan stone forests, was also formed from subcutaneous karren. The shapes are determined mainly by the characteristic distribution of variously thick and at the top mostly thin rock beds on which the stone forest developed at various levels. The dimensions and oblong shapes of the pillars were predetermined

by faults and cracks that vertically criss-cross the rock strata. The rock features and their rock relief clearly point to the importance of their underground formation, while reshaping by rainwater slowly progresses down the pillar.

The rock is practically the same throughout the geological profile. There is biomicrosparitic limestone all along it, with an almost 100 % $CaCO_3$ content – limestone which expresses similar sedimentation conditions along the profile and indicates an equal response to erosion and corrosion processes throughout, regardless of the thickness of the layer. The thickness of the layers crucially affects, and is clearly reflected in, the morphological shape of the individual rock pillars.

In the upper part of the stone forest pillars mostly stand individually. They are smaller in cross-section and rock strata are the thinnest. The bottom parts of the pillars formed on the thick rock strata are more stout and closer to one another. Where the layers are thinner, the notches are more expressed. They disintegrate faster and the tops are thus relatively level. Where the top layers are thicker, the tops become sharp. In the lower part of the stone forest, where the rock pillars are fewer, the pillars were formed on the thick rock layers and are generally thicker at the bottom and taper towards the top.

All the rock features which reflect the genesis of the stone forest are well developed. The subcutaneous rock features are the large subcutaneous channels on the rock faces and the subcutaneous channels and cups on the larger tops. The combined rock features are the channels that lead from the subcutaneous channels and cups located on the tops and subcutaneous holes between the bedding-planes. The exposed subcutaneous rock features are reshaped by rainwater which hollows the flutes, channels and scallops.

# SHILIN – THE FORMATION OF STONE FORESTS ON VARIOUS ROCK

4

MARTIN KNEZ, TADEJ SLABE

Stone forests are unique karst surface landforms (1). The Lunan stone forests developed from underground karren. Where this type of surface is highly developed in China, it is defined as 'shilin'. The extensive stone forests composed of many several-metre high pillars are an international tourist attraction, and to karstologists they offer a unique insight into the formation of karst landscapes. The development of stone forests has been presented many times (*Yuan*, 1991; *Sweeting*, 1995; *Ford et al.*, 1996; 1997; *Song* and *Wang*, 1997; *Frančišković-Bilinski et al.*, 2003; *Song* and *Liang*, 2009), and descriptions of their forms even more often (*Chen et al.*, 1986; *Song*, 1986; *Hantoon*, 1997; *Chen et al.*, 1998; *Maire et al.*, 1991; *Song* and *Liu*, 1992; *Song* and *Li*, 1997; *Yuan*, 1997; *Yu* and *Yang*, 1997; *Zhang et al.*, 1997; *Zhang, Geng et al.*, 1997; *Knez* and *Slabe*, 2001a; 2001b; 2002; *Šebela et al.*, 2004). An increasing emphasis has also been placed on the study of anthropogenic influences on the karst landscape and on its protection (*Kranjc* and *Liu*, 2001). The development of caves under stone forests and their influence on the formation of the forests have also been examined (*Šebela et al.*, 2001). This article compiles our current knowledge about the formation of the stone forests and their rock relief, which are the result of the way rock was formed and of characteristic processes on various carbonate rock.

**1** A stone forest as a unique landform on the karst surface landscape.
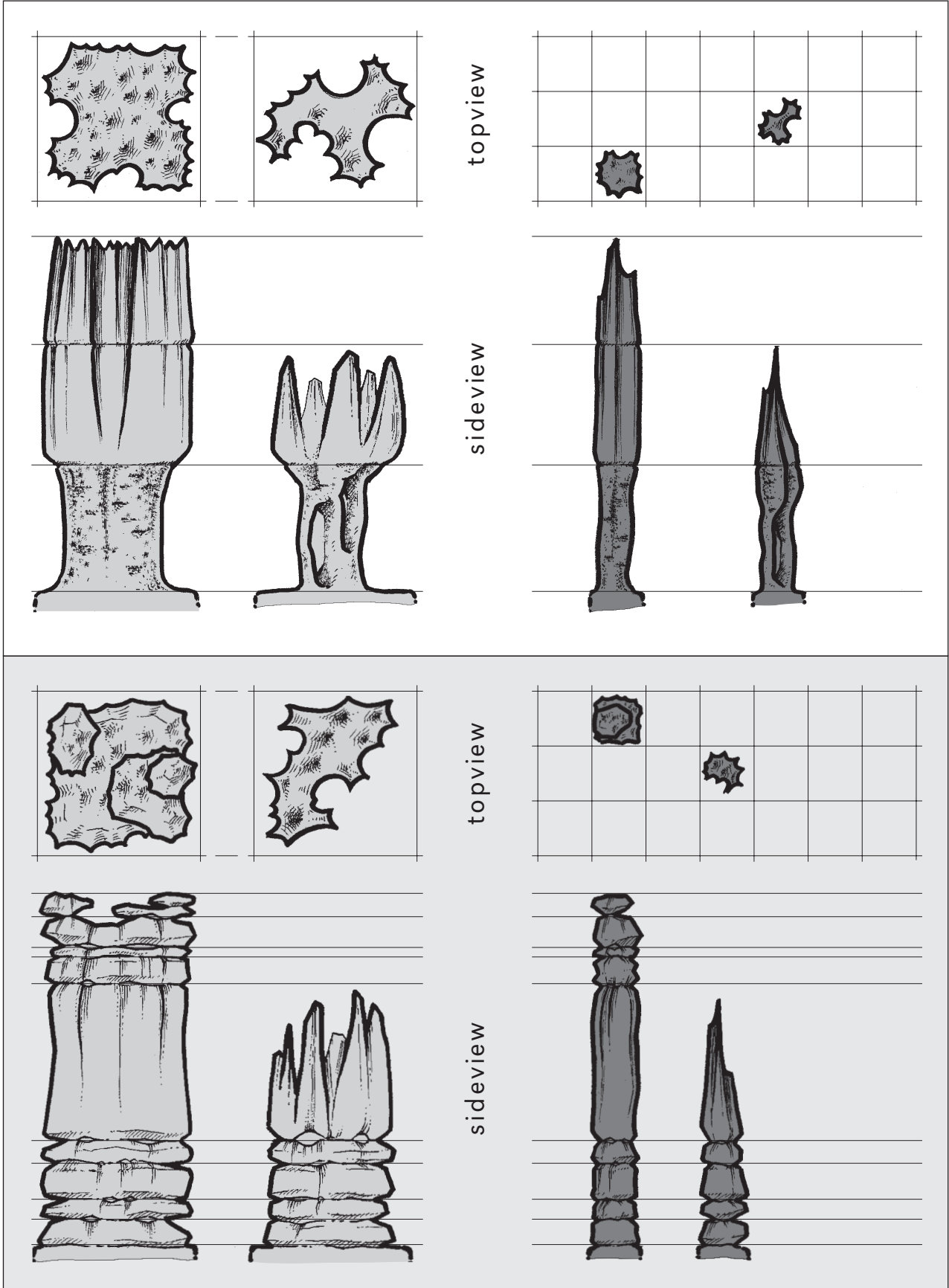
**2** Typical shapes of pillars in the *Lunan* stone forests.

The chapter covering a close interdependence of stratification, fissuring and composition of the bedrock with various processes in diverse conditions in the formation of the karst landscape is the core of this article and is illustrated by an accompanying drawing (2). The prevailing process of the carbonate rocks formation is their dissolution – corrosion in different conditions and caused by different factors. At the formation of the stone forests the most important is dissolution of the rock below sediment and soil and denudation of the rock due to rainwater, but also below vegetation. The most effective is the first one as organic substances in the soil with increased rate of organic carbon (*Slabe*, 1995, 66; *Urushibara-Yoshino et al.*, 1999) accelerate dissolution of carbonate rocks.

Of course, the sketch is simplified, but it offers a general insight into interweaving of diversity of the stone forest forms and pillars that comprise them. The rock relief of the stone forests reveals subsoil processes, hollowing of the rock by rainwater, and diverse transformation of the subsoil rock forms later by rainwater.

## 4.1 MATERIALS AND METHODS

For fifteen years, karstologists from the Karst Research Institute of the Scientific Research Centre of the Slovenian Academy of Sciences and Arts have been systematically involved in research of the stone forests in Yunnan Province.

Using various methods we have collected numerous new findings about the formation and development of the stone forests, karst landscape, epikarst areas, and hollowing of the aquifer in the immediate proximity of developing underground karren.

In the areas studied we conducted geomorphological, geological, structural and hydrogeological mapping and geodetic surveying. In the laboratory in Postojna we conducted experiments in the modeling of rock forms in plaster (*Slabe*, 2005).

In the field we selected rock samples and in the laboratory made microscopic preparations and conducted lithological, petrological and stratigraphical studies. The results of calcimetric analyses of carbonates were very important. Many noncarbonate sediments were analysed using a standard paleomagnetic analysis. The dissolving of the surface of carbonates at several locations was also tested with micrometric measuring.

## 4.2 GEOLOGY

The stone forest area consists of Early Permian carbonates of the Qixia and Maokou formations. These are two of the most important basal formations from which numerous stone forests emerged in the southern Yunnan province of Lunan. Typical for the Qixia formations are micrite limestone with intercalated dolomite and dolomitized limestone with intervening layers of schist. In the lower part of the Maokou formations, limestone alternates with dolomite and dolomitized limestone. In the upper part we find a succession of limestone layers that in some places are thin and in others several metres thick as well as solid limestone that contains several decimetres large nodules of chert in individual horizons. The main lithologic properties of the Maokou formations are roughly similar to those of the Qixia formations, except that in Maokou carbonates we do not find a major influence of late diagenetic dolomitization and in some places a considerable secondary porosity. However, both show a strong diagenetic alteration of the basic rock, which is undoubtedly also a consequence of the intensive volcanic (basalt lava) activity during the transition from the Paleozoic to the Mesozoic era. The rock contains an extremely high percentage of carbonate.

In the area studied we find considerable variations in thickness, porosity, and degree and type of dolomitization, in the components of inclusions, and in the colour of individual layers that are reflected in the formation of the stone forests (*Knez*, 1998).

What is macroscopically most noticeable in the geological profiles, is the different thickness of layers which varies from ten centimetres to many metres, according to some data, even more than 30 m (*Song*, 1986). In the stone forests we encounter rock sequences composed of several-metre thick homogeneous and compact layers where karstification is advancing considerably faster on tops, along bedding planes and individual fissures, and below the surface as well as sequences of thin-layered (10 cm and more) limestone where intensive karstification is already accelerating along numerous lithologic junctions. In the geological profiles we find an alternation of thickly- and thinly-stratified carbonate as well. Where the layers are thinner, the pillars can be much thinner due to more rapid corrosion.

In some places we encounter thicker segments of very porous layers where the intercrystal porosity exceeds 20 % in most cases. Typical for them are dolosparite and dolomicrosparite of the grainstone type. Diameters of light brown and in some places extremely pure and almost completely transparent dolomite grains reach one millimetre while their average diameter is one third of a millimetre. In contrast to the homogeneous and compact rock, a segment of the porous layers does not karstify merely along the lithotectonic junctions but across the whole profile in accordance with the stage of porosity. The rate of karstification of such rock is substantially greater and additionally accelerated locally below the surface.

Late diagenetic dolomitization is also typical of some layers. Where increased porosity and dolomitization appear in the same layers, more intensive karstification is found as well. A special example is the dolomitization of only individual smaller fields in such a way that otherwise homogeneous, compact and impermeable rock becomes freckled. Dolomitized limestone is therefore less influenced by karstification than pure thickly-stratified limestone. To a lesser degree, we see that dolomite fields, usually with a diameter of a few centimetres, protrude from the rock.

Layers with inclusions more resistant to karstification protrude from the profiles as well. One example is the chert that is the result of allochemical early diagenetic processes. Less soluble inclusions macroscopically influence slower karstification only locally while microscopically corrosion is substantially more intensive at the junctions between the inclusions and limestone.

### 4.3 THE FORMATION OF STONE FORESTS

More or less horizontal layers of the rock of various thickness and composition are criss-crossed by vertical fissures or cracks. Each of these features can have an important influence on the formation of the network of stone pillars in a forest, on their size and shape, and consequently on the rock relief as well. They interact in various combinations, fostering a vast diversity of stone forests. As a rule, however, one of the features of the rock or one of the factors of their shaping is dominant: a) the influence of fissuring of the rock on the shape of a stone forest and the size of stone pillars, b) the influence of rock strata on the shape of stone pillars, c) the influence of rock composition on the shape of stone pillars, and d) the influence of subsoil factors on the shape of stone forests (2).

Exposed subsoil karren is reshaped by rainwater. The long-lasting development of stone forests allowed creation of large karst forms. Due to the development of caves

beneath the forests and the erosion of alluvium and soil that previously covered the carbonate rock, exposure takes place faster than dissolving of the rock by rainwater.

### 4.3.1 *Fissuring of the rock and its influence on the shape of a stone forest and the size of stone pillars*

Networks of pillars distribution, i.e. ground plans of stone forests, are congruent with fracturing of the rock, in this case largely vertical, and take various shapes. Pillars can be linked in rows between distinct fault areas or close together, or a stone forest or parts of it can consist of individual wide or narrow pillars. Cracks between pillars have thus been corroded to various widths ranging from a few dozen centimetres to ten metres and more. This diversity in the network of the pillars can occur in the same forest, as for example in the Naigu stone forest.

As a rule, pillars with smaller cross-sections occur with a dense network of fissures (provided, of course, they are not diminished primarily by corrosion) and larger pillars occur with a sparser network. The latter, which can often be described as larger rock masses as well, have broader tops dissected into several points on the thickly-stratified rock.

The Naigu stone forest (3) lies 20 km east of the Major stone forest and is an important tourist site. This stone forest is composed of larger rock masses and smaller pillars that stand together or individually. The unique form of the forest is defined primarily by the fracturedness and texture of various beds of the rock from which the stone forest formed at different levels. The dimensions of the pillars are dictated by joints and fissures that vertically criss-cross the rock layers. The shape of the pillars, which are frequently undercut, and their rock relief clearly reflect an importance of the subsoil formation and reshaping by rainwater progressing slowly down the pillars.

**3** *Naigu* stone forest.

The stone forest lies alongside two tectonically slightly elevated ridges. The joints that border the joint zone are extremely strong, and the intermediate joints that largely run in a northwest-southeast direction are several kilometres long and deep. The pillars formed on a package of Lower Permian carbonate rock of the Qixia formation more than one hundred metres thick. The properties of the rock throughout the geological cross-section are very different, and from the morphogenic viewpoint we therefore divide the layers into three groups from the bottom up: a) layered micrite and nonporous limestone, b) porous and heavily dolomitized limestone, and c) massive and striped dolomitized limestone.

The pillars developed on different levels of the described rock beds and their shapes correspond to this. The most characteristic shape of the pillars is mushroom-like, and there are distinct notches along the porous and heavily dolomitized beds. This is the consequence of faster underground corrosion and hollowing of the most porous part of the rock, whose surface disintegrates relatively quickly. The pillars whose tops are in the porous and heavily dolomitized beds are narrower and mostly without characteristic or regular shapes dictated by the factors of their development. Stratified and nonporous limestone often forms wider bases of the pillars composed of porous and heavily dolomitized and massive and striped dolomitized limestone. The shape of the subsoil rock teeth as a rule does not reflect the different texture of the rock.

The most distinctive are subsoil and composed rock forms. Subsoil rock forms include large channels on the walls of the pillars and channels on the broader tops. Composed forms include the channels leading from the subsoil channels or subsoil cups found on the tops. The deepening of the subsoil cups and water flowing along the channels caused the dissection of the tops of the pillars, particularly the larger ones, into points with funnel-like notches between them.

Subsoil rock forms, as a rule larger ones, developed on all types of the rock in the Naigu stone forest. The rock influenced their shape, especially that of the smallest ones which often have jagged edges on the dolomitized rock. Flutes hollowed by rainwater are a less distinctive rock form in Naigu. Their occurrence and development are primarily influenced by the texture of the rock. Subsoil rock forms developed on the majority of beds of different rock, but only a few are found on porous and heavily dolomitized beds. Here we find subsoil tubes. When these beds of rock are found at the tops of the pillars, smaller rock forms hollowed by rainwater hardly occur. In places these are only rainwater pits or rainwater shapes larger subsoil rock forms. The rock relief therefore developed relative to the position of the beds in the pillars.

The gradual and diverse development of stone forests, which of course is connected with the development of caves below them, is also confirmed by traces of the development in the Bayun Cave in its central part. From the cave sediments and rock relief we can distinguish several periods of the development in the epiphreatic part of the aquifer, and then a rapid drop of the underground water that probably caused the faster growth of the stone forest (*Šebela et al.*, 2001).

### 4.3.2 *Rock strata and their influence on the shape of stone pillars*

The rock from which stone forests developed consists of strata of a different thickness and composition. This is reflected in the shape of the stone pillars, particularly in their cross-sections, in the shape of their tops and in their rock relief.

The shape of the pillars that develop on the thick and uniformly composed rock strata shows hardly any influences but rather reflects the more or less uniform develop-

ment from subsoil karren to a stone forest. The central part of the Lunan stone forests is an example. Narrower pillars have pointed or blade-like tops and relatively flat or subsoil undercut walls. Wider stone pillars, however, often have broad tops dissected into many points with notches between them.

Longitudinal sections of the pillars on thin rock strata (Pu Chao Chun) are often jagged since they are dissected by wall notches occurring along the bedding planes, or their shapes reflect the uneven resistance of the different rock strata to the factors of their formation. Cross-sections of the pillars are of various sizes and shapes. Thinner strata disintegrate faster and therefore the pillar tops are relatively flat having typical rock relief. Where the strata are thinner, as a rule, the pillars are narrow. Subsoil tubes occurring along the bedding planes can develop into subsoil channels when they occur on the top of a stone pillar or be reshaped by rainwater.

Pu Chao Chun (4) is a smaller stone forest located 15 km south of the Major stone forest. Its rock pillars are located on a ridge where their network is the densest, and on the hillslope below. Its shape is defined primarily by the unique distribution of variously thick beds of the rock, mostly thin in the upper parts, on which the stone forest developed at different levels. Dimensions and an oblong form of the pillars were dictated by joints and fissures that vertically criss-cross the rock beds. The shape of the pillars and its subsoil rock forms clearly reflect their subsoil formation and their transformation by rainwater slowly progressing down the pillars.

The rock changes little across the geological profile. Throughout, we trace mainly biomicrosparitic limestone with an almost hundred-percent proportion of $CaCO_3$, limestone that in this profile shows similar sedimentation conditions and that regardless of the thickness of the beds shows the same response to the influence of erosion and corrosion processes. The thickness of the beds has a decisive influence and clearly reflects the morphological appearance of the individual rock pillars.

In the upper part of the stone forest, the pillars are mostly individual and of smaller diameters, and the rock beds are the thinnest here. The lower parts of the pillars which are formed on the thicker beds of the rock, are stouter and stand closer together. Along the thinner beds there are distinct notches. Here, the beds disintegrated faster and the tops left beneath them are often flat, while if the beds above them were thicker, the tops are sharp. In the lower part of the stone forest, where there are fewer rock pillars, the pillars formed on the thick beds of the rock and as a rule therefore are wider at the bottom and narrower towards the top.

**4** *Pu Chao Chun* stone forest where rock strata play an important role.



41
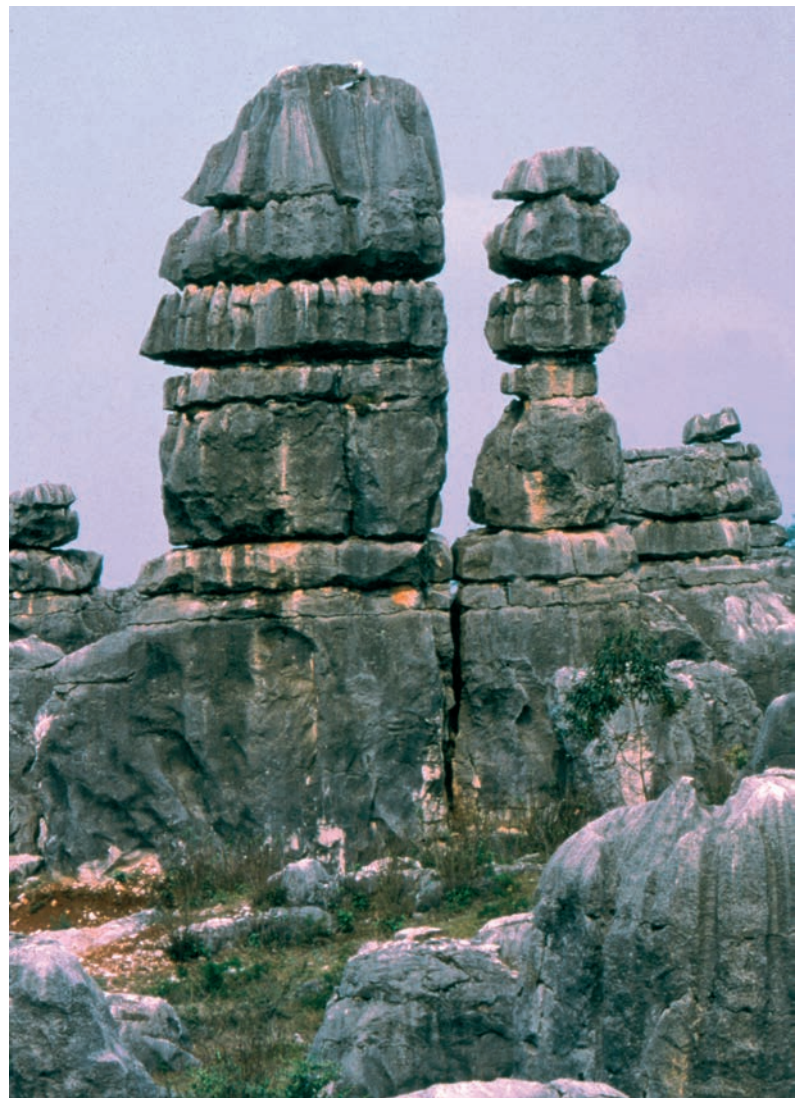
All types of the subsoil rock forms that reveal the development of the stone forest are well developed. These include large subsoil channels and scallops, as well as channels and solution cups on the wider tops. The latter channels often developed from subsoil tubes along the bedding planes and were uncovered when the upper beds disintegrated. Subsoil notches developed where long-lasting layers of soil surrounded the walls. A distinct proportion of the rock relief consists of the composed rock forms divided into those that occurred due to direct interaction of subsoil factors and rainwater and those whose unique shape is the consequence of transformation of subsoil forms by rainwater. The composed rock forms are channels that lead from subsoil channels and cups at the tops and hollows between the bedding planes of the rock. Funnel-shaped mouths formed on the edges. Exposed subsoil rock forms were transformed by rainwater that hollowed flutes, channels, and rain pits, and on vertical and overhanging walls, rain scallops are present that occured due to water trickling down the rough surface of the rock. Solution pans most often occur on the bottoms of exposed subsoil rock forms.

### 4.3.3  *Rock composition and its influence on the shape of stone pillars*

Rock composition, particularly if it is diverse, may decisively influence the shape of stone pillars, as much their longitudinal sections as the size of their cross-sections.

Porous strata are often perforated below ground and disintegrate more rapidly on surface as a result (Naigu, Lao Hei Gin). Pillars are most narrow at the level of the porous strata. Above them forms typical of overhanging walls and below them of gently sloping wall sections occur. The pillars break fastest along them. The tops of the pillars occurring on such rock are most often of irregular shapes.

Rock strata with less soluble components usually protrude from the walls, and if they are at the top, the tops are broader than the lower parts of a pillar and pillars therefore acquire characteristic mushroom shapes. These are particularly distinct if the pillars occur on the rock whose lower strata are relatively more soluble, porous, or disintegrate rapidly (Naigu).



**5**  *Lao Hei Gin* stone forest where rock composition decisively influenced a shape of stone pillars.

The Lao Hei Gin stone forest (5) lies 18 km north of the Major stone forest. Individual and clustered rock pillars and larger blocks of the rock transformed by corrosion and erosion occupy about 2 km². Where the pillars are clustered, there are only cracks or fissures between them. The pillars developed on various levels of almost horizontal rock beds, and their shapes correspond to this. The larger clusters of the stone pillars are composed of several dozen pillars. There are only individual pillars and rock teeth on a relatively large area of the stone forest. Some pillars have a shape of square towers and others of mushrooms. They are often composed of several blocks, remains of the rock beds between bedding planes and fissures. The individual pillars are either relatively large, wide and high or wide and low (1–2 m).

In the area of the Lao Hei Gin stone forest, the original limestone is heavily diagenetically altered: under the microscope, we can observe subhedral to euhedral grains of dolomite in the rock that form hipidiotopic to idiotopic structures. With the exception of the upper part, the rock pillars are roughly built of dolosparites and dolomicrosparites of the grainstone type.

An important difference in individual packages of the layers was in the determination of various degrees of secondary porosity and recrystallization, which are also reflected in the morphological appearance of the stone pillars. The lower parts of the pillars are composed of dolosparites to dolomicrosparites of the grainstone type in which secondary porosity is barely noticeable. The central part of the pillars is composed of very secondary-porous dolomites. On average, the crystals of dolomite are smaller than the crystals in the lower package of the layers and at the same time are less pure. The upper parts of the pillars are again composed of secondary almost nonporous limestone and dolomites. Only the tops are composed of recrystallized secondary nonporous limestone. Dolomite rock disintegrates mostly into grains.

The strongly secondary porous central parts of the pillars below the ground as well as on the surface weather and disintegrate faster. As a rule, tall pillars therefore have a distinct mushroom shape because the nonporous beds are more durable and extensive. In places, the upper parts of the pillars no longer exist, and only low pillars that formed in the lower nonporous rock and protrude from the ground as basalt remain. The heavily porous rock in the central part of the pillars is often hollowed by subsoil tubes that have been formed by rainwater trickling down the pillars. The rare tops of the pillars formed on such rock have in most cases irregular shapes.

The rock relief is composed of all the characteristic groups of subsoil forms, forms hollowed by rainwater, and composed rock forms. To a considerable extent, the texture of the various rock beds determines their features.

The first complex of subsoil forms includes various subsoil channels that occurred due to continuous flowing of water along the contact of the wall and sediment that covered the rock and filled cracks along vertical fissures. The diameter of the largest channels reaches several metres. They dissect all four different complexes of the beds. On the tops of the tallest pillars they were transformed by rainwater while the porous middle beds weathered too quickly for the channels to remain on them for a longer time. Thus the channels are mostly a characteristic of the lower pillars and rock teeth. Subsoil scallops which occur at relatively permeable contacts between the rock and sediments are also preserved as a rule on the nonporous beds or on the only recently uncovered heavily porous beds.

The wider tops of the pillars and teeth are dissected by medium-sized and smaller subsoil channels and subsoil cups (*Slabe*, 1999, 259) that developed under the soil that

partially covered the rock, i.e. due to permeation of water through the soil and its flowing along the contact with the rock. The larger channels on the upper parts of the pillars are composed rock forms. They occur due to the water flowing from subsoil channels on the wide tops of the pillars or lead from funnel-shaped notches. At the bottoms of the latter there are or used to be subsoil cups. At the edges of the tops are therefore larger or smaller funnel-shaped mouths most frequently reshaped by rainwater. They are especially distinct on the non-porous beds, or when the top is in the limestone rock, reaching lower lying heavily porous beds. Their distribution and shape – relatively narrow and deep – are determined by the fracturedness of the rock and indentation of the rock circumference by the texture of the rock.

Half-bells occur at the longer lasting levels of soil and sediments surrounding the pillars (*Slabe*, 1998; 1999).

Rock forms hollowed by rainwater, especially smaller ones like flutes and rain pits, do not occur on the rock described above. The rock is coarsely rough and only those rock forms whose size exceeds individual elements of the texture and structure occur on it. The exception is the smaller, highest-lying part of the stone forest where flutes occurred on the tops of limestone teeth. The dissection of most of the tops is therefore determined by the texture and fracturedness of the rock. From subsoil cups distinctly dissected and rough solution pans occur, and only the bottoms of those covered by a thin layer of sediment and overgrown remain flat and relatively smooth. On the upper part of the steep walls there are rough features similar to channels which are mostly very narrow, relatively deep, and of an angular shape; their diameters measure 1–10 cm and they are 2–3 m long.

### 4.3.4 *Subsoil factors and their influence on the shape of stone forests*

Subsoil factors created the pointed tops of narrow subsoil teeth and channels penetrating broad teeth (6) and caused undercutting of the pillars. At the levels where sediment and soil surrounded the stone pillars for a long period, larger notches or half-bells de-



**6** Subsoil channels on the top of a stone tooth.

veloped. Below the surface, the pillars were most often hollowed out along the bedding planes and more porous rock strata. The narrowest stone pillars can also be subsoil hollowed. Subsoil factors working only on individual parts of the stone pillars, as in cases when their tops are covered with soil and vegetation, most distinctly dissect them vertically when water trickles through the soil and corrodes the rock or when it flows from the soil down the pillars. Rainwater sharpens the pillar tops, reshapes the traces of their original subsoil formation, and with time also carves unique shapes distinctly reflected in the rock relief (7).

**7** Reshaping of subsoil features (channels) by rainwater.

45

Laboratory experiments of the karst rock features formation in plaster of Paris either appearing in the caves or on the karst surface proved to be useful (*Slabe*, 1995; 2005). Highly soluble gypsum, the solubility at 20 °C is 2.5 g/l (*Klimchouk*, 2000, 160), gives an opportunity to observe how plaster features change if they are exposed to various conditions and different factors such as water flow, water drainage through fine-grained sediments, water percolating through soil or trickling at the contact of sediment and plaster. The features in plaster are generally similar to the features developing on other carbonate rocks, but due to its high solubility they occur faster and, as a rule, they are smaller. But in a good deal they help to disclose the way how soluble rocks are shaped. We attempted to verify descriptions of various subsoil and epikarst rock features with experiments on the formation of subsoil karren (*Slabe*, 2005).

We sliced a plaster cube into small columns with 6 cm square cross-sections and heights of 30 cm. The separated columns were placed tightly side by side in a large bucket and covered with soil. We tried to recreate conditions dominating in the Lunan stone forests. We drilled small holes in the bottom of the bucket and then filled it with water. We provided a continuous supply of water to keep its surface 5 cm above the soil surface. Slowly, water started to penetrate the soil and then flowed through the holes in the bottom of the bucket. During the experiment, which with breaks lasted almost 400 hours, small subsidences appeared in the soil. Part of soil was carried out of the bucket by water and part of soil filled spaces where dissolved plaster had been removed. Before the conclusion of the experiment, after a day or two of a 'dry period', water required 1–2 minutes to fill the cavities between plaster and soil and flow out of the bucket through the holes in the bottom.

The results of the experiments can be summed up into three complexes. The fissured block of plaster generated the subsoil stone forest with single rock pillars controlled by vertical fissures in plaster and by water flowing vertically through the block of plaster, transporting sediments and dissolving plaster along them. Along the fissures plaster quickly dissolves. Two thirds of it dissolved and between the pillars distinctive fissures developed. Pointed upper parts of the pillars are the effect of the uniform vertical water flow through the soil. When the karst surface is being denuded, due to various interventions, similar subsoil features, i.e. stone teeth and stone forests, occur.

There are clearly visible traces of various ways water percolates down the model in the upper section through the vadose zone and in the lower part there are traces of water flowing through the locally flooded section. Water percolates most uniformly to plaster through the upper, most permeable soil layer, but it also flows along the contact between soil and plaster, carrying grains of soil with it and depositing them on plaster. Small recesses form characteristic of epikarst rock features on the rock. Subsoil scallops are found lower on the central section of the columns where the contact between the rock and soil is still quite permeable. As sediment we used soil that preserved a loose contact with plaster. Subsoil scallops may be found on the most vertical and overhanging walls of carbonate rocks shaped subcutaneously that are being formed in a vadose zone by water percolation along the uniformly permeable contact between the rock and sediment around.

In the lower section, a locally flooded zone developed where channels formed. Horizontal notches occur at the upper level of this zone. Such type of the carbonate rock

formation can be seen in the areas that are often flooded either the contact between the rock and sediment is poorly permeable or the rock is reached by underground water. Along the 'bedding planes', several-story networks of above-sediment anastomoses developed. Paragenetic formation of the rock in locally flooded areas at the contact of the rock and sediment is a frequent characteristic of cave ceilings and more or less horizontal bedding-planes and fissures or basal conglomerates in flysch. The origin of the ceiling channels was explained by an exact experiment (*Slabe*, 1995, 66).

In short, the experiment augmented and in many ways also confirmed our previous knowledge about the formation of the rock features (*Slabe*, 1998; 1999). The experiments proved to be useful this time also, they confirm and widen the conclusions about the subsoil formation of the soluble rock but, of course, they answer only a part of questions and this is why they must continue.

## CONCLUSION

Numerous examples of stone forests that developed in almost identical conditions show that the diverse shape of the pillars is primarily a consequence of the properties of the rock, from distribution and density of joints and fissures in the rock and its stratification to its composition. However, we must also consider the significance of the effect on their shaping by the subsoil factors and transformation by rainwater, that is the course of their development in various periods.

The strata of the Lunan stone forests which formed in Early Permian carbonates are mostly horizontal or inclined by 5–10°. Due to the vigorous tectonic action, they are fractured by numerous vertical and subvertical joints and fissures.

Diverse fracturing, stratification, and rock composition are reflected in the shapes of the stone forests and their stone pillars. In the same stone forest which developed on the diversely composed rock, pillars may be of various but typical shapes, the consequence of their development on different levels of a diverse rock column.

The shape of stone pillars occurring on thicker and uniformly composed rock strata reflects primarily the development from subsoil karren into a stone forest, and the traces of subsoil factors are gradually reshaped by rainwater. Cross-sections of stone pillars occurring on thin rock strata are often jagged, and their tops (even of thinner pillars) which as a rule are pointed, are often flat, the consequence of the rapid disintegration of thin strata. Porous rock strata are most often perforated below the ground and disintegrate faster on the surface; the pillars are therefore narrower and the tops on such rock have no characteristic shapes. More resistant rock strata protrude from the cross-section. The tops of the narrower pillars are sharp, formed as much by subsoil factors as by rainwater. The broader tops, however, are dissected by points and funnel-like cups.

The unique development of the stone forests is also reflected in their rock relief. Rainwater gradually reshapes the subsoil rock relief. The most distinct and particularly the largest rock forms are subsoil and composed rock forms. Subsoil rock forms include scallops, large channels, notches, half-bells, and subsoil channels and cups on broader tops. Composed rock forms include channels that lead from subsoil channels or subsoil cups and dissect pillar walls. Many pillars are undercut below the ground, while their tops have been reshaped by secondary subsoil rock forms and forms carved by rainwater. The rock relief of broader stone pillars is unique as well, particularly of those with broader tops, either on thick rock strata where secondary subsoil forms occur or on tops that developed due to the disintegration of thin rock strata when subsoil tubes oc-

47

curring along bedding planes developed into subsoil forms or large channels that were reshaped by rainwater. Both forms indirectly influence the shape of the pillar walls, due to water flowing from them and carving channels. As a rule, smaller rock forms do not occur on dolomite rock, on very porous rock, or on rock filled with larger inclusions.

The development of stone forests and their rate of growth in a particular period are also influenced by the position and development of karst caves below them, i.e. by the manner water – and the sediment and soil with it – flows from the karst surface. Various periods can also be determined from the karst caves. In the Baiyun Cave below the Naigu stone forest we can identify the periods characteristic of the cave development in epiphreatic conditions when water flowed rapidly through the cave and deposited gravel, then the periods of cave flooding during which the cave has been filled with fine-grained sediment, and the following period of the rapid deepening of the central tunnel by a water current that swept away most of the sediment from the cave. This last event which was a consequence of the rapid intermittent lowering of the water table below the stone forest made possible the faster growth of the cave as well (*Šebela et al.*, 2001).

# KARREN OF THE MUSHROOM MOUNTAIN (JUNZI SHAN) IN THE EASTERN YUNNAN RIDGE, A KARSTOLOGICAL AND TOURIST ATTRACTION

5

MARTIN KNEZ, TADEJ SLABE

The stony tops of cones (fengcong) of the mountain range in Shizong County (Yunnan Province) reveal interesting and unique development of karren on subsoil and bare rock, mainly formed under tree growth and in individual places, especially on the peaks where rock relief carved by rainwater dominates (1).

The way of its formation is to a large extent dictated by in parallel with stratification stylolitized rock, which at first glance (regional macroscopic level) appears as thinly layered carbonate. We can define karren on the Mushroom Mountain (Junzi Shan) as a special type (*Fornós* and *Ginés*, 1996).

The area has been organized for tourists, and a professional description of the attractive karst surface is necessary for development of the modern karst-related tourism.

**1** Unique development of karren and unique relief on the karst surface.

Researches there have been carried out in the scope of studying the Lunan stone forests (*Chen et al.*, 1998; *Knez*, 1998; *Knez* and *Slabe*, 2001a; 2001b; 2002; 2006; 2007; *Slabe*, 1998; *Šebela et al.*, 2001) and other forms on the karst surface in southern Yunnan.

## 5.1   THE SITE, ITS GEOMORPHOLOGICAL DESCRIPTION AND GEOLOGICAL FEATURES

The highest point of the Mushroom Mountain, one of the mountains of the eastern Yunnan ridge, reaches an altitude of 2409 m. The area of interest around the mountain occupies several square kilometres.

Several dozen metres high rocky cones (2) form tops of the mountain range that rises above the edge of flatlands where the county seat, the town of Shizong is located. The mountain range is largely overgrown with tree vegetation, and only a few of the hill tops and until recently denuded individual parts of lower-lying karren are bare.

The Mushroom Mountain is one of the most attractive sites in eastern Yunnan and boasts a wide selection of plant and animal species. Over 150 wild animal species live in the area and we also find there 1500 plant species, including twenty varieties of azaleas. The largest associations of some of the world's rarest plants and animals, discovered in China, are among them, too.



**2**   The Mushroom Mountain area.
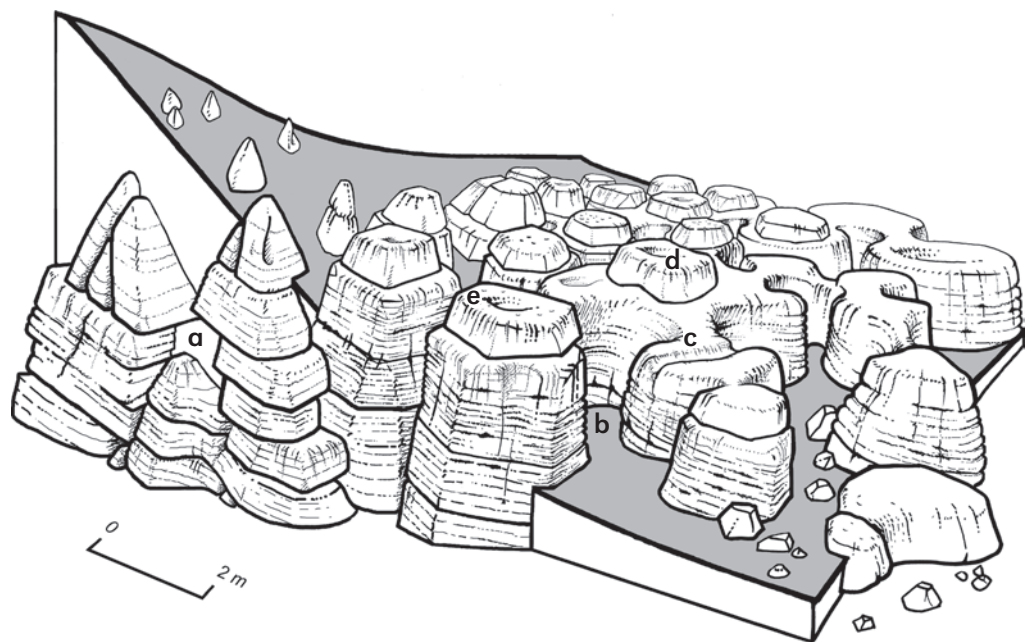


**3**   Development from subsoil karren to karren with flat tops: a – subsoil karren; b and c – subsoil channel; d – solution pan; e – rain pits and flutes.

Karren whose upper plates are oriented 160° towards northwest with a dip between 8 and 12° (1, 3) is composed of Middle Triassic marly limestone and marly dolomitized limestone of the Gejiu carbonate group. Rock is heavily stylolitized in parallel with stratification. Limestone and dolomitized limestone are mostly dark grey and in places medium or very light grey.

Dark grey limestone in the lower part of the studied rock is dense and very compact. Its stratification (4) almost completely covered by stylolitization (5) is very even in the entire area. In the lower part, the layers or the rock horizons from ten to several dozen centimetres thick dominate while from the stratigraphic viewpoint the layers of the upper section of the bare rock are only a few centimetres thick on average. The layers or the rock horizons are separated from each other by stylolites, in places marked by several

**4** Stratification is very distinct on denuded rock.



**5** Stratification is almost completely covered by stylolitization.

51

**6** Stylolites are in places only a few millimetres apart (thin section, diameter 2 cm).
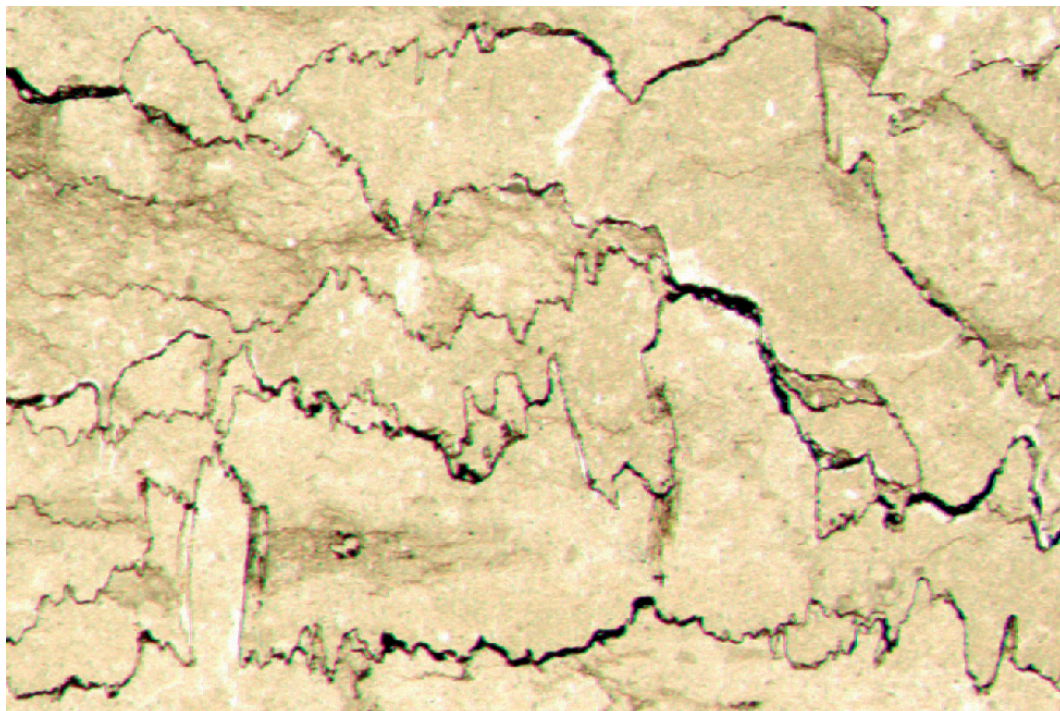
millimetres thick sheets of clay. The veins of calcite in the rock are almost imperceptible. Numerous stylolites are certainly characteristic of this limestone and in places they are only a few millimetres apart (6). The denuded rock along the stylolites weathers very quickly. There are no observable fossilized remains in them and no recrystalized rock. Moss and lichen along the corrosion-widened stylolites greatly accelerate the speed of weathering on the surface of the rock.

Medium grey to medium light grey rock is late diagenetic slightly dolomitized limestone. It is greatly cracked with dominating fissures that are largely perpendicular to the layers. In these layers, there are frequent several cubic centimetres large sections filled with coarse crystal calcite and in places with terrigenous sediment. Weathering is greatly accelerated along fissures or calcite veins. Corrosion is further accelerated by moss and lichen that colonize mainly fissures on denuded rock where biocorrosion rapidly dissolves it (7).

**7** Corrosion is additionally accelerated by moss and lichen.



In places, very light grey and slightly grainy limestone contains unidentifiable particles of fossil remains that are fused in horizons parallel to the layers.

Except for samples 9 and 10, the samples taken on the Mushroom Mountain contain a high percentage of total carbonate, almost 100 % in the case of sample 8 (Table 1). Samples 1 to 5 are dark grey limestone from the lower part of the studied strata, samples 6 and 7 late diagenetic dolomitized limestone containing more than 60 or 70 % of dolomite, sample 8 is light grey limestone, while samples 9 and 10 were taken from laterally filled noncarbonate sand pockets.

| sample | CaO (%) | MgO (%) | calcite (%) | dolomite (%) | total carbonate (%) | CaO/MgO (%) | insoluble residue (%) |
|--------|---------|---------|-------------|--------------|---------------------|-------------|------------------------|
| 1 | 51.82 | 1.89 | 87.13 | 8.66 | 96.34 | 27.42 | 3.66 |
| 2 | 54.06 | 0.80 | 91.13 | 3.69 | 94.82 | 67.58 | 5.18 |
| 3 | 54.56 | 0.64 | 95.77 | 2.95 | 98.72 | 85.25 | 1.28 |
| 4 | 50.92 | 3.26 | 82.76 | 14.94 | 97.70 | 15.62 | 2.30 |
| 5 | 52.88 | 1.49 | 90.68 | 6.82 | 97.50 | 35.49 | 2.50 |
| 6 | 34.04 | 14.27 | 25.31 | 65.28 | 90.59 | 2.38 | 9.41 |
| 7 | 34.15 | 16.77 | 19.30 | 76.72 | 96.02 | 2.04 | 3.98 |
| 8 | 55.46 | 0.60 | 96.86 | 2.77 | 99.63 | 92.43 | 0.37 |
| 9 | 54.28 | 0.56 | 35.19 | 2.58 | 37.77 | 96.93 | 62.23 |
| 10 | 27.54 | 0.36 | 48.24 | 1.66 | 49.90 | 76.50 | 50.10 |

**Table 1**
Calcimetric data of the samples from the Mushroom Mountain.

## 5.2 KARREN AND THEIR ROCK RELIEF

### 5.2.1 *The shape of karren*

Karren, reaching one or two metres in height, have characteristic flat tops (1, 3); only individual vertical cracks between them where fissures developed are deeper. Within a uniform level defined by contacts between the strata of rock or stylolites, they often spread over extensive areas either between the cones or on their tops. For the most part, the slopes of these cones are stepped, intersecting numerous rock strata. The uniform level of karren tops gives a unique stamp to the landscape. Subsoil enlargements of vertical karren cracks are relatively narrow so that the rocky surface often completely dominates; only individual zones covered by soil are wider.

### 5.2.2 *Karren rock relief*

The greater part of the surface is overgrown with trees (2). Karren under the trees are thus to a great extent covered by lichen and moss. Underneath, subsoil channels and solution pans are formed, criss-crossing the tops entirely in some places. Due to their characteristic long-term shaping, the karren are rounded and their surface is more or less smooth. The karren that were denuded not long ago are similar although the tree growth above them has been removed, but rainwater is leaving increasingly visible traces on them.

**8**  A solution pan and solution flutes.



The karren which dominate the tops of the cones and have been denuded for a long period have already been reshaped by rain to a great extent. First rain pits were formed on gently sloping surfaces, and flutes are the prevailing form on the dissected karren tops and their edges (3, 8). Channels were formed between flutes on more extensive gently sloping karren tops. Water from the flutes runs into these channels, forming branched networks in

*Karren of the Mushroom Mountain (Junzi Shan) in the eastern Yunnan ridge*

**9**   Subsoil rock relief.

**10**   Subsoil karren teeth.

the direction of the slope of the rock strata. Rainwater scallops form on overhanging parts of the rock wall. Flat karren tops foster the formation of solution pans as well (8) which often develop from subcutaneous cups. Another consequence of the karren shaping by rain is sharpening of their tops, naturally more pronounced on the narrower parts of the rock in a thicker network of cracks.

Subsoil rock relief (3, 9) is an important trace of the development and shaping (*Slabe*, 1999; *Slabe* and *Knez*, 2004). Karren originally starts as a subsoil form. Under soil and sediment, more or less vertical fissures begin to appear where water trickles downward along the contact of soil and rock as well as along junctions in the rock. Subsoil channels develop and subsoil shafts form that reach one metre in diameter, often with a funnel-shaped mouth in the upper part. The water that seeps through sediments and trickles downward on the walls dictates and continues to dictate the pronounced dissection of the edges of rock masses with semicircular notches of subsoil channels. Horizontal or gently sloping subsoil channels with cross-sections often shaped like an inverted Greek letter omega continue to dissect the karren tops as well. A good part of them are still filled with soil. In places, smaller subsoil tubes form along junctions in the rock, often linked in anastomoses. In their lower part, water also flows down these tubes in the areas of denuded karren. Vegetation also penetrates them.

Pointed or blade-like karren tops (3, 10, 11) form under the soil (*Chen et al.*, 1998; *Knez*, 1998; *Knez* and *Slabe*, 2001a; 2001b; 2002; 2006; 2007; *Slabe*, 1998). This became evident when earthworks revealed sections of subsoil karren. Their flat tops are for the most part a trace of the shaping of denuded, mostly thin-layered rock.

*Karren of the Mushroom Mountain (Junzi Shan) in the eastern Yunnan ridge*

**11** Pointed subsoil karren tops.

*Karren of the Mushroom Mountain (Junzi Shan) in the eastern Yunnan ridge*

The study of the rock relief of karren and stone forests and their development opened a number of questions regarding the way of the forming their tops exposed to rain. The rock relief is often formed on the top of the legacy of older, especially subsoil relief.

We exposed smaller plaster cubes with 40 cm long edges to rain (*Slabe*, 2005). The shaping of plaster blocks took two forms. When exposed to rain, the planes of various inclinations below ridges and the vertical planes below horizontal tops took characteristic shapes. Overhanging planes, however, took their own characteristic shapes.

In the central part of the plane inclined at 36°, vertical, narrow, long, and shallow scallop-like recesses were the first to form after ten hours, and narrow channels formed in the lower part of the plane. The ridge was dissected by small semicircular notches, below which flutes began to form. Gradually, three different sections of the planes were created (12). The upper sections became covered with flutes, the central parts were relatively smooth, and channels developed on the lower parts. This is the characteristic shaping of a plane, as illustrated in the book by Ford and Williams (2007). The flutes grew slowly downward from the ridge and became deeper. At first, their shape was indistinct because the ridges between them were rounded. The size of young flutes did not deviate significantly from the size of 'mature' flutes. On the plane inclined at 27°, the flutes are 3.6 cm long and 0.7 cm wide on average, and 0.5 cm deep in the upper part. As they progress downward, they become shallower and wedge out. On the surface with a 36° inclination, they are 4 cm long, 0.8 cm wide and 0.5 cm deep in the upper part. On the steepest, 63° surface, their most distinct parts are on average 7 cm long, 0.5 cm wide and 0.3 cm deep in the upper part. On steeper surfaces, flutes are therefore longer and slightly narrower.

Individual channels (Hortonian-type runnels; *Ford* and *Williams*, 2007) formed on the lower sections of the inclined surfaces (27°, 36°, 63°) (12). They were initially relatively flat, 0.5 cm wide and 10 cm long, with larger flat surfaces between them. First, channels started mainly to deepen. Their cross-sections took the form of an inverted Greek letter omega. Rainwater gradually sharpened the ridges between them. The channels widened to two centimetres. Thus, a network of channels formed in the lower section, which at first develop as collectors of water from the upper section of the inclined plane and later when they become deeper and their ridges begin to be shaped by rainwater, flutes form on the ridges as well. In this way, the denuded tops of the present karren are also shaped. Flutes and solution pans are found on all the longer denuded tops, i.e. mainly on the tops of the cones.

A special type of a channel (also called Hortonian-type dissolution channels by



**12** The relief of plaster of Paris plane exposed to rain.

*Ford* and *Williams*, 2007) formed on the vertical planes where water flowed from the horizontal tops. At first, channels with 3 mm diameters formed that meandered slightly. They were most pronounced in the upper sections of the planes below the ridge serrated by small semicircular notches. The channels reached to the bottom of the vertical planes. At first they became deeper and their cross-sections acquired the shape of the Greek letter omega. There were larger undissected surfaces between the channels, but eventually they covered the greater part of the plane. The channels gradually began to coalesce with the larger channels reaching up to 3 cm in diameter while the smaller channels remained hanging on the ridges between them. In a similar way, the rock relief of the pillars in the Spanish El Torcal stone forest was created. The upper parts of the vertical plaster block planes directly exposed to rain gradually became less steep, and by the end of the experiment, they deviated from the vertical by 3 cm. Becoming ever more directly exposed to rain, the ridges between the upper parts of the channels therefore became sharp and the channels became semicircular. Channels are gradually reshaped into flutes. The horizontal karren tops on the Mushroom Mountain also acquire these forms. Smaller wall channels also form due to water flowing from the tubes that developed along the rock contact points (bedding planes, stylolites).

We cut two channels, 1 cm in diameter, in two surfaces inclined at 63° and 36° to represent subsoil channels. Their diameter grew by 1 cm, and smaller meandering channels, very distinct in the lower parts, were carved in the channel bottoms. The mouths of the channels became funnel-like, 3.5 cm wide, and the first was dissected by flutes. This shape is a frequent and characteristic form for the tops of stone forests and karren originally shaped below soil (*Knez* and *Slabe*, 2002), and the karren of the Mushroom Mountain are no exception, especially since this shape is actually the prevalent form on their walls and the edges. The more or less vertical walls of subsoil channels are reshaped by water flowing from the flat tops and rainwater.

Whole plaster blocks acquire characteristic shapes. The plaster blocks become sharp because the upper parts of originally vertical planes incline inward and are therefore increasingly exposed directly to the rain. However, on the plaster blocks with horizontal upper planes, the vertical side planes bow in concavely with their edges protruding 3–4 cm. The tops on the Mushroom Mountain are flat, and those of the recently denuded karren have been only partially reshaped by rainwater. Their shape is conditioned primarily by pseudo-thin stratification of the rock, which is in the process of disintegration.

## 5.4 AN OLD CAVE UNDER THE TOP OF A CONE

An old cave that opens just below the top of one of the cones illuminates yet another period of the development of this part of the karst. It is a more or less horizontal passage that reaches 10 m in diameter. The rock relief (*Slabe*, 1995) on its walls, which are only partly covered by flowstone, reveals a manner of forming the cave as well as wider geomorphological and hydrogeological conditions when water once flowed through it.

The circumference of the passage is dissected by ceiling pockets and large scallops (13), indicating a slower flow of water in the phreatic zone of the aquifer. Typically, the size of the ceiling pockets exceeds one metre, they are often coalesced, and a number of pockets together usually form a cupola (14).

Humidity which to a large extent condenses on the circumference of the cave (especially on the ceiling of the entrance section) played an important role in the formation of the current appearance of the cave. Flowstone that once largely covered the ceiling and

walls is preserved only in small patches. This indicates that before the cave became open to external influences, it had been filled for a very long time with flowstone brought in by water percolating from the surface. Over time, flowstone corroded by condensed moisture, which even partly reshaped the old traces of the water course. At the top of the ceiling pockets carved by the swirling water in the primary period of the cave's development, there are smaller pockets carved by moisture condensed from the air. They reach up to half a metre in diameter, have steep edges, and can be clearly distinguished from the semicircular tops of the old pockets. The quantity of the water that to a large extent condenses in them and to a smaller extent on the walls below them was so great that it flowed down the walls in small streams. This led to the formation of narrower and partly meandering smaller channels that lead downwards from the pockets. The tops of the pockets formed due to condensation are smooth.

This indicates that a slow stream of water had flowed through the cave in the phreatic zone even before this part of the karst rose above the surroundings and the surface was dissected into cones. This vertical dissection of the karst must have been relatively rapid, otherwise the described rock forms would have been at least partly reshaped by developments in the changing hydrological conditions. The shape of the surface in front of the entrance to the cave which could be defined as a roofless cave (*Knez* and *Slabe*, 2002) indicates the gradual disappearance of the cave during the characteristic dissection of the karst surface above the deeply developed vadose zone.

**13** Large scallops in the cave.

**14** A ceiling cupola in the cave with channels carved by condensed moisture.

## CONCLUSION

Karren with predominantly flat tops that formed along stylolites and bedding planes of rock dictated special features of this karst landscape, which is attractive and interesting for tourists as well as for researchers. Their features and rock relief clearly reflect the geological conditions and development.

The carbonate rock in the area of the Mushroom Mountain has a very even and gentle dip of strata (8–12°). Throughout its geological history, Triassic rock covered by very thick younger layers underwent the diagenetic process of chemical dissolution and stylolitization which occurred in parallel with stratification.

Generally speaking, an outcrop of layers influenced by stylolitization indicates thin stratification, while the rock only recently denuded appears to be substantially more massive or apparently thickly layered.

The weathering along the stratification and stylolitization below the soil is not pronounced. Under the ground (a few dozen centimetres below the surface) rock teeth of relatively regular conical shape form. Due to the thin stratification and dense stylolitization, rock teeth of this shape only rarely protrude on the surface or they resist erosion and surface weathering only for a short period.

Once denuded, the rock rapidly reveals its true characteristics. Corrosion and erosion processes, especially along the contacts of layers and stylolites, intensively affect the outcrops. In a relatively short period of time and with the extensive help from moss and lichen (biochemical corrosion), the rock along these contacts becomes heavily weathered.

On a fresh outcrop, we can observe a thin sheet of clay (insoluble remains) between individual layers or horizons of the carbonate rock. This phenomenon resembles the structure and development of the El Torcal stone forest in Spain. There are two possible reasons for the appearance of this thin, even laminar clay: either the clay is synsedimentary (El Torcal stone forest) or more probably it is the residue of a very strong diagenetic process of stylolitization. There is no doubt that the laminar clays, regardless of their origin, are one of the basic reasons for the type of weathering we see on the Mushroom Mountain.

Due to the thin horizons of the rock between individual layers and stylolites and due to the laminar clay, the conical rock teeth or even the rock pillars cannot last long on the surface. On the contrary, the surface shows a trend of 'leveling' according to stratification and in its 'final' or current state appears as a 'karst pavement'.

Subsoil karren with conical tops dissected by subsoil rock relief were exposed from beneath the soil. On the surface, flat tops formed gradually. Below tree vegetation, subsoil karren are to a great extent covered by moss and lichen, under which they acquire their characteristic shape. On the bare surface they are reshaped by rainwater that carves flutes and solution pans.

An old cave that opens below the top of one of the cones is attractive and speleologically interesting. It reveals the period when this part of the karst was formed before its dissection into hills and cones and when this part of the karst aquifer was still deep under the water table.

The Mushroom Mountain is certainly an exceptional karst area. Further karstological studies will reveal even more of its particularities and make it an even greater tourist attraction.

# THE EXPLOITATION POLICY OF THE EARTH SCIENCE RESOURCES IN THE THREE PARALLEL RIVERS AREA

6

CHUXING HUANG, SHIYU YANG

After the movement of the Himalayas, the intense collision of the Eurasian and Indian plates led to the formation of the Three Parallel Rivers flow, a marvelous, spectacular geological phenomenon in the northwest part of Yunnan Province. The Jinsha, Lancang and Nujiang rivers extend here in a long, narrow region. Three Rivers is only 66.3 kilometres away at the weakest point. The elevation difference between the canyons of the Nujiang and Lancang rivers amounts to nearly 6000 m. The rivers run parallel for more than 170 km. This special geological phenomenon features many types of high-quality geological landscapes that are rare in China and abroad. At present, the local government is actively preparing a UNESCO World Natural Heritage declaration for the Three Parallel Rivers area.

## 6.1 THREE PARALLEL RIVERS AREA

### 6.1.1 *Three Rivers overview*

The name Three Rivers refers, as mentioned above, to the Jinsha, Lancang and Nujiang rivers. The Jinsha River originates in the Tanghla Mountain of Geladandong in Qinghai Province and represents a section of the Asia's largest river, the Yangtze. After Tibet and Sichuan it enters Yunnan Province near the town of Deqen Yangla. The length of the river in the tourist area is 380 km and features the Tiger Leaping canyon, the First Bay on the Yangtze River (1) and other famous geological phenomena.

1 The First Bay on the Yangtze River.

The Lancang River originates in the Qinghai's Tanghla Mountain and flows through Tibet and Yunnan. After leaving the canyon, it drops considerably and flows out of Yunnan at Jinghong. It continues as the Mekong River, Laos and Mjanmar's boundary river, and winds along the border between Laos, Thailand and Cambodia before finally entering Vietnam. It empties out into the South China Sea in the Pacific Ocean south of the Ho Chi Minh city, totalling a span of 1612 km.

The Nujiang River originates in the southern part of the Qinghai's Tanghla Mountain. After crossing the border, it continues as the Salween River and pours into the Andaman Sea in the Indian Ocean at Moulmein in Mjanmar.

### 6.1.2   *Three Parallel Rivers area defined*

From the geographical point of view, the Three Parallel Rivers area should include the Diqing Tibetan Autonomous Prefecture Deqen, Chungtien, Weixi; Nujiang Lisu national minority Autonomous Prefecture Gongshan, Fugong, Lushui, Lanping; Dali Pai national minority Autonomous Prefecture Dali, Pinchuan, Jianchuan, Heqing, Eryuan, Yunlong; Lijiang area Ninglang, Lijiang and 15 city counties. Geographically, it is located between the latitudes of 25°30' and 29°15'N, and between the longitudes of 98°5' to 101°15'E. The area covers 68,908 km² which accounts for 17.48 % of the total area of the entire province. At the end of 1998 the area had a population of 3,094,000 which accounted for 7.47 % of the total population of the province.

Looking from the geological angle, the Qinghai-Tibet-Western Yunnan crustal motion way is mainly unceasing nearness of tectonic plates that has led to a fierce collision making an intense raising fold by the huge pressure function of all construction kinds of deposit in the Tethys Ocean. It formed the Himalayas-Hengduan grand mountain range including the Three Parallel Rivers area and the Lijiang Yulong Snow Mountain, two scenic spots of national importance. Through the process of extinction of the marine shell a strong magmatic activity extended into the mainland; rocks, geological structure, mineral resources and landscape fabric became highly complex and characteristic of this region. From this point of view, the studies of the Three Parallel Rivers area tend to regard this area and the Lijiang Yulong Snow Mountain together, even a proper attention to the area has been influenced by a new tectonic movement.

Looking from the landform angle, the entire region belongs to the Hengduan Mountains. The Qinghai-Tibet and Yunnan plateaus are the first-level landform turning point, high in the north and low in the south. Relative heights range from 1000 to 4500 m. The region is known for three already mentioned famous rivers flowing from north to south. In the north of the region, the first-level branch of the Irrawaddy (Salween) River, the Dulong, sets a boundary that extends from the Nujiang's Pula downwards to the Yangtze River's Tuoding. Its length is only 66.3 km. Especially the Nujiang and Lancang rivers are divided just by Nu Sierra. From Nujiang's Buna, Lisadi, to Lancang River's Mianyaji,

**Table 1**
Hydrological characteristics of the Three Parallel Rivers area in Yunnan Province.

| Rivers | Catchment area (km²) | The catchment area accounts for the entire province total area (%) | Main current length (km) | The elevation of entering and flowing out (m) | Rivers average profile (%) | Annual production water volume (hundred million m³) | | |
|---|---|---|---|---|---|---|---|---|
| | | | | | | normal year | ample flow year | arid year |
| Jinsha River | 109,026 | 28.5 | 1560 | 2400 – 1420 | 0.129 | 456 | 536 | 388 |
| Lancang River | 88,655 | 23.2 | 1170 | 2357 – 1373 | 0.164 | 502 | 597 | 417 |
| Nujiang River | 33,484 | 8.7 | 547 | 1400 – 1760 | 0.179 | 280 | 308 | 258 |

Bidu, it is only 18.6 km. Near the latitude of 27°30'N, the beds of the three rivers begin to drop from east to west. The elevation of the river surfaces are: 2100 m (Jinsha River), 1900 m (Lancang River) and 1600 m (Nujiang River) (Table 1).

From the geographical point of view, the landform is most often considered as one unit. As for travelling, it focuses on the scenic spots and nature conservancy areas. The part which is slated to be included in the Declaration as a World Natural Heritage Site represents the third batch of state-level key scenic spot areas that were announced by the State Council in 1998. They extend over more than 34,000 km². The central scenic area is more than 17,000 km² in size including 10 nature conservancy areas and 9 scenic spots. It is the biggest nature conservancy in the world. Our country has declared it a cultural heritage site.

## 6.2 THREE PARALLEL RIVERS AREA GEOLOGICAL TOURISM RESOURCES TYPE

In the natural tourist resources there is a geological landscape with an ornamental and scientific expedition value which forms the geologic body and its phenomenon represented by crust mineral rock composition entity in the earth. With the predominant factor in endogenous or exogenous geological processes, the geological landscape is a manifestation sum of geological phenomena and structure trail under certain natural conditions.

Characteristics of the geological landscape, its origin, widespread scientific and cultural connotation have decided mystery and interest of this landscape and its ornamental value as tourist resources.

### 6.2.1 *Danxia landscape*

The region includes the Liming, Liguang and Meile townships in Lijiang Naxi Autonomous County. It is an important component of the nationally rated scenic Laojun in the Three Parallel Rivers area. Its total area is 240 km², composed of red sand, gravel, and powder detritus in the eogene system's great heavy film. The red sandstone layer forms steep crags of approximately 80 m. The landforms of the Qiangui Mountain are especially unique. Because steep multistage crags grow on the same hillside, three unusual landscapes can be seen here from sunrise to sunset within one day.

### 6.2.2 *Glacier landscape*

According to statistics, in this region there are 118 peaks higher than 5000 m and nearly 800 peaks between 4000 and 5000 m. In the area with an altitude of more than 3600 m world-wide landforms of glacial erosions and moraines cover 12,520 km² and snowfields, more than 4200 m high, occupy 5000 km². There distribute 424 glacial erosions or drift-dammed lakes. Typical are the Meili, Baima, Daxiao and Haba Snow Mountains, Yulong Mountain, etc. The glacier in the area is a low-latitude, high-elevation mountain glacier.

Since the Quaternary period the global climate has warmed up gradually. When the large-scale Quaternary ice age ended, glacial recession formed many issues of glacier vestiges in the Three Parallel Rivers area. It constitutes a unique series of glacier geology landscapes and tourist routes. In addition, the research of the composition of the

**2** The *Yulong* Snow Mountain glacier.

glacier landforms, deposits, and fluctuation changes in the snow line may determine characteristics and the scale of the glacier and its capacity to sustain weathering by cold. It reflected the climate and wet change degrees, and contrasted the glacier developing process. The good state of preservation of the Yulong Snow Mountain glacier vestige (2) is an advantage in reconstructing the ancient snow line.

### 6.2.3  *Karst sinters*

Karst landscape in the area is unusual and features many types. As a representative of the high cold karst landscape, Baishuitai is a famous scenic site in the area. The zone of transition slopes steeply to the gentle slope in the Baishui spring whose elevation is more than 3000 m and forms approximately 100 m tall, 300 m wide step-shaped sinter. Tianshengqiao natural bridge and Xiagei spring are representatives of the hot water sinters. Tianshengqiao bridge is located at the hillock 10 km upstream from the town of Zhongxin in Zhongdian. The bridge is 40 m tall, 10 m wide and 15 m long (3). Its surroundings include four or five hot springs with the maximum water temperature 54 °C (4). There appear three parallel crevasses, more than 100 m long, 1–5 m wide and 15 m deep. The smooth broken wall of the straight shape is a sign of the new structural activity. This provides a good location for the karst hot spring research and protection in the area. The Xiagei spring which lies approximately 5 km east of the Tianshengqiao bridge has in fact 13 hot springs appearing in an area of nearly 600 m². The famous cavern in the area is the Wujing limestone cave. According to the reports, limestone caves have once been discovered in the Baishuitai and Hutiao canyons, too, but because of difficult transportation only a few researches have been conducted there.

**3** The *Tianshengqiao* bridge.



**4** One of the hot springs in *Shangri-La*.

### 6.2.4 *Complex traveling geological landscape*

Niru has canyons, waterfalls, sinters and lakes, whose plant belt divides obvious and its ecological protection is good.

### 6.2.5 *Canyon landscape*

Hutiao canyon (5) includes Shanghutiao, Xiahutiao (Daju to Shigu), the First Bay on the Yangtze River and other famous scenic sites. Two sections of a drop in the Shangri-La canyon, not being big, have been primarily caused by distorting large-scale jointing (there are local faults). The strata and rock control are obvious, the surrounding snow mountain's present ice is occupying during withering away and its decline. A modern glacier stretches on the snow mountain that is now in recession. Under extrusion of the Mts. Nu and Yunling, the Lancang River becomes exceptionally vigorous. Just as Hilton writes in his Lost Horizon: "The appearance of the mountain is nearly vertical which has fallen a crack" and "the valley is far, and has been seemed a little dizziness".

**5** *Hutiao* canyon of the *Jinsha* River.



The Nujiang gallops between Mount Meili (also called the Biluo Snow Mountain) and Mount Gaoligong. The elevation of the two mountains reaches 4000–5000 m, but the Nujiang River bed is only 760 m a.s.l. Thus the famous Nujiang grand canyon formed. Along the river there live the Lisu, Nu, Drung, Pai and Tibetan national minorities, and the Lemo people. The precipitous natural scenery and the primitive culture of these peoples result in a beauty that embraces the wonderful wild area.

The Three Parallel Rivers area is a zone of transition in our country from the first to the second level of a landform unit (i.e. from the Qinghai-Tibet plain to the Yunnan-Guizhou plateau). In the region a new tectonic movement is intense. The erect rock layer belt, the crushed zone, the extrusion belt, their complete set of NW and NE structures (Chung-tien-Nixi-Beizilan) grow. The new tectonic movement is visible in the canyon landform of the Three Parallel Rivers area. It is an extremely scientific examination and scenic site and a geoscience scientific research, teaching and practical base.

### 6.2.6 *Running water geological process landscape*

It is in the area the main outside power geological process because the running water rapids and erosion power were greatly strengthened. They have created the Hutiao canyon, grand canyons of the Lancang and Nujiang rivers, and other marvelous sights. In addition, there are also brooks, waterfalls, Danxia landform, terraces, heart beaches,

and so on, e.g. the sister waterfall beside the Lancang River. The stack landforms, heart beaches, side beaches and terraces can only be seen in Shigu, Daju.

### 6.2.7  *Plateau lake landscape*

Because of the long-term glacier activity, many lakes in the region were formed by glacial erosion, such as the Bita and Napa seas, Shudougang Lake, and others. The scenery and environment are elegant, clear, primitive and interesting as a regional tourist attraction. Also their structure and compound origin can be noticed. Because the lakes were created in many periods of glacial activity, it constituted forms of the complete evolutionary process of the lakes in the region.

### 6.2.8  *Ornamental stones and minerals to be watched*

This refers to the stones formed by natural forces which have a value as aesthetic, contemplative, exhibit and collectible objects including rocks without carving, minerals, fossils, meteorites, etc., for exhibitions, collecting, teaching, installation or gardening purposes. We distinguish eight categories: of singularity, workability, and rariness, and of natural, scientific, artistic, regional and commercial characteristics. The area mainly features marble, yuhua stone (Yangtze River's Hutiao canyon to the Xingwen section, Lancang River's Yan Men to the Weixi section), green mudstone, serpentine (Lancang River's Deqen to the Yan Men section), as well as all kinds of mineral rock specimens and valuable jade, such as calcium fluoride and tungsten beryllium ores on the Haba Snow Mountain, Scarlet Mountain copper mine in Zhongdian, and so on.

### 6.3  characteristics of the tourism resources in the three parallel rivers area

### 6.3.1  *Physiographic characteristics*

Because this area lies at the suture line of the Eurasian and Indian tectonic plates, characteristics of the Hengduan Mountains extrusion are exceptionally obvious. Schistosity, lineation and vertical rock layer grow. Three crag class set characteristics are evident, in particular snake greenstone. All kinds of landforms are present and rivers are sincere; moreover, bends, headward erosion, glacier vestiges, levels of the surface and other Quaternary geological phenomena are obvious. The area represents an important and unique era in the evolution of the Earth's crust.

### 6.3.2  *Biodiversity*

Rising from the Lancang River edge, the area belongs, successively, to the subtropics, warm temperate, temperate, cold temperate, subfrigid and frigid zones, from low to high. This kind of an alpine belt cover type of the vertical distribution parallels the Northern Hemisphere distribution of the subtropical to the polar vegetation. In the Three Parallel Rivers area, the advanced plants have 210 branches with more than 1200 classes which altogether numbers 6000 species. Representing less than 0.2 % of Chinese land, it features 20 % of the advanced plants in our country. There are 173 species of mammals, 417 of birds and 59 from a crawling class.

Because the Meili Snow Mountain is located at a low latitude, climatic vertical distribution there is remarkable. After the area had gone through geological processes, the mountain became the channel and convergence point for plants onset and retreat from north to south. The Quaternary glaciers became a refuge for many plants and animals and have preserved many otherwise lost plants. Fir, spruce, hemlock, yew, Lancang Huang, Yunnan pine, *Pinus armandii*, and others have been included in the key state protection of plant varieties. Also rare animals find refuge here, such as the Yunnan golden monkey, a white-lipped deer, an antelope and the Tibet chicken, among other first-level or second-level protected animals.

The area has numerous snowy mountains, glaciers, mountain lakes, open plateaus as well as mountain canyon landforms. There live 14 national minorities with a population of approximately 880,000 people. Eight of them are unique to the region. The UNESCO Heritage Committee declared that as long as an item achieves four standards, it may be declared a World Heritage Site. According to the Chinese authoritative experts' demonstration, the Three Parallel Rivers area conforms to the four world natural heritage standards.

### 6.3.3 *Unusual natural scenic beauty*

In this region the snowy peaks stand in great numbers. The Meili Snow Mountain is situated at the head of eight big mountains in the Tibet area. It is among the small number of mountain peaks that have not been conquered by human beings. The American explorer Loke, the British writer Hilton and numerous modern scholars and tourists, they all are full of praise for beautiful scenery of the area, and have left behind many works. The Three Parallel Rivers area is one of the world's most concentrated distribution regions of the natural landscape.

### 6.4 DEVELOPMENT STRATEGIES FOR THE GEOLOGICAL TOURISM RESOURCES IN THE THREE PARALLEL RIVERS AREA

Because of the new tectonic movement as well as human aggressive development activity the tourist resources in the area have experienced varying degrees of destruction. In addition, a sharp increase in tourism in recent years revealed the lack of the effective management in the tourist environment.

In the area the snow line has risen. The forest is in a sharp decline. Grass cover has degenerated. Soil erosion, landslides and collapse are obvious. For example, the newly built road in the Hutiao canyon creates unstable banks on both sides. In order to open up the People's Bank plank road from bottom to top, towards the Bita marine tourism attractions in Zhongdian County, its planners did not hesitate to cut down several thousand mature trees to pave the way. During the restoration and reconstruction of a Buddhist temple in the Diqing Tibet area, the construction took place on such a large scale that it had an influence on the original cultural monument. On the Mingyong glacier on the Meili Snow Mountain hotels were built in the scenic area; tourists can directly reach the lower part of the glacier which is seriously polluted and shows signs of retreat.

The clash between human and natural phenomena grows daily more prominent. According to predictions, by 2010 the population of the northwestern Yunnan Province would reach 3,351,000, that is 257,000 more comparing with 1998. This fact will certainly put more pressure on crucial resources and environmental capacity. In this part

of Yunnan Province, village residence places burning firewood occupy its total number separately 78 % and their population 79 %. Every year at least 129,200 hectares of the forest vanish because of using the firewood. The natural protective forest project is achieving only less than 40 % of entire forest consumption. If the issue of energy substitutes for local residents is not solved as soon as possible, in 50 years the northwest of Yunnan Province will gradually be left without its precious natural tree cover.

Ecological environment of the river valley is changing for the worse, soil erosion and pollution becoming more evident. The population is concentrated in the river valley area where the access to only very limited resources is possible. Twelve of the 15 city counties are poverty-stricken. The poverty of the local communities, outdated technical education and the traditional approach to the way of economic growth dictate exploitation of natural resources and preserve the low level of development. All this creates huge pressure and leads to destruction of ecology and resources in the area.

### 6.4.1 Strategy for protecting the development and sustainable use

As already seen, tourist resources of the study area are in the initial development phase without making deep-seated minding and reflecting their scientific and cultural connotations. It pauses merely in satisfies in the low level which the tourist seeks and also lacks the practical and feasible protective measures. Because of travelling vulnerability and renewability of the geoscience resources, the studying of the tourist resources' origin and their scientific and cultural historical value as soon as possible is essential to promote the tourist resources brand in the area, and to protect the development and sustainable use.

### 6.4.2 Comprehensive development strategies for geoscience tourism, eco-tourism and cultural diversity tourist resources

The area bounds several regions and is a zone of transition for exchange and integration of three civilizations: on the northern side for the Tibet culture, in the west and south for the southeast South Asian subculture, and in the southeast for the mainland cultural contact. The Three Rivers natural valley channel links the northwest of Yunnan and the surrounding civilizations.

Integration and the conflict between different national cultures have been frequent, resulting in a diverse population mix in this region, forming a multi-cultural blend of interactive human networks. In addition, the transportation system is inconvenient, having been under natural conditions for a long time, thus preserving numerous national characters, styles and national culture characteristics, religious sites and settlements. The diversity of national cultures makes the region one of the richest historical cultural heritage areas not only in China but world-wide.

### 6.4.3 Perspective for the action and development

The number of glaciers in the area, for example, is high and their types are complete. The remnant of the ancient glacier and the ancient snow line are clear and well preserved that could increase scientific curiosity and interest in the popular science tourism but also provide a good base for studying glaciers. The karst series have ascending springs, descending sources, and also have hot and cold springs. This area is not suitable for the

large-scale purely commercial tourist activity, but has characteristics suitable for eco-tourism. Tourists mainly go to this area in order to return to the nature, to the original conditions. This area should be developed in the direction of the environmental tourist education and as a scientific research base for academic exchanges.

### 6.4.4 Tourist resource unit exploitation and tourist route's union with the neighbouring area

The Three Parallel Rivers area is situated in Yunnan, Sichuan, at the intersection point of the Tibet's three provinces. It features numerous tourist hot spots which have been developed or are waiting to be developed in the vicinity; they are known as the Golden Triangle for Travel, a virgin tourist country awaiting development. Shangri-La grand canyon extends northeast for 200 km, towards Sichuan's Daocheng. Beautiful snowy peaks, initial alpine meadows, a simple national character and styles are rapidly making a new tourism hot spot of it. Meili Snow Mountain lies approximately 40 km to the northwest; it is the Tibetan brine well from which one can enjoy the scenery of the upper reaches of the Lancang River. At the time, this area is famous for its Tea-Horse road (south ancient Silk road). The ancient salty mineral ruins of the brine well and a well-preserved Catholic church more than 150 years old speak of the activities of foreign missionaries in the second half of the 19<sup>th</sup> century and about the religious contradictions and ethnic conflicts which existed in the Tibet area. They have deep cultural connotations and historic importance. Towards east, there lies the World Heritage town of Lijiang and lives the world's last remaining matriarchal clan community (the Mosuo people) of Lugu Lake. To the south is Dali as a state-level historical and cultural city. The southwest features famous tourist spots such as Xishuangbanna, Ruili, Baoshan and Tengchong. In planning tourist routes, full consideration should be given to the areas surrounding the tourist spots. Generally speaking, attention should be paid to the following points: avoiding duplicate roads and back roads so that tourists can appreciate, as far as possible, most of the landscape in a limited time; at the same time, we must consider how to satisfy tourism of various levels and tourists with different demands. Because the Three Parallel Rivers area is far away from the big and medium-size cities and the transportation is inconvenient, according to our country's holiday characteristics, the time for sight-seeing will be limited. Therefore we must be careful not to act alone, but to establish joint tourism plans (*CLTGI*, 1991; *CNST*, 1993; *GDR*, 1989; *Plan of Protection*, 2001; *TYTG*, 1995; *Yunnan gardening bureau*, 1999).

# VEGETATION OF THE STONE FOREST

PING WANG, HONG LIU

<span style="font-size:3em;float:right">7</span>

The stone forest is located in the core area of the karst plateau in the eastern region of Yunnan Province. It lies in the upper part of the Zhujiang River watershed. The Bajiang River and its branch, the Dakehe River, flow through this region. Their downcutting is not strong, disintegration of the plateau surface slight, and plateau topography has not been changed much by river erosion (*Yang*, 1991). The altitude is mostly between 1700 and 1950 m, only one summit being higher than 2200 m. The altitude of the Major stone forest district reaches about 1750 m and that of the Naigu stone forest approximately 1820 m. The relief slopes from northeast to southwest. The main mountains are Mt. Gui, Mt. Jiupan, Mt. Dayang and Mt. Dafo. The highest of them reaches more than 2000 m in height. The main part of the stone forest is located in the karst district between Mt. Jiupan (East Mountain) and Mt. Dafo (Western Mountain). The main physiognomical features of this area are a plateau, hills, low mountains, solution depressions, fields, stone forests, stone teeth, fengcong, fenglin, isolated peaks, valleys, sinkholes, karst caves, lake basins, and river valleys (*Zhang*, 1984). Stone forests and stone teeth can mainly be found near lake basins, depressions, river valleys and on the plateau surface.

The climate of the stone forest is strongly affected by the north subtropical monsoon (*Wang* and *Shou*, 1989). According to the climate data collected by the Shilin Meteorological Station over the last 17 years (*Information collection*, 1984), the annual average temperature is 15.6 °C, the mean monthly temperature of the hottest month (July) 20.6 °C and the mean monthly temperature of the coldest month (January) 8.4 °C. Annual average temperature range is 12.2 °C. Annual average amount of rainfall is 964 mm. The rainy season lasts from May to October and contributes about 87 % of annual rainfall while only about 13 % of annual rainfall is contributed in the dry season between November and April. The solar radiation is 5656.5–5731.9 MJ/m². Annual average sunshine duration is 2318 hours and the ratio of sunshine 53 %. For about 270 days a year the annual mean daily temperature is higher than 10 °C and accumulated temperature of ≥10 °C is 4857.7 MJ/m². The annual average frost season lasts 113 days.

The main strata in the stone forest area were formed in the Later Palaeozoic age and some of them in the Proterozoic, Early Palaeozoic and Cenozoic ages. The types of rock are limestone, dolomite, marl, sandstone, shale, basalt and others. The landscape of the Major stone forest developed in the limestone of the Maokou age in the Early Permian epoch while the Minor stone forest developed in the limestone of the Qixia age (*Zhang*, 1984).

In the stone forest the distinct soil belongs to the puna red soil zone of the karst plateau of eastern Yunnan (*Wang et al.*, 1996). The types of soil formation parent material are mainly ancient red weathered crust, proluvial formations, alluvial deposits, lacustrine deposits, slope deposits and others, weathered and shaped by the rocks described above since the Tertiary period. With the long-term interaction of local soil formation factors such as the plateau subtropical bioclimate, parent material and others, the following four soil types were developed: red earth, limestone soil, purple soil and paddy soil. The red earth and limestone soil are the main while the purple and paddy soil are the minor soil types in this area.

### 7.1.1   *Vegetation types*

*Vegetation of the stone forest*

Current wood vegetation in the stone forest area mainly belongs to a secondary forest although primary vegetation can also be found. Only a few semi-humid, evergreen, broad-leaved forests grow in this region. Based on the field evidence, this kind of a forest was a dominant vegetation type in the past. It can be found not only on a soil-mountain but also on a stone-mountain, especially on stone teeth mountains with stones and soil. After the evergreen, broad-leaved forest was cut or burned, the region turned into shrub and grass-land. This kind of vegetation is very limited in the stone forest area. If this area is strictly protected, after decades or one hundred years shrub and grass-land will change into a climatic climax community – a semi-humid, evergreen, broad-leaved forest.

Except for agricultural land, the secondary vegetation is dominant, such as the young *Pinus yunnanensis* forest, bush-grass representing deserted mountains, and the *Pinus armandii* forest. The latter can scarcely be found in this region. Most of the *Pinus yunnanensis* and *Pinus armandii* forests are artificial. Some of them occur on limestone hills with low cover and density. The high density *Pinus yunnanensis* forest can only be found around Changhu Lake (Long Lake) and its area is very small. The *Pinus yunnanensis* savanna is one of the dominant vegetation types. According to the local climate environment, this kind of vegetation can develop into the *Pinus yunnanensis* forest. However, because the physical environment is harsh, featuring much gravel, a thin soil layer and drought, this process would be very slow and possibly even unsuccessful.

**Table 1**
Classification of the vegetation in the stone forest of *Yunnan*.

| Vegetation type | Sub-vegetation type | Formation | Association |
|---|---|---|---|
| I. Evergreen broad-leaved forest | (I) Semi-humid evergreen broad-leaved forest | (1) *Cyclobalanopsis glaucoides* forest formation | a) ass. *Cyclobalanopsis glaucoides, Olea yunnanensis* (Yuehu Lake, 1900–1960 m)<br>b) ass. *Pistacia chinensis, Cyclobalanopsis glaucoides, Olea yunnanensis* (Great stone forest, 1760–1850 m) |
| II. Warm coniferous forest | (I) Warm coniferous forest | (1) *Pinus yunnanensis* forest formation | a) ass. *Pinus yunnanensis, Myrsine africana, Pyrus pashia* (Changhu Lake, 1880–1890 m) |
| | | (2) *Pinus armandii* forest formation | a) ass. *Pinus armandii, Quercus franchetii, Myrsine africana* (Ziyun Cave, 1750–1790 m) |
| | | (3) *Cupressus duclouxiana* forest formation | a) ass. *Cupressus duclouxiana, Pinus yunnanensis* (Shifeng temple, 1790–1870 m) |
| | | (4) *Juniperus formosana* forest formation | a) ass. *Juniperus formosana, Pinus armandii, Cotoneaster microphyllus* (Yuehu Lake, 1890–1950 m) |
| III. Savanna bush | (I) Warm savanna bush | (1) Medium grassland formation containing *Pinus yunnanensis, Campylotropis polyantha* | a) ass. *Heteropogon contortus, Schizachyrium delavayi, Pinus yunnanensis* (Ziyun Cave, 1760–1840 m) |
| IV. Bushes | (I) Warm limestone bush-grass | (1) *Myrsine africana* bush-grass formation | a) ass. *Myrsine africana, Sophora velutina* (Great stone forest, 1790–1820 m) |
| | | (2) *Millettia velutina* bush-grass formation | a) ass. *Millettia velutina, Spiraea martinii* (Naigu stone forest, 1820–1890 m) |
| V. Meadow | (I) Warm meadow | (1) *Cynodon dactylon* meadow formation | a) ass. *Cynodon dactylon, Centella asiatica* (the bank of Yuehu Lake, 1870–1940 m) |
| VI. Aquatic vegetation (vegetation of the lakes) | (I) Community of emergent plants | | a) ass. *Phragmites australis* |
| | (II) Community of floating plants | | b) ass. *Potamogeton tepperi* |
| | (III) Community of submerged plants | | a) ass. *Ottelia acuminata* var. *yunnanensis*<br>b) ass. *Chara* spp. |

In the stone forest area, a semi-humid, evergreen, broad-leaved forest, which has been strongly disturbed by local people, is a traditional vegetation type (*Jin* and *Peng*, 1998). It is also a typical vegetation type in the middle area of the Yunnan plateau. The dominant species in this kind of vegetation are *Cyclobalanopsis glaucoides, Olea yunnanensis, Pistacia weinmannifolia, Pistacia chinensis, Sapindus delavayi, Albizzia mollis*, and *Neocinnamomum delavayi*. In addition, savanna vegetation is another important type of vegetation. Because of strong human interference and very tough physical environment, that is arid and features much gravel and poor soil, this kind of vegetation is a relatively stable vegetation type. It is difficult for it to change into a forest. The dominant species of this vegetation type include *Myrsine africana, Sophora velutina, Sophora davidii, Delavaya yunnanensis, Diospyros mollifolia, Sarcococca ruscifolia, Toxicodendron delavayi, Indigofera cinerascens* and others. These are typical species of shrubs on the limestone-mountain. They all grow on limestone and have xerophilization characteristics, with small leaves, hairiness, many thorns, thick sap, and a peculiar smell. The community takes this shape in the process of adapting to the arid, fragile habitat.

According to the field survey from the stone forest area (*Jin* and *Peng*, 1998) and classification system Vegetation of Yunnan (*Wu* and *Zhu*, 1987), there are 6 vegetation types, 8 sub-vegetation types, 9 formations, and 14 associations (Table 1).

### 7.1.2  *Shared floristic elements of the tropical and temperate zones*

In the floristic zones of China the stone forest belongs to the Yunnan plateau subregion, the East Asiatic kingdom, China-Himalaya inferior district of forest plant, highlands of Yunnan (*Wu* and *Wu*, 1998). Again, typical vegetation in this area comprises a half-moist, evergreen broad-leaved forest and a *Pinus yunnanensis* forest. The floristic elements include both tropical and temperate species. According to the species composition of the communities, most belong to one of the four plant families (Fagaceae, Theaceae, Lauraceae and Magnoliaceae). The representative species are *Cyclobalanopsis, Lithocarpus, Castanopsis, Schima, Ternstroemia, Machilus, Cinnamomum, Michelia*. Other species belong to the families of Rosaceae, Pinaceae, Cupressaceae, Corylaceae, Ericaceae and Rhamnaceae. The representative species are *Pyrus, Photinia, Pinus, Cupressus, Carpinus, Rhododendron, Pieris, Vaccinium*, and *Rhamnus*. In addition, some species are typical tropical species and can also be found in this area, e.g. *Pistacia, Toxicodendron, Celtis, Zanthoxylum, Pittosporum, Platycarya, Olea*. The Paleotropic kingdom and the East Asiatic kingdom wonderfully overlap in the plateau district of the middle regions of Yunnan Province (*Wu* and *Zhu*, 1987).

### 7.1.3  *Endemic species of the Yunnan plateau*

As mentioned above, the majority of the species belong to the China-Himalaya zone in East Asia, and some belong to the tropical and temperate zones. However, in this area the endemic species are very rich (*Wu* and *Zhu*, 1987), such as *Pinus yunnanensis, Cyclobalanopsis glaucoides, Lithocarpus dealbatus, Castanopsis orthacantha, C. delavayi, Cinnamomum glanduliferum, Machilus longipedicellata, M. yunnanensis, Celtis yunnanensis, Olea yunnanensis, Cupressus duclouxiana, Sapindus delavayi, Carpinus monbeigiana, Corylus yunnanensis, Keteleeria evelyniana*, etc. Moreover, *Pinus yunnanensis* is one of the important endemic species of southwest China. It is a common and very important species in Yunnan Province. The *Pinus yunnanensis* forest is one of the big-

gest forests in Yunnan. It is also one of the significant forests in the stone forest area. In general, the species composition of the vegetation in the stone forest is similar to the vegetation composition of the whole central Yunnan plateau; some deciduous trees also form specific elements of the local vegetation, for instance *Albizzia mollis*, *Quercus dentata* var. *oxyloba*, etc.

## 7.2   THE DOMINANT PLANT COMMUNITIES IN THE STONE FOREST

As noted above, the vegetation in the stone forest belongs to the half-moist, evergreen broad-leaved forest and *Pinus yunnanensis* forest zones, according to the Yunnan vegetation classification system. In general, the ecosystem in this area can be divided into terrestrial and aquatic ecosystems. The terrestrial ecosystem can be divided into the following subsystems: community of an evergreen broad-leaved forest on the limestone (the forest of the *Cyclobalanopsis glaucoides* formation*), Pinus yunnanensis* formation, *Pinus armandii* formation, *Cupressus duclouxiana* formation, *Juniperus formosana* formation, a type of rare-tree bush grass, a sub-type of bush grass of limestone, meadow, etc. The aquatic ecosystem consists of Changhu and Yuehu lakes' ecosystems. Because the ground substance is water and bottom-mud sediment with the special habitat vegetation, ecological series are formed by hygrophytes, emergent plants, floating plants, submerged plants, etc.

### 7.2.1   *Cyclobalanopsis glaucoides forest formation*

This community occurs in the northwest of Changhu Lake and around Yuehu Lake. The altitude ranges from 1900 to 1960 m. The area is flat; limestone, stone teeth and broken stone are major elements of its landscape. The red lime soil can be found in rock cracks. In general, stone dominates in most parts. Only in the flat land there is more soil than stone on the ground. The plant community consists of the evergreen broad-leaved forest and the young forest generated by logging. The crown of the evergreen arbour forms the shape of a globe or hemisphere. Their branches and leaves are abundant. Normally, in this community which is 5–8 m high and its coverage about 85–95 %, the broad-leaved trees always mix with some deciduous trees. The main community structure consists of the following three layers: arbour, shrubs and herbage. There are about 108 species in the community (*Peng*, 1988).

The arbour layer is 6–9 m high and consists of 15 tree species, 13 of them beeing evergreen broad-leaved species and two of them deciduous broad-leaved species. The dominant species are *Cyclobalanopsis glaucoides*, *Machilus longipedicellata*, *Olea yunnanensis*, *Cinnamomum glanduliferum*, *Schima argentea*, *Quercus dentate*, *Magnolia delavayi*, and others. Their formation belongs to the China-Himalaya zone. These trees have some common characteristics, such as small, thick leaves with leathery qualities and hard, villous surface in the back of a leaf. The trunk is crooked, the bark thick with an inner bark which is obviously adapted to the drought environment. The prevalent colour of the arbour layer is dark green. In winter, the deciduous trees are reddish brown and in early spring they are yellowish-brown. This community has a seasonal appearance (1, 2).

The shrub layer grows very well. It's height is 1–3 m and coverage 60–70 %. In the community there are 44 different species, 32 of which are evergreen and 12 are machaka. The dominant species are *Myrsine africana*, *Zanthoxylum armatum*, *Pistacia wein-*

1 Semi-humid evergreen broad-leaved forest in *Bailong tan* village.

2 Semi-humid evergreen broad-leaved forest in Great stone forest.

*mannifolia, Ligustrum quihoui, Rhamnus leptophyllus, Toxicodendron succedaneum,* etc. Lianas appear at the edge of the forest including *Milletia dielsiana, Smilax mairei, Kadsura induta, Periploca forrestii*, and others.

The herbaceous layer is undeveloped. Its coverage is about 10 %. Few herb species occur below the forest, however, in the forest gap. They grow intensively. There are 49 different species in the layer. Some of them are shade plants, such as *Carex longipes, Ophiopogon bodinieri, Oplismanus compositus, Disporum cantoniense, Polystichum tsus-simense, Agrostis myriantha*, etc. Some of them are sun plants, e.g. *Capillipedium dissititolium, Erianthus rufipilus, Rabdosia eriocalyx, Agrimonia pilosa* var. *nepalensis*, etc.

The spectrum of plant life forms is dominated by Phanerophyte, representing about 42.5 % of the total number of plants. They are followed by two other kinds of plants, Hemicryptophyte and Cryptophyte. In terms of plant life forms in the area, the environment reflects the warm, drier climate characteristic of the subtropical zones. This kind of the community is characteristic of the forest restoration stage. The trees grow very vigorously, the cover density grows and the community's environment is also recovering.

### 7.2.2   *Pinus yunnanensis forest formation*

Most of the *Pinus yunnanensis* forests in this area are artificial and were planted by local people. The area covered by natural forest is small. The species in the young forest differ from those in the middle aged forest. A large old forest can only be found around Changhu Lake and is a historical representative of such forests. It is the best natural *Pinus yunnanensis* forest in the stone forest area (*Ou*, 1988).

This kind of a forest is distributed on the gentle slope of limestone around Changhu Lake. The altitude ranges from 1880 to 1890 m. Some limestone can be found lumped on the ground reaching 0.5–1 m in the height. Red lime soil always mixed with small stones can also be found in the area. The height of the community is about 20 m, its coverage 85–95 %. The tree's canopy looks like an umbrella, which is a typical morphological feature of a pine forest. The community contains 74 plant species. Its structure is very simple and can be divided into three layers: the top layer is the arbour layer, the second is the weak bush layer and the lowest is the very well developed herbaceous layer (3).

The coverage of the arbour layer is 70 % and consists of *Pinus yunnanensis*. The breast height diameter (DBH) values of these pine trees range from 20 to 25 cm. The maximum DBH is 50 cm. Trees of medium age are 10–15 m high and their DBH is 12–14 cm. Their tops are spread out and branch forks hang down, most establishing are solid and sumptuous. The base of the stem is thick and distorted, although they look graceful. The bark is dun.

The bush layer is 50–150 cm high, its coverage 15–20 %. Species diversity of this layer is very poor. Except for the young *Pinus yunnanensis*, seedlings and saplings blend with the evergreen broad-leaved trees here, such as the following: *Cyclobalanopsis glaucoides, Lithocarpus, Pistacia weinmannifolia, Quercus dentata* var. *oxyloba, Olea yunnanensis*, and so on. This indicates that the protogenesis vegetation of this area is an evergreen broad-leaved and mingled forest. *Pinus yunnanensis* grows after the protogenic vegetation has been destroyed. The greatest percentage and coverage degree of the plants belong to *Myrsine africana, Pyrus pashia, Cornus oblonga, Cotoneaster microphyllus, Berberis pruinosa*, and *Pistacia weinmannifolia*.

The height of the herbaceous layer is 0.3–1.0 m and its coverage 50–70 %. Herbage

**3** *Pinus yunnanensis* forest in Great Stone Forest.

grows vigorously and the diversity of grass is quite rich. The standing grain grass is obviously the dominant species. There are nearly 40 kinds of plant species in the area which represent about 54.5 % of the total number of plant species for this community. The following are the plants that are the most numerous and feature the highest coverage degree: *Eulalia pallens*, *Eremopogon delavayi*, *Themeda triandra* var. *japonica*, *Arundinella setosa*, *Calamagrostis parvifiorum*, *Arthraxon hispidus*, etc.

The life-form spectrum mainly belongs to Hemicryptophyte and Phanerophyte. Both of them account for 38 % of the total number of species. Among the Phanerophyte, the short Phanerophyte, accounted for more than 2/3, which shows the climatic conditions of warm coniferous trees of the subtropical zone of Yunnan, and the second-class natural disposition characteristic of the *Pinus yunnanensis* forests formation. The limestone area with so many tall trees has not only increased the biological versatility of the vegetation in the area of the stone forest but has also added to the beautiful garden scenery of the stone mountains.

### 7.2.3   *Pinus armandii forest formation*

The area of the *Pinus armandii* forest is not very big in the stone forest region. Most of the trees were planted by local people. One reason is that this area is a typical karst stone landscape. Another reason is that the arid soil is not suitable for growing of the *Pinus armandii*. But this formation appears in the soil mountain areas and half stone-half soil mountain areas near the stone mountain. A typical one can be found around the Ziyun Hole near the stone forest (*Jin* and *Peng*, 1998).

This community is distributed in a small half stone-half soil area. It is surrounded by stone hills in the limestone mountain region. Its altitude is 1750–1790 m, with a slope of about 20°. The height of the limestone above the surface is 0.5–1.0 m and its floor-space

probably 10–30 %. There are many stones but little soil which is the original mountain red earth developed from the limestone.

The height of the community is about 7–9 m and the coverage 80–95 %. The even crown layer is composed of conical crowns of the trees. It appears light blue-green and looks pretty and graceful. The vertical structure of the community consists of 61 plant species in three layers: the arborous tier, bush tier, and grass family tier. However, the arborous layer has only two kinds; it is obviously the only excellent forest.

The height of the arbour layer is the same as that of the community and its coverage is 70–80 %. *Pinus armandii* is the dominant species; however, *Pinus yunnanensis* can sometimes also be found. The trees are 20–25 years old and their DBH is 8–12 cm. The trunk is perfectly straight and round, and the branch is neat and grows fine. The density of the forest is medium; there are nearly 2700 trees in each hectare. The bark is smooth and lichen adapted to the living at the base of the trunk.

The height of the bush layer is 0.5–0.6 m, and the coverage 10–20 %. There are arbours in this layer, such as *Castanopsis, Quercus franchetii, Albizzia mollis, Engelhardtia colebrookeana, Pistacia weinmannifolia*, etc. They are plants growing in the stone mountain or on arid land, especially *Quercus francheti. Myrsine africana* has the same characteristic among the bush. Besides, there are *Rubus obcordatus, Zanthoxylum armatum, Vaccinium fragile, Lyonia ovalifolia*, etc. Among the herbaceous half-bush the *Lespedeza juncea* var. *sericea* and *Elsholtzia rugulosa* are common, too. Only in the wooden rattan the crawling low *Ficus tikoua* could be seen on the ground.

The height of the herbaceous layer is 0.1–0.35 m, and the coverage is 20–40 %. It is composed of many kinds of species; however, it is difficult to find the dominant ones. Both Xerophytes and Mesophytes are present, e.g. *Gerbera delavayi, Hedyotis uncinella, Ligusticum daucoides, Cassia mimosoides, Lysimachia christinae*, etc. There are a few anti-sunshine and wet liking plants, for example *Aiasliaea bonatii, Athyrium dissitifolium*, and others.

The *Pinus armandii* formation is the kind of community that grows up rapidly, and the one that gives esthetic appearance to a forest. As long as there are suitable soil conditions present, they can all be fostered artificially that can also increase the variety of the vegetation in the scenic spot.

### 7.2.4 *Cupressus duclouxiana forest formation*

*Cupressus duclouxiana* (also called the towering cypress) is the typical community in the limestone mountain region of southwest China and the area of dry-warm river valleys. It can tolerate high temperatures and drought stress and adapt to different kinds of environment. At present, this kind of a tree is planted on the stone and soil hills. Normally, the natural *Cupressus duclouxiana* forest is a low density forest. However, a *Cupressus duclouxiana* artificial forest can be formed by close planting and can occur in a small range. A typical example can be found in the Stone-Peak Temple near the stone forest (*Ou*, 1988).

This community is distributed on the low mound of limestone with elevation of 1790–1870 m and the slope of 10–35°. The surface consists of many uncovered limestones, and their size and height are different, too. They cover an area of 30–50 %. They cannot be distributed evenly, and stone teeth account for half. The habitat is the half-stone, half-soil one and the soil is red lime-earth. The community is dark green, towering tree-tops are shaped by the numerous *Cupressus duclouxiana* trees; the forest ap-

pears quite graceful. The height of the community is 10 m, close to the ridge it is lower and amounts to 5–7 m. Its coverage is 70–80 %, in intensive locations 95 %. The main big covered-degree layers are the arbour and the herbaceous layers. The vertical structure of this community is obviously divided into three layers of which the arbour layer is the main one.

The arbour layer is of the same height as the community. Its covered-degree is about 70 %. The dominant species is *Cupressus duclouxiana* while *Pinus yunnanensis* and *Pinus armandii* are seen occasionally. There are 33–41 *Cupressus duclouxiana* trees per 100 m². Their DBH is 5–13 cm. The trunk is very straight and the growth luxuriant.

The height of the bush layer is 1–1.2 m and its coverage 5–15 %, at the specific locations reaching 40 %. There are a lot of species, but of few quantities. Some woody plants also occur in this layer, such as *Cyclobalanopsis glaucoides, Pistacia weinmannifolia, Olea yunnanensis, Pistacia chinensis, Carpinus monbeigiana, Neocinnamomum delavayi*, etc. *Myrsine africana* and *indigofera cinerascens* are the most common types of the bush; however, their quantity is not large. The other kinds can tolerate drought stress, which leads to small leaves, more thorns and villous surfaces.

The herbaceous layer is 0.1–0.4 m high with coverage of 45–70 %. Plants are more frequent in the forest gap and at the forest edge. There are many kinds that are mixed and no dominant species. Drought-resistant grass is relatively common and includes species, such as *Arthraxon hispidus, Heteropogon contortus, Schizachyrium delavayi, Arundinella setosa*, etc. Plants adapted to dark and moist are hardly seen. However, on the rock surface the specific Epiphyte can be seen, such as *Asplenium varians*.

Under certain soil conditions the *Cupressus duclouxiana* forest can grow on vast limestone hills. This type of vegetation can rapidly change the appearance of the bare stone and arid mountains. The ecological appearance is more beautiful than at the *Pinus armandii* formation.

### 7.2.5  *Juniperus formosana forest formation*

In the scenic spot of the stone forest the *Juniperus formosana* community has already grown into a forest which is only distributed around Yuehu Lake. The area is very small being protected as a scenic forest. It is the best known *Juniperus formosana* community that has already grown into a forest in the Kunming area. It is also a kind of an artificial forest. The community is distributed in the low limestone hills at 1890–1950 m a.s.l. The height of the community is 7–15 m and its coverage 50–75 %. The appearance of the crown-canopy is dark green. Under the forest the stone peaks interlock and stand in great numbers, the arbour tree coverage alternates with stone outcrops, so the forest coverage rate is low. The structure can be divided into three layers: the arbour, bush and herbaceous layer. The arbour layer is the major one. The number of plant species is 94; among them the arbour layer features 6, the bush layer 23 and the herbaceous layer 65 kinds. The habitat is arid but the species diversity is rich (*Ou*, 1988).

The height of the arbour layer is different and the coverage is 40–60 %. *Juniperus formosana* is the dominant species and its breast-height diameter 15–20 cm. It looks graceful and straight, but individual trees cannot be distributed evenly. In the forest gap, despite stone teeth, there is enough sunshine for the trees. With the poor growing situation, this layer grows together with a small amount of *Pinus armandii, Pinus yunnanensis* and *Cyclobalanopsis glaucoides*.

The height of the bush layer is 0.4–0.8 m with the coverage of 25–40 %. They cannot

be distributed evenly. Common is *Cotoneaster microphyllus* being able to bear drought. In addition, there are the bush species with small leaves and much stingy, such as *Pyracantha fortuneana*, *Berberis wilsonae*, *Osteomeles schwerinae*, *Elsholtzia rugulosa*, *Myrsine africana*. The wooden rattan is as follows: *Ficus tikoua*, *Berchemia floribunda*, etc.

The height of the herbaceous layer is less than 0.4 m and its coverage about 30 %. They grow in bushes but they cannot be distributed evenly. They are common in vacant forest gaps. The style varies, the number of individual items is not large. The layer of this kind which likes sunshine and can stand aridity, preponderates together with grass. It includes species, such as *Heteropogon contortus*, *Bothriochloa intermedia*, *Arthraxon hispidus*, *Arundinella setosa*, etc.

In the life-form spectrum of plants most of these species are Hemicryptophyte, some of them are Phanerophyte and Therophyte. Very few species are Chamaephyte and lianas.

### 7.2.6    *Savanna community*

Savanna is widely distributed in the stone forest area. The representatives of this community whose elevation ranges from 1760 to 1840 m a.s.l. are *Heteropogon contortus*, *Schizachyrium delavayi* and *Pinus yunnanensis* near the Ziyun Hole (*Peng*, 1988).

The community is located in the limestone mountain area where, historically, the evergreen forest appeared first. Because of intensive human activity there is no forest here yet. The hillside is gentle, with a slope of 10–20°. Facing southwest, however, the uncovered parts of the ground limestone are different in height, 0.6–1.2 m on average. It accounts for more than 50 % of the ground. Rock is abundant and soil scarce. There is red lime-soil between the stones, deep and loose. The top soil has been occupied by the grass layer, and plants grow in the rock fissures.

The grass layer is the main layer of the community. Medium-sized grasses create its main physiognomy while species occur on the stones or among them. Above the grass is the shrub layer which makes the community look disorderly. In total, there are 74 kinds of higher plants, including ferns.

The height of the herbaceous layer is 0.3–0.6 m and its coverage 40–60 %. This layer is mainly composed of heliophile grasses. In total there are 12 species, with *Heteropogon contortus*, *Schizachyrium delavayi* and *Themeda triandra* var. *japonica* being the most common. *Heteropogon contortus* is the dominant species of this layer and is also ubiquitous in the area. It can be seen as an indicator of an arid or semi-arid habitat. *Schizachyrium delavayi* is the representative species of the Yunnan middle plateau. In addition, *Themeda triandra* var. *japonica* and *Arundinella setosa* are also common in the area.

The highest individual plants in the shrub and tree layer can reach 3–5 m, and the coverage 10–25 %. Individual plants in this layer are randomly distributed. *Pinus yunnanensis* is the dominant species, and *Pistacia weinmannifolia*, *Pinus armandii*, *Pistacia chinensis* and *Broussonetia papyrifolia* are the most common tree species. *Toxicodendron succedaneum*, *Pyrus pashia*, *Camellia pitardii* var. *yunnanensis*, *Coriaria nepalensis*, *Campylotropis polyantha*, *Incligofera mairei*, *Sophora davidii*, *Spiraea martinii*, *Inula cappa* and *Cotoneaster microphyllus* are the most common species in this layer (4).

The current existence of this ecosystem indicates that the *Pinus yunnanensis* forest, *Cupressus duclouxiana* and *Juniperus formosana* can be used in the practice of reforestation.

**4**   Savanna community.

### 7.2.7   *Cynodon dactylon meadow formation*

*Cynodon dactylon* meadow formation is a warm grass meadow and considered a kind of intrazonal vegetation. There is only one association type of this formation in the area of the stone forest, namely, ass. *Phragmites australis* which is distributed on the banks of Yuehu Lake (*Ou*, 1988).

This community occurs on the alluvial coast of the old lake banks at altitudes between 1870 m and 1940 m a.s.l. surrounded by a shrub-forest or a forest. There would have been meadows around the lake if the large pieces of limestone had not occupied the lake banks. Under present conditions the meadow can only be found on alluvial terrain or soil caused by washing the slopes. In the rainy season floods may make this kind of community wet thus the underground water level may suppress their development. The ground surface is very smooth, mainly composed of sandy, alluvial soil.

The herb layer is the only layer of this community. It is low, with the height of only 0.05–0.15 m. Shrub species occur occasionally, with some individual plants reaching 0.2–0.5 m in height; however, they cannot compose a unique layer. There are 64 kinds of plant species, including 58 herbaceous and 6 shrub species. The community's total coverage is 45–90 %, mainly contributed by herbaceous species. The other 10–55 % of the local area is covered by exposed alluvial and lime rocks.

*Cynodon dactylon* is the dominant species of the herb layer; it used to be called the iron line grass. Another common species is *Centella asiatica* which is a creeping mesophyte plant found in shady areas with many individual plants that live in patches. *Paspalum distichum, Dichrocephala integrifolia, Taraxacum mongolicum, Kummerowia striata, Medicago lupulina* and *Oxalis corniculata* are drought-endurance species in the area, and there are some other species which are seldom found here, such as *Arthraxon*

*hispidus, Arundinella setosa* and *Micromeria biflora.* Colonial shrub species account for very little within the total coverage.

The existence and surroudings of this ecosystem indicate that this community is restricted by the level of the lake and underground water. Once this restriction is diminished, the community may develop towards a tree-grass coexistence ecosystem.

### 7.2.8  *Myrsine africana formation*

The limestone *Myrsine africana* shrub is common in the stone forest area. The following will consider *Myrsine africana* and *Sophora velutina* as representatives of the area (*Jin* and *Peng*, 1998).

The community is found at an elevation of 1790–1820 m, mainly on the gentle slope of the limestone-mountain; the slope grade is 10–15°. On the ground there are some irregular uncovered limestone-lumps whose general height is 1.0–2.5 m, the highest reach 3–4 m. The stony outcrops occupy more than 50 % of the area with little soil between them. The soil there is relatively thick and belongs to the rendzina type. This kind of habitat is comparatively arid.

The physiognomy of the community is light green, with disordered shrub-forest clumped together in some areas while others occur scattered and divided by large rocks on the ground. The height of this community is between 0.6 and 1.5 m, with total coverage about 60 %; in sparse places it is only 40 %. It is hard to divide the height structure clearly into two layers because shrub and herb species are almost of the same height and always coexist.

Woody plants are the most common species in this community. Their height is less than 1.5 m. The shrub layer is composed of such plants and includes 28 species; 6 of them are tree species, 4 are small tree species and 3 shrub species. This layer in total makes up 40 % coverage of this community. *Myrsine africana* and *Sophora velutina* are the indicative species. A xeromorphic shape typical of shrub species is a characteristic feature of this kind of habitat. The small-leaved shrub species, such as *Myrsine africana, Sophora velutina, Sophora davidii, Campylotropis polyantha*, etc.; the thorny species, such as *Sophora davidii, Rhamnus leptophyllus*, and *Prinsepia utilis*; the species with cilium like *Rubus parvifolius, Elsholtzia rugulosa, Indigofera cinerascens*, etc.; the small trees regenerated after big trees have been cut down, such as *Pistacia weinmannifolia, Ehretia corglifolia, Neocinnamomum delavayi, Albizzia mollis, Ilex micrococca*, etc. – they all suggest that the community may develop into a forest after long-term protection. The species of the small arbour consist of the following: *Delavaya yunnanensis, Diospyros mollifolia, Rhus chinensis, Toxicodendron delavayi*, etc. These are all adapted to the semi-arid habitat. *Delavaya yunnanensis* and *Diospyros mollifolia* are mainly found in the areas of the dry-warm river valleys. In the limestone-mountain region, *Pterolobium punctatum* can develop into big wooden-rattan attached to the rock outcrops; red infructescence of this species looks very aesthetic.

The coverage of the herb layer is 20–50 %, and the species height varies a lot. On average, the layer is 0.3–0.5 m high while some inflorescences can reach over 1 m. The total number of species in this layer is 64. Most of them occur in an open area, indicating that they can withstand drought. They include *Pteridium revolutum, Arthraxon hispidus, Heteropogon contortus, Schizachyrium delavayi, Themeda triandra* var. *japonica*, etc. Among them, only *Pteridium revolutum* can be found everywhere in the community; the rest occur randomly and occupy few areas. In general, all these species share the

same ecological characteristics such as small leaves, hairiness, thick sap, noxious smell and drought resistance.

If this kind of the community is well protected and developed, it may lead to a semi-moist evergreen broad-leaved forest with the indicator species *Cyclobalanopsis glaucoides* and *Pistacia weinmannifolia*. Because the habitat is arid, the succession is relatively slow, and if accompanied by frequent cutting or burning, the community may degenerate and turn into the tree-grass coexistence type.

### 7.2.9   *Millettia velutina formation*

This community is found mainly in the Naigu shilin and is seldom seen in other regions. However, it is still representative of the area because the dominant species of this formation are not *Myrsine africana* and *Sophora velutina* but *Millettia velutina*. It grows in the form of shrub in the limestone-mountain region and shares the same environment with other shrub species, such as *Spiraea martini* and *Zanthoxylum armatum*. These species are suitable for growing in the limestone habitat. There are also other species in the community, e.g. bush, arbour, twining, herbaceous and others. They are all adapted to the stone-mountain habitat. The areas where this community is distributed lie in the elevation ranges between 1820 and 1890 m and they all belong to the limestone mountain-regions. The slope varies a lot, from flat areas under the cliffs to rough slopes, with grades below 20°. This community is mostly south-facing. The ground shares the same characteristics with the community above: various stones are located on the surface, and plants can only be found in the soil between the stones. The physiognomy shows light green crowns between gray limestone, and this changes with different ranges of the mountain and topography. The height of the community is 1.0–1.5 m and its total coverage about 50 %. The density is uneven: in sparse places it can reach 35 % and in dense places up to 65 %. It is difficult to classify the height structure of the layers because the herb species have almost the same height as the shrub species.

The height of the shrub layer is the same as that of the community. Its coverage is 30–45 %. Except for the rock covered surface, *Millettia velutina* is regarded as the dominant species in the community. The other common species is *Spiraea martini*. Both are hairy and drought tolerant and they are the indicator species of the community. There are 35 kinds of species in the layer, among which the number of shrub species is 22 and of the tree species 6 which include some small trees and tree sprouts after the main stem has been cut down (*Jin* and *Peng*, 1998). Shrub species contribute most to the composition of this community, and all the woody plants share the same characteristics of the drought tolerant plants. They are hairy and have thorns, small leaves, thick sap, bad smell, and so on. This phenomenon is common for the plants on the stone mountain, especially for those of the shrub species.

The height of the herb layer is 0.8–1.0 m, and the coverage 20–40 %. There are 52 herb species developing well. The most common is *Cymbopogon distans*, a resource plant that can grow in the limestone mountain areas or hot-dry river valleys. Though the number of other herb plants is large, their quantity and coverage is small. Most species are drought tolerant. It is rare to see herb plants in a shady habitat. Most of the herb plants belong to the Poaceae and Compositae families.

This kind of the community is a special type in the shrub forests of the limestone areas; it should be protected in order to keep the diversity of the stone-mountain vegetation type in the scenic spot of the stone forest.

### 7.2.10 *Aquatic vegetation*

The aquatic vegetation in the area of the stone forest grows in many lakes, such as Yuehu, Changhu and Yuanhu lakes. Among them, the vegetation in Changhu Lake is more representative than in the others. It can be divided into five types that reach from the lake centre to the riparian area (*Li*, 1988).

The community of *Pasparum distichum* and *Cynodon dactylon* belongs to the Hygrophyte type. The plants in this community are distributed on the beach in the south part of the lake. The coverage can reach 80 %, while the height of plants varies a lot. The compositions include aquatic and terrestrial plant species, 20 in total. The dominant species are *Pasparum distichum, Cynodon dactylon, Linmophila sessilifiora,* and others. *Linmophila sessilifiora* is a common aquatic plant found in the temperate and tropical zones in Asia.

The community of *Phragmites australis* is a community type emergent plant, found by the lake beach south of Changhu Lake at a depth of 0.5 m. Its total coverage is about 70 %, in some areas only 20–30 %. The dominant species is *Phragmites australis* whose height is 1–1.5 m. There is also *Salix* sp., growing in the water. Together with the aquatic species, it makes the upper strata of the community. In the lower strata there are many other plants, for instance *Xanthium sibiricum, Plantago majo*r and others.

The community of *Potamogeton tepperi* is a floating-leaf plant type of the community, scattered in the southern part of the phytal zone and in the northeast lake bay. Its coverage can reach 100 %.

The community of *Ottelia acuminata* var. *yunnanensis* is located around the circle of Changhu Lake. It is a submerged plant community distributed in the lake bay near the lake inlet or outlet, and in the water areas near the island in the north. The coverage of this community is 90 %. Its dominant species is *Ottelia acuminata* var. *yunnanensis*. The leaves are submerged, while the flowers bloom on the surface. It always lives together and looks like a clump. Other species in this community include *Potamogeton tepperi, Myriophyllum spicatum, Hydrilla verticillata, Potamogeton malainus, Chara* spp. and *Schoenoplectus* spp.

*Chara* spp is a submerged plant community distributed north of the island in Changhu Lake. The depth of the water is 2.0–2.5 m. The community with the height 30–40 cm reaches the coverage of 50–70 %. The common species are *Chara* spp. and *Myriophyllum spicatum.*

The local flora of Changhu Lake includes the following five submerged plant species: *Myriophyllum spicatum, Ottelia acuminata* var. *yunnanensis, Hydrilla verticillata, Potamogeton malainus, Najas graminea,* and one kind of floating-leaf plants, *Potamogeton tepperi.* In addition, *Linmophila sessilifiora* exists in the form of a Hygrophyte around Changhu Lake. In total, seven lake-plants are typical of the Yunnan-Guizhou plateaus. They are of a relatively poor composition; however, this represents the characteristics of the local flora.

# THE EFFECT OF SOIL EROSION ON EVOLUTION OF THE LUNAN STONE FOREST – AN EVIDENCE FROM THE STALAGMITE AND FIELD OBSERVATION

BINGGUI CAI, HONG LIU, GUOAN WANG

The Lunan stone forests landscape attracts millions of visitors each year because of its exceptional appeal. Pinnacle karst of this area is characterized by a much greater morphological variety and evolutionary complexity. Previous studies from the last two decades have demonstrated that pinnacles of the Lunan stone forest were mainly shaped through subsoil corrosion, together with light modifications of the upper parts by direct rainwater corrosion (*Yu et al.*, 1985; *Song*, 1986; *Zhang*, 1984; 1997; *Song* and *Li*, 1997; *Ford et al.*, 1996; *Lin*, 1997b). Ford also mentioned that the formation of the stone forest might be at least partly related to deforestation and soil erosion. The modern denudation rate of carbonate rock in the Lunan stone forest karsts has been well studied (*Liu* and *Wu*, 1998; *Tian et al.*, 2003). However, a few studies had addressed an important impact of soil erosion on evolution of this forest. In this study, a stalagmite record of the Holocene flood history and *in situ* observed soil erosion rates in this area were used to illustrate an evolution mode of the Lunan stone forest landscape.

## 8.1 METHODS AND RESULTS

### 8.1.1 The *study site*

The Lunan stone forest (103°10'E–103°40'E, 24°30'N–25°03'N; 1700–1950 m a.s.l.) is located in Shilin County, around 87 km southeast of Kunming in Yunnan. It has a total area of 350 km² with magnificent and spectacular landform, exhibiting a complicated evolution, and is now a world natural heritage site. This area is located in the subtropical plateau climate zone and is strongly affected by the Asian monsoon system. Most of rainfall (70–80 %) occurs during the rainy season (June–October). The mean annual temperature and precipitation recorded by the nearby meteorological station are 16.3 °C and 936.5 mm, respectively.

### 8.1.2 *Description of the stalagmite and ICP-MS $^{230}$Th dating*

The stalagmite NG02 was collected in a shallow pocket cave in the vicinity of the Naigu stone forest. This cave developed at a depth of 5–10 m below the surface; it is about 50 m long and 2–6 m wide. Overlying the cave, vegetation comprises secondary successional shrubs, grasses and a few pine trees. Some stone teeth with heights of 3–5 m were also found above the cave. This type of a cave is common in the Lunan stone forest area. Their development was always restricted to the regional major fracture and it has a good hydrodynamic relationship with surface water (*Liu* and *Zhou*, 2003). As a result, a lot of

mud was carried by floods through some big fissures which made the cave muddy. Many remnant marks of flood levels can be distinguished on the wall at different heights in the cave. The stalagmite NG02 grew at the bottom of the wall. Its base was found 30 cm higher than the flood level when it was sampled after a heavy rainstorm while its top was much lower than some remnant marks of the flood levels on the wall.

The short stalagmite NG02 reaches 9 cm in height and 14–18 cm in diameter. The specimen was halved along the growth axis and one of the halves was further cut into a 3 cm thick plate (1). The sample consists of grey to yellow microcrystalline calcite and exhibits well-defined growth lamina interrupted by five clay layers. Most of the laminations are opaque, and some are quite dark, owing to relatively high concentrations of organic matter. No evidence for recrystallization or dissolution was observed in these sections, as the calcite crystals exhibit a subtle palisade structure and lack solution hollows. The thickness of the lentoid clay layers, named CS-1, CS-2, CS-3, CS-4 and CS-5 from top to base, varied from 1–5 mm. The colour and texture of the clay looked similar to those of detrital sediment on the cave floor and to the soil overlying the cave.

1 Sections of the stalagmite NG02, sampled from the *Naigu* stone forest, a and b indicating two sides of the plate. The red arrow points to the five clay layers (CS-1 to CS-5) while the blue one points to the sub-sample locations drilled for uranium dating.
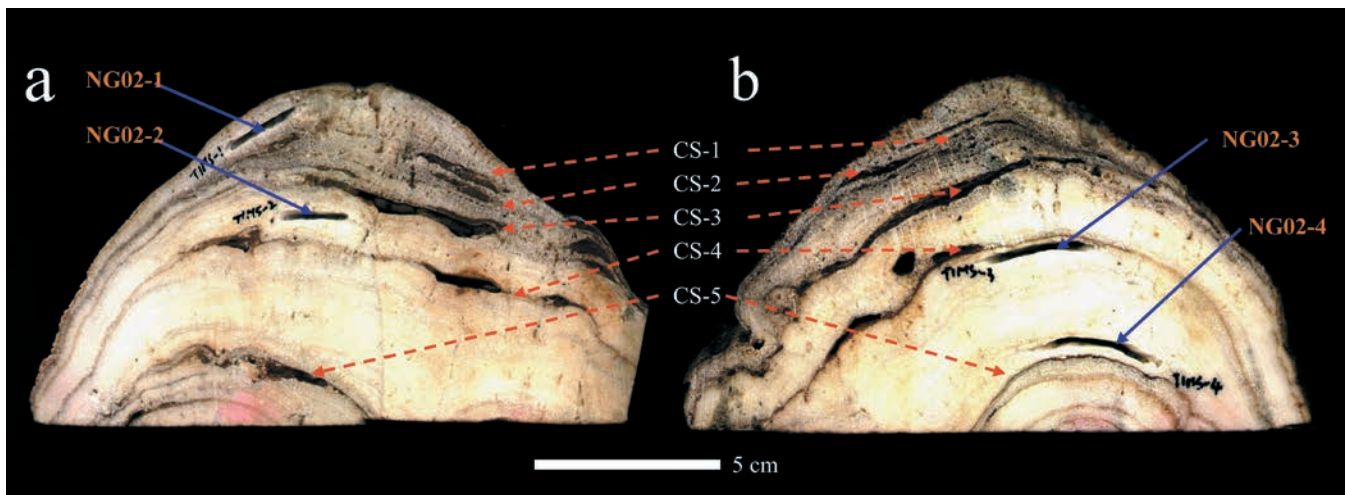


Four powdered samples were drilled for $^{230}$Th dating, using a 0.9 mm carbide dental bur. Samples were drilled along growth bands and weighed between 300 and 500 mg. Isotopic measurements were made on the magnetic sector inductively coupled plasma–mass spectrometer (ICP-MS, Finnigan element) in the Department of Geology and Geophysics, University of Minnesota. The results are shown in Table 1.

**Table 1**
U, Th isotopic composition and $^{230}$Th ages of the stalagmite NG02.

| Sample no. | $^{238}$U (ppb) | $^{232}$Th (ppt) | $^{234}$U* (measured) | $^{230}$Th/$^{238}$U (activity) | $^{230}$Th age (yrs) (uncorrected) | $^{230}$Th age (yrs) (corrected) |
|---|---|---|---|---|---|---|
| NG02-1 | 42.83 ± 0.08 | 12,200 ± 150 | 132.5 ± 5.3 | 0.0735 ± 0.0019 | 7130 ± 200 | −260 ± 3680 |
| NG02-2 | 33.45 ± 0.05 | 12,170 ± 100 | 120.6 ± 5.3 | 0.0797 ± 0.0016 | 8040 ± 170 | −1830 ± 4700 |
| NG02-3 | 19.55 ± 0.03 | 2,553 ± 20 | 113.6 ± 6.3 | 0.0185 ± 0.0015 | 1230 ± 150 | −1640 ± 1720 |
| NG02-4 | 35.78 ± 0.07 | 10,200 ± 80 | 120.9 ± 6.2 | 0.0688 ± 0.0012 | 6910 ± 130 | −750 ± 3700 |

$\lambda_{230} = 9.1577 \times 10^{-6}$ y$^{-1}$, $\lambda_{234} = 2.8263 \times 10^{-6}$ y$^{-1}$, $\lambda_{238} = 1.55125 \times 10^{-10}$ y$^{-1}$.
*$\delta^{234}$U = ([$^{234}$U/$^{238}$U]$_{activity}$ − 1) × 1000.

Corrected $^{230}$Th ages assume the initial $^{230}$Th/$^{232}$Th atomic ratio of $4.4 \pm 2.2 \times 10^{-6}$. Those are the values for material at secular equilibrium, with the crustal $^{232}$Th/$^{238}$U value of 3.8. The errors are arbitrarily assumed to be 50 %.

Unfortunately, the absolute values of all four ages are uncertain, with large errors ($2\sigma$) resulting from significant uncertainty in the initial $^{230}$Th (assume the initial $^{230}$Th/$^{232}$Th atomic ratio of $4.4 \pm 2.2 \times 10^{-6}$), owing to the low uranium and high $^{232}$Th concentration. Therefore, it is impossible to establish the chronology for the stalagmite NG02. We cannot even determine the exact time at which the clay layers were deposited. However, the $^{230}$Th ages do tell us that this stalagmite was formed during the Holocene.

### 8.1.3    *Experimental observation of soil erosion*

Two plots, located 1.5 km south of the Major stone forest, were chosen for experimental observation of soil erosion. One was located in the headstream of the gully and consisted of an escarpment and a gentle slope. The soil on this plot was relatively incompact and was covered by very sparse grass (2.a). The other lay several hundred metres away where grass-land surrounded the base of stone teeth (2.b).

In order to evaluate the soil erosion rate, 10 cm-long steel nails were embedded into soil at different vegetation and micro-topography sites on 22 June 2002. For each embedding the cap of the nail was kept at the same level as the ground surface. Then the lengths of the steel nails which exceeded the ground surface were measured on 2 October 2003 (2.c). The results are listed in Table 2. Here we did not calculate the annual corrosion rate because our experiment was to cover almost two rainy seasons, but only a little more than one hydrological year. The real corrosion rates should thus be a little less than those listed in this table.

| Site 1 – headstream of a gully | | | | Site 2 – base of stone teeth | | | |
|---|---|---|---|---|---|---|---|
| Steel nail no. | Vegetation | Slope | Erosion rate (mm) | Steel nail no. | Vegetation | Slope | Erosion rate (mm) |
| 001 | bareness | 20° | 24 | 101 | bareness | 0° | 5 |
| 002 | bareness | - | - | 102 | grass | 0° | 0 |
| 003 | bareness | 25° | 18 | 103 | bareness | 23° | 8 |
| 004 | bareness | 30° | 30 | 104 | grass | 0° | 1 |
| 005 | bareness | 10° | 19 | 105 | grass | 0° | 1 |
| 006 | grass | 3° | 15 | | | | |
| 021 | bareness | 40° | 20 | | | | |

**Table 2**
Soil erosion rates determined by pre-embedded steel nails.

It was observed that the erosion values ranged from 0 to 30 mm. Those at the headstream plot were much severer than those at the base of the stone teeth. Erosion values on bare ground at the headstream varied from 15 to 30 mm. Some of the steel nails that had been pre-embedded in precipitous bare ground in this plot had washed out, indicating that the headstream had trended back at least 10 cm. Relatively, soil erosion at the base of the stone teeth was much weaker, with values varying from 0 to 8 mm. Different soil erosion rates between different sites should be due to their different vegetation cover and micro-topography. Therefore, it is difficult to get an exact absolute value of the soil erosion rate. However, it is reasonable to deduce that the soil erosion rate in this region is significant on some sites with spare plants under the present climate regime.

**2** Field photos showing the soil erosion observation plots and scallops of stone teeth: a – Plot 1, headstream of the gully; b – Plot 2, base of stone teeth; c – the white arrow points to a pre-embedded steel nail after erosion; d – a series of scallops of stone teeth formed by sub-soil corrosion; e – fresh surface of stone teeth without aerial algae.



## 8.2 DISCUSSION

### 8.2.1 *Interpretation of the clay layers in the stalagmite NG02*

Detrital minerals in the stalagmite may originate from drip water, flood water and/or cave air dust (aeolian deposit). As a result of the thin overlying bedrock of the study cave, the drip water in this cave contains a lot of detrital minerals, and stalagmites in this cave were 'dirty', resulting in uncertain $^{230}$Th ages with large errors. However, the formation of the clay layers (1) in the stalagmite NG02 should not be assigned to the drip water and/or aeolian deposition because of the following evidence: the thick clay layers consisted entirely of loose clay which was similar to those of the flood deposits in the

cave, with a thickness of up to 5 mm. There were sharp interfaces between the soil layers and the adjacent laminated calcite. There was no evidence of any calcitic cementation. Therefore, the formation of the clay layers in the stalagmite could potentially be attributed to the flood events.

The base of the stalagmite was found 30 cm higher than the flood level when it was sampled after a heavy rainstorm while its top was much lower than some remnant marks of the flood levels on the cave wall. The relatively low position of the stalagmite NG02 in the cave allows it to be capable of recording larger flood events. When an intense rainstorm occurred, flood water could carry a lot of mud into the cave and submerged the stalagmite. The mud might be deposited on the top of it after the flood waters finally receded. Then the clay deposit might be clothed by calcite precipitation when the stalagmite accepted the drip water again. Therefore, a series of clay layers in the stalagmite among the gray-yellow calcites precipitated by dripping water might record several high intensity flood events (possibly in centenary frequency).

### 8.2.2 *Evidence for the formation of the Lunan stone forest*

With its various marvelous pinnacle karst scenes, the Lunan stone forest attracts professional karst scientists from all over the world and brings millions of visitors to the wonderland which displays great morphological variety both as individual features and as groupings that occur. Such richness of forms and their distribution can be attributed to the combination of the varied limestone and dolomite lithology and to the complex evolutional history (*Ford et al.*, 1996). The stone forest of Lunan developed in pure, massive carbonate rocks, with gentle dips in the beds, from 2° to 8°, in tropical humid climate conditions when this region was at low altitude of 20°N (*Zhang*, 1984; 1997; *Song* and *Li*, 1997; *Lin*, 1997b). The morphological features of the most individual columns of the Lunan stone forest can be divided into two parts: the upper pinnacle crests and vertical solution troughs with sharp karren ridges, flutes, gullies and pits on the surface, and the lower smooth column with several horizontal scallops, habitacle, and a hole (*Liang*, 2000). The upper part was formed by erosive water chemically and mechanically eroding the carbonate rocks. Therefore, the origin of the Lunan stone forest can initially be explained in terms of rainwater dissolution (*Song* and *Li*, 1997). In the 1980s, many karst geologists noticed the effect of subsoil weathering on the development of the Lunan stone forest. They stated that the stone forest might have been developed under the soil and then modified by rainwater dissolution after exposure (*Song* and *Li*, 1997).

An experiment on the modern denudation rate of carbonate rock in the Lunan stone forest karst showed that the subsoil corrosion rate, uneven along the soil profile, was three times as great as the sub-aerial corrosion rate (*Liu* and *Wu*, 1998). The modern active horizontal habitacles of stone teeth and stone forest were observed to be distributed at a depth of 40 cm below the soil surface, owing to the soil $CO_2$ concentration and soil water content distribution pattern along the soil profile (*Liang*, 2000). This indicates that there should be a preponderant part at a given depth (e.g. 40 cm) under the soil surface where subsoil weathering is the greatest. The existence of the preponderant part of subsoil corrosion makes it reasonable to deduce that the stone teeth and/or stone forest possibly might be cut through, even resulting in collapse, if the soil is kept stable for long enough time periods. Therefore, the effect of soil erosion on the stone forest development should also be emphasized. When significant soil erosion occurs, the preponderant part of the subsoil corrosion might move downward, and the horizontal scallop which previ-

*The effect of
soil erosion on
evolution of the
Lunan stone forest
– an evidence from
the stalagmite and
field observation*

ously formed might move upward, and finally be explored (3). This exploration process might keep the isolated column (pillar) from 'overcorrosion'. Conversely, if the soil erosion rate is much greater than the carbonate rock corrosion rate, the soil might become thinner, and carbonate rock corrosion might slow down. Accordingly, there should be equilibrium between soil erosion and rock corrosion.

Flood events recorded by the stalagmite NG02 compared with *in situ* observed values of the soil erosion rate imply that a rapid soil erosion process in the Lunan stone forest karst should be expected. As we observed, soil erosion on the bare ground surface was quite significant during a normal year. Soil erosion would be much more intense during a period of rainy years, as indicated by the stalagmite NG02. In this case, the soil erosion rate should be much greater than the carbonate rock corrosion rate; consequently, the soil surface moved downward while the stone column moved upward, relatively speaking. This might lead the preponderant part of subsoil corrosion to move downward and begin to form a new horizontal scallop below the previous one if the soil went into another stable period (3). Based on the equilibrium between soil erosion and rock corrosion, periodically occurring soil stable and erosion cycles might form a series of horizontal flutes at different depths of the stone column. A broad distribution of a series of horizontal scallops on the surface of isolated stone columns (pillars) of the stone forest and stone teeth (2.d) sustains this hypothesis of the stone forest formation.

These periodically occurring soil stable and erosion cycles are consistent with the observed morphological features of the stone forest and stone teeth, suggesting that long term subsoil corrosion under a stable soil status was periodically interrupted by a series of abrupt soil erosion events, and this alternation corrosion process plays an important role in the formation of the Lunan stone forest.

**3**   The evolutionary
model of the scallops
of the stone forest.
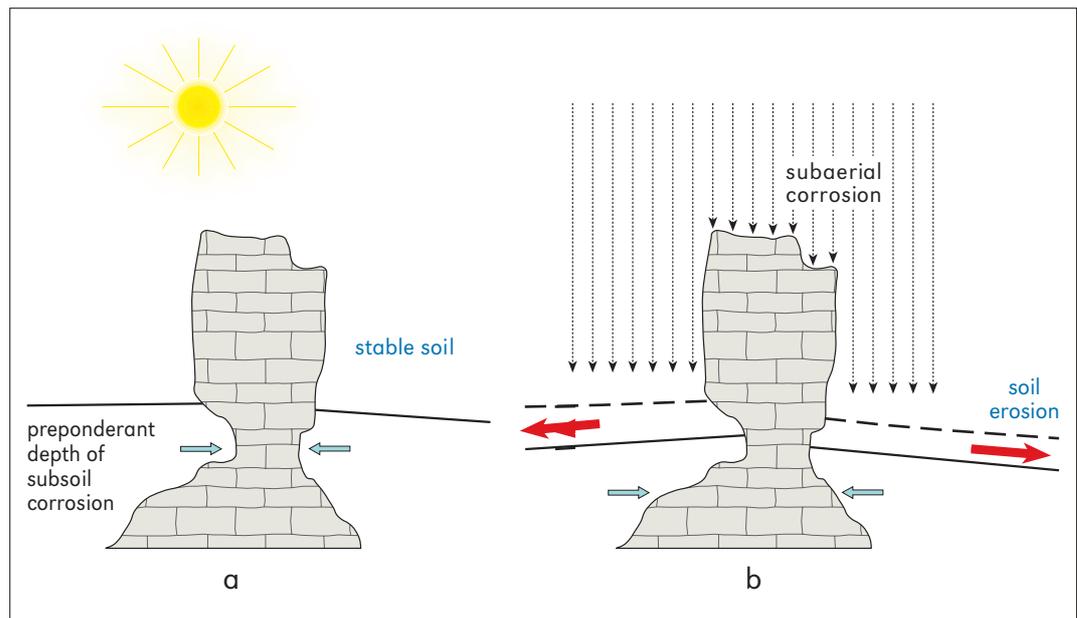
# CHARACTERISTICS AND FORMATION MECHANISM OF THE TUFA LANDSCAPE IN TIANSHENGQIAO IN ZHONGDIAN COUNTY

9

CHUXING HUANG

In Yunnan Province valuable tourist tufa geological resources are gathered within Shangri-La County. In general, development and protection of tufa resources are still at the elementary stage and only on the superficial level. Moreover, their significance has not been recognized yet. Carbonate tufas are very sensitive to water and climate, and the carbonate tufa resource is also very fragile. However, no corresponding protective measures have been applied to the tufa tourist geological resource at Tianshengqiao, thus making some parts of it face diminishing and exhausted commodities. Therefore we have investigated and analysed the tourist karst tufa landscapes within the Tianshengqiao area intending to provide a scientific basis for the protection of such resources all over the county.

## 9.1 CHARACTERISTICS OF THE LANDSCAPE AT TIANSHENGQIAO

### 9.1.1 *Rock characteristics of the landscape formation in the wider area*

Carbonate rocks are the material foundation forming karst landscapes. Zhongdian County covers an area of 11,330.46 km², 4786.27 km² of them are of carbonate surface which occupies about 42.2 % of the total territory (*Dong*, 1996).

The scenic carbonate rocks in Tianshengqiao date mostly from the Devonian to the Carboniferous periods, some of them from the Lower Permian and the Middle and Lower Triassic periods. Part of the rocks are from the Tertiary and the Quaternary and some marbles from the system of the metamorphic rocks (*Yunnan Bureau of Geology*, 1985).

East of the Jinsha River scenic rocks cover 35 % of the total eastern area and are exposed in the plot; to the west of the Jinsha River fault they are exposed in the strips lining the Lancang River; in other areas the exposed scenic rocks lie scattered.

The Yulong and Haba Snow Mountains consist of carbonate rocks from the Paleozoic era. In the eastern area clastic rocks of the Tertiary period are mixed with marlites and calcareous rocks.

In the districts of the Nujiang and Lancang rivers, especially in the areas along both sides of the Lancang River, calcareous rocks are less exposed in relative terms and appear in an interlayer. But in these districts faults are well developed and conducive to rainwater seepage and erosion.

The Gaoligong and Biluo Mountains consist of a set of migmatites. East of the Biluo Snow Mountain the rocks change from porphyry and diorite. Along the east side of the Nujiang River and in the southern section of the Lancang River lots of sandy shale, mudrock and almond basalt are distributed. Along the sides of the Lancang River fault, mauve sandstone is formed in the chalk and shale.

### 9.1.2   *Regional structural characteristics of the landscape*

Along the west side of the Jinsha River, from the Low Paleozoic to the Low Permian system, is a set of formation series similar to geosynclinal sediment. In detail, the Low Paleozoic stratum mainly consists of a flysch formation and is mingled with basic volcanic rock formations. In general, rocks from the Middle Silurian are mixed with volcanic rock; this is particularly well developed in the Early Permian period. Tianshengqiao lies near the north-south Suoge-Xuejiping fault on the western side of the Jinsha River. The fault is wide and deep formed in the early stages of the Permian but still active at present. The hot liquid of the gabbro igneous rock effuses up through this fault and is a precondition for forming tufa landscape.

The Jinsha fault is a large-scale ductile shear zone. Its structure was transformed in the Indo-Chinese epoch and has characteristics of a left-lateral sense of shear. The structure in the Yanshanian has characteristics of a right-lateral sense of slip. After the Himalayan epoch the structure changed and has the nature of left-lateral overriding. These NNW left-lateral sense faults obviously controlled the development of the sediment basin in the Cenozoic and are also an intensively active seismic belt in modern times. They have the characteristics of a push-twisted shear in the activities of the left-lateral slide faults.

According to the research of J. Luo and others, the Qinghai-Tibetan plateau has been entering an integral lifting stage from the Middle Pleistocene till now (*Luo et al.*, 1994). In western Yunnan there are three different types of mountain chains from east to west. Of these, the Ailou Mountain has sunk eastwards over a long period of time. The research by B. Chen and others indicated that the both sides of the Jinsha River had obviously a different history of the structural development (*Chen et al.*, 1992). On the eastern side ophiolite is developed. The rocks from the Zhendan to the Cambrian system are a formation of clasolite mingling with lava; the rocks from the Ordovician system to the Low Permian epoch are carbonate rock. The strata are continuous, the quality of rock is stable and fossils are abundant. From the Permian to the Triassic systems, the rocks are a formation of flysch and marine lava facies. The major structures exist in the Middle and Upper Trias.

### 9.1.3   *Basic morphological patterns of the landscape*

Tianshengqiao lies about 10 km to the east of the capital of Shangri-La County. The Shuodugang River flows from east towards west and cuts through the tufa bank at Tianshengqiao. In this way a natural limestone bridge appears consisting of limestone and hot water tufa. The bridge is 40 m high, 10 m wide and 15 m long (1).

Tianshengqiao is situated in a small basin surrounded by mountains. The mountains are lower in the south and higher in the north, 70–80 m above the modern river bed, and consist of lumpish rocks from the Trias. Cliffs abound on the south shore, interlaced with narrow cracks and karst interstices, forming rugged topography. In the cracks there are three hot springs, with a maximum temperature of 54 °C (*Geng*, 1989). They are sulphur springs formed in different stages: the east side was formed at an earlier and the west side at a later stage. The materials from the later stage lie above those from the earlier stage. Both shores have also formed canyon landforms and the cliff surfaces are full of small burrows. The Shuodugang River circumvents the natural bridge and forms a turn of 180°. In dry seasons, the flow volume is around 2 m³/s (*Yunnan Bureau of Geology*, 1985). The natural bridge took shape by erosion and weathering over a long period of time.

*Characteristics and formation mechanism of the tufa landscape in Tianshengqiao in Zhongdian County*

**1** The *Tianshengqiao* natural bridge.
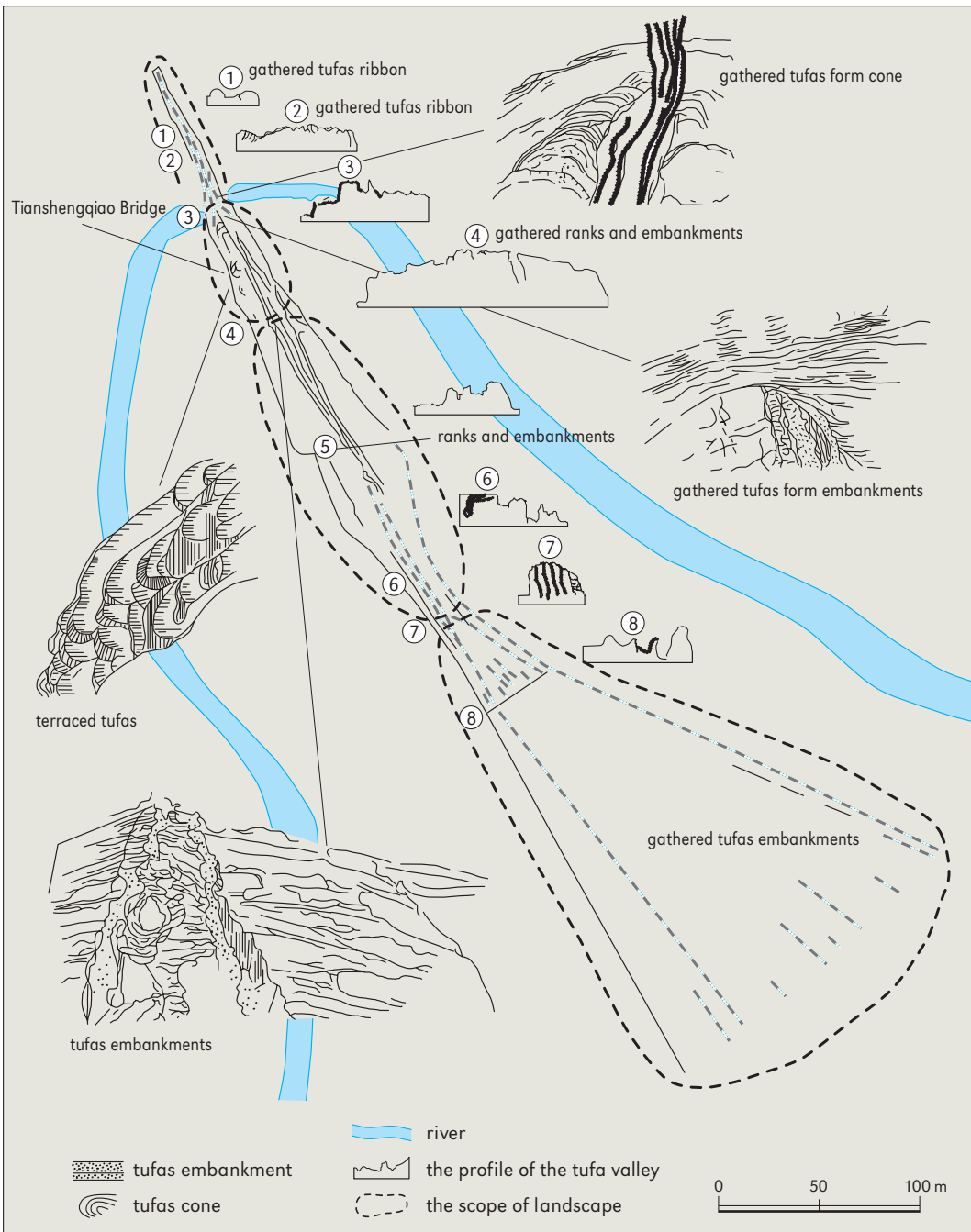


**2** The sketch of tufas in the natural bridge.

The water volume of the hot springs in Tianshengqiao is high and in general the water temperature is more than 50 °C. Calcium carbonate is deposited at a relatively high speed and the estimated sedimentation speed is 1–5 cm/yr. According to the characteristics of the relatively high sedimentation speed, it is estimated that the bank of the natural tufa was formed comparatively late. By comparison with other tufas in surrounding areas, it was formed not earlier than 5000 years ago.

## 9.2 CHARACTERISTICS OF THE NATURAL BRIDGE TUFA LANDSCAPE

The tufa bank at Tianshengqiao extends NW-SE, converging northwestwards and stretching out southeastwards (2, 3). There are three tufa strips on the bank, lying laterally in parallel or in echelon formation to a length of hundreds of metres. From the amount of the material sedimentation of tufa they tend to decrease northwestwards. Travertine flows from cracks in the middle towards the sides forming travertine waterfalls. The deposits on the east side are thick, from the top to the river bed surfaces in modern times. But on the west side much bedrock is exposed. Thus the east side is steep and the west side gentle.

### 9.2.1 *Regional characteristics of the tufa landscape*

The tufa landscape at Tianshengqiao mainly consists of four parts (2).

A striated tufa dike and ridge is distributed in the north of the scenic spot, with the steepest section at Tianshengqiao, 40 m high and 5–10 m long. The lower stratum is composed of a thick layer of calcareous rocks and the upper one is covered with a very thick layer of tufa. There is a natural bridge formed by water of the Shuodugang River eroding through the calcareous band.



**3** The tufa embankment on the *Tianshengqiao* natural bridge.

A tufa bank formed by overlapped cones occurs mainly in the mid section of the east side, i.e. in the 'coloured tufa' area. Hot tufa rises along structural cracks, forming tufa cones. These cones are aligned with the direction of the fault, over time they connect and a tufa bank takes shape.

Terraces and dikes occur in the middle of the west side of the scenic spot which has many hot springs. The topography is gentle. Because of intermittent lifts and the north-south structure, the structure of this area moves westwards. Thus multiple-layered tufa terraces come into being accompanied by tufa banks.

Many parallel dikes occur in the southeast area of the scenic spot. Because hot tufa is lifted up along several parallel cracks, many tufa banks in different sizes take shape laterally.

The tufas at Tianshengqiao have different shapes in different development stages and in different structural sections. In general, bundle-shaped tufa banks converge north-westwards and spread out southeast. The walls of the fault cliffs are smooth, rising vertically like spades. Travertines grow in the direction of the cracks, converge northwards and spread out southwards, breaking into two branches, one growing at a 50° angle and the other at 140°.

### 9.2.2 *Morphological characteristics of the tufa landscape*

At Tianshengqiao, the tufa landscape in the early stage exists in a linear pattern and later gradually changes to dot and planar patterns. The major patterns are as follows:

A tufa bank is the major type of the natural bridge landscape. The major composition parts of the natural bridge include in the lower layer calcareous rocks from the Triassic and an overlaid tufa screen, tufa waterfalls and tufa cones.

Tufa cones are arrayed in a certain direction. Connections between the cones form tufa banks. In the later period, tufa cones were scattered on tufa banks or in low-lying areas.

Tufa terraces appear in a crescent shape and flank tufa banks.

Tufa screens and waterfalls lie on Triassic calcareous rocks.

### 9.2.3 *Structural characteristics of the tufa landscape*

The structural pattern is the structural form of the exposed mineral materials of tufa. Owing to differing physiochemical conditions and environmental characteristics in different places, various structural patterns exist. The major patterns include:

Foam and sponge patterns appear in the middle of the natural bridge. While a hot spring was rising, $CO_2$ escaped at the same time and then the hot spring cooled down rapidly, thus forming tufas in foam, sponge, porous and beehive forms.

A strip pattern appears on two sides of the cracks where spring water rose up. Because the spring water cooled down slowly, $CaCO_3$ crystallized and formed crystals. Such tufas are relatively dense and hard and their parts may contain mineral materials; thus colour strips exist.

### 9.2.4 *Composition characteristics of the tufa landscape*

Composition types mean different types of the structure and spatial composition rules of tufas at different periods. At Tianshengqiao the tufa landscape includes the following composition types:

Compound superposition: Owing to the actions of structural movements, tufa banks, cones, screens and waterfalls were in different periods superimposed on one another, these from the later period atop those from the earlier period.

A ladder pattern: This is mainly the composition pattern of tufa waterfalls and water screens. Over a period of time, because of the changes in the water passageway along a certain direction, while tufa from a later period superposed tufa from an earlier period, at the same time tufa also changed its position along with changing of the water passageway, and a ladder pattern appeared.

A sawtooth pattern: The cause is similar to the ladder composition. This pattern is typical in a tufa bank. In the process of rising up of a hot spring, the spring diverged asymmetrically, and deposits existed on two sides in different volumes. And in the place where hot water rose up, a concave sawtooth formed, and on the both sides convex sawteeth formed.

An imbricate pattern: Tufa screens and waterfalls were imbricated in different periods, the former in one period and the latter in the other period.

A layering corrugation pattern: When the lower bedding was uneven, a hot spring formed ripples while flowing. Deposition happened in a place where the velocity of the flow changed relatively fast, thus forming the corrugation pattern.
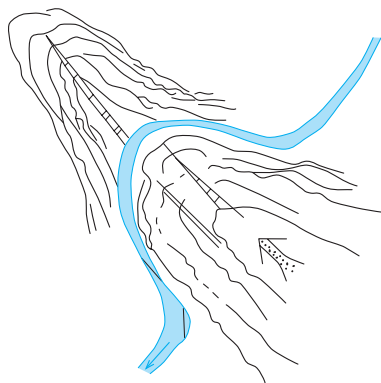
### 9.3 THE MODEL OF THE NATURAL BRIDGE FORMATION

The natural bridge lies exactly at the convergence of the north-south and north-west faults. Especially to the west of the north-south Suoge-Xuejiping fault, lava is widely visible; but to the east, strata from the Carboniferous and Devonian meet in conformity. So the fault is an active one (*Dun*, 1999). The hot liquid emerging from the natural bridge is mostly related to the activity of this fault. In terms of the regional structure, the SE-NW fault ends at the northwestern end of the natural bridge; in terms of the landform pattern, this area is surrounded by mountains. Naturally, the scenic spot is a gathering place for the surface and underground water. Moreover, underground thermal geysers form here.

For the natural bridge tufa, the process from the material beginning to the final formation can be divided into the following six stages:

a) the material preparation stage during which the water cycling system and thermal stress field come into being. Where carbonate strata appear widely, the regional north-south and west-east faults overlap and a hotspot exists. Magma activity is intense, and granite porphyry and granodiorite porphyry lie in dislocation. Highly mineralized hot water and its conduits come into being, thus providing the pre-requirements for the formation of the tufa landscape (4);



**4** The material preparation stage of the natural bridge formation.

**5** The rudimentary stage of the natural bridge formation.
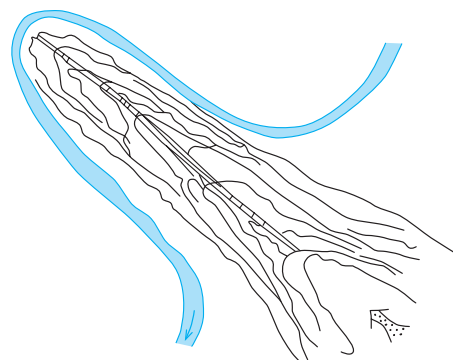
b) the rudimentary stage when at the hotspot where the faults meet, cracks in the limited north-west tension fracture are breached, the spring wells up, and on the south side of the Shuodugang River to the south, tufas are scattered in a northwest direction (5);

c) the development stage. Along with the increasing growth of tufa deposition, the up-welling passageway of water is blocked by the tufas formed earlier and hot water moves north-westwards along the fault and tufa banks. The river bed moves west-wards along with the development of tufa banks, circumvents them and forms a sinuous path (6);

d) the thriving stage. While tufa banks spread north-westwards, they continuously converge. A gushing tufa concentration spot comes into being and a peak period of tufa depositi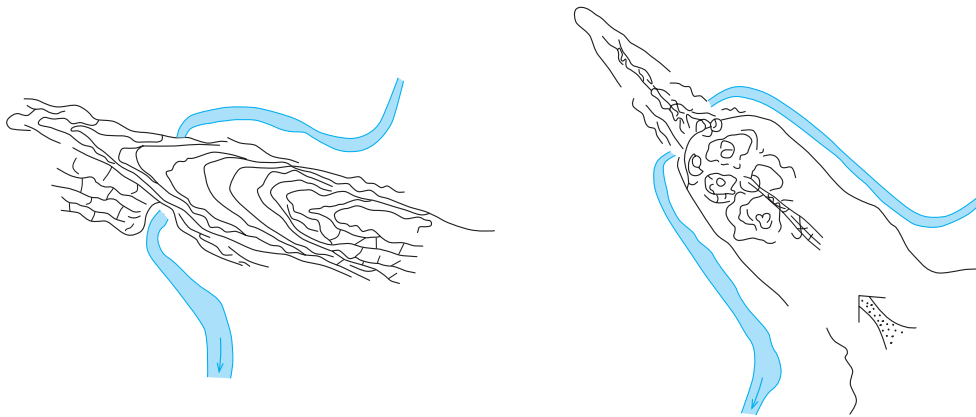on appears. Dot tufas such as tufa cones, screens, waterfalls and ladders develop. The hot spring upwells along the new water passageway and deposit; and imbricate tufa, ladder tufa, tufa screens and cones come into being. Tufa banks are connected on a large scale. Lateral screens and waterfalls develop in parallel. Tufas pile up and cover the river passage (7);

**6** The development stage of the natural bridge formation.



**7** The thriving stage of the natural bridge formation.

e) the declining stage when tufa banks cannot move forwards; bank-shaped tufas gradually become sharp-ended. But tufa screens and waterfalls on the tufa banks continue to develop (8);

f) the extinction stage during which corrosion and erosion begin. The deposition speed of tufa becomes slower than the corrosion speed. River water rapidly corrodes and erodes calcareous rocks on both sides. The river bed is undercut, the 'bridge opening' is widened, and today's natural bridge comes into being (9).



**8** The declining stage of the natural bridge formation.



**9** The extinction stage of the natural bridge formation.

97

# CHARACTERISTICS OF THE CAVE DEVELOPMENT IN THE SHILIN AREA

## 10

HONG LIU, YAN ZHOU

Shilin County takes its name from the shilin karst landscape. It lies 86 km southeast from Kunming, the capital city of Yunnan, and is located in the southern part of the Yunnan karst plateau. Over 350 km² of the 900 km² karst region could be identified as shilin which comprises the national Shilin Karst Landscape Nature Reserve. Widespread Paleozoic carbonate strata, pure and thick, provided fundamental conditions for the karst cave development. From Linkoupu, Hemocuen, and Xiaojianshan in the north to the Yizheng, Suoyishan, Dadieshui and Guishan regions in the south, numerous caves have been recorded (1).
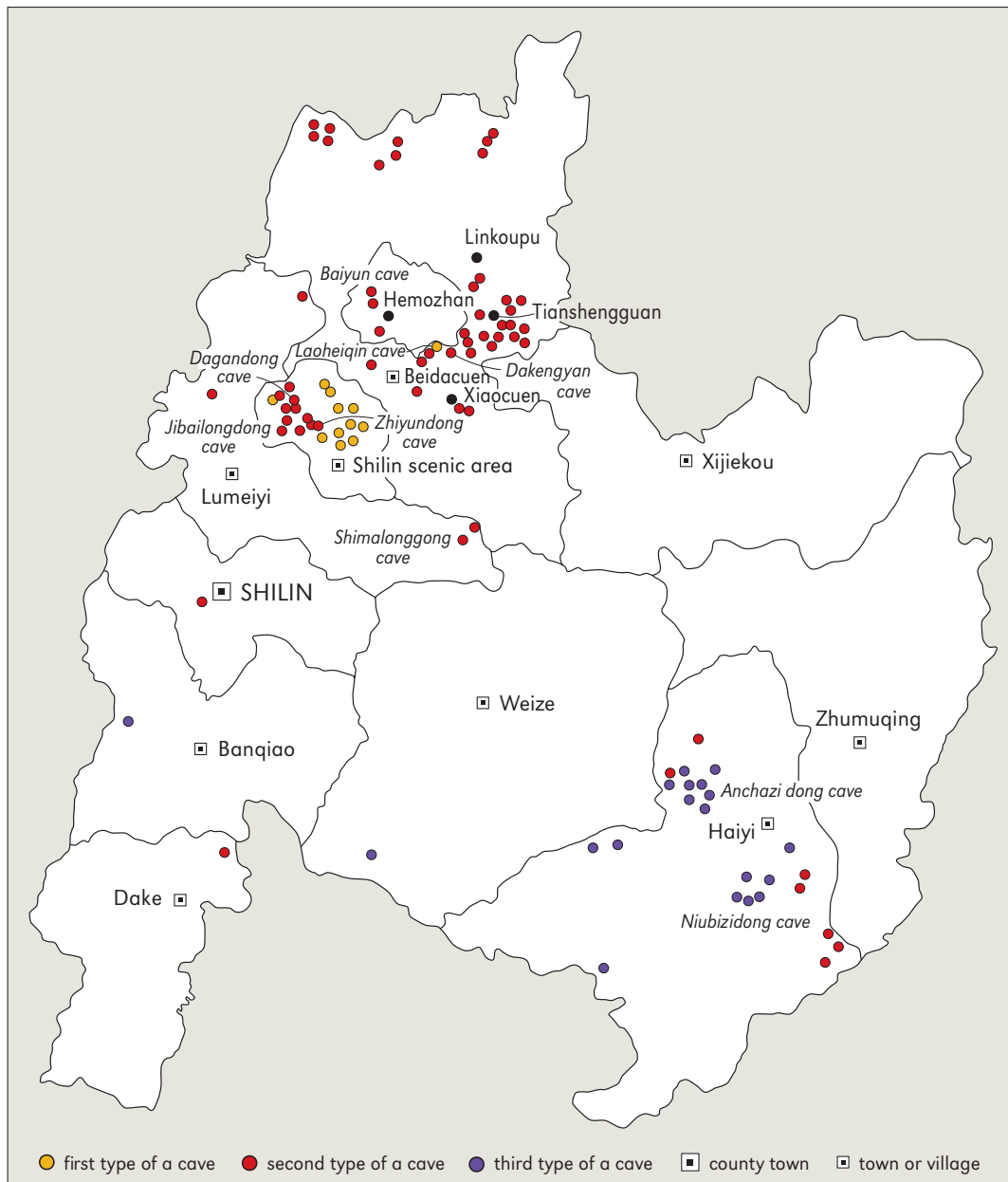


**1** Cave distribution map of *Shilin*.

*Characteristics
of the cave
development in
the Shilin area*

Between 1998 and 2001 three caving expeditions were carried out in this area by cave research teams of Yunnan Institute of Geography, Yunnan University, and Hongmeigui Caving Club, respectively. In total, over 70 caves have been explored. Among them, the deepest shaft is over 132 m deep and the longest horizontal cave stretches 1320 m in length. It is one of the extreme cave development areas in Yunnan Province.

## 10.1 CLIMATE AND HYDROLOGY

The study area belongs to the low latitude plateau subtropical climate, in the nature of "no frost in winter, no broiler in summer, every season was spring, with dry and wet seasons clearly defined." The annual temperature is 15.5 °C and precipitation is 967.9 mm. The annual variation in precipitation amounts to 34 %. The wet (rainy) season lasts from May to October, the dry season is from November to April. From 80 to 88 % of rainfall occurs in the wet season. The annual average humidity is 75 %.

The area belongs to the Nanpanjiang River drainage area in the upper reaches of the Zhujiang (Pearl) River. Generally, in immense karst areas there is a lack of surface streams; however, along the skirts of the Lunan basin many big springs have appeared, such as the Heilongtan, Bailongtan and Fenglongtan springs. Some of them have properties of an ascending spring. The main stream is the Bajiang River which rises in the Shanshenmiao Mountains, and runs in a NE-SW direction through Naigu shilin, Beidachun, Tianshengqiao, Lumeiyi and Banqiao villages. At the end it meets the Nanpanjiang River at the village of Lufong. It is about 48 km long and has a drainage area of 705.6 km². In its upstream area (above Tianshengqiao village), the appearance of a surface river alternates with that of an underground river. There are about 80 lakes in the Shilin area, of them the Changhu, Yuehu and Yuanhu lakes are larger and form the regional karst water drainage bases together with the Dadieshui waterfall.

In Shilin County the percentage of the forested area is over 36.3 %; however, most caves that have been found, are located in cultivated areas or in open grassland.

## 10.2 GEOLOGY

Widespread pure and thick Paleozoic carbonate strata provide fundamental conditions for the karst cave development in the study area. Its overlying formations are the Ermeishan group ($P_2\beta$) and the red strata of the Eogene (E). The former rock is continental tholeiite; the feature of many periods of effusive rhytms is obvious (*Zhang, Geng et al.*, 1997; *Hydrogeological team*, 1977). Most cap rocks have been moved by erosion and denudation; only a few remaining rocks have been spotted in the west mountainous area and in the central carbonate rock area. The Permian Daoshitou group ($P_1d$) is a suite of littoral facies to marsh facies black shale, thin to medium thickness of fine-grained quartz sandstone and thin layers clay-bearing microcrystal limestone, 23–43.3 m thick in total, which forms the relative impermeable layer of the Qixia group ($P_1q$), Maokou group ($P_1m$) karstic aquifers and a confined roof for underlying Carboniferous and Devonian carbonate aquifers. It has a great influence on the ground-water systems and cave development in the shilin area (2).

From the tectonic point of view, Shilin is located at the southwestern extremity of the Niutoushang rise, the southwestern edge of the Yangtze peneplatform, sandwiched by the Shizong-Mile and Xiaojiang fault zones. The structural deformations are mainly brittle, with the secondary folded deformation. In a S-N direction the Yanshan move-

ment has formed gentler and wide anticlines, in which the fractured structure and the folds are well developed, and the S-N and NE-SW direction structure dominant. The dips in the anticlinal strata are gentle, 2–25°.

In addition, denseness of fissures in carbonate rocks originates from different ages. What is more, the strikes of joints are quite different with respect to the age of the rock. Devonian strata are dominant by 40–50° and 315–338° two conjugate shear joints. There are three main joint systems, 320°, 10° and W-E developed in the Carboniferous and two main joint systems, 330–340° and 40–60°, in the Permian rocks. In the main Shilin scenic area, the strike of the dominant crevices is 315–338°, 45–60° and 285–300°, respectively (*Šebela*, 1996). The dips of fissures are near straightness, between 75–90°. The existence

**2** Geological map of *Shilin*.

of these vertical joint systems is a prerequisite for the shilin development. Though there are no big fault zones, these fissures amplified the secondary water permeability of the carbonate rocks, which provided good elements for the cave development in the Shilin area.

101

The caves of Shilin can be divided into three groups based on the shape of a cave, its geomorphological position and evolutionary differences.

*Characteristics of the cave development in the Shilin area*

The first type is a fracture-like cave, formed by enlargement of meteoric water flowing along the fractures. There are innumerable caves of this type that have developed in the shilin landform areas. They are small, 0.5–2 m wide and 20–40 m deep, or they converge to 20–30 cm wide dissolved fractures at depths of 20–40 m. Their development is strictly controlled by the dominant fractures of the region. Naturally, such caves have a good hydraulic connection with peripheral fractures (3). On the walls of the caves it is common to observe traces of water flood levels, channels and some other flowing water reliefs.

This type of caves is actually an outcome of shilin evolution. Its concentration in the shilin areas suggests that at the time when the shilin underground was formed, the ground-water was buried at a shallow level or that uniform ground-water levels were formed in some areas owing to the violent lateral connectivity of such caves. Ubiquitous lakes and pools in the developed areas of the shilin landscape suggest this possibility.

The second type of caves is a horizontal cave, which is widespread in the fengcong-shallow depression areas. Owing to their thin overlying strata, most merely 10–30 m

**3**   Map of the *Laoheiqin* Cave.



Surveyed by: Xiaoping Chen, Andrej Mihevc & Hong Liu
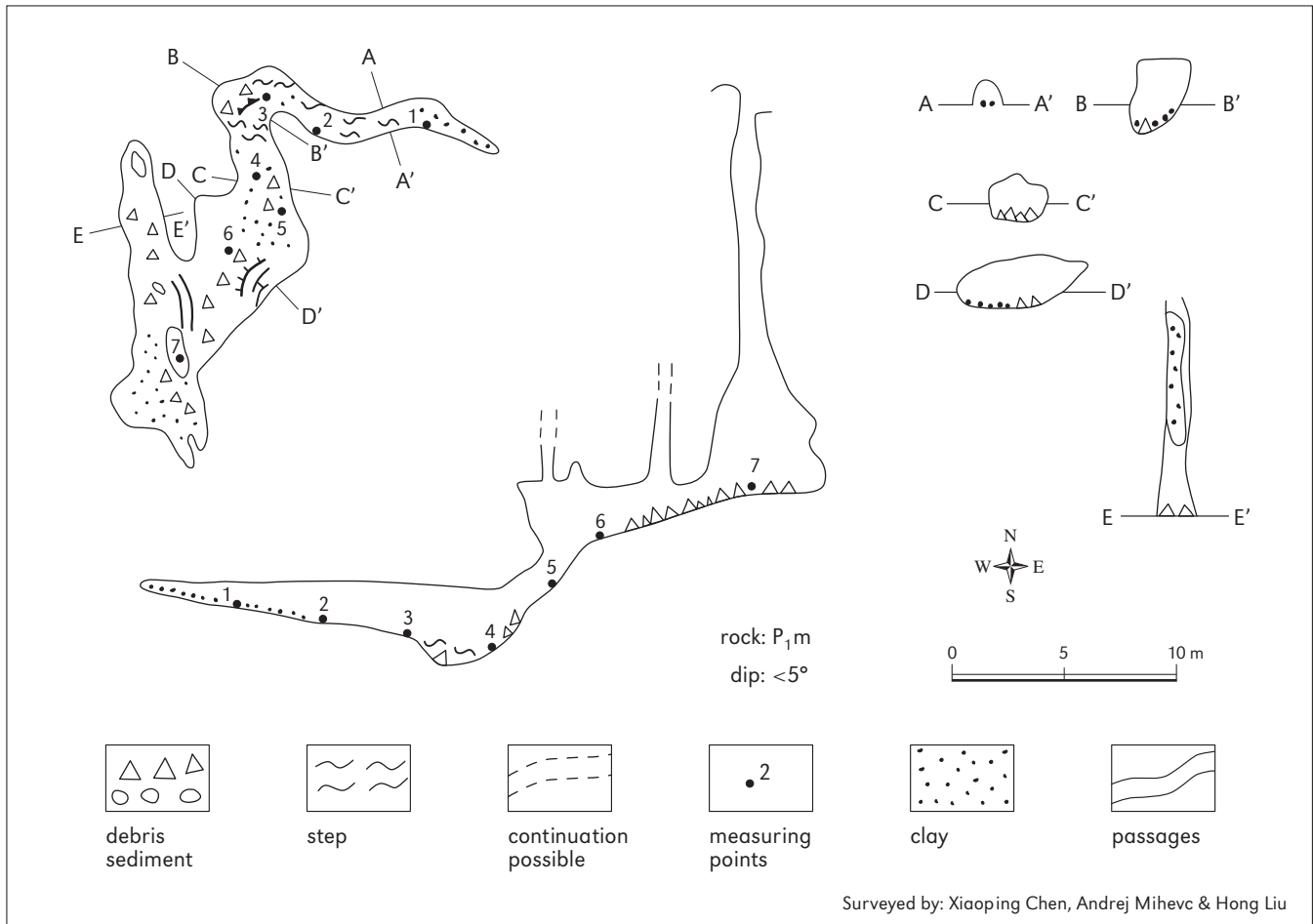
thick, such caves are normally decorated with windows; collapse phenomena are serious (4). From the perspective of both, their shape and genesis, this type of caves is the most complicated. Judging from the rock relief and sediments, the caves in the west have suffered several rounds of sediment-filled or half-filled processes. The evolution of the caves shows a character of different paragenesis stages.

The third type of caves is an inclined cave. Ordinarily it appears in combination with deep shafts or collapsed valleys as entrances (5). This type of caves mainly developed in the outer zones of the shilin landform, in mountainous areas, especially in the Guishan Mountain, Haiyi. The landform of the surface is the fengcong-depression; the groundwater is buried deep, around 150–200 m below the surface.

Seasonal flooding played an important role in the development of such caves. Without exception, gigantic scallops, 2–3 m in diameter and 3–4 m deep, could be found in the caves showing that they were flooded because of the limited cave passage discharge in the wet season. Speleothems are seldom found in them. At the bottom of the caves or near narrow passages, thick sediments were piled up. This type of caves was the main ground-water flow channel that is normally connected at the bottom of the cave with the modern ground-water river. Because of the neotectonic movement and surface river trenching, the function of the radial drainage system of the surface depression failed; no more water flows into the caves through the entrances now, except in seasonal cases.

**4** Map of the *Shimalonggong* Cave.



Surveyed by: G. Lowe, H. Greaves, E. Lynch & Hong Liu

rocks: D$_3$i + C$_1$ds
dips: 5–15°

projection: 45°

| | | |
|---|---|---|
| passages | clay | debris |
| pools | continuation possible | overlay |

underground river

Surveyed by: G. Lowe, H. Greaves, E. Lynch & Hong Liu
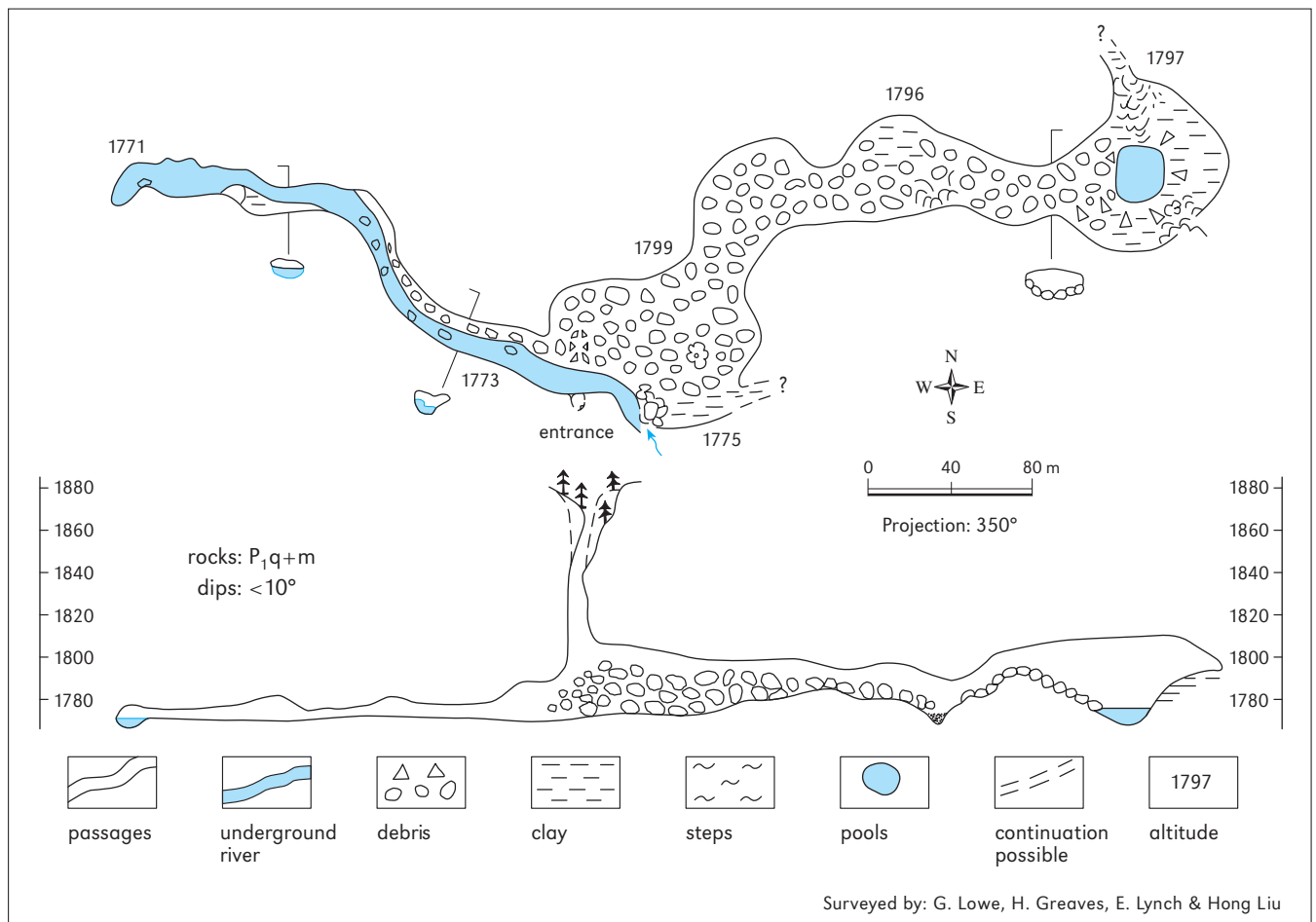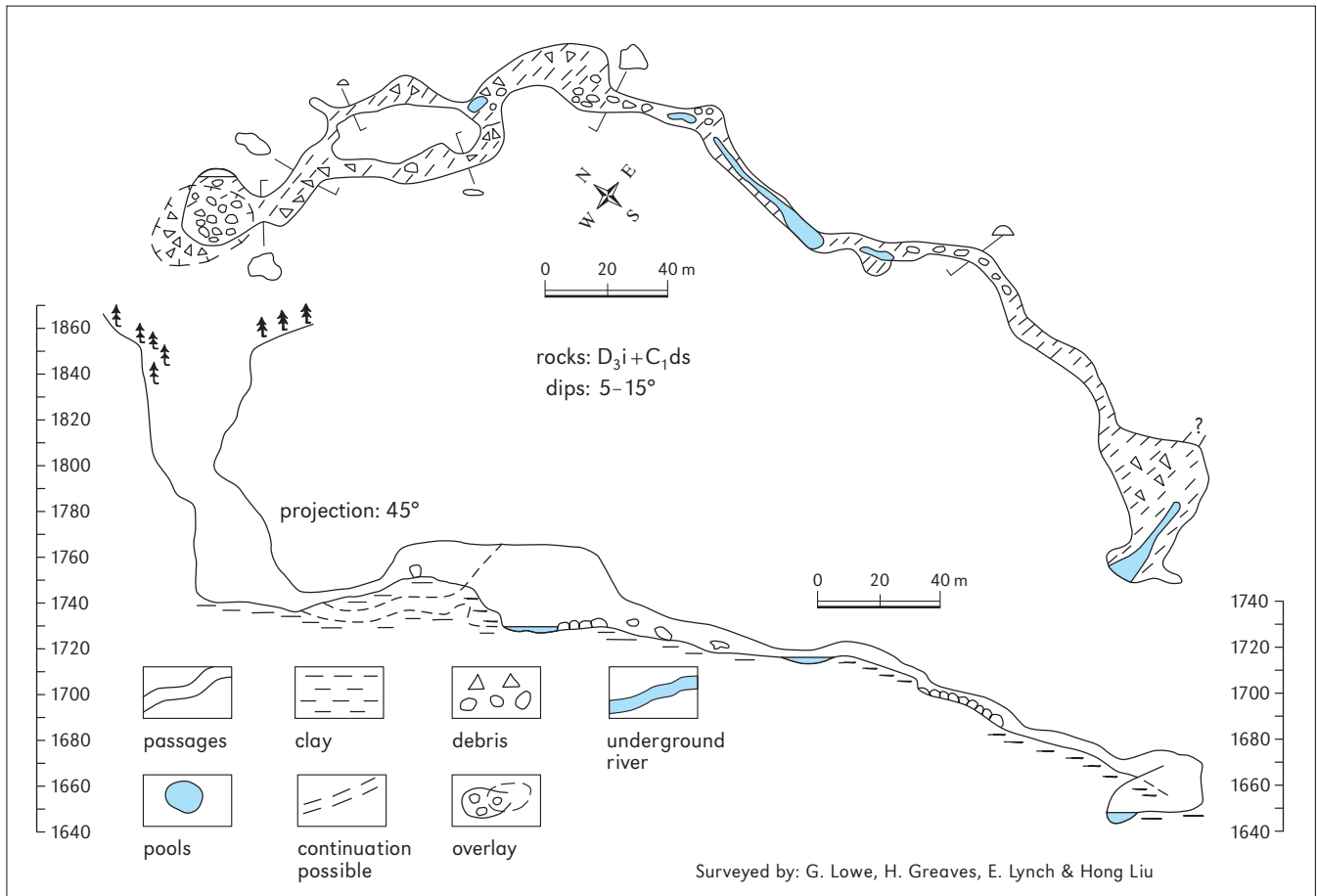
**5** Map of the *Niubizi* Cave.

## 10.4 CHARACTERISTICS OF THE CAVE DEVELOPMENT

A cave is one of widely developed subsurface karst forms. According to field surveys and statistical data, there are more than 100 caves in the Shilin area. It is believed that more and more caves will be found with further investigation.

Though quite different in scale, shape and cave sediments, caves also reveal some common characteristics of their development.

### 10.4.1 *Stratified cave development*

Stratification of the cave development reveals characteristics of cave and karst landform evolution. In the study area, up to the karstic mountains, plane surfaces and hills have caves developed in them at altitudes 1800–1950 m, down to 1500 m in the Bajiang valley. Most of them, however, occur in the zone between 1700 and 1935 m. They could be divided into three layers. The 1850–1900 m altitude zone is the layer with the most developed caves; nearly 50 % of the caves known today are located in this zone. Secondly, the 1900–1950 m and 1700–1750 m layers also contain caves of comparative concentricity zones; in total, they represent 38 % of the known caves.

Some caves, the Dixiashilindong Cave for instance, have three layers of passages, each of them connected by a shaft 7–10 m deep. Most of the caves have two layers of passages or only some varieties on cross-sections of cave passages. For example, the Qinghuadong Cave in Linkoupu village north of the study area could be divided into two layers: a fossil (dry) and a water cave.

104

The Zhiyundong, Zhuerdong and Dagandong caves are distributed at three different elevations and embody stratified characteristics in a small area of less than 2 km².

### 10.4.2 Selectivity of the cave development on carbonate strata

There are obvious differences in the number of caves in different carbonate strata. The majority of the caves developed in carbonate rocks from the Permian $P_1m$, $P_1q$ groups, Carboniferous $C_1ds$, $C_2w$, $C_3m$ groups, Devonian $D_2q$, $D_3i$ groups and Sinian $Z_bdn$ group. Among them, more caves developed in the carbonate rocks of the Maokou $P_1m$ group than in the Sinian carbonate strata.

According to the statistical data for 45 caves, nearly 93.3 % of the known caves developed in Permian and Carboniferous carbonate rocks (Table 1). The caves in Permian rocks account for 51.1 % and Carboniferous carbonate rock caves for 42.2 % of all the caves.

This result may be biased. Besides the lithological factors, it is also related to the area size of the Permian and Carboniferous outcrops. In addition, the strata of the key areas are related.

**Table 1**
Statistical data of the caves in the different rock formations.

| Strata | Number of caves | Percent of total |
|---|---|---|
| Maokou group ($P_1m$) | 14 | 31.1 |
| Qixia group ($P_1q$) | 9 | 20.0 |
| Maping group ($C_3m$) | 2 | 4.4 |
| Weining group ($C_2m$) | 9 | 20.0 |
| Shangsi group ($C_1ds$) | 8 | 17.8 |
| Qujing group ($D_2q$) | 1 | 2.2 |
| Yidadequn group ($D_3i$) | 1 | 2.2 |
| Dengying group ($Z_bdn$) | 1 | 2.2 |
| Total | 45 | 100.0 |

### 10.4.3 Dominance of small and medium scale caves

On the basis of the cave classification by Bögli (1980), caves that are shorter than 50 m and have a floor (or bottom) area of less than 500 m² are called small caves. Those with a length between 50–500 m and a bottom area of between 500–5000 m² are medium-sized caves; bigger than those are large-scale caves. The caves in the Shilin area include all three scale types; however, small and medium scale caves absolutely predominate. The majority of the caves are 50–300 m long.

The longest cave is the Shimalonggong Cave. Its entrance is a 105 m-deep shaft which connects with an internal ground river 1.2 km long. The next longest cave should be the Dagandong Cave (its entrance is less than 200 m north of the Zhiyundong Cave). Over 618 m cave passages have been surveyed (some passages were flooded, owing to heavy rain, and could not be completely explored). The passages and the geomorphological location suggest that it is not shorter than 1 km. Wayaodong, for example, the shortest cave, is only 20–30 m long. The length of the tourist caves, the Zhiyundong, Jibailongdong, Baiyundong, and Dieyundong caves, is 200–400 m, so they belong to the medium-scale caves.

The width of most caves is in the range of 2–15 m; only some passages in the Shimalonggong, Niubizi and Dagandong caves can attain widths of 30–56 m. The statistics on the cave passage width show that 10–15 m wide passages stand first on the list. In the second place are those that are 5–6 m wide. They account for 18 % and 15.6 % of the total number, respectively.

The height of cave passages in the Shilin area is mostly in the range of 3–25 m. Passages, reaching 4–5 m in height, are dominant and represent 20 % of the total number; those with heights of 10–15 m are the next and account for 15 %.

So far, the deepest cave is the Niubizidong Cave in the Hehe village, Guishan Township. The total depth of the Niubizidong Cave is 205 m. The entrance is a 132 m-deep shaft, with a diameter of 50 m at the opening. There is another big shaft nearby. Because the two shafts are close and so bear a resemblance to the nose of a buffalo, local people call them the Niubizidong (Buffalo's Nose) Cave. The second deepest cave (around 110 m) is the Shimalonggong Cave located near the Weiboyi village.

### 10.4.4 *Caves as part of modern ground river channels*

In addition to a small number of caves such as the Jibailongdong, Zhiyundong, Dieyundong and some other small caves that have developed near the tops of karst hills in the shilin areas, the majority are ground river caves, which account for 80 % of the known caves.

In general, in the source area of the Bajiang River, free of headwater erosion, it means that the caves are normally small and shallowly buried. Downstream, with the groundwater hydraulic gradient increasing, a few large, deeply buried caves have developed. If we take for example the Tianshenguang-Beidacun underground water system, it turns out that the ground-water is less than 20 m under the surface. However, in some places the ground-water even comes to the surface in the Tianshenguang village because of the collapsed roof. The caves are less than 200 m long, except Yangshidong Cave. After the ground-water breaks down the water impermeable layer, the Duoshitou group rocks ($P_1d$), it goes even deeper under the surface, e.g. 35–40 m around the Dakenyan area. And one kilometre to the southwest of the Laoheigin shilin area it reaches the depth of 50–60 m.

In the karst highland near the Weiboyi village, the ground-water was buried 105 m deep. In the Shimalonggong Cave there is a big underground river, which during the rainy season discharges 4–5 m³/s of water flowing into the Dongfanghong reservoir.

Because of the shallowly buried ground-water, many windows have developed along the course of ground rivers, such as in the Xiangshidong, Qifengnandong, Guanyindong, and Pipadong caves. In some places, ground-water even turns into a surface river. The surface river between the Yingguohua and Guanyindong caves, for example, was formed by a ceiling collapse. As a result of the collapsed roof, natural bridges remained in the Shilin area. The best known one is the natural bridge of the Tianshengqiao (Natural Bridge) village. Because of its close relationship with the hydrological environment of the Shilin stage landform and cave development, the importance of this natural bridge has been emphasized in many previous studies (*Zhang*, 1984).

### 10.4.5 *The control of cave strikes by structure fissures*

Measurement results indicate that caves primarily developed along the structure fissures in the rocks. The statistical data about 207 structure fissures in the Dieyundong, Jibailongdong, Zhiyundong, and Baiyundong caves have shown that in 23.7 % of the four caves the channel follows a N0–10°W direction, and in 16 % a N30–40°W direction (6). The third, most frequent direction is N110–120°E which occupies 12.5 % of the total length (*Kogovšek et al.*, 1999).

In the Zhiyundong Cave, the main fissure direction is NW-SE. 47.1 % of the principal passage follows a N30–40°W direction. The study showed that regional fissures strictly controlled the extended directions of the shafts and caves in the shilin areas. In particu-

lar, in some small areas, like the shafts be-
hind the Shilin administration buildings
and those behind Wrestle Performance
Ground, they extended primarily along
one fissure. Dips in the fissures of the Shi-
lin area were vertical or around 70–80°. In
most cases, the trails of the fissures could
be clearly identified on the ceiling of the
cave; broken zones occurred only rarely.

Nevertheless, the strikes of cave devel-
opment in the western and eastern parts
differ significantly that concerns the evo-
lution of the regional water system. In the
west, the direction of cave passages is pre-
dominantly N-S, while in the east the E-W
or near E-W direction dominates.
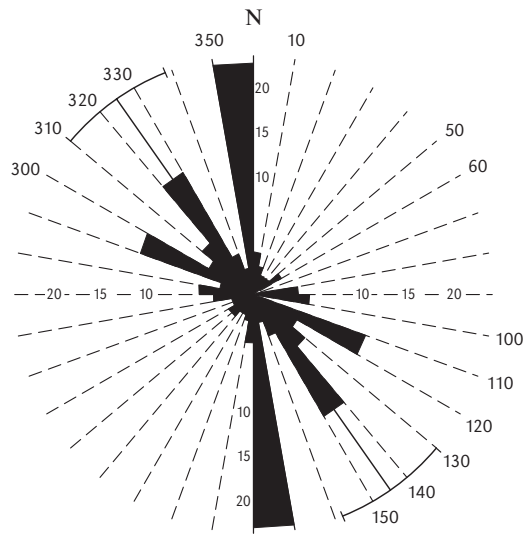


**6** Rose diagram of the passages for the Dieyundong, Jibailongdong, Zhiyundong and Baiyundong caves (from *Kogovšek et al.*, 1999).

## 10.5 PALEOENVIRONMENTAL AND SPELEOGENETIC CONCERNS

The cave origin is a matter relevant to the regional paleoenvironment, global climate
change in the Cenozoic and the uplift of the Yunnan plateau. Since the end of the Yang-
tze tectonic movement, the Shilin area was located in a lowland region, south-southwest
of the Niutoushan Old Land, so the surface water and ground-water systems broadly
developed from north to south (*Zhang, Geng et al.*, 1997). The Haixi movement caused
the study area to rise up and become the land permanently, and the Yunnan movement
fissured the Permian carbonate strata, which provided the fundamental conditions for
paleo-karst development. In Late Permian, Ermeishan basalt effused and covered a great
part of this area. Hydrothermal recrystallization occurred in carbonate rock. The im-
pact of recrystallization and calcite veins on the development of caves and ground water
systems is not yet quite clear, but it is certain that they have had a great influence on the
rock relief (*Knez*, 1998; *Slabe*, 1998).

The results of the caves' survey suggest that no large cave systems may have formed
before the basalt effused because there were no basalt remains; scorch marks have been
found in the caves.

The Yanshan movement further enhanced the fossil landscape which established the
surface water and ground-water flow system patterns. In the Middle Eocene, especially
the impact from the discrepant uplift of the first stage Himalayan movement, ancient
Lunan Lake appeared and the Palaeogene Lunan red stratum was deposited directly
over Permian carbonate rocks and basalt. The SEM (scan electron microscope) stud-
ies of the sedimentary facies along with quartz have indicated that in the Palaeogene,
diastrophism in the Shilin area was relatively quiet. Under the influence of weather al-
ternating with xerothermic (hot and dry) and wet heat, the Shilin area underwent strong
denudation, and the Yunnan peneplain formed. The appearance of the ancient Lunan
Lake formed a closed water flow system in the shilin that may be the cause of differ-
ences in the ground-water system evolution between the eastern and western parts. The
eastern part was under water and thick Palaeogene sediments were deposited; however,
the eastern part became the erosion zone of the lake.

The Permian Daoshitou group (P$_1$d) rocks suggest that a relative impermeable layer between the karst aquifers of the east and west broke down at that time. In order to adapt the changing discharge base, ground-water systems in the east looked for a short cut to discharge towards west, and broke down the impermeable layer of the Daoshitou group (P$_1$d) rocks around Dakenyan. The Eocene period was a warm period globally. The Shilin area had suffered heavy eluviation in the hot and humid climate conditions.

In the Late Tertiary, the Yunnan peneplain was gently uplifted, higher in the northwest, inclining towards east and south. In the early Oligocene the ancient Lunan Lake constringed towards southwest and disappeared finally and the rudiment of the Bajiang River formed (*Zhang, Geng et al.*, 1997). Subsequently, the tectonic movement of the study area turned into a longer period of relative quiet once more. Under hot, wet climate conditions, the karst was extremely developed, and the shilin stage peneplain formed. According to Lin's studies, the altitude of the Lunan basin was perhaps lower than 600–800 m, still under the tropical climate during the Middle Pliocene to the Early Pleistocene (*Lin*, 1997b). The cave systems and the underground water systems were likely formed at that period.

After the Early Pleistocene, in particular the Middle Pleistocene, the Yunnan highland was sharply uplifted to about 1000 m, and the Shilin area was lifted to its present positions, 1700–2000 m a.s.l. From that time, shilin was divorced from tropical climate and shifted to subtropical climatic conditions. The contemporary Bajiang River carved deep into the ground and made earlier ground-water systems turn into fossil caves.

The Jibailongdong, Dieyundong and Zhiyundong caves – such in N-S direction dominated caves have been thought as N-S extended early stage paths of ground-water systems – developed along the contact zone between the Lunan basin's edges and carbonate rocks (*Zhang*, 1984). Some Palaeogene sediments still remained at the top of the Jibailongdong Cave. The cave passage was obviously extended to the N0–10°W and NW-SE along two group fissures. It is clear that those fissures did not cut through the Palaeogene strata. This means that fissure systems in the Permian carbonate rocks already existed, and perhaps the rudiments of the ground-water flow systems had been formed before the Palaeogene sediments were deposited. Most caves in the E-W direction are modern ground-water channels, possibly formed after Daoshitou group (P$_1$d) rocks broke down.

It has been proven by water tracing experiments in the Tianshenguang-Beidacun ground-water system (*Kogovšek et al.,* 1997; 1998; *Kogovšek* and *Liu*, 1999) that cave systems and ground-water systems are very complicated in this area. It seems that the N-S and E-W water systems co-exist. During the low water level period, the E-W ground-water systems demonstrate better connectivity, while during the high water-level period the situation is somewhat different. Not only did some tracers appear in the south Xiaocun village, but also sequences of the tracer peaks appeared and the values of tracer concentrations at sample points were different. All that suggests that beside the current flow system, there existed another abandoned, earlier cave system that dominated with N-S direction passages and played a role in the floods. The behavior of the karst aquifer is very complex.

Obviously, the rock relief and sediments of the caves in the western part show characteristics of multiphase paragenesis (*Šebela et al.*, 2001; 2004). The remains of pebble sediments and ceiling channels in the Baiyun Cave, Naigu shilin, suggest that the cave has experienced several alternations of fast water flows and flood water (*Šebela et al.*, 2004). Judging from the shapes of the cave passages, speleothems and rock reliefs, the

Zhiyundong, Jibailongdong and Dieyundong caves were also infilled or half-infilled by sediments on many occasions.

Paleomagnetic analyses of four samples from the 1.75 m sediment profile in the Baiyun Cave suggest all samples to be part of an old period of cave infilling around 780,000 years BP, except for one from the upper part of the profile which probably belongs to the time period 112,300–117,900 years BP (*Šebela et al.*, 2001). Based on Dr Tan's work on the Shilin area, where one or two clay layers in the stalagmites were commonly found, TIMS dating shows they belong to the Holocene (*personal communication*).

In contrast to the keyhole-shape or I-shape sections of the cave passages in the narrow zones, there are different layers of fluvial gravel sediments in the wide passages.

# BAIYUN CAVE – THE LONGEST CAVE IN THE NAIGU SHILIN

<span style="float:right">**11**</span>

JANJA KOGOVŠEK, TADEJ SLABE, STANKA ŠEBELA, HONG LIU, PETR PRUNER

The Naigu shilin is situated 20 km east of the central Lunan shilin and around 70 km southeast from Kunming (1). It covers an area of 8 km² (*Salomon*, 1997) and is an important tourist attraction.

Baiyun Cave in the Naigu shilin (2) is open to the public. It is situated at an altitude of 1700 m with the general direction in NW-SE. The cave is 380 m long and its passage is up to 25 m wide (3). A small water flow which occurs in the northern part of the cave flows parallel with the tourist path; at the southern part of the cave the water flow leaves the cave and reappears on the surface. The ceiling of the Baiyun Cave is only a few metres high (4), yet it is several tens of metres thick.

We accomplished geological, geomorphological and chemical researches of the cave (*Šebela et al.*, 2001) as a base for future studies of caves and shilins. A sample of flowstone was taken for a Th/U analysis from the top of our profile of cave sediments (5). Due to impurity of the sample, the age of flowstone was not sufficiently proved.

## 11.1 GEOLOGY OF THE BAIYUN CAVE

In southern Yunnan we found structures of the Eocene to the Miocene age and Middle Cenozoic structures. During Late Cenozoic time, an unhomogeneously distributed extension has been expressed by numerous Quaternary basins along the southern part

**1** Tectonic situation in the area of *Kunming, Yunnan*. The dark star represents the *Naigu shilin*.

**2** *Naigu shilin* and karst caves.
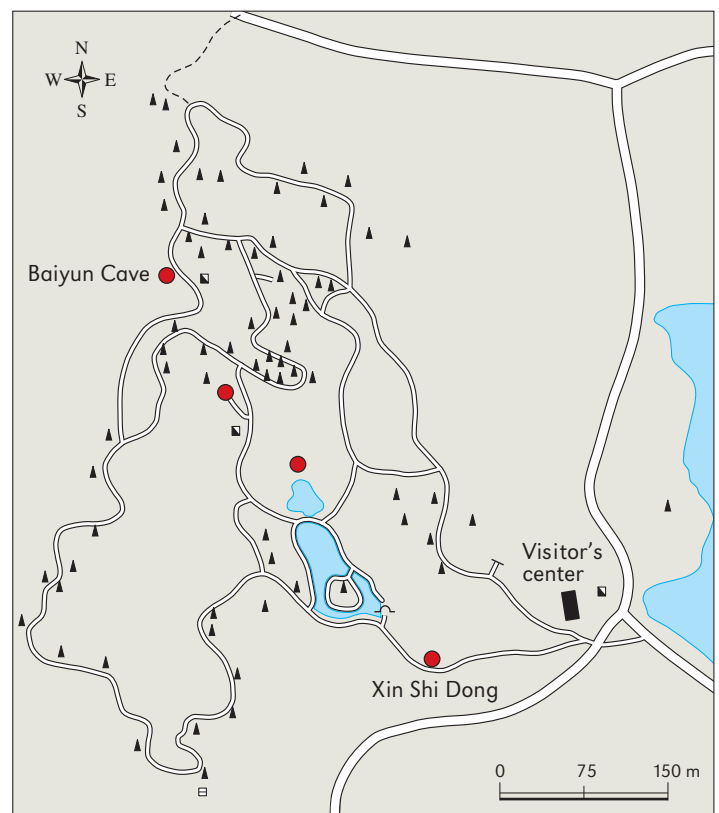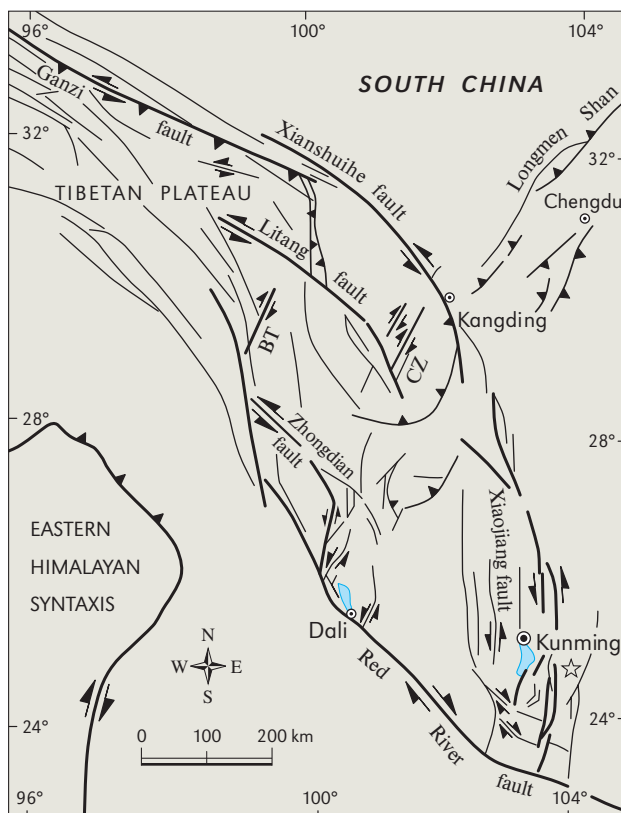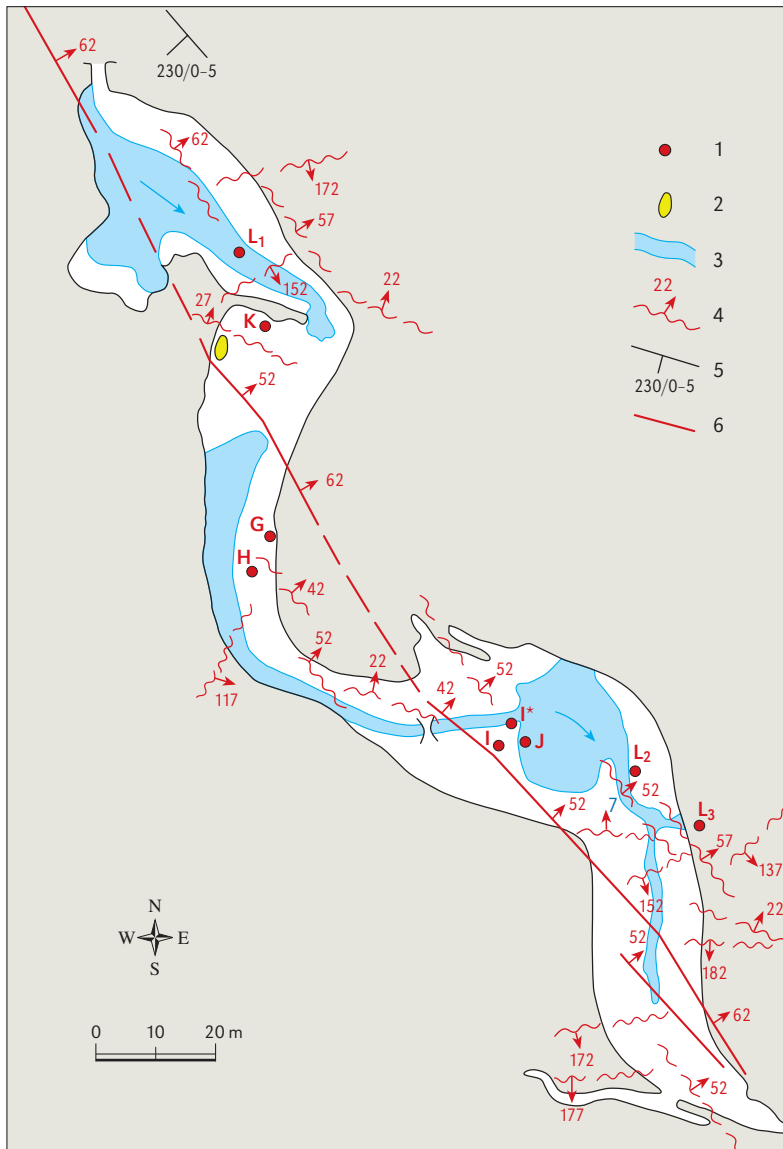
of the Xianshuihe-Xiaojiang fault system (1). Quaternary basins and lakes north of Dali and within the southern part of the Xiaojiang fault zone are areas of the local active extension (*Wang* and *Burchfiel*, 2000).

The crust west of the Xianshuihe-Xiaojiang fault system rotates clockwise relative to the crust in South China. The left-lateral Xianshuihe-Xiaojiang fault system is the major crustal boundary that separates these two crustal sections. The Pliocene-Quaternary sedimentary fill in pull-apart basins associated with this fault system indicates that this fault system was initiated at least 2–4 Ma ago (*Wang et al.*, 1998).

The region north-east to east of the Eastern Himalayan syntaxis is subjected to the right-lateral shear between the syntaxis and South China east of the Xianshuihe-Xiaojiang fault system (*Wang* and *Burchfiel*, 2000).

Regarding the tectonic situation, the Baiyun Cave is situated a little east of the Xiaojiang fault system, which runs in the general direction N-S. The cave has 36.6 % of its passages in the direction N0–10°W and in the second place 27 % in

**3** Ground-plan of the *Baiyun* Cave with geological elements and position of water samples.

1 – points in the cave where chemical measurements of percolating water have been performed;

2 – position of the sediment profile taken for paleomagnetic and Th/U analyses;

3 – water flow;

4 – strike and dip of fissures;

5 – strike and dip of a bedding-plane;

6 – the most expressed joint in the cave.

**4** A passage in the *Baiyun* Cave.
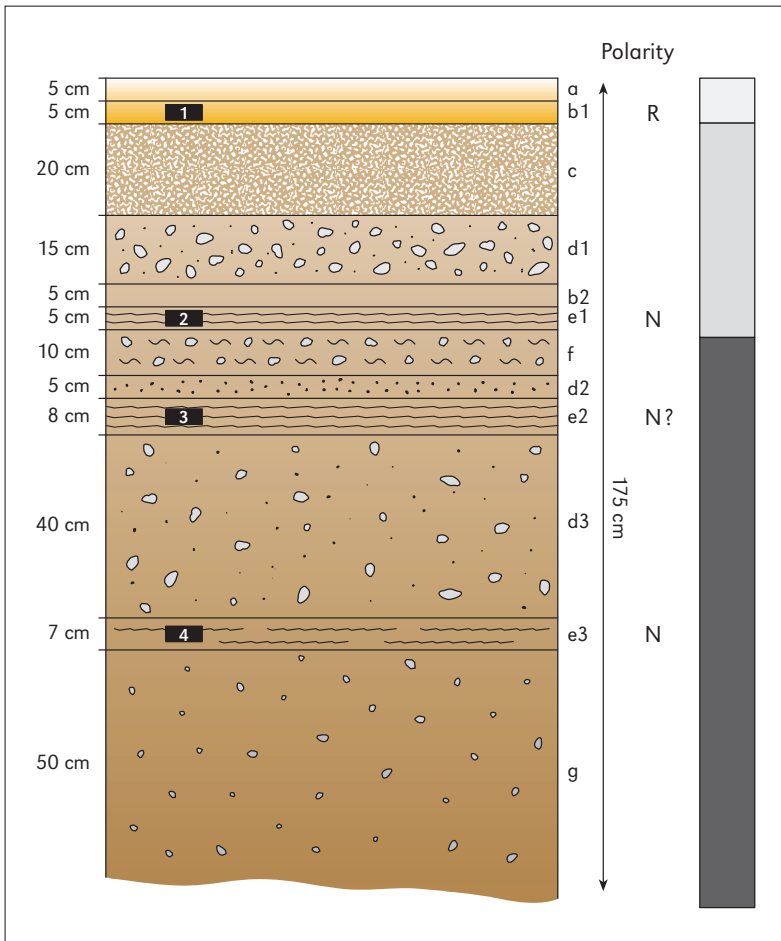
**5** The profile of cave sediments taken for paleomagnetic analyses.
a    flowstone (d = 5 cm);
b1  reddish sandy clay (d = 5 cm);
c    sandy clay with brown flowstone (d = 20 cm);
d1  gravels cemented into conglomerate
     (d = 15 cm);
b2  reddish sandy clay (d = 5 cm);
e1  laminated sandy clay (d = 5 cm);
f    sandy clay with uncemented gravels (d = 10 cm);
d2  conglomerate (d = 5 cm);
e2  laminated sandy clay with rare gravels
     (d = 8 cm);
d3  conglomerate (d = 40 cm);
e3  laminated sandy clay (d = 7 cm);
g    conglomerate with smaller gravels than in layers
     d1, d2 and d3 (d = 50 cm).

Black boxes are samples for paleomagnetic analyses.
1    reverse polarity R;
2    normal polarity N;
3    normal polarity (?) N?;
4    normal polarity N.



Passage orientation, Baiyun Cave

Calculation Method ............Frequency
Class Interval.........................10 Degrees
Filtering .....................................Deactivated
Data Type ...............................Bidirectional
Rotation Amount .................0.0 Degrees
Population...............................41
Maximum Percentage .........36.6 Percent
Mean Percentage .................20.0 Percent
Standard Deviation..............10.71 Percent
Vector Mean...........................330.66 Degrees
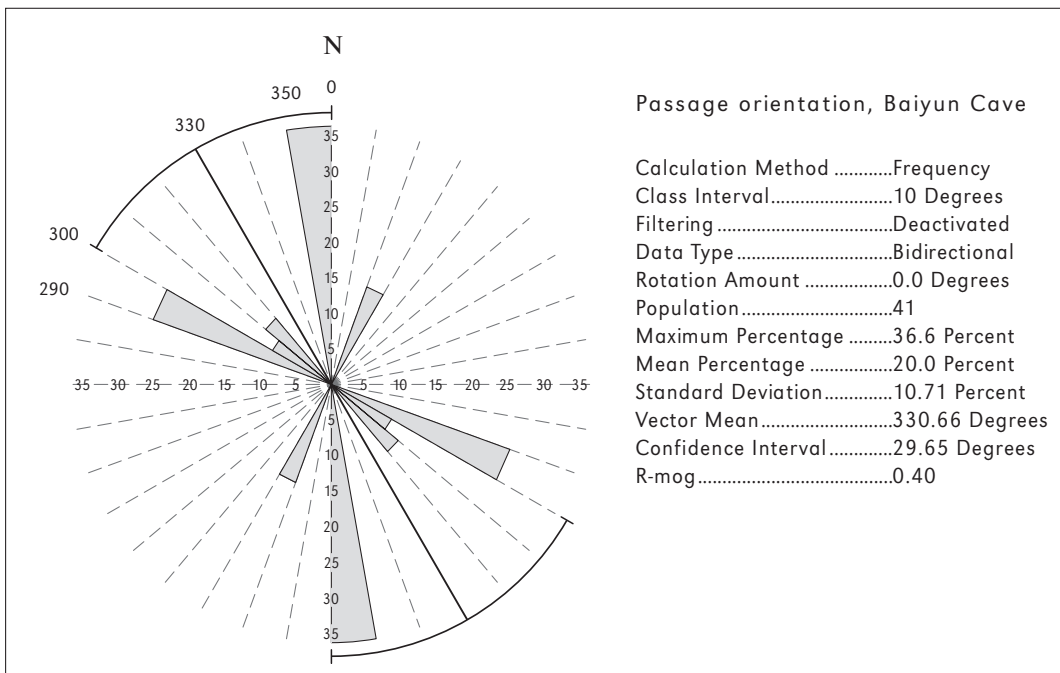Confidence Interval .............29.65 Degrees
R-mog.......................................0.40

**6** Rose diagram of the passage orientation in the *Baiyun* Cave.

the direction N60–70°W (6). The Naigu shilin is formed in carbonate rocks of the Qixia group. The rock is limestone, dolomitized limestone and Lower Permian chert. Qixia group carbonate rock is mostly thick-bedded to massive.
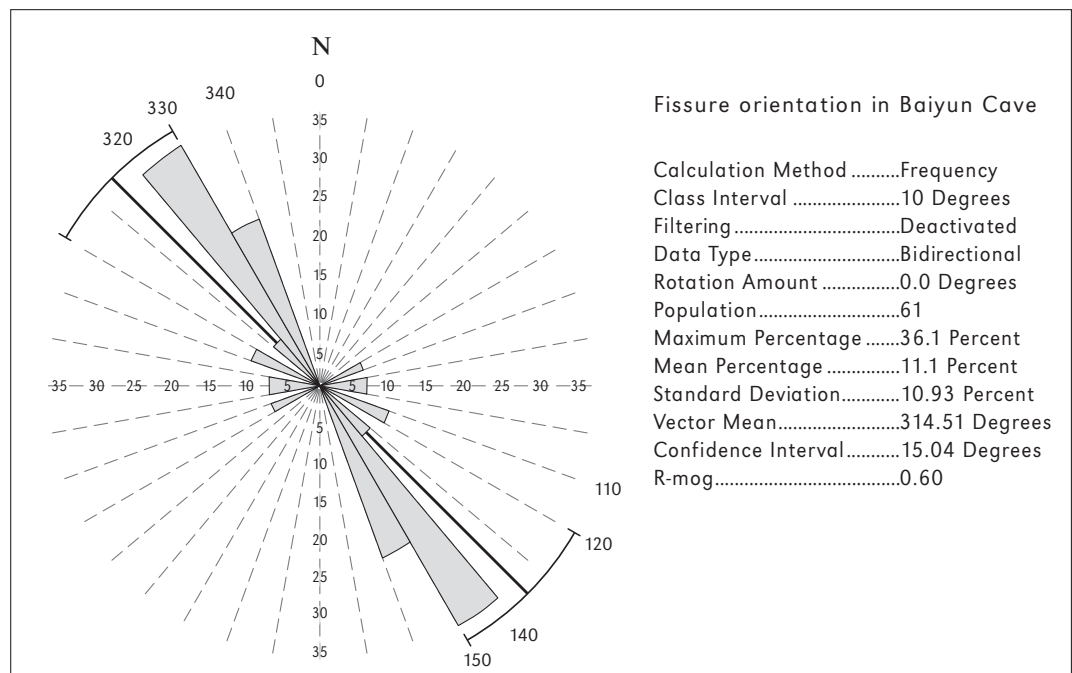
The base of the lowest exposed part of the Qixia formation where the Baiyun Cave is developed (7) is composed of light-brown to orange massive and homogeneous carbonate (*Knez*, 1998).

Fissure orientation in Baiyun Cave

Calculation Method ..........Frequency
Class Interval ......................10 Degrees
Filtering ..................................Deactivated
Data Type..............................Bidirectional
Rotation Amount ................0.0 Degrees
Population .............................61
Maximum Percentage .......36.1 Percent
Mean Percentage ...............11.1 Percent
Standard Deviation............10.93 Percent
Vector Mean.........................314.51 Degrees
Confidence Interval...........15.04 Degrees
R-mog.......................................0.60

The prevalent fissure direction in the cave is N30–40°W (36.1 %) (8) while the second prevailing direction is N20–30°W (23 %).

The prevailing fissure direction and prevailing direction of cave passages of the Baiyun Cave do not compare well. The dip direction of the bedding planes 230°/0–5° also does not match with the most common cave passage direction.

Some fissures on the cave ceiling are filled with calcite, as for example the fissure 57° in the northeastern part of the cave (3). Slightly southern fissure 22° is opened for percolating water. In the middle part of the cave ceiling channels are developed inside the fissure with the dip direction 52°. In the northern part of the cave the prevailing dip directions of the fissures are 52–62°, in the southern part they are 172° and 177°. The dip direction 22° is more rarely represented, but where it occurrs it is strongly expressed and opened for vertical percolation of the water.

**9** View towards the *Naigu shilin*.

The direction of the Baiyun Cave is parallel with the surficial valley, i.e. with the morphological depression in the Naigu shilin (9). The cave is developed under the morphologically lowest part between two morphologically higher shilins. For the development of the cave the almost horizontal bedding planes, tectonically broken and karstified, are important. Only in the northern part of the cave we had the chance to measure the dip direction of the bedding planes 230°/0–5°. On the surface we found limestone with cherts and beneath those a breccia layer. The fissures observed in the cave are not horizontal, but curved for 5–10°.

In the cave we did not find any fissured zones known from Slovene karst (*Šebela*, 1998), we can talk just about single or some parallel fissures or joints as there are in the Ozarks of Missouri (*Šebela et al.*, 1999). Fissures can be several metres long, they resemble faults but no movement was detected on them.

## 11.2  CAVE ROCK RELIEF IN THE BAIYUN CAVE

Cave rock relief is composed by different types of various rock features which completely covered traces of the former or older cave formation. Most of them are of paragenetic origin. Rock features may be due either to traces of water flows or traces of water flow above fine-grained sediments that filled the cave (10).

There is a large channel on the ceiling, up to 8 m wide and up to 2 m deep. Its bottom is flat. Below there are corrosion notches evidencing different levels of sediments that had filled the cave. Some of them are still completely filled up. Water flowed above the sediments. The rim of the channel is covered by small scallops indicating a fast water flow transporting and depositing mostly gravel sediments and incising upwards into the ceiling and thus transforming traces of the older development phases of the cave. The shape of the channel shows fast deposition, distinctive entrenchment into the ceiling and its relatively short time lasting transformation.

Today less water flows through the cave, it deepened the cave river-bed into a larger channel but seasonally the cave is flooded. At vertical fissures the river-bed walls are

*Baiyun Cave – the longest cave in the Naigu shilin.*

**10** Rock features in the *Baiyun* Cave.

dissected into small pillars and knives. Their upper parts, seldom reached by flowing water, are larger, downwards they even wedge out. On the upper part of the bottom channel there are small scallops evidencing the seasonal fast flow. The consequence of frequent variations of the water level are below-sediment rock features, below sediment channels and pits (*Slabe*, 1995, 71) found in leeward places of the lower part of the channel in the river-bed and on its upper part where the channel widens.

One of the more distinctive parts of the cave rocky relief are channels and anastomoses above sediment making a network over a significant part of the main channel ceiling. The above-sediment channels are from 0.05 to 0.5 m in diameter. The deepest have preserved omega shaped cross-section, typical of such channels (*Slabe*, 1995, 62). The crests between smaller channels are usually pointed because of the faster water flow. The network of anastomoses is at several levels, due to gradual prevailing of selected channels during the long-lasting infill of the cave by fine-grained sediments where such features develop (*Slabe*, 1995, 67). Some channels are still filled up by fine-grained sediments.

The rocky surface that is no more reached by the water flow is thinly weathered. This is due to the less moisture condensation on the rocky rim.

### 11.3 CAVE SEDIMENTS

In the Baiyun Cave we found many remains of cave fillings. Because we wanted to find out the age of deposition of the cave sediments we sampled the profile in the northern part of the cave (3, 5).

In front of the cave, at the northern entrance (7) and inside the limestone bedding-plane (230°/0–5°), gravels can be found. Some are more, others less rounded. In some parts gravel can be cemented to conglomerate. The thickness of the layer with gravel and conglomerate in front of the cave is 10–15 cm. Gravel is from sandstone, bazalt and quartz. Minerals as mica, quartz, calcite, and Fe-minerals can be detected in the gravel. The cement has a brown colour and contains a lot of carbonates.

Gravel can be found in different levels showing more generations of cave fillings. The periods of gravel fillings have exchanged with clay fillings. In the northern part of the cave we sampled a 1.75 m thick profile for paleomagnetic analyses (3, 5). These are samples 1 to 4. The upper part of the profile is covered with 5–10 cm thick flowstone. At the place of our sampling profile the flowstone is 5 cm thick. The layer b1 is 5 cm thick reddish sandy clay, sample 1 was taken from it. Below we have a 20 cm thick layer c of sandy clay with brown flowstone. The next is a 15 cm thick layer of gravel (d1) cemented into conglomerate. The prevailing gravel has diameters of 3 cm and less, all gravels are not well rounded. We can find the same layer in the lower part of the profile twice more (d2 and d3). The uppermost layer of gravel cemented into conglomerate (d1) is followed by 5 cm thick laminated sandy clay (e1) from which sample 2 was taken. The layer f represents sandy clay with uncemented gravel, 10 cm thick. The second layer of conglomerate d2 (d = 5 cm) is followed by laminated sandy clay with rare gravel (e2). Sample 3 was taken from this 8 cm thick layer. The lowest conglomerate layer (d3) is 40 cm thick. Sample 4 was taken from the layer e3 (laminated sandy clay, d = 7 cm). The lowest part of the profile (d = 50 cm) represents conglomerate with smaller gravel than in the three upper conglomerate layers.

Conglomerate or uncemented gravel can be found all over the cave. In the northeastern part of the cave the thickness of the gravel layer is 1–1.5 m. In the southern part of the cave there is a place with gravel (d = up to 10 cm) deposited above the anastomoses channels. This cave infilling is situated on the ceiling 4 m above the tourist path; this profile is vertically higher than our profile (3). Regarding the stratigraphic position of both profiles, our sampled profile should be older.

Four samples of the cave sediments (5) were taken for paleomagnetic analyses. Laboratory procedures at the Institute of Geology, Czech Academy of Sciences, were based on progressive demagnetization by an alternating field (AF) to detect components of remanent magnetic polarity in different intervals and to determine moduli and directions of remanent magnetization.

Sediments were sampled into small plastic cubes 20 × 20 × 20 mm. In the laboratory they were measured on the JR 5 spinner magnetometer (*Jelínek*, 1996). All samples were demagnetized by alternating field procedures, up to the field of 1000 Oe in 14 steps. The LDA-3 (Agico) apparatus was used for AF demagnetization.

The remanent magnetization of the samples in their natural state (NRM) is identified by the symbol $J_n$, the corresponding remanent magnetic moment by a symbol $M$. Graphs of normalized values of $M/M_o = F(t)$ were constructed for each analysed specimen.

The volume magnetic susceptibility $k_n$ was measured on the KLY-2 kappa-bridge (*Jelínek*, 1973). Separation of the respective remanent magnetization components was carried out by the multi-component Kirschvink analysis (*Kirschvink*, 1980).

The principal magnetic parameters and the mean values of the moduli of $J_n$ and $k_n$ are documented in Table 1. Values of the moduli of natural remanent magnetization $J_n$ and those of volume magnetic susceptibility $k_n$ of studied sediments in their natural state show big scatter. Samples are characterized by low magnetic (5, sample 3) up to high magnetic with reverse paleomagnetic polarity (5, sample 1).

| No. of 4 samples | $J_n$ (nT) | $k_n \times 10^{-6}$ (SI) | Polarity |
|---|---|---|---|
| 1 | 881.529 | 1172 | R |
| 2 | 37.615 | 1200 | N |
| 3 | 2.144 | 692 | N? |
| 4 | 38.487 | 1447 | N |
| Mean value | 239.944 | 1128 | |
| Standard deviation | 370.709 | 273 | |

**Table 1**
Principal magnetic and paleomagnetic parameters of the samples from the *Baiyun* Cave.
$J_n$ natural remanent magnetization;
$k_n$ volume magnetic susceptibility.
Polarity of samples (N normal, R reverse) derived by the multi-component analyses.

Directions of remanent magnetization inferred by the above given procedures were tested using the multi-component analysis of Kirschvink (1980). A-components of remanence are mostly of a viscous or chemoremanent (weathering) origin, they can be removed by an alternating field with an intensity of 10 up to 60 Oe. Normal and reverse C-components are the most stable in an AC field of 200 up to 1000 Oe.

## 11.4 CHEMICAL PROPERTIES OF THE WATERS IN THE BAIYUN CAVE

The surface above the cave is dissected by numerous protruding rocks and rocky teeth. The pockets in between are filled up with soil where lush vegetation grows during the whole year, yet differently intensively.

The climate of the studied area can be classified as subtropical with an average annual precipitation of 796 mm, average relative humidity of 75.3 % and average annual temperature of 15 °C (for the period 1980–1992). Each year from May to September is the rainy season with 80–88 % of total annual precipitation and the dry season is from October to April (*Kogovšek et al.*, 1997). Due to the relatively high temperature and high humidity during the summer, the circumstances to develop $CO_2$ in soil are favourable in this period.

Red soil which is present today on the surface developed in the tropical climate from sediments originated from the weathered remains of non-carbonate rocks, schist, sandstones, Upper Permian basalt, Eocene lake sediments, and others.

Weathered remains are enriched on silico-ferrous minerals like quartz, opal, amorphous silica, goethite, hematite, sericite, siderite, etc. A sample of red soil from the Central shilin contains 96 % of quartz, 2 % of chloride, 1 % of muscovite and kaolinite and hematite in traces (*Zupan Hajna*, 1998).

Red soil has an important role for dissolution of carbonates. To determine which components of precipitation can be rinsed from the soil, we occasionally soaked the ground samples in distilled water (5 g in 500 ml for 6 days) and after spinning them, we determined in the soil from shilin 170 mg/100 g silica, 50 mg/100 g calcium, 3.6 mg/100 g magnesium, 5 mg/100 g chlorides, and 9 mg/100 g nitrates (*Kogovšek*, 1998).

The Lunan shilin's red soil has the silica/alumina ratio of 2.7–2.8 and pH of 7.8–8.1. The $CO_2$ content of the soil air relates to the quantities of the three main kinds of the soil microbes present and is from 1.3–4.25 % at 16,200–136,000 total microbes number/gram. The modern Lunan soil microbe content is only 60 % of that at the lower altitude at Pingxiang, Guangxi (*Lin*, 1997a).

In the Baiyun Cave tiny percolation and some smaller trickles prevail beside a stream flowing near the tourist path. When visiting the cave, we analysed samples of these waters. While we took samples in the field, we measured the water temperature to the exactness of one tenth of a degree and conductivity (EC, ref. temperature 20 °C) to 1 % of measurements (July 1996 with the LF 91 – WTW apparatus, September 1997 and November 1998 with the LF 196) and also the pH of the samples (pH 90 – WTW apparatus). The comparison and intercalibration of both conductivity meters indicated a fairly good correspondance. In October 1999 we measured EC, temperature and pH with the Multiline-meter WTW apparatus. Carbonate, Ca, and Mg contents were determined titrimetrically, according to the standard methods (*Standard Methods for the Examination of Water and Wastewater*, 1992).

### 11.4.1 Results of the physical measurements and chemical analysis

After intensive rain there are numerous tiny drippings and some smaller trickles in the cave, in the dry period the discharge diminishes substantially and some drippings and trickles dry up. This indicates a relatively well-karstified and permeable cave roof allowing gradual and relatively fast draining of the recharge area of trickles until they are dry.

High carbonate levels and high total hardness of percolation water show intensive rock disolution. One litre of rain dissolves and transports from the cave ceiling 280–370 mg of $CaCO_3$. Contemporary measurements of conductivity (EC) show linear interdependence with concentration of carbonates and with total hardness (11, Table 2). In percolation water we determined a low content of silica, in concentrations from 0.2–0.3 mg $SiO_2$/l.

We sampled the percolation waters and water stream in the Baiyun Cave at different hydrological conditions: in September 1997 at high water level after more intensive rain, in October 1999 at lower discharges and in November 1998 at very low discharges when at some places dripping was not active.

The water stream flowing through the cave has in its initial part ($L_1$) a high carbonate level (Table 2) from 235 to 325 mg $CaCO_3$/l (4.09–6.52 meq/l) and high total hardness like the percolation water in the cave that is oversaturated and deposits sinter. Its water does not contain solid particles at higher discharges as is the case with the nearby superficial streams. The relatively large passage allows good air circulation, so on the relatively short way through the cave the carbonates are deposited (up to 80 mg $CaCO_3$ from one litre). Calcium is deposited mostly, while magnesium remains in solution due to
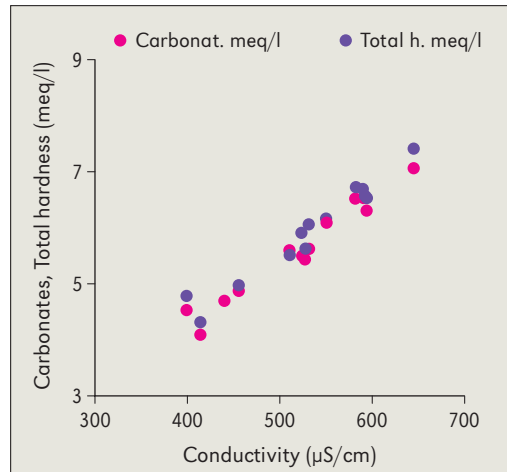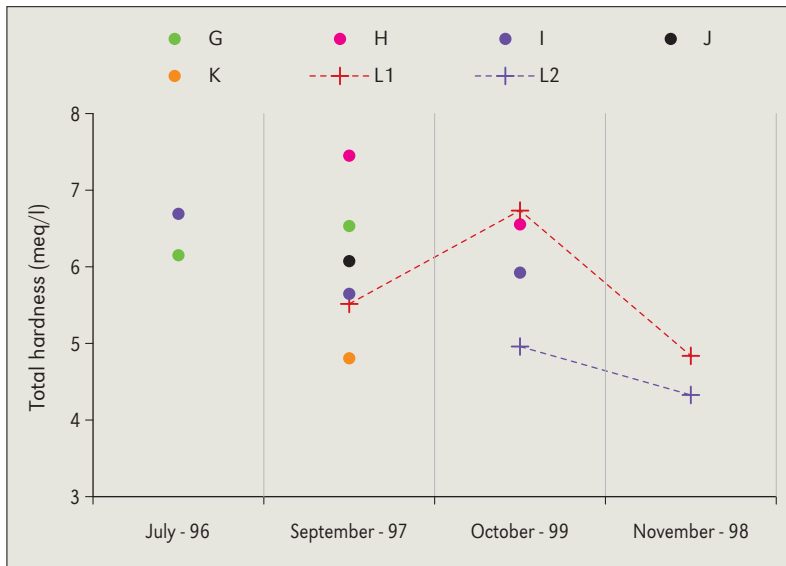


**11** Linear correlation between conductivity and carbonates, total hardness.

**Table 2** Chemical characteristics of the percolation water (drippings and trickles G, H, I, J, and K) and of the water stream (L1 – at the initial part of the cave; L2 – at the end of the cave) in the Baiyun Cave and L3 – at the spring.

| Month | Place | Discharge (ml/min) | T (°C) | SEC (µS/cm) | pH | Carbon. h. (meq/l) | Ca (meq/l) | Mg (meq/l) | Total h. (meq/l) | Ca/Mg ratio | Noncarbon. h. (meq/l) |
|---|---|---|---|---|---|---|---|---|---|---|---|
| July | G–96 | 100 | 17.3 | 550 | 7.75 | 6.08 | | | 6.16 | | 0.08 |
| September | G–97 | 50 | 17.6 | 594 | 7.44 | 6.32 | 5.35 | 1.19 | 6.54 | 5.5 | 0.22 |
| October | G–99 | dry | | | | | | | | | |
| September | H–97 | 10 | | 645 | 8.03 | 7.05 | 5.75 | 1.67 | 7.42 | 3.4 | 0.37 |
| October | H–99 | | | 591 | 7.88 | | 5.12 | 1.44 | 6.56 | 3.6 | |
| July | I–96 | 400 | 18.0 | 590 | 7.15 | 6.52 | | | 6.68 | | 0.16 |
| September | I–97 | 50 | 16.4 | 527 | 7.97 | 5.43 | 4.27 | 1.36 | 5.63 | 3.1 | 0.20 |
| October | I*–99 | | 16.9 | 524 | 7.94 | 5.50 | 4.36 | 1.56 | 5.92 | 2.8 | 0.42 |
| September | J–97 | 100 | 16.4 | 532 | 7.88 | 5.63 | 4.47 | 1.59 | 6.06 | 2.8 | 0.43 |
| September | K–97 | | | 398 | | 4.54 | 2.63 | 2.16 | 4.79 | 1.2 | 0.25 |
| September | L1–97 | several l/s | 16.8 | 511 | 7.63 | 5.59 | 4.63 | 0.88 | 5.51 | 5.3 | |
| October | L1–99 | 0.1 l/s | 16.4 | 582 | 7.29 | 6.52 | 5.36 | 1.36 | 6.72 | 3.9 | 0.20 |
| October | L2–99 | | 16.5 | 455 | 7.50 | 4.86 | 3.72 | 1.24 | 4.96 | 3.0 | 0.10 |
| November | L1–98 | | 16.4 | 441 | 7.44 | 4.70 | 3.95 | 0.88 | 4.83 | 4.5 | 0.13 |
| November | L3–98 | | 17.9 | 413 | 7.20 | 4.09 | 3.51 | 0.80 | 4.31 | 4.4 | 0.22 |

**12** Chemical properties of percolated water in the *Baiyun* Cave.

the higher solubility. According to these properties, we conclude that the water of the water flow is collected from a wider vadose area, probably geomorphologically lying higher, outside of the cave area, providing its abundance, as it appears in the cave as the water flows with discharge up to some litres per second. During high discharge (several l/s in September 1997) it reached the lower carbonate level and lower total hardness (12) than they are during medium discharges (0.1 l/s in October 1999). This is characteristic for the percolation water in the vadose zone after abundant rain when large flood waves are formed. The lowest levels of carbonates and total hardness were defined at the lowest discharges (November 1998) when the water flow becomes the water probably only from a limited part of the less permeable recharge area. Also that is accordingly with observations of the water dynamic in the vadose zone that reflects in the water chemical composition (*Kogovšek* and *Šebela*, 2004).

The Ca/Mg rate of percolation water is from 2.8 to 5.5. These levels also show the presence of dolomite in the cave roof. Only water flowing into a rimstone pool (K) (13, 14, Table 2) had lower calcium and little higher magnesium levels and therefore the lower ratio Ca/Mg = 1.2. Probably the inflow water deposited $CaCO_3$ previously as is shown by substantially lower calcium and carbonate levels in the water. We suppose also a possible influence of evaporation. The non-carbonate admixture level in the sampled water was from 0.1 to 0.4 meq/l.

Waters flowing into the Baiyun Cave today are oversaturated and deposit a part of carbonates in the cave. The total hardness of percolation waters reaches high values, up to 370 mg $CaCO_3$/l, what means dissolution in the cave ceiling which is a little slow, due



**13** Sampling the water flowing into the rimstone pool.

to weak dripping and small trickles. More intensive is dissolution in the recharge area of the water flow that reaches discharges of several litres per second and total hardness of 336 mg $CaCO_3$/l. In comparison with oversaturated water in Škocjanske jame, Slovenia, where percolation water reaches the values of 300 mg $CaCO_3$/l (*Kogovšek*, 1984), dissolution in the wider vadose zone of the Baiyun Cave is higher. Unfortunately, our measurements did not include the detailed observation of the flood waves directly after intensive and abundant rainfall that could give a lot of information on the water dynamic.

CONCLUSION

The rock relief of the cave indicates several periods of the cave development. The oldest rock features in the cave are above-sediment channels and anastomoses belonging to the time when the cave was entirely filled by sediments. In the upper part these were fine-grained sediments which condition the origin of such type of rock features. A large ceiling channel covered by small scallops developed when faster water flowed in the upper part of the cave depositing gravel. This water flow partly transformed the above-sediment rock features. In some places gravel is stuck on. The youngest period of the cave evolution is shown by the floor channel which is a narrow part of a deepened river-bed; this flow seasonally flooded the cave and caused below-sediment rock features.

The origin and development of cave passages in the Baiyun Cave (15) is tightly connected with formation of a superficial part of the shilin and especially with the ground-water level. An active water flow may still be seen in the cave today. The cave consists of one important cave passage developed in the general direction NW-SE. The most frequent fissure directions do not correspond with the most frequent passage direction. 59.1 % of all the surveyed fissures are in the N20–40°W direction with the confidence interval of 15.04°. The cave passage is developed in two main directions having 50° of

difference (6). The prevailing passage directions are N0–10°W (36.6 %) and N110–120°E (27 %). At the northern entrance into the cave we measured a dip of the bedding planes 230°/0–5°. Due to paragenesis, additional strata could not be measured in the cave. The cave passage does not strictly follow the fissure directions and also not the dipping of the strata N140°E.

In 1999 the most frequent passage directions of four caves, three of them near the Lunan shilin and one in the Naigu shilin, were shown by a rose diagram (*Kogovšek et al.*, 1999). The most common passage direction is N0–10°W (23.7 %), on the second place is direction N140–150°E (16 %) and on the third direction N110–120°E (12.5 %). The passage in the Baiyun Cave corresponds to the directions N0–10°W and N110–120°E.

In all probability, the most frequent directions of the Baiyun Cave passage reflect the wider geological setting of the terrain. The north-south direction is parallel to the Xiaojiang fault and the direction N110–120°E to the southern Red River fault (1). Considering that the region around Kunming is tectonically active (*Wang* and *Burchfiel*, 2000) and considering the age of the cave sediments in the Baiyun Cave (112.3–117.9 ka BP) (16) and several older periods of the cave development we can rank this cave at least in the Upper Pleistocene (less than 800 ka ago). It was determined from the absolute age analyses of the related secondary carbonate accumulation (*Yu* and *Yang*, 1997) that the earliest modern shilin had begun to evolve in the Naigu region in the Late Pliocene (about 2 million years ago).

In speleomorphological meaning the cave developed from an anastomoses network and some channels evolved in smaller and in one larger cave passage. In the cave there is evidence of alternating of several periods of depositing the sediments and periods of fast water flows and flood waters. Due to tectonic changes a sharp collapse of the ground-water level followed and the river-bed started to incise.

The total hardness of percolating waters in the Baiyun Cave reaches high values what means intensive dissolution of carbonates in the cave ceiling. The water flow in the cave mainly collects water from the vadose zone in the wider vicinity of the cave. Because the percolation water and water flow in the cave are oversaturated with the high content of carbonates, to 370 mg $CaCO_3$/l, an important part of them is deposited in the cave.

For paleomagnetic analyses only four oriented samples have been investigated of the 1.75 m thick profile. Magnetostratigraphic investigations defined normal and reverse polarity. The top part of the profile (5) shows reverse polarity (sample 1); the other part shows the long normal magnetozone (samples 2, 3, 4). The correlation with standard paleomagnetic scales is problematic because there are more possibilities (16). Sample 1 which is highest in the profile (5) probably belongs to the reverse Blake event (112.3–117.9 ka BP). Samples 2, 3 and 4 with normal polarity belong to the Brunhes chron (they are younger than 780 ka BP).

We think that the long-lasting periods of relatively frequent smaller variations of underground water can slower the development of the shilin at the surface. Younger, dramatic lowering of the ground-water level probably caused faster development of the shilin. Modern formation of the shilin at the surface is, beside other factors, influenced by the intensive dissolution of those lowered parts that are covered by soil and vegetation thus generating greater quantities of $CO_2$ and more intensive dissolution of the rock which results in over-saturated water in the cave.

The formation of the Baiyun Cave is directly connected with the development of the Naigu shilin. The formation of the karst underground and surface features depends on the regional tectonic deformation on the Cenozoic extension of the studied area.



Ma

excursion (R)
26.0–27.1 kyr B.P.

excursion (R)
37.4–46.8 kyr B.P.

the Blake event (R)
112.3–117.9 kyr B.P.

Brunhes
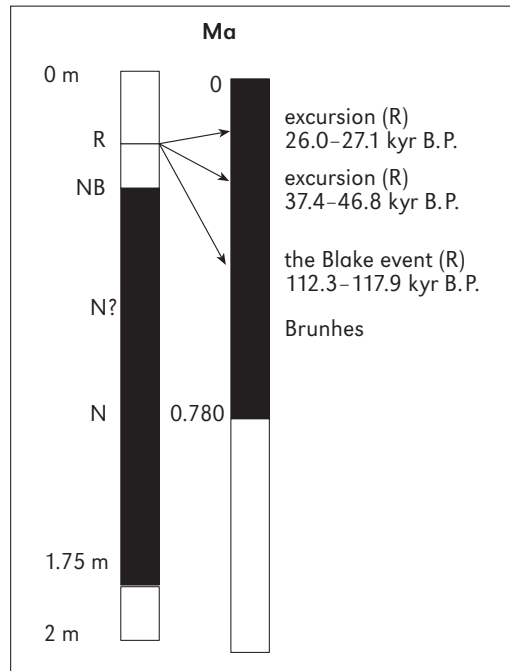
*Baiyun Cave – the longest cave in the Naigu shilin*

**16** The correlation of the *Baiyun* Cave profile with standard paleomagnetic scales.

# SHUILIAN CAVE IN THE UPPER REGION OF THE CHANG JIANG RIVER

**12**

MARTIN KNEZ, JANJA KOGOVŠEK, ANDREJ KRANJC, HONG LIU, TADEJ SLABE, METKA PETRIČ

Three of the largest East Asian rivers, Chang Jiang (Yangtze), Lancang Jiang (Mekong), and Nu Jiang (Salween), take rise relatively close in the eastern part of the Tibetan high plateau, but reach the ocean thousands kilometres apart: Chang Jiang in the Yellow Sea near Shanghai, Lancang Jiang in the South China Sea at Hoshiminh in southern Vietnam, and Nu Jiang in the Andaman Sea near Yangon (Myanmar). In the east where the Himalayan arc narrows and turns southeast- and southwards the mentioned rivers cut in deep parallel valleys. At a length of 250 km they flow almost parallel, distant from one to another for mere 20–50 km. Then the Chang Jiang turns east in its famous First Bend, while the other two rivers continue southeast and south, respectively. Characteristic for this section of the northwestern most part of Chinese Yunnan Province are parallel mountain chains consisting of peaks above 6500 m, intermediate plains and deeply cut valleys (to 3000 m of depth) of these three rivers (*Du*, 2007). Owing to geologic and physiographic reasons, landscape beauty, ecologic characteristics and extraordinary biologic diversity, China founded the Three Parallel Rivers National Park in this territory and in its frame a number of protected areas that were inscribed in 2003 to the UNESCO World Heritage List as Protected Areas of the Three Yunnan Parallel Rivers (1). The core of the protected region measures almost 9400 km² and the transitory zone additional 7600 km². It is situated between 28°12' and 26°40' north geographic latitude (*Unesco*, 2007).
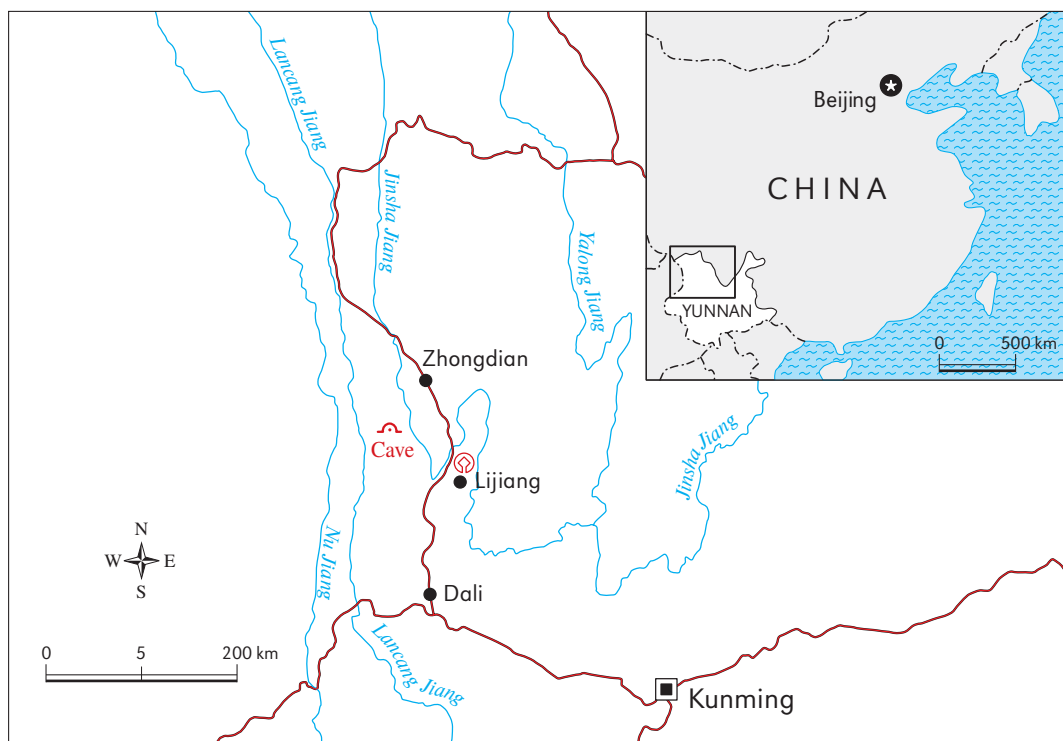


**1** Location of the studied area (drawn by F. Drole).

**2** *Jinsha* River.

Among rocks in this territory there are also carbonates, and they are karstified. One of the most well known landscape attractions is a narrow and deep gorge through which the Chang Jiang (in this area called Jinsha, meaning the Golden Sand) roars, the canyon being called the Tiger Leaping gorge. A large part of the eastern slopes of the Jinsha River valley, several ten kilometres above the First Bend, consists of limestones. Owing to very steep and uniform slopes, surface karst phenomena are rare, but the karst is manifested by typical karst hydrology. Above the bottom of the valley, usually 50–150 m high, a number of strong karst springs occur from which water flows in surface streams into the Jinsha River (2).

One among these karst springs is also the original Shuilian spring cave situated near the town of Zhongdian (Zhongdian County, renamed into Xianggelila meaning Shangri-La). The river flows here in its bed which is partly cut into solid rock, and partly in alluviums. The alluvial gravel and sand bars are especially extensive in sheltered sites. The foot of a slope, several tens of metres above the river, is gently inclined, and there the village of Chang Yue extends. Rocky slopes rise above it, very steep interrupted at several places with vertical cliffs. About 70 m above the river two entrances open to the Shuilian Cave. The brook flows from the lower entrance and falls a little below as a waterfall several tens metres deep. About ten metres above it is the dry entrance. The splashing waterfall (3) gave the cave its name, Shuilian meaning the Water Curtain.

Hydrologic characteristics of the wider area are strongly influenced by the position of the Chang Jiang River and by the geologic contact of rocks of various permeability. The river that plays here the regional erosion basis has cut down its bed deep into the metamorphic rocks. Therefore the contact of metamorphosed sandy siltstones forming a hydrogeologic barrier with overlying metamorphosed calcitic siltsones extends in this area about 50 to 100 m above the river. Springs occur at the contact discharging water from the carbonate aquifer. Some of them are used for energy generation owing to their favourable position above the river valley bottom. Water is canalized in pipes to hydro-

126

**3** Water falling from the *Shuilian* Cave making a 'water curtain'.

electric stations that take advantage of the water gradient for electric energy production. The observed spring from the Shuilian Cave, however, is not used for this purpose. The water is led into the village to a smaller mill wheel.

This part of the Three Parallel Rivers territory underwent a rapid and strong tectonic uplift, and the big high energy rivers deeply cut down their valleys accordingly with the uplift. This is indicated by morphology of the slopes as well as by karst hydrology. Erosion processes as deepening of the valleys were faster than underground karstification. The underground discharge was not able to cope with the surface processes and it lagged behind them. As a result several karst springs, including the one of the Shuilian Cave, were left 'hanging' about 100 m above the valley floor. Similar phenomena can be found also in the Slovenian alpine karst where karst water in a number of springs, as in the case of Savica, Soča and Boka, takes rise high in the slopes above the floor of the valleys that were during Pleistocene additionally deepened by glaciers.

The valley slopes of the Three Parallel Rivers are presently almost bare or they are overgrown with sparse bushes, typical for arid regions, and partly by scarce pine tree woods. This is a result of the human interference with the natural environment. During the times of the highest population pressure on the land all possible surfaces were used for agriculture and a lot of woods were cut down. This did not affect vegetation only, but had wider and long-term consequences. One of them was also a radical increase of soil erosion which is recorded in sediments. They can be observed at many places in cuts of small valleys and ravines that descend from the slopes towards the river. On the fluvial sediments (sand and gravel) the soil deposits might be up to several metres thick. The profiles clearly show that the soil did not form *in situ* but was deposited there by other processes, perhaps as colluvial soil (4).

As the climate is relatively dry, the forest does not renew readily. At present, the societal and economic circumstances changed. In many places the abandoned culture terraces can be seen and the trees and woods are getting more abundant. Reforestation

127

**4** Quick change from deposition to erosion illustrated by sediments: fluvial sand (grey) covered by thick soil (reddish brown).

is in course everywhere. Owing to hard accessibility, reforestation is carried out mainly by planes that sow pine-tree seeds from the air.

The Shuilian Cave, the entrance of which is situated 70 m above the average water level of the Chang Jiang River, is 1190 m long (5). In the entrance part it consists of two passages that after the first third of the cave joined into a unique water passage. The upper passage is old and dry and through the lower passage flows the water stream that discharges in the waterfall.

Position, shape, geologic, speleomorphologic and hydrogeologic investigations shed light on the way of the cave formation and the most important stages of its evolution, but also on the characteristics of the karst aquifer, the waters that flow along the contact with less permeable rocks, and the development of the rapidly incising canyon of the Chang Jiang River.

## 12.1 GEOLOGIC STRUCTURE

In the narrow surroundings of the cave Lower and Middle Devonian rocks are exposed. The belt of the Devonian beds extends SE-NW and is separated from the beds in the northeast and southeast by two deep faults. In the northeast Devonian rocks are in the contact with Upper Carboniferous limestones and shales and in the southwest with Middle to Upper Silurian limestones and dolomites. All the beds mentioned are strongly folded or tilted to almost vertical positions. Along both faults that delimit the Devonian beds compression occurred in geologic history which led to the forming of a folded

128

**5** Survey of the *Shuilian* Cave by Erin Lynch.

## C3-1 Shuǐ Lián Dòng
### Water Curtain Cave 水帘洞
(47G-A8-1)

Qi Zong, Deqin
Yunnan, P. R. China
中国云南德钦犹其宗

WGS84 UTM 47R 0551716 3056182
Altitude 1965m　海拔1965米

Length 1,190m　长度 1,190米
Vertical range +97m　垂直幅度 +97米

Surveyed to BCRA Grade 5d
by Hong Meigui CES January 2004

Cartography by Erin Lynch

### PLAN
平面图

Scale 1:2000
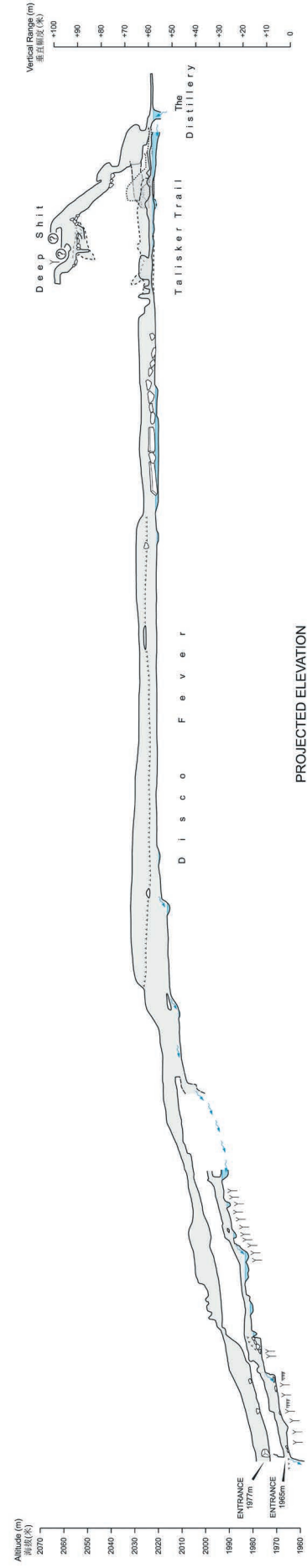比例尺 1:2000

0　10　20　30　40　50　100m

N

Deep Shit

Talisker Trail

The Distillery

Disco Fever

The Writing's On The Ceiling

submerged shaft
bat roost
deep
sump (open)

ENTRANCE 1965m
ENTRANCE 1977m

2023m 2027m 2047m 2062m 2025m 2023m 2022m 2023m 2006m 2013m 2016m 1982m 1959m 1986m
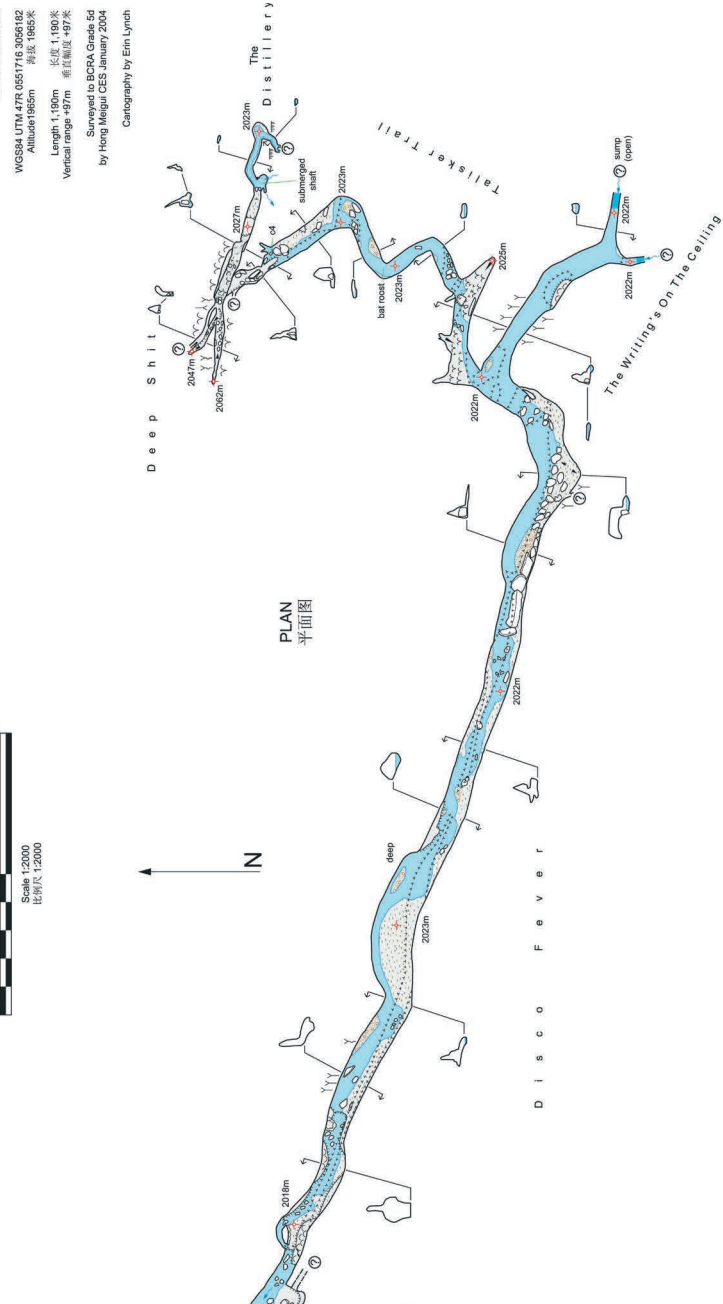
### LEGEND

| | | | | |
|---|---|---|---|---|
| Passage walls | | 861m Altitude | | Mud/clay |
| Unsurveyed/assumed walls | | Guano | | Cobbles |
| Underlying passage | | Unexplored | | Large breakdown |
| Drip line | | Water flow | | Boulders |
| Cliff with climb (3m) | | Water | | **Elevation symbols** |
| Ceiling height change | | Drip/inlet | | Ledge/traverse |
| Ceiling channel | | Sump | | Ceiling channel |
| Slope (points downhill) | | | | |

Stalagmite · Stalactite · Column · Curtain · Soda straws · Popcorn · Calcite mound · Flowstone

Survey symbols are based on the US 1999 standard. All measurements are in metres. All cross sections are to scale. All altitudes are in metres above sea level and are based on BCRA Grade 5 surveys from GPS points in the WGS84 datum. Altitude values are for individual survey stations, which are not a consistent height above the passage floor. For lists of survey team members and the original survey data, see www.hongmeigui.net

### PROJECTED ELEVATION
剖面图
090° – 270°

Vertical Range (m)
垂直幅度 (米)
+100 +90 +80 +70 +60 +50 +40 +30 +20 +10 0

Altitude (m)
海拔 (米)
2070 2060 2050 2040 2030 2020 2010 2000 1990 1980 1970 1960

Deep Shit
Talisker Trail
The Distillery
Disco Fever

ENTRANCE 1977m
ENTRANCE 1965m

129

structure in which the beds dip on an average 80° in the northeast, and between 30° and 60° in the southwest.

The cave formed at the contact between Lower and Middle Devonian rocks (6). Lower Devonian rocks are calcitized and metamorphosed sandy siltstones and Middle Devonian high grade metamorphic calcitic siltstones of high carbonate content (Table 1).

Calcitized and metamorphosed sandy siltstones are finely bedded and of a red brown colour due to the presence of iron oxides. Alizarine colouring is intense, calcite contents exceed 60 % (sample 1) (Table 1). The preponderance of sparitic calcite is observable also macroscopically. Aggregates of polycrystalline quartz attain 0.5 mm. Quartz contents are estimated at 5–7 %. Iron oxides impregnate the rock and in addition they occur in irregular aggregates and on original schistosity planes with muscovite and sericite particles. The rock is cut by calcite veins of several generations.

**Table 1**
Calcimetric data of rock samples. Samples 1–3 are calcitized and metamorphosed sandy siltstones of the lower Devonian age; samples 4–9 are Middle Devonian metamorphosed calcitic siltstones.

| Sample | CaO (%) | MgO (%) | Calcite (%) | Dolomite (%) | Total carbonate (%) | CaO/MgO (%) | Insoluble residue (%) |
|---|---|---|---|---|---|---|---|
| 1 | 33.64 | 1.93 | 56.34 | 7.74 | 64.08 | 17.43 | 35.92 |
| 2 | 41.18 | 3.20 | 65.99 | 13.83 | 79.82 | 13.64 | 20.18 |
| 3 | 50.47 | 0.81 | 87.09 | 3.68 | 91.77 | 62.31 | 8.23 |
| 4 | 55.29 | 0.56 | 97.27 | 2.58 | 99.85 | 98.73 | 0.15 |
| 5 | 55.21 | 0.62 | 96.97 | 2.85 | 99.82 | 89.00 | 0.18 |
| 6 | 55.18 | 0.64 | 96.87 | 2.95 | 99.82 | 86.22 | 0.18 |
| 7 | 55.09 | 0.58 | 96.77 | 2.67 | 99.53 | 98.37 | 0.47 |
| 8 | 55.12 | 0.56 | 96.97 | 2.58 | 99.55 | 98.42 | 0.45 |
| 9 | 55.18 | 0.64 | 96.86 | 2.95 | 99.81 | 86.06 | 0.19 |

Calcitized and metamorphosed sandy siltstones, a few decimetres thick, that lie just below the metamorphosed limestones are finely laminated, the laminas being up to 2 mm thick. The cross-bedding pinches out lentiformly at the contact with the Middle Devonian beds. In areas where calcitization has not been entirely completed, the rock is of alternating reddish brown and dark grey colours. Reddish brown lenses contain iron oxide minerals, most probably limonite. Colouration with alizarine red is very intense, the indicated calcite contents being high, between 80 % and 90 % of the total rock (samples 2, 3) (Table 1). The rock consists of sparitic calcite (at least 70 %). In very low amounts polycrystalline quartz is present (to 5 %), and in traces sericite-muscovite (up to 2 %), the rest being represented by iron oxides, chiefly limonite. The latter occurs as impregnations and is concentrated on schistosity planes that apparently coincide with the bedding planes.

The original rock of the calcitized and metamorphosed sandy siltstone was most probably silty sandstone or sandy siltstone. The rock was metamorphosed and most probably strongly calcitized during speleogenesis.

Heavy metamorphosed calcitic siltstones of the high carbonate contents (samples 4–9) (Table 1), higher in the cave profile, are bedded with the beds up to several 10 cm thick. The rock is strongly altered. The original rock was sedimentary, most probably calcitic siltstone and fine grained sandstone that were later metamorphosed to marble-like rock (7). During this process iron oxides separated from phyllosilicates owing to substitution by calcite.

A smaller part of the lower extent of the passage was formed by erosional processes in the less permeable beds of calcitized and metamorphosed red sandy siltstones. The

**7** Fine grained sandstone that was later metamorphosed to marble-like rock.

reason for the high calcite contents in these beds are also abundant fissures filled with sparitic calcite.

On dissected sides of the passage variable resistance of individual carbonate beds in the vertical direction is observable.

The rocks in this area became densely fissured as a result of intense tectonic activity. Later, the fissures, mostly up to 1 mm wide, became filled with calcite cement. A somewhat stronger fault, along which the shift can be seen, occurred in the central part of the passage.

## 12.2 ROCK RELIEF OF THE CAVE AND THE SHAPE OF PASSAGES

The cave rock relief and longitudinal and transversal sections of passages give insight into the way of water flow through the cave, the mechanism of shaping the cave and the most important stages of its development.

The rock relief can be divided into two groups of rock features. The first group assembles rock features that indicate slower water flow through the cave when it was inundated, and the second group features that indicate faster water flow velocities. The latter comprise traces of the present water flow in the lower part of the water passage and in conduits of smaller cross-section, before the discharge, along the entire periphery. The cave originated and has been shaped at the contact of underlying calcitized and metamorphosed sandy siltstones and intensely metamorphosed calcitic siltstones of which the periphery of the passage's upper parts consists. The prevailing process in the lower parts is consequently mechanical erosion and in their upper parts dissolution of rocks. With the first process the cave is evolving also today.

Traces of the water flow through the formerly flooded cave are large scallops and ceiling pockets (8) as well as wall pockets. They were shaped by the slower water flow. They arose in the beds of metamorphosed calcitic siltstones. Large scallops (*Slabe*, 1995) with diameters of up to 0.7 m are best preserved on the passage walls. The deepest ones, to 15 cm, occur at the bedding planes. The most characteristic features are the pockets. They can be simple or composed. Some of them are several (up to 3) metres high. The deepest ones that formed at the fissures tend to narrow upwards. They consist of several floors or their tops may be composed of several pockets. They are elongated along the fissures, composed, they may be stringed one next to the other. In places, they are fastened together into ceiling cupolas. On parts of the ceiling that were

**8**   A ceiling pocket.

shaped along a well expressed vertical fissure, a ceiling channel (9) can form whose top developed into pockets. The ceiling channel is in places several metres high, while in other places it completely pinches out. On such places, on the walls of the ceiling channels and on the walls of the cupolas vertical and semi-circular notches occur that may be several metres long. At the bedding planes and at the widest open parts of the contacts of different rocks several metres deep wall pockets formed. Their upper part is dome-like shaped, but the lower part is more or less horizontal. Such a shape is governed by the lower, less carbonate containing rock or sediments that deposited in the lower part of the wall pocket and that preserved it from faster rock dissolution. Quite often several smaller pockets are connected into a wall cupola, and they rise, like connected into a vertical channel, one above the other.

Characteristic rock features are also wall notches (*Slabe*, 1995). They formed at the contact of two different rocks and at the bedding planes. Some of them are asymmetrical and semicircular. Their upper semicircular part is in metamorphosed calcitic siltstones and the flat bottom on the underlying less permeable rock (5). In other places wall notches are better developed in the lower, less carbonate rock, while the metamorphosed calcitic siltstone stands out as a projecting step in the wall. Elsewhere, there are no morphologic features at the boundary between two rocks. The wall notches are often ribbed with scallops and dissected by wall pockets.

Most of the upper part of the passage circumference has been shaped by water that has been lastingly condensing in the upper parts of the passage. On the ceiling and walls remains of sinter are found, an indication of the changed microclimatic conditions in the passage. The cave obviously became wider beeing opened to exterior influences. The surface of the rock and of sinter is finely dissected. At the better soluble parts of the rock, mainly cut by fine cracks that pass through the rock in various directions, small etchings formed that reach up to 1.5 cm in depth.

The lower parts of the passage that are frequented by the water flow were shaped predominantly by a mechanic action of the water load that included also sand and smaller pebbles. So, potholes, scallop-like shapes and wall notches, wall pockets and floor channels were formed. Longitudinal wall notches with a diameter of decimetre-size are developed along the bedding planes. Some of them deepen small wall pockets. Their diameters may attain half a metre. They are the result of the mechanical action of the water flow that tears off the rock particles and chisels the rock with the transported material it drives into whirling. Along the entire water passage and also on the floor of dry parts of

**9** A ceiling channel.

*Shuilian Cave in
the upper region
of the Chang Jiang
River*

**10** A cross-like shape of
the cave passage.

the cave floor channels can be traced. They represent a trace of cutting of the water flow into the rocky floor over the entire surface and in broader parts of the cave also of periodic smaller water streams that flowed only over the lowest parts of the channel. The surface of the channel has been mechanically smoothened and rounded, especially somewhat higher, 1–1.5 m above the floor, in the reach of higher waters. Potholes are chiseled into the floor of the channel that measure up to 0.75 m in diameter. However, the smaller ones measure only a few cm. In the prevailingly calcitized and metamorphosed sandy siltstones the water flow that whirls along the rough surface of the rock consisting of grains excavates also scallop-like elongated hollows, up to 3 cm long. Also these features are mostly the consequence of mainly mechanical excavation of the rock by mass of the water current which also carries insoluble particles. In the entrance part of the cave the walls and sinter are covered by mosses and liverworts that finely dissect their surface.

From the transversal sections of the passages various ways of formation of the cave at the contact of two rocks can be deduced. Water that filled the empty space in the flooded zone first percolated along the contact cut by vertical cracks. At the crack a vug formed that first spread along the contact of the beds of different rocks and then spread upwards into the fissured upper part in the metamorphosed calcitic siltstone. In the flooded zone consequently a cross-like shape formed with a larger, higher upper part (10). After lowering of the water level the water current kept eroding only into the calcitized and metamorphosed sandy silstone and it deepened and widened the lower part of the passage. Certain smaller passages preserved the prevailingly round cross-section. Their larger part formed in the metamorphosed calcitic siltstone. In the lower, metamorphosed sandy siltstone, however, they formed below a semicircular floor channel (11). Such passages did not form at distinct fissures. The cross-section of the larger passages, on the other side, indicates that they originated from joining of several smaller

**11** Cross-section of the passage with the larger upper part developed in the rock of higher carbonate content.

circuits. Their ceiling consists of several arches. The contact of the described rocks was not of uniform permeability, however. The higher water permeability at the vertical fissures was mentioned already. The parts of highest permeability assumed the part of water conduit, while the impermeable parts of the contact remained preserved. In more spacious parts of the passages pillars can be seen that are as a rule the narrowest at the contact, they are often indented by circular wall notches, while upwards they widen into the vault of the cave ceiling.

## 12.3 HYDROGEOLOGICAL CHARACTERISTICS

On the day of our visit water flowed from the Shuilian Cave through the lower passage at 1965 m a.s.l., while in the interior we reached water through the upper dry passage after approximately 150 m. The discharge was not measured, but was estimated at about 100 to 200 l/s.

The basic physical parameters of water were measured and a sample for the chemical analysis collected. In the cave that has developed at the contact of two lithologically differing rocks, the water current was cut into underlying metamorphosed sandy siltstones. There were no appreciable discharges of percolating water through the ceiling consisting of carbonate rocks on the day of our visit. An exception was a smaller trickle of water in which the specific electric conductivity was measured.

The river has several surface affluents. Two of them encircle the recharge area of the Shuilian spring. In the field we visited the left affluent that flows into the river about 1.5 km northwards. Also in this ravine that is equally cut into metamorphosed sandy siltstones several springs were observed in the slope above the river bed. The highest contribution to the flow of the surface stream comes from a larger spring near Shuilian, situated higher up in the ravine just above the river-bed at the contact with metamor-

**12** A spring near *Shuilian* recharges the left affluent of the *Jinsha* River.

phosed calcitic siltstones (12). At the spring the basic physical characteristics of water were measured and a sample for the chemical analysis collected (Table 2). The discharge of the spring was estimated to 200–300 l/s. The described situation was recorded in the time of low to medium waters at the beginning of the rainy period. In view of climatic conditions higher flows can be expected after the rainy season peak towards the end of the summer.

**Table 2**
Physico-chemical characteristics of the sampled waters (28 May 2007): T – temperature; SEC – specific electric conductivity; Ca + Mg – total hardness; Ca – calcium; Ca/Mg – ratio calcium/magnesium; Cl⁻ – chlorides.

| Place | T (°C) | SEC (µS/cm) | Carbonates | Ca+Mg | Ca | Ca/Mg | Cl⁻ (mg/l) |
|---|---|---|---|---|---|---|---|
| | | | (meq/l) | | | | |
| Water flow in Shuilian | 9.2 | 154 | 1.73 | 1.72 | 1.48 | 6.4 | 2 |
| Spring near Shuilian | 9.3 | 165 | 2.01 | 1.88 | 1.52 | 4.2 | 1 |
| Percolating water | | 355 | | | | | |

Above the river and the spring, the slope rises steeply, and it reaches about 10 km eastwards the high plateau with an altitude over 4000 m a.s.l. There are exposed rocks of very low permeability on which precipitation water collects in small lakes and surface streams. At the contact with carbonate rocks of higher permeability it sinks underground. It is possible that it also flows to the observed springs, but additional investigations would be needed to verify this connection.

## 12.4 RESULTS OF THE WATER ANALYSES

The ground-water in the Shuilian Cave sampled at the spring near the entrance on 28 May 2007 displayed the temperature of 9.2 °C and specific electric conductivity (SEC) of 154.4 µS/cm. The low SEC value was confirmed also by the chemical analyses. The water contained only 1.73 meq/l carbonates (106 mg $HCO_3^-$/l), and total hardness of 1.72 meq/l (86 mg $CaCO_3$/l). Calcium concentration was 1.48 meq/l (30 mg $Ca^{2+}$/l), and

followingly the ratio Ca/Mg = 6.4. The water contained only 2 mg Cl⁻/l and low sulfates concentration, only a few mg/l (Table 2).

The relatively low water temperature indicates longer residence in the wide and high hinterland while the low SEC and hardness indicate the absence of the flow through easily soluble carbonate rocks which would lead to dissolution of carbonate minerals and higher values of their constituents in the water.

A possible source of water is the surface stream from the area of very low permeable rocks on the high plateau about 2000 m higher. With respect to chemical characteristics of water in the cave we presume a rapid flow through the metamorphosed calcitic siltstones, a respectively continuous flow along their contact with the metamorphosed sandy siltstones not much different from the flow in the Shuilian Cave. In percolating water (Table 2) that is fed into the cave through the ceiling, a considerably higher value of SEC (355 μS/cm) was measured which reflects its percolation through the higher carbonate containing rock and more abundant dissolution of carbonates. Since the samples were collected at the beginning of the rainy season and considering our knowledge of the water flow through the vadose zone in the Slovenian karst (*Kogovšek*, 2007; *Kogovšek* and *Petrič*, 2006), we presume that the first rainfalls at the beginning of the rainy period were used mainly for filling up the vadose zone of the karst part of the catchment that had been drained during the previous drought period. For this reason the discharge from it was low at the time of our sampling which resulted also in the chemical composition of the spring water. Probably, a larger contribution of water from the vadose zone with the higher carbonates' concentration can be expected in the rainy season. Of course, this could be established only with appropriate additional measurements and analyses.

Also the larger spring, the spring near Shuilian, that feeds the left affluent of the river 1.5 km northwards displays physico-chemical characteristics very similar to those of the spring from the Shuilian Cave, as evident from Table 2.

The close chemical correspondence of the two examined springs indicates very similar recharge areas (possibly some parts are common to both), and a very similar underground flow.

CONCLUSION

Shuilian Cave originated at the contact between underlying little permeable Lower Devonian calcitized and metamorphosed sandy siltstones and overlying higher permeable Middle Devonian metamorphosed calcite siltstones.

The formation of the cave at the contact of rocks differing much with respect to erosion and corrosion led to the rise of typical cross-sections. The rock relief with preserved traces of the slow water flow in the flooded zone bears evidence of the rapid change of hydrologic conditions from phreatic to epiphreatic and to vadose ones. This change has been the consequence of the rapid deepening of the river valley. In less permeable rocks the hanging water flow is preserved. Hydrogeologic position of the springs and physico-chemical characteristics of their water permit the conclusion that the Shuilian Cave and neighbouring springs are recharged by water from the vadose zone in the metamorphosed calcitic siltstones and by water from the high plateau, approximately 2000 m above the river.

# SPELEOGENESIS OF SELECTED CAVES IN THE LUNAN SHILINS AND CAVES OF THE FENGLIN KARST IN QIUBEI

<div style="text-align:right">13</div>

STANKA ŠEBELA, TADEJ SLABE, HONG LIU, PETR PRUNER

Yunnan is famous for its attractive karst landscapes, especially shilin, fengcong and fenglin. The development of caves beneath shilins in the vicinity of Lunan is closely connected with shilin formation. Most of waters percolating through shilins run through the caves and are responsible for their formation. The study of the cave speleogenesis deepens knowledge about both the development of shilins and karst structure.

Two different locations in Yunnan were chosen for karstological studies. The first area is in the vicinity of the Central Lunan shilin, about 100 km southeast from Kunming, the provincial capital. The second area, named Puzhehei, lies in the southeastern part of Yunnan near the town of Qiubei (1). The locations are linked to two different types of karst: stone forest (shilin) and tower or cone karst (fenglin or fengcong) (*Ravbar*, 2002; *Lowe* and *Waltham*, 1995).

Shilin is a type of pinnacle karst formed on a plateau of gently dipping limestone (*Knez* and *Slabe*, 2002). Fengcong karst is identified by its clustered limestone hills (*Lowe* and *Waltham*, 1995).

Fengcong is almost the equivalent of cone karst; its closely packed hills are conical rather than hemispherical, with intervening dolines and disjointed valleys. Fenglin karst is identified by its isolated limestone hills and is almost the equivalent of tower karst (*Lowe* and *Waltham*, 1995).

In the vicinity of the Central Lunan shilin, we accomplished structural geological mapping and speleomorphological studies of three karst caves (Jibailong Dong, Dieyun Dong and Ziyun Dong). A further locality, the Baiyun Cave in the Naigu shilin, is situated 20 km to the east of the Central Lunan shilin (*Šebela et al.*, 2001). In the area of cone karst in Puzhehei morphological studies of the Guangyin Dong Cave were accomplished. Paleomagnetic analyses of cave sediments were performed at Institute of Geology, Czech Academy of Sciences.

The principal aim of this study was to identify the significant geological and speleomorphological properties that influence formation and shaping of karst caves. In addition, we aimed to determine the age of sediment infillings in the chosen karst caves. A comparison between the structural geological and morphological properties of caves developed beneath shilins, foot caves at the bottom of fenglin, and older caves higher on the fenglin has especially been taken into account.
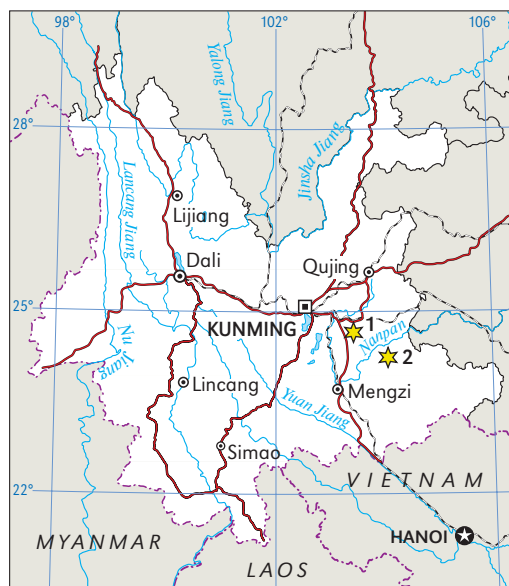


**1** Geographical position of the study areas in *Yunnan* Province, south China. 1 – *Lunan* shilin, 2 – *Qiubei, Puzhehei* district.

Recent investigations about Chinese karst are numerous (*Luo et al.*, 2003; *Gu et al.*, 2002; *He et al.*, 2001; *Song* and *Liang*, 2001; *Šebela et al.*, 2004; *Knez* and *Slabe*, 2010). Frančišković-Bilinski and others analysed karst tufa from Guangxi and determined the Pleistocene and mostly Holocene age (*Frančišković-Bilinski et al.*, 2003). They sampled tufa and travertine deposits mainly from karst freshwater springs, whereas we sampled karst cave sediments such as clay and loam (*Šebela et al.*, 2001). They used different methods such as $^{14}C$ analysis, whereas we used paleomagnetic studies.

## 13.1 REGIONAL GEOLOGY OF THE STUDIED AREA

Upper Devonian, Carboniferous and Permian shallow-water carbonates build the south China tower karst, south from Kunming. Near Kunming basalt rock is interbedded with Upper Permian limestones. Such vulcanism indicates regional extension and localizes rifting of the carbonate platform at the end of the Permian. Southeast of Kunming, Lower-Middle Triassic, mostly shallow-marine carbonates are generally conformable on the Permian. The Upper Triassic, Jurassic and even Eocene red beds are unconformable, often at a low angle, upon Palaeozoic and Proterozoic rocks of Kunming region, which appears to have formed a broad north-south trending high or horst since the Early Mesozoic. Around Kunming, the basal unconformity of the Mesozoic-Tertiary continental sequence seems to be a distal onlap over a region mostly structured by Late Palaeozoic extensional blockfaulting. Cenozoic deformations have been strong (*Leloup et al.*, 1995).

The studied area shows tectonic deformation because of the movement in Asia caused by the thrust of the Indian collision. The great geological discontinuity that separates Indochina from China results from the Cenozoic strike-slip strain. This suggests that this narrow zone acted as a continental transform plate boundary in the Oligo-Miocene. Extrusion of Indochina alone accounted for 10–25 % of the total shortening of the Asian



**2** Regional geology of southern China (after *Wang* and *Burchfiel*, 2000; *Leloup et al.*, 1995).
1 – *Lunan shilin*;
2 – *Puzhehei*;
A – rose diagram of the direction of cave passages based on the *Jibailong Dong*, *Dieyun Dong*, *Ziyun Dong* and *Baiyun* caves;
B – rose diagram of the direction of fissures in the caves.
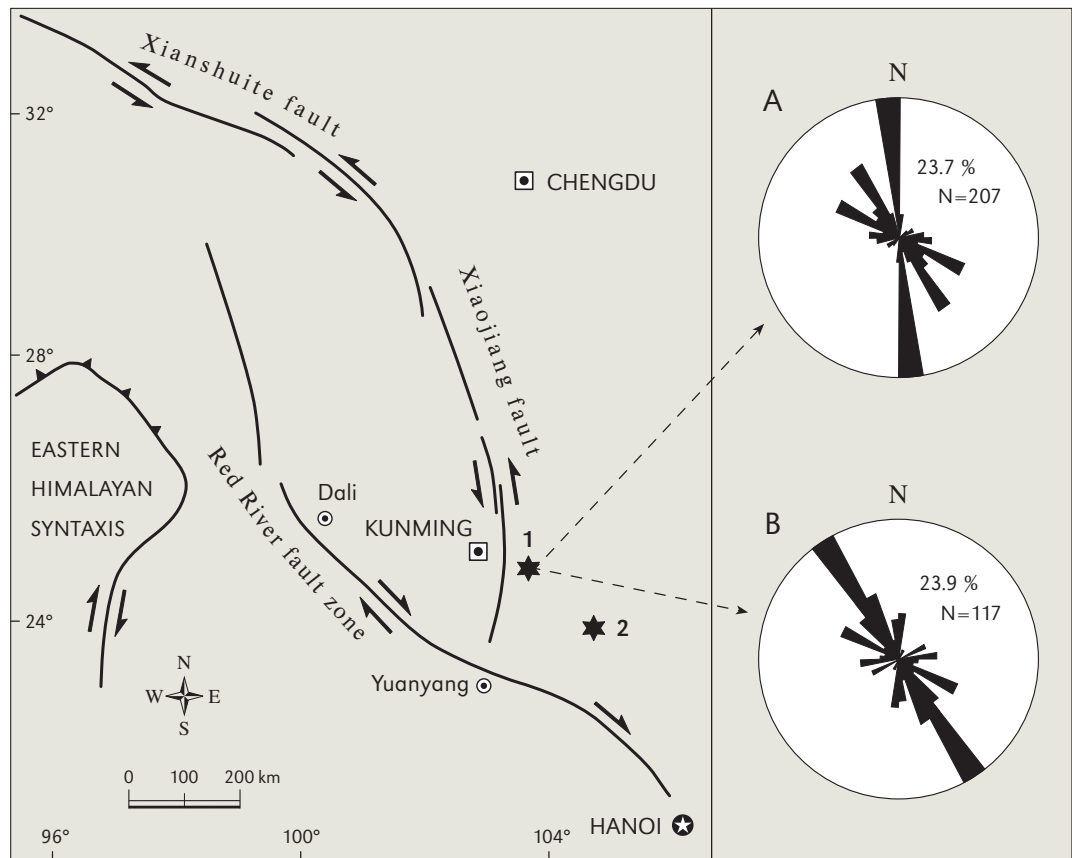
continent. Indochina was extruded towards the southeast as a result of the India-Asia collision (*Leloup et al.*, 1995).

Present-day tectonic styles and rates cannot be extrapolated far into the past because the deformation of Asia started only with the onset of collision, prior to −50 Ma. The large-scale left-lateral shear followed by a reversal to right lateral occurred along the Ailao Shan-Red River zone in the mid-late Cenozoic (*Leloup et al.* 1995).

The Red River fault zone (2) is the major geological discontinuity that separates South China from Indochina. Motion along the Red River fault zone switched from left lateral in the Oligo-Miocene to right lateral in the Plio-Quaternary. Estimates have ranged from 200–250 km right lateral to more than 1500 km left lateral (*Leloup et al.*, 1995). The current dextral slip-rate is 2–8 mm/yr (*Allen et al.*, 1984). The present-day stress field is NNW-SSE shortening. The Ailao Shan-Red River shear zone is mostly strike-slip with transpression in the NW and transtension in the SE (*Briais et al.*, 1993).

South of Kunming, steep E-W to NE-SW striking cleavage is found locally in the Mesozoic sandstones. We interpret these NE-SW to E-W folds and cleavage to result from late Neogene-Quaternary NNW-SSE shortening, compatible with left-lateral slip on the Xiaojiang fault (2), right-lateral slip on the Red River fault zone (*Tapponier* and *Molnar*, 1977) and with the SSE-directed impingement of the Kunming-Chuxiong block against the north-eastern edge of Indochina (the Red River fault) (*Leloup et al.*, 1995).

The focal mechanisms of the 1966 earthquakes on the N-S striking Xiaojiang fault imply a left-lateral slip along it. A normal component of the slip on the roughly N-S faults south of Kunming has created several Quaternary half-grabens, some of them filled by lakes (*Tapponier* and *Molnar*, 1977).

During the late Cenozoic, an inhomogeneously distributed extension has been expressed by numerous Quaternary basins along the southern part of the Xianshuihe-Xiaojiang fault system (2). Quaternary basins and lakes north of Dali and within the southern part of the Xiaojiang fault zone are areas of local active extension (*Wang* and *Burchfiel*, 2000).

The Pliocene-Quaternary sedimentary fill in pull-apart basins associated with the left lateral Xianshuihe-Xiaojiang fault system indicates that this structure was initiated by at least 2–4 Ma ago (*Wang et al.*, 1998).

Samples for the paleomagnetic analysis are CH 1–9. Fissures on the groundplans are coded in degrees with dip-direction/dip-angle (for example 90°/80°).

## 13.2 CAVES IN THE VICINITY OF THE LUNAN SHILIN

The Lunan shilin is one of the most known tourist attractions in Yunnan. Karst caves are found below densely packed pinnacles. The Baiyun Cave (*Šebela et al.*, 2001) in the Naigu shilin is a well-visited show cave. Jibailong Dong, Dieyun Dong and Ziyun Dong are also the show caves. Structural geological and speleomorphological investigations have been performed in the studied caves. Paleomagnetic analyses of clastic cave sediments from three different profiles provided additional informations about the age and formation of the caves.

### 13.2.1 *Jibailong Dong*

The cave (1730 m a.s.l.) is 460 m long (3). Both cave entrances were dug out from cave sediments. The passage is developed mostly in Permian thick-bedded limestone. In the

**3** Geological map of the *Jibailong Dong* Cave.
A – rose diagram of the direction of cave passages;
B – rose diagram of the direction of fissures in the cave;
1 – ground-plan of the cave passage;
2 – position of the sediment profile taken for the paleomagnetic analysis;
3 – dip-direction/dip-angle in degrees of the limestone bedding-plane;
4 – anticline;
5 – dip-direction/dip-angle in degrees of the joint;
6 – horizontal movement along the fissure;
7 – dip-direction/dip-angle in degrees of the fissure to the broken zone;
8 – extrapolated continuation of the fissure.
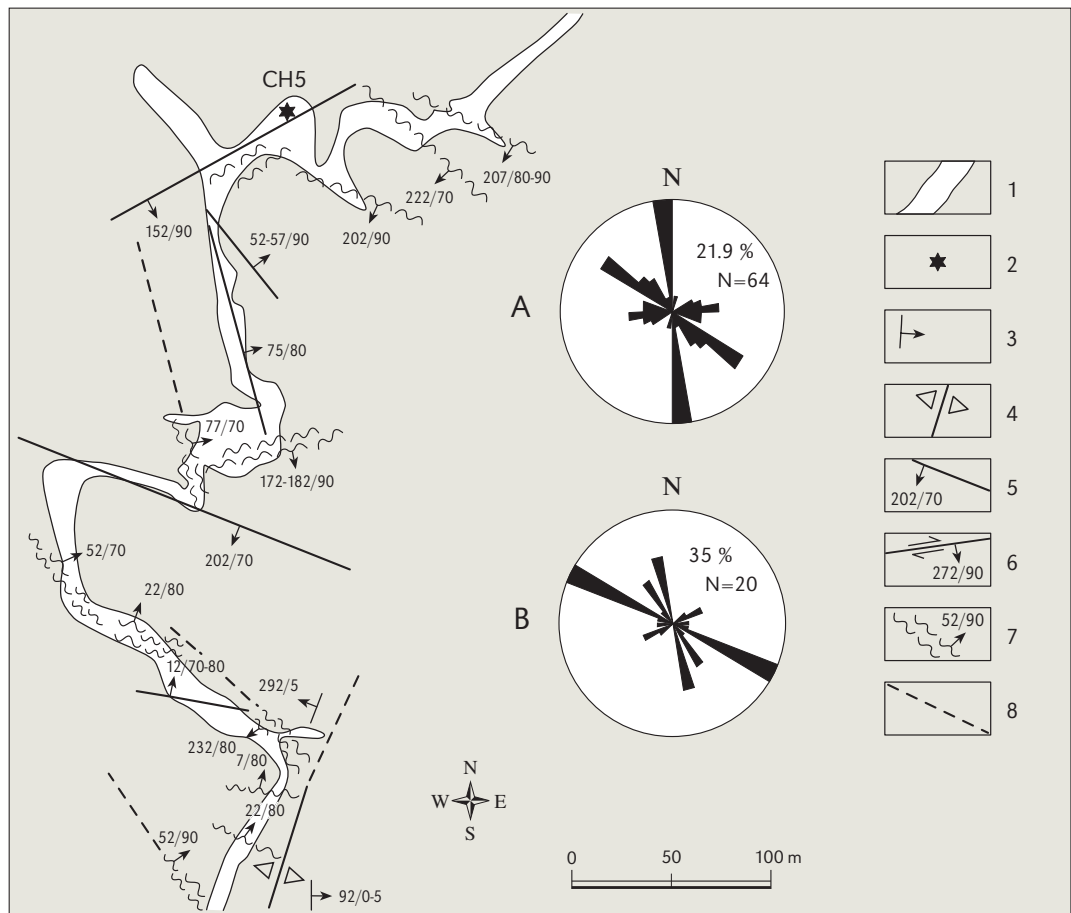
southern part of the cave a NE-SW trending anticline has been detected. The dip angle of the bedding-planes is 0–5°. In some parts the cave passage is formed along fissures. In the northern part of the cave the passage, up to 15 m high, is developed inside the fissure 75°/80°. Inside the fissure 202°/70° we observed collapse blocks stuck on the ceiling.

Sediments were sampled for paleomagnetic analyses in the northern collapse chamber of the cave (4) from a profile of about 1 m thick. The upper part belongs to flowstone and below this unit the sediment layers are inclined due to sliding. Sample CH 5 was taken from the upper part of a 0.15 m thick layer of laminated loam. The cave sediments are fine-grained, containing mostly quartz; they have been deposited into the cave by the underground water flow.

The Jibailong Dong passage orientation is the most varied of the four studied caves. Four main passage directions are observed: N0–10°W (21.9 %), N50–60°W (17 %), N80–90°E (9 %) and N40–50°W (9 %). The most frequent fissure orientation measured in the cave passage is N60–70°E (35 %), the second direction N10–20°W (20 %), the third one N30–40°W (15 %) and the fourth one N60–70°E (10 %). The passage which is developed along distinct fractures, as noted above, runs in the directions of N0–10°W and NW-SE.



**4** Profile of cave sediments taken for the paleomagnetic analysis in the *Jibailong Dong* Cave.
A – flowstone (d = 30 cm);
B – linked layers of loam caused by sliding (d = 50 cm);
C – laminated loam (d = 15 cm);
D – massive loam (d = 30 cm);
CH 5 – a sample for the paleomagnetic analysis, normal polarity.
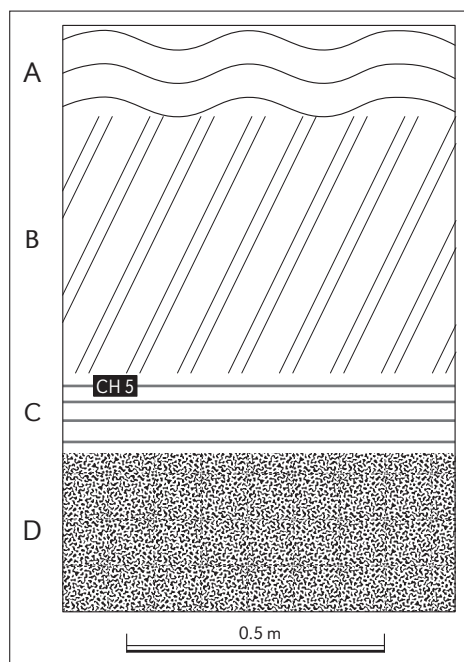
## 13.2.2 *Dieyun Dong*

The artificially dug northern cave entrance is situated at 1715 m a.s.l. The cave is 280 m long (5). The strongest fissure changes direction from 260°/70° on the north to 265°/90° in the middle part and finally to 270°/80–90° in the southern part of the cave. The fissure widens into a lens shape. No slip along the fissure was detected. At the natural cave entrance the bedding-planes were measured at 170°/5° and the rock is mostly Permian thick-bedded subhorizontal limestone.

The most frequent passage orientation is N0–10°W (48.7 %), the second direction N0–10°E (23 %) and the third one N50–60°E (15 %). Prevailing fissures are oriented N0–10°E (40.9 %) and N0–10°W (35 %).
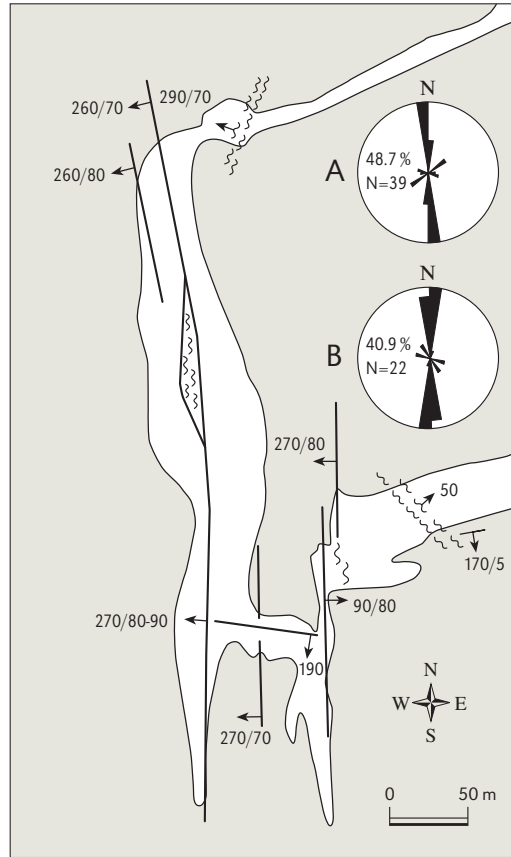
## 13.2.3 *Ziyun Dong*

The cave (7) is 360 m long and is situated at 1755 m a.s.l. The predominant thick-bedded Permian limestone dips towards west and northwest at 5°. Along the 172°/90° joint a small 0.5 cm-horizontal slip with dextral movement was determined. Most fissures run in the NW-SE direction.

The general passage orientation is NW-SE (6). The most frequent orientation of the passage is N30–40°W (47.1 %), in the second place are two directions, N90–100°E (16 %) and N60–70°W (16 %). Most fissures in the cave are oriented N40–50°W (35.7 %) and N50–60°W (28 %). Lastly is the direction N80–90°E (22 %).

## 13.2.4 *Baiyun Cave*

Baiyun Cave is more precisely described in Chapter 11. Here we will just summarize some important facts about fissures, cave passage orientation and cave sediments.

Gravel in the 380 m long Baiyun Cave can be found at different levels and implies several generations of cave infillings. The periods of gravel infilling have alternated



**5** Geological map of the *Dieyun Dong* Cave.
A – rose diagram of the direction of cave passages;
B – rose diagram of the direction of fissures in the cave.
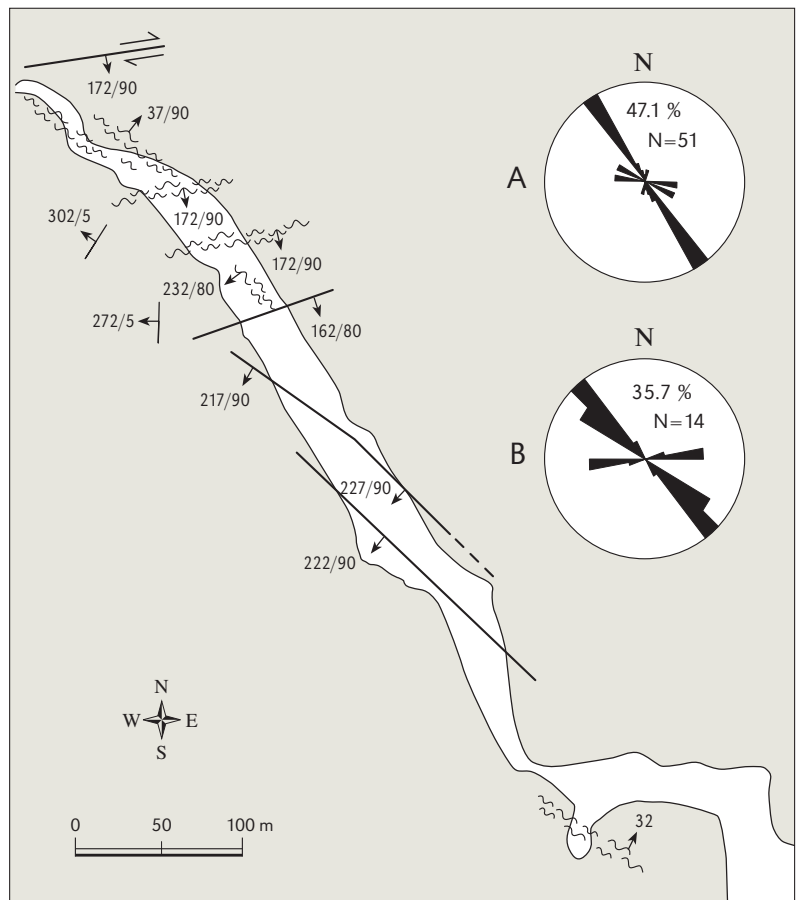


**6** Geological map of the *Ziyun Dong* Cave.
A – rose diagram of the direction of cave passages;
B – rose diagram of the direction of fissures in the cave.

with clay infillings. In the northern part of the cave we sampled a 1.75 m thick profile for paleomagnetic analyses (samples CH 1–4). The profile contains sandy clay, as well as pebbles cemented into conglomerate. The prevailing pebble diameters are 3 cm and less; none are well rounded. Conglomerate and/or uncemented pebbles can be found in different parts of the cave.

Cave passages are mostly oriented in the directions N60–70°W (34 %) and N0–10°W (30 %). The prevailing fissure direction in the cave is N30–40°W (36.1 %) and the second one N20–30°W (23 %). The direction N60–70°W, which is the most common direction of the cave passage, represents just 10 % of all the fissures in the cave.



**7** The entrance to the *Ziyun Dong* Cave.

The basic statistics, giving the most frequent directions of the studied cave passages (2.A) at distribution intervals of 10° and a population of 207, indicates that most passages (23.7 %) have developed in the direction of N0–10°W. The second prevalent direction is N30–40°W (16 %) and the third one N60–70°W (12.5 %). The interval of confidence is 13.93°, with the standard deviation of 5.76 %. The results represent the most frequent directions for the total of 1478 m of passages, representing the four caves (Jibailong Dong, Dieyun Dong, Ziyun Dong and the Baiyun Cave).

The rose diagram for fissure orientation includes a population of 117 measurements (2.B). The maximum percentage of 23.9 % belongs to the N30–40°W direction, 13 % represent N20–30°W direction and 11 % belong to the N60–70°W direction. The N-S (N0–10°W) direction represents 6 % and the N0–10°E direction 7 %. The standard deviation is 5.84 % and the confidence interval 13.67°.

Through geological mapping we found that many passages run along fractures. In this manner we were able to follow a well-defined fracture in the ceiling of Ziyun Dong running in the NW-SE direction. The fractures in the cave ceiling are mainly subvertical. The main passage in Dieyun Dong running in the N0–10°W direction corresponds to the direction of the ceiling fracture.

The results of the surface geologic mapping of the fractures in the Central Lunan shilin from 1996 (*Chen et al.*, 1998) show that 20.79 % of all the fractures are oriented in the direction of N30–45°W which corresponds to the second most frequent direction of the cave passages, N30–40°W (16 %). It is interesting that in the Central Lunan shilin only 5 % of the surface fractures lie in the N0–15°W direction whereas this is the most frequent direction of all the studied cave passages.

We do not have a large amount of data on directions and dips of bedding-planes, as the studied caves developed in the thick-bedded Lower Permian deposits, mostly limestones. For the most part, the beds are subhorizontal and/or dip at a 5° angle.

From the speleological point of view, the caves in the vicinity of the Lunan shilin can be divided into two groups. The first group represents active caves that are situated near the actual water table level and can be periodically flooded. The second group includes old, dry caves.

The caves which are permanently or periodically flooded have a relief typical of epiphreatic conditions. More rapid water flow formed smaller scallops and ceiling pockets. The below-sediment cave rocky relief was formed in the period when the cave was filled with fine-grained sediment, the latter showing frequent oscillations of the water level.

The consequence of frequent variations of the water level in the Baiyun Cave are below-sediment rock features, and below-sediment flutes and pits (*Slabe*, 1995, 71) found in leeward places of the lower part of the channel in the river-bed and on its upper part where the channel widens.

The second type represents old and dry caves. In those caves traces of former older water flows are preserved. There are also infillings with the cave sediments that were deposited by slower or faster water flows, depending on regional changes of the water level. Continuous infillings caused paragenetic shapes of the cave relief. Especially the Baiyun Cave shows paragenetic deformation of the original passage. One of the more distinctive parts of the cave rocky relief in the Baiyun Cave are the above-sediment channels and anastomoses which make a network over a significant part of the main channel ceil-

145

*Speleogenesis of selected caves in the Lunan shilins and caves of the fenglin karst in Qiubei*

ing. The above-sediment channels are from 0.05 to 0.5 m in diameter. The deepest have preserved an omega-shaped cross-section which is usually typical for such a channel (*Slabe*, 1995, 62). The crests between smaller channels are usually pointed because of younger transformation with faster water flow. The network of anastomoses is at several levels, due to gradual prevailing of selected channels during long-lasting infill of the cave by fine-grained sediments where such features develop (*Slabe*, 1995, 67). Some channels are still filled up with fine-grained sediments. Paleomagnetic studies of the cave sediments provide evidence of younger but distinct periods of flooding of the old

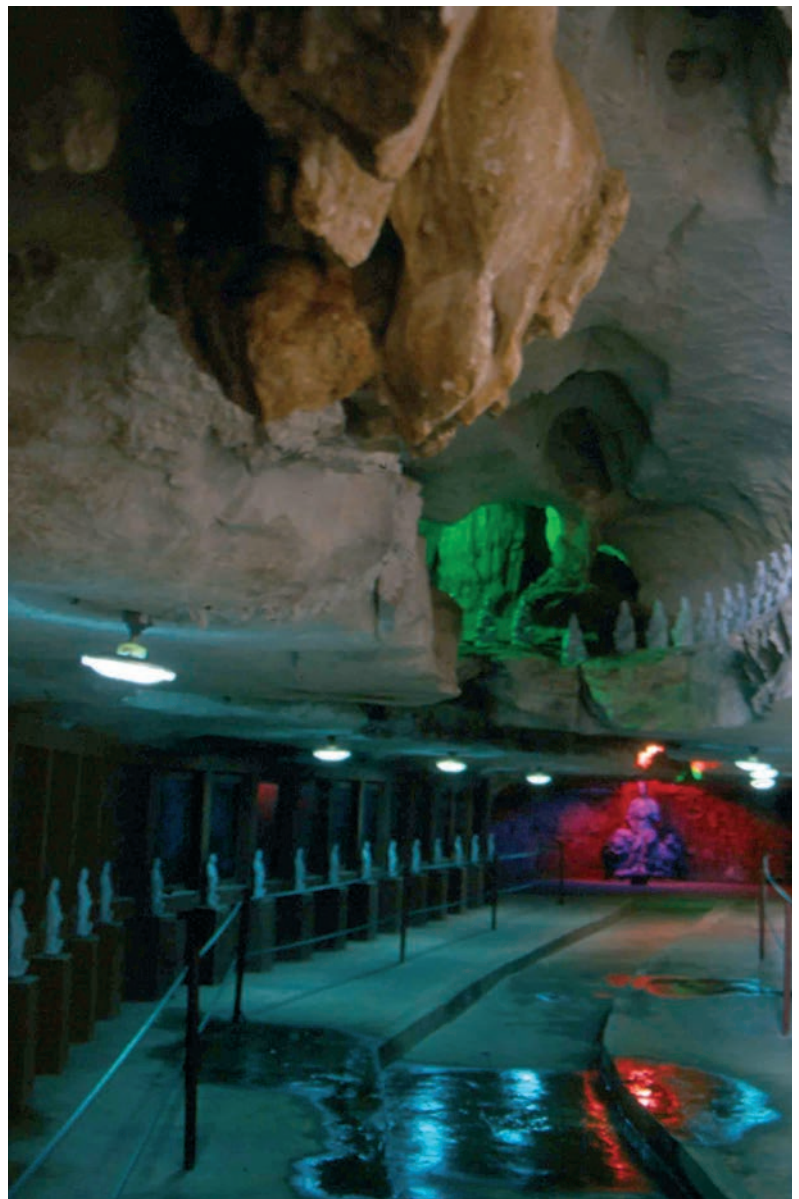**9** The landscape of cone karst (*fengcong*), *Puzhehei*.



146

*Speleogenesis of selected caves in the Lunan shilins and caves of the fenglin karst in Qiubei*

**11** *Guangyin Dong* Cave.



caves. Today those caves are subjected to water percolation through the cave ceiling and to humidity condensed from the air. Because in the old and dry caves near the Lunan shilin we do not usually find traces of gradual reshaping of the cave relief with faster flows, we assume that lowering of the water level was rapid. The exception is the Baiyun Cave where narrower indentation of the floor channel was found. The cave relief forms of older periods are today situated much higher than the actual water level. The rapid lowering of the water table can be connected with the development of surficial stone forests, shilins, which form more intensely in the periods of water table lowering.

## 13.4 SELECTED CAVES IN THE FENGLIN KARST OF PUZHEHEI

The karst area of Puzhehei (2) is built of Triassic and dolomitic limestone. The region of attractive scenery includes 16 lakes (1375 m), numerous fenglin, fengcong (8, 9, 10) and caves. The principal studies were performed in the Guangyin Dong Cave (11, 12) which is a typical foot cave (13), about 150 m long and situated at

*Speleogenesis of
selected caves in
the Lunan shilins
and caves of the
fenglin karst in
Qiubei*

**12** *Guangyin Dong* Cave.

**13** The entrance to the *Guangyin Dong* Cave.
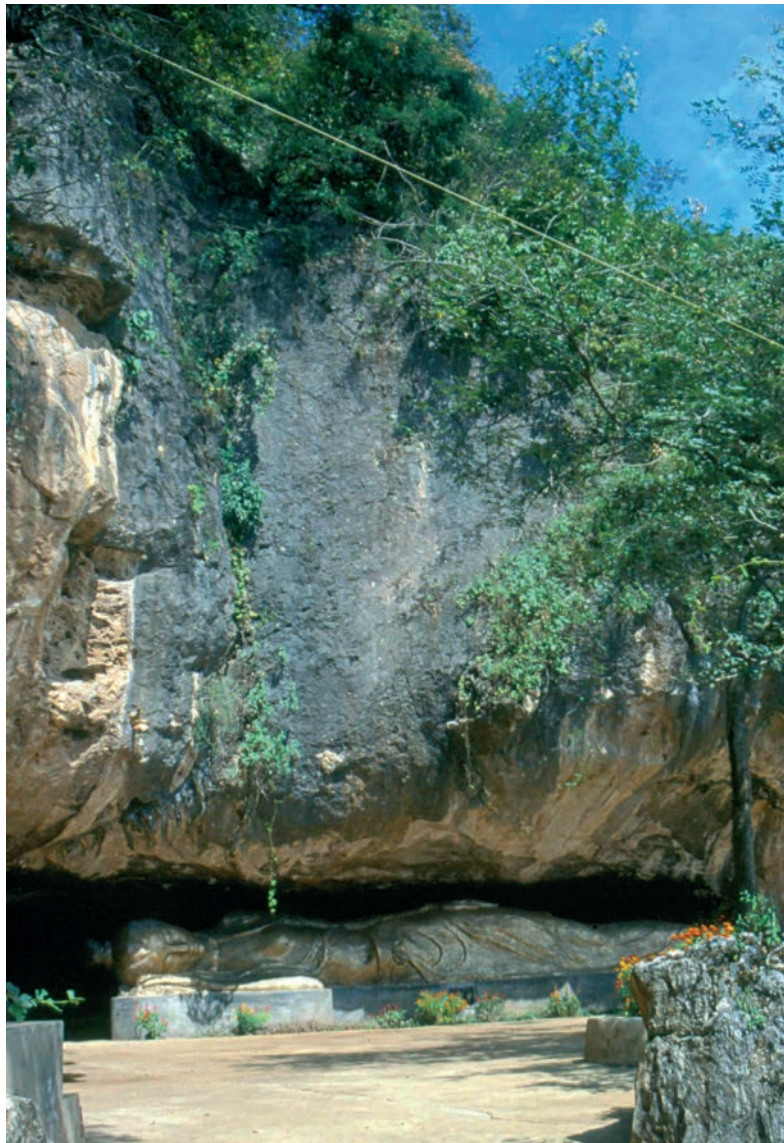


the lake water table level. Samples of cave sediments (CH 6–9) were collected for paleomagnetic analysis (14). The lowest part of the 1.7 m thick profile is situated 2 m above the lake. Sample CH 9 was taken from the upper part of the cave which is about 8 m higher than the lower profile. Samples CH 8 and 7 were taken from loamy layers that differ in colour. Sample CH 6 came from reddish loam.

At the bottom of the fenglin foot caves are numerous. They represent systems of mostly dense passages with up to 5 m in diameter. We assume that most passages developed from the bedding-plane anastomoses. Passages developed at different levels. Caves on lower levels are filled with water or are periodically flooded. Passages situated above the water level are dry and frequently filled with cave sediments and flowstone. The rocky relief of water passages, with middle-sized scallops and ceiling pockets, shows its formation in the presence of the slower water flow. Below-sediment notches and pockets, remnants of frequent changes in the water level and deposition of smaller quantities of fine-grained sediments, are situated along the bedding-planes. Passages situated at

higher levels exhibit more periods of development. Frequently, above-sediment channels and along-sediment notches are found which are remnants of cave sediment infillings. The distinct above-sediment rocky relief shows that the periods of cave infillings with fine-grained sediments and increases of the water level were relatively continuous.

Older caves, more than 10 m high, are frequent on the fenglin. They have higher and larger passages, large ceiling pockets and cupolas, but no scallops. They have been formed by continuous and slow water flow as is characteristic for phreatic conditions. In those higher caves big stalagmites and flowstone piles are common.

In front of many entrances into karst caves situated on different altitudes flowstone could be found. There are also so-called unroofed caves, remains of denudation of the karst surface (*Mihevc et al.*, 1998).
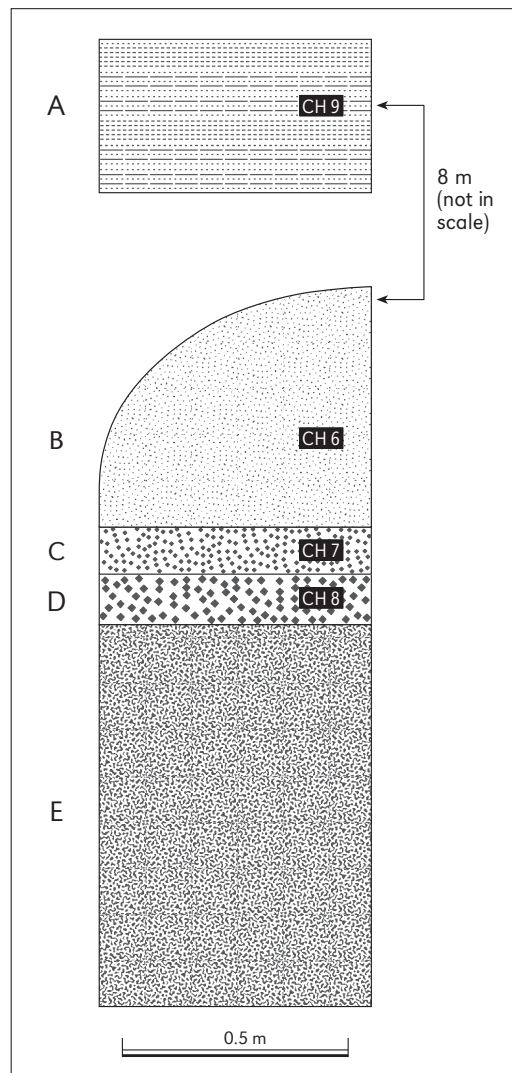


*Speleogenesis of selected caves in the Lunan shilins and caves of the fenglin karst in Qiubei*

**14** Profile of cave sediments taken for the paleomagnetic analyses, *Guangyin Dong* Cave, *Puzhehei*.
A – reddish loam (d = up to 100 cm);
B – reddish loam (d = up to 50 cm);
C – yellowish loam (d = 10 cm);
D – loam (d = 9 cm);
E – loam cut by the cave pathway (d = less than 100 cm);
CH 6–9 – samples for the paleomagnetic analysis, all normal polarity.

## 13.5 RESULTS AND DISCUSSION ABOUT PALEOMAGNETISM AND THE AGE OF CAVE INFILLINGS

From three different caves, Jibailong Dong (CH 5) near the Lunan shilin, Baiyun Cave (CH 1–4) in the Naigu shilin, and Guangyin Dong (CH 6–9) in Puzhehei, nine samples of cave sediments (loam and clay) were taken for paleomagnetic analyses. Laboratory procedures performed at the Institute of Geology, Czech Academy of Sciences, were based on progressive demagnetization by the alternating field (AF) to detect components of remanent magnetic polarity in different intervals and to determine values and directions of remanent magnetization.

Sediments were sampled into small plastic cubes $20 \times 20 \times 20$ mm. In the laboratory they were measured on the JR 5 spinner magnetometer (*Jelínek*, 1996). All samples were demagnetized by alternating field procedures, up to the field of 1000 Oe in 14 steps. The LDA-3 (Agico) apparatus was used for AF demagnetization.

The remanent magnetization of samples in their natural state (NRM) is identified by the symbol $J_n$ and the corresponding remanent magnetic moment by symbol $M$. Graphs of normalized values of $M/M_o = F(t)$ were constructed for each analysed specimen.

The volume magnetic susceptibility $k_n$ was measured on the KLY-2 kappa-bridge (*Jelínek*, 1973). Separation of the respective remanent magnetization components was carried out by the multi-component Kirschvink analysis (*Kirschvink*, 1980).

149

| No. of sample | $J_n$ (nT) | $k_n$ ($10^{-6}$ SI) | Polarity |
|---|---|---|---|
| CH 1 | 881.529 | 1172 | R |
| CH 2 | 37.615 | 1200 | N |
| CH 3 | 2.144 | 692 | N? |
| CH 4 | 38.487 | 1447 | N |
| CH 5 | 37.950 | 1821 | N |
| CH 6 | 94.658 | 3359 | N |
| CH 7 | 1.205 | 134 | N |
| CH 8 | 7.151 | 504 | N |
| CH 9 | 1.102 | 110 | N |
| No. of samples | 9 | 9 | |
| Mean value | 122.427 | 1160 | |
| Standard deviation | 269.888 | 952 | |

The principal magnetic parameters and the mean values of the $J_n$ and $k_n$ are documented in Table 1. Values of natural remanent magnetization $J_n$ and those of magnetic susceptibility $k_n$ of studied sediments in their natural state show large differences. The samples are character-ized by low magnetic (sample CH 3) up to high magnetic parameters with reverse paleomagnetic polarity (sample CH 1).

Directions of remanent magnetization inferred from the above given procedures were tested using the multi-component analysis of Kirschvink. A-components of remanence are mostly of the viscous or chemo-remnant (weathering) origin; they can be removed by the alternating field with an inten-sity of 10 up to 60 Oe. Normal and reverse C-components are the most stable in the AC field of 200 up to 1000 Oe.

Eight of the nine analysed samples showed normal polarity (15). Only sample CH 1 (Baiyun Cave) was deposited in a period of reverse polarity. The correlation with stan-dard paleomagnetic scales is problematic and there are many possibilities. We consider that the upper part (CH 1) of the sampled profile in the Baiyun Cave probably belongs to the reverse Blake event (112,300–117,900 years BP) (*Šebela et al.*, 2001). For all other samples we can conclude that they are younger than 780,000 years and were deposited during the Brunhes Chron.

**15** Direction statistics of eight samples for the paleomagnetic analysis.
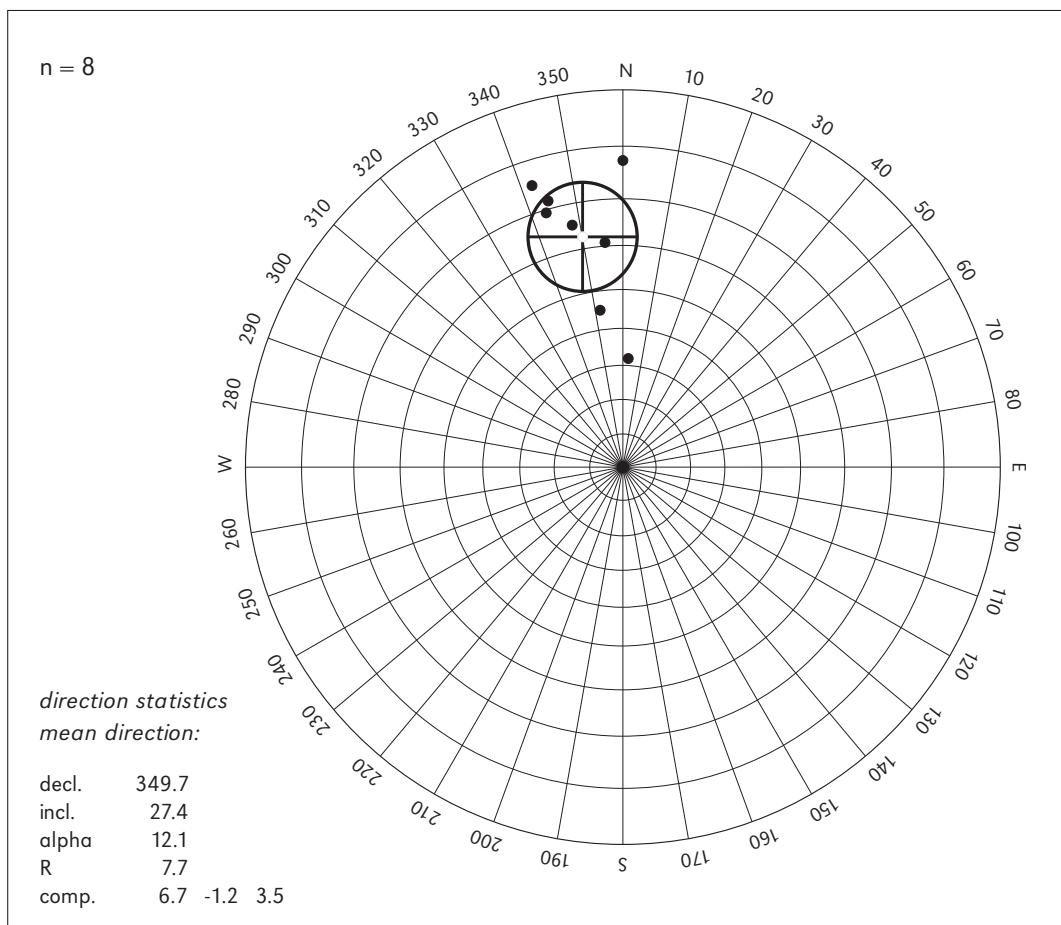
## CONCLUSION

China is famous for its attractive karst landscape characterized by shilin, fengcong and fenglin. Although Yunnan has mostly been known for vast areas of shilin karst, fengcong and fenglin karst areas are also getting more and more popular. The scientific co-operation between Yunnan Institute of Geography (P. R. China) and Karst Research Institute ZRC SAZU (Slovenia) has been continuous since 1995 (*Chen et al.*, 1998). Slovenia is a country of Classical karst and China has a rich karst landscape. Geological, geomorphological, speleological, hydrological, paleomagnetic and chemical studies which have been included into this project are important for understanding the formation and development of karst areas not just in Yunnan but also world-wide.

In the vicinity of the Lunan shilin (1), in a diameter of 30 km, all four karst studied caves are formed below shilin karst topography. The paleomagnetic analysis of five samples of cave sediments taken from two of the karst caves (Baiyun Cave and Jibailong Dong) was accomplished. The upper part of the profile taken in the Baiyun Cave probably belongs to 112,300–117,900 years BP (*Šebela et al.*, 2001). All other samples are part of an older period of cave infilling around 780,000 years BP and thus probably belong to the Upper Pleistocene. We need to stress that the oldest cave sediments have probably been removed. The Baiyun and Jibailong Dong caves are much older than the age of the deposited cave sediments is. From the absolute age analysis of related secondary carbonate accumulation it was determined (*Yu* and *Yang*, 1997) that the earliest modern shilin had begun to evolve in the Naigu region, where the Baiyun Cave is situated, in the Late Pliocene (about 2 Ma BP).

The caves formed below shilins can be divided into two groups. The first group represents the caves that are situated near the actual water table level. These caves can be flooded periodically. The caves which are permanently or periodically flooded have a rock relief typical of epiphreatic conditions. The second group includes the old and dry caves with traces of several developmental stages. The oldest rock features in such caves are above-sediment channels and anastomoses belonging to a period when the caves were entirely filled by sediments. Large ceiling channels covered by small scallops developed when faster water flowed in the upper part of the Baiyun Cave. This water partly transformed the above-sediment rock features. The youngest period is shown by the floor channel which is a narrow part of a deepened river-bed.

We think that the long-lasting periods of relatively frequent smaller variations of underground water, almost at the same water table, slowed down the development of the shilin at the surface. Younger, significant lowering of the ground-water level probably caused faster development of the shilin.

The karst area of Puzhehei (1) is a typical fenglin and fengcong landscape with lakes and numerous foot caves. The caves are developed on different levels, such as on the level of the lake or higher on the fenglin. Many of them traverse the fenglin. Four samples (CH 6–9) of cave sediments were taken from the Guangyin Dong Cave. Paleomagnetic analyses suggest that the cave sediments are younger than 780,000 years (Brunhes Chron). The rocky relief of water passages, with middle sized scallops and ceiling pockets, shows its formation in the presence of the slower water flow. Below-sediment notches and pockets are situated along the bedding-planes and are remnants of frequent changes in the water level and deposition of smaller quantities of fine-grained sediments. Passages situated at higher levels show more periods of development. They frequently have above-sediment channels and notches that are remnants of cave sediment

infillings. The distinct above-sediment rocky relief shows that the periods of cave infillings with fine-grained sediments and the rise of the water level were relatively continuous. Larger cave passages situated on higher cone elevations are remains of slower water flows and represent development in phreatic conditions. It appears that these caves were formed before shaping of the karst surface into cone forms.

Detailed structural-geological mapping was carried out in four karst caves (Jibailong Dong, Dieyun Dong, Ziyun Dong and Baiyun Cave) near the Lunan shilin. Further geological maps including measurement of fissures, joints and bedding-planes were accomplished (3, 5, 6). In the studied caves the bedding-planes are mostly subhorizontal and in most cases the caves are formed within massive or thickbedded Permian limestone or dolomitic limestone. The bedding-plane dip angle generally does not exceed 5°. Gentle folds, such as an anticline in the Jibailong Dong (3), are present. As has already been pointed out (*Sweeting*, 1995), the structures in the limestones of the Lunan shilin are open synclines and anticlines.

In our study of the caves we did not detect a really good example of a fault. There are many fissures and linear joints along which displacement is not visible. Some small displacement was determined at the northern entrance of the Ziyun Dong Cave along the vertical NE-SW trending joint.

Statistical evaluation of the most frequent directions of the passage (3.A, 5.A, 6.A) and fissure orientation (3.B, 5.B, 6.B) is illustrated by rose diagrams. The best comparison between the passage and joint orientation is between the rose diagrams of the Dieyun Dong Cave (5) where the passage is significantly developed along the N-S trending fissures and joints.

The united data including all four studied caves show that most passages (23.7 %) are oriented in the direction N0–10°W, being followed by the directions N30–40°W (16 %) and N60–70°W (12.5 %) (2.A). The most frequently oriented fissures (23.9 %) are evaluated in the N30–40°W direction (2.B) which is the second common orientation of the cave passages. Fissures in the general direction N-S (N0–10°W and N0–10°E) represent 13 % (6 % + 7 %), being 10 % less than N-S oriented passages.

In the Baiyun Cave (*Šebela et al.*, 2001) the most frequent cave passage directions reflect the wider geological setting of the area. The Xiaojiang fault is parallel to the N-S direction and the southern Red River fault to the direction of N60–70°W (2). Because both faults are still tectonically active (*Wang* and *Burchfiel*, 2000) and because the studied area (2.1) is situated 50 km from the Xiaojiang fault and 200 km from the Red River fault, we assume that the general directions of both active faults influence the most frequent directions of the fissures as well as cave passages. The closest Xiaojiang fault more strongly influences the cave passage orientation (2.A), while the more distant Red River fault prominently influences the fissure orientation (2.B).

# THE PILOT STUDY OF TWO CAVES, ROCK SHELTERS AND ROCK ART ALONG THE JINSHA RIVER (UPSTREAM OF THE YANGTZE)

14

HONG LIU, PAUL S. C. TAÇON, XUEPING JI, GUAN LI

At precisely the time when we were preparing texts for this book, we embarked on a journey to explore caves along the Jinsha River. We explored two caves right at the end of the Tiger Leaping gorge, named Xiahutiao by the locals. Nearby, a number of rock art sites turned up on both sides of the Jinsha River in the area that belongs to Diqing Tibetan Autonomous Prefecture and the Lijiang subprovincial administrative region. During the expedition, 7 of 52 rock art sites were surveyed and recorded. This paper will give a brief introduction to the research and findings of this trip.

Tiger Leaping gorge is famous worldwide for its spectacular features. At an altitude of less than 1700 m the Jinsha River flows between the Yulong Snow Mountain and the Haba Snow Mountain, which both reach over 5000 m a.s.l. At its narrowest part the gorge is less than 30 m wide. However, it is also of interest to geomorphologists and geologists. Owing to the rapid neotectonic uplift and strong river erosion, the river from the beginning to the end of the gorge, in 18 km of air distance, falls for 100 m, from 1795 to 1695 m (1).

Several groups of tectonic structures meet here and their relationship is very complicated and tectonically complex (2).
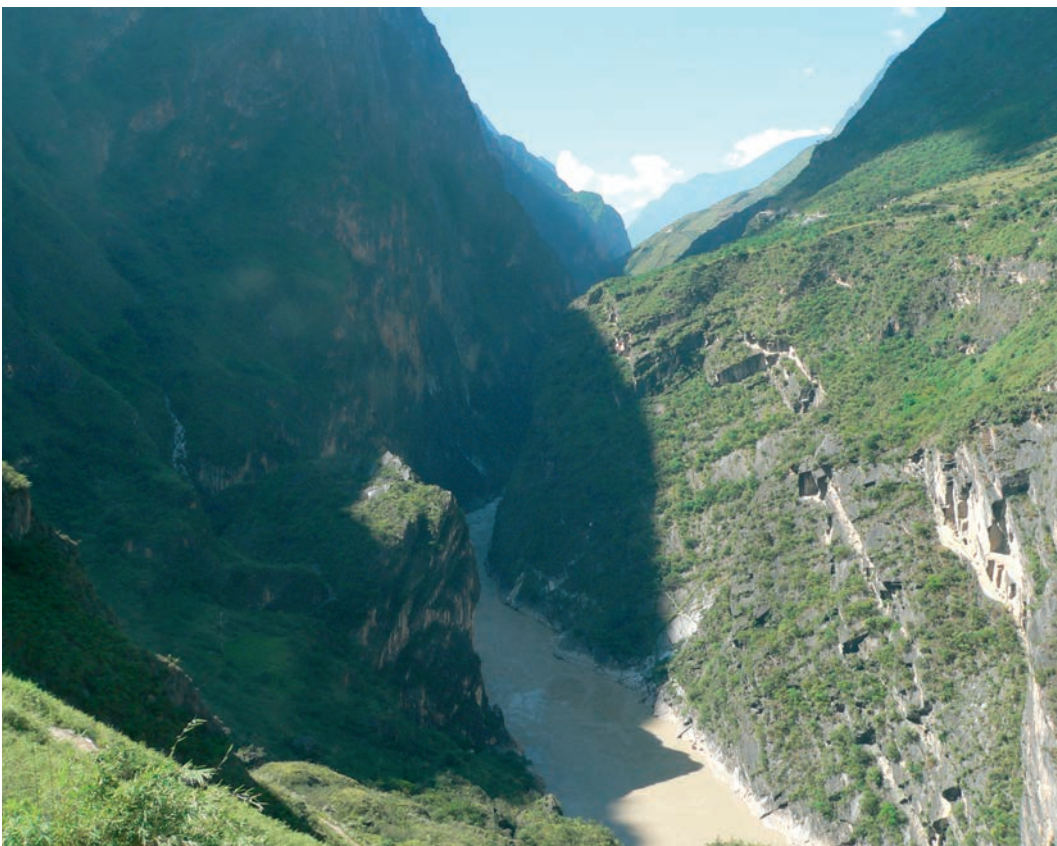


**1** *Xiahutiao* – the end of the Tiger Leaping gorge.
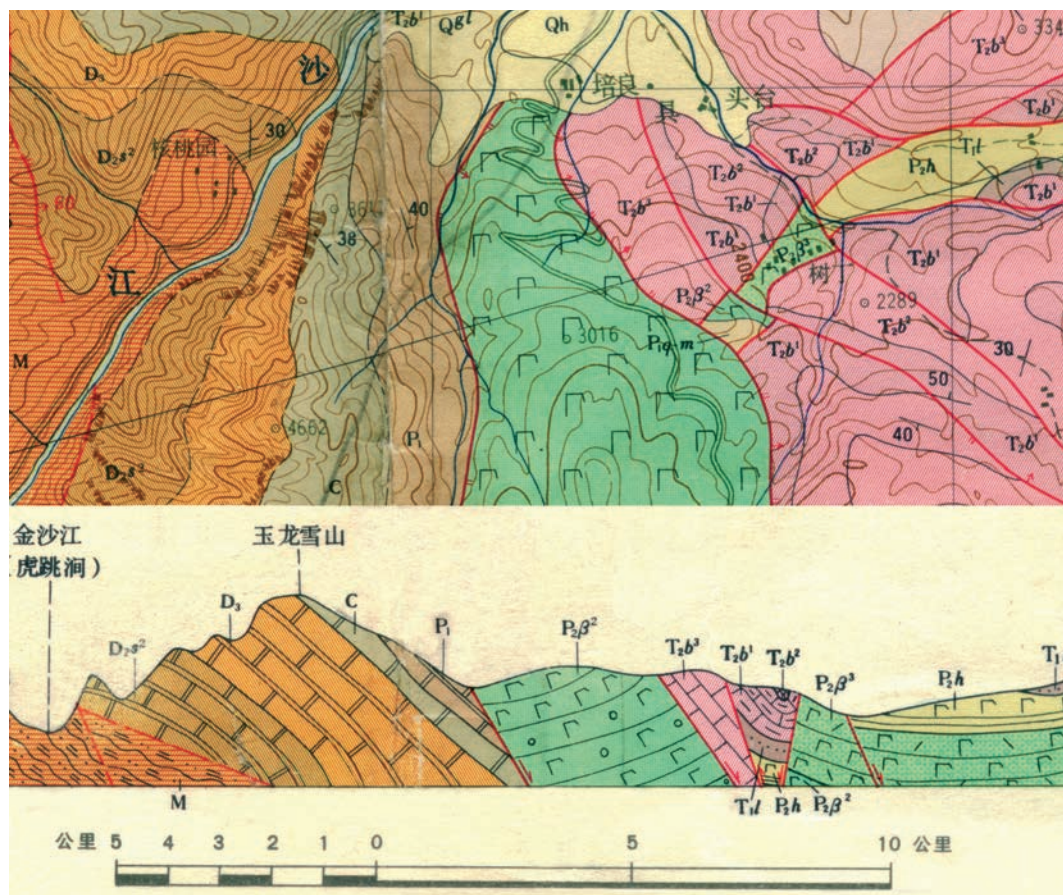
**2** Geological map of the Tiger Leaping gorge.

The outcrops of carbonate rocks are from the Devonian, Carboniferous, and Permian periods. Later Devonian ($D_3$) is a set of limestone, dolomitic limestone and sandwiched marble. Middle Devonian ($D_2s^2$) is thin to block marble. The Carboniferous stratum (C) is grey, cyanish grey, thin to massive continuous carbonate sedimentary rock, influenced by tectonic compression; it is partly metamorphosed in the same way as Devonian rocks. Permian carbonate rocks ($P_1$) are a group including marble intercalated with crystalline limestone. These carbonate rocks frequently appear along the Jinsha River in the form of cliffs.

Because of the foehn effect, the Jinsha River gorge has characteristics of a dry-hot valley climate. Sparse shrubbery grows on steep slopes and rocky land. Three levels of river terraces, at 1700 m, 1850 m, and 2000 m, can be identified around the village of Daju. They are scattered at different elevations along the river. Levels of the caves could be divided along the river in the same way (3). Since the 1950s, a number of instances of rock art have been discovered along the Jinsha River valley. To date, 52 sites have been recorded, but no detailed studies have been carried out because of a lack of accurate dating.

## 14.1 TWO CAVES

On this expedition the Wanrendong and Xiaodong caves in Xiahutiao, right at the end of the Tiger Leaping gorge were explored. They developed in Permian carbonate rocks (2) and are located at different elevations, 1710 m and 1774 m a.s.l. (4). There is one cave that could be seen on the opposite side of the Jinsha River at the same altitude. In front of the entrance to the Xiaodong Cave there is a platform, 80–100 m wide and slightly inclined to the river. Both caves are short, which is a common characteristic of the caves located around the gorge.

154

**3** A cave on the opposite side of the *Jinsha* River on the same level as the *Wanrendong* Cave.
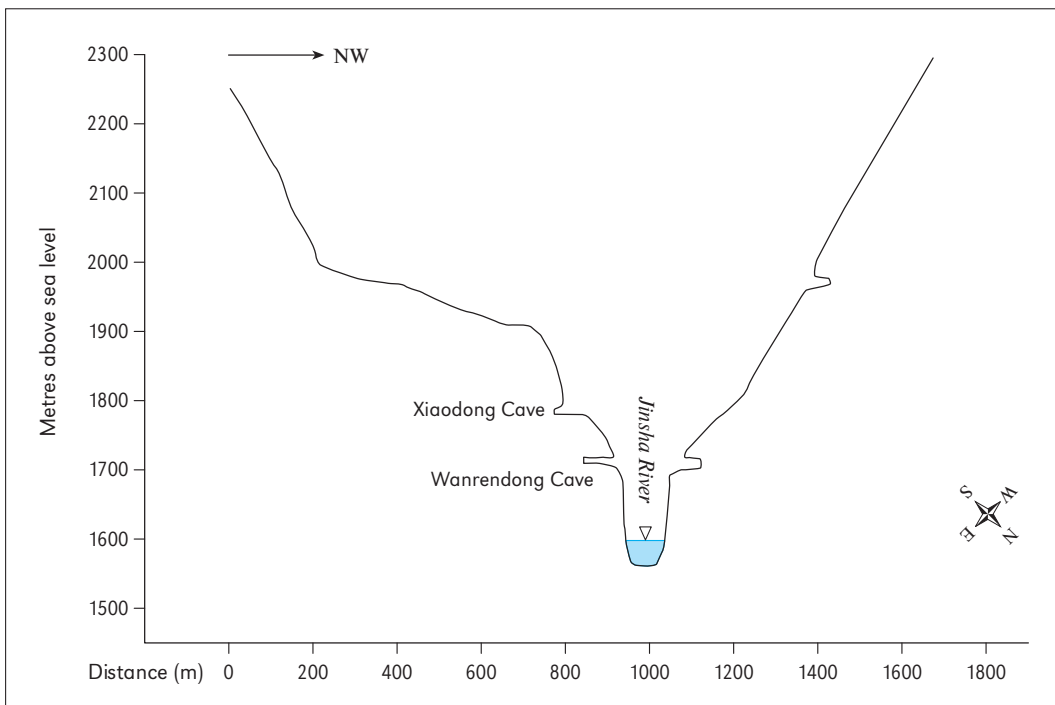


**4** Location diagram of the caves and the *Jinsha* River in *Xiahutiao*.

### 14.1.1  *Wanrendong Cave*

Wanrendong Cave got its name because local people believe that over 10,000 persons could hide in it. In strong contrast with its large entrance, the cave is short, only 42 m long and features a 4 m height difference of the cave floor (5, 6). It consists of three big chambers, free of speleothems, except for thin flowstone curtains partly on the wall at the end of the cave, and on the ceiling of the entrance. At the entrance there is an artificial rock wall made by the locals to keep goats inside.

*The pilot study
of two caves,
rock shelters and
rock art along
the Jinsha River
(upstream of the
Yangtze)*
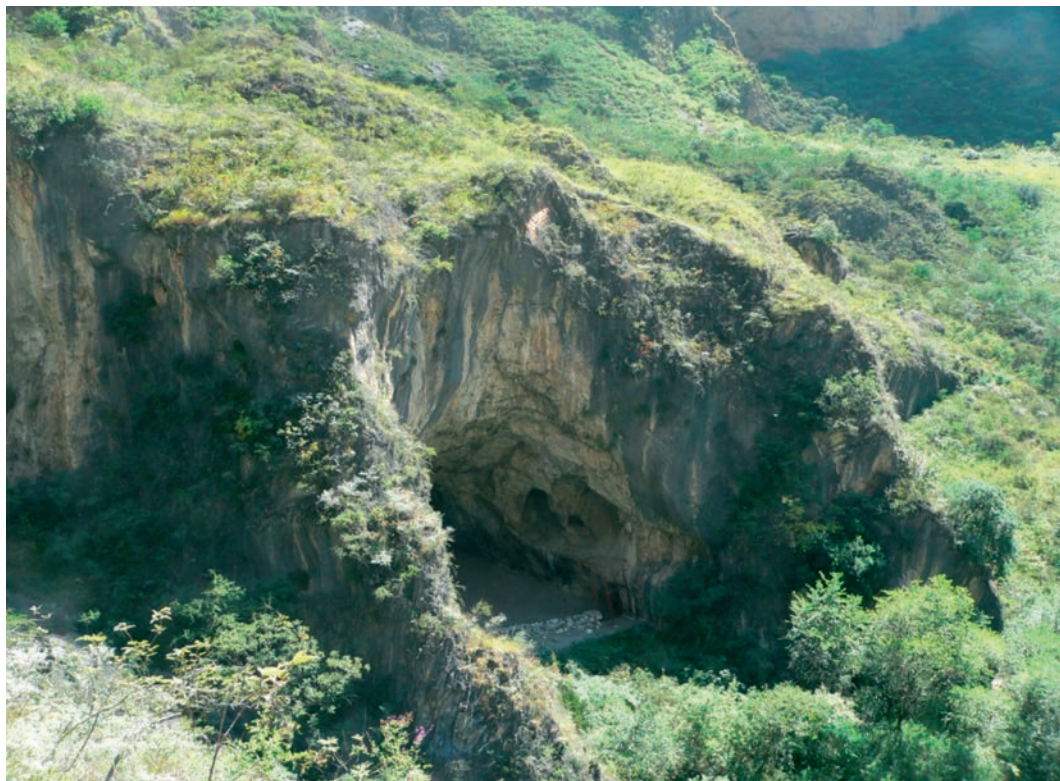
**5**   The entrance of the
*Wanrendong* Cave.
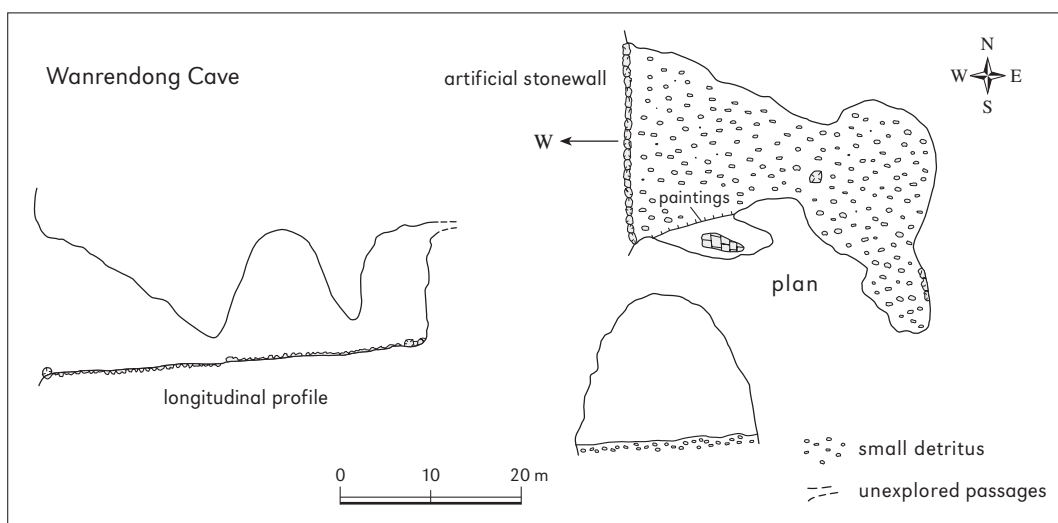


**6**   Map of the *Wanren-
dong* Cave.

The floor is slightly inclined to the outside. Sediments are only detritus, small pieces of limestone and marble rocks without gravel or any kind of material carried a long way by water. Towards the end of the cave, the content of rock powder increases. These sediments should come from the weathered rocks on the upper parts of the mountain and are carried in by a temporary surface flow. In terms of speleogenesis, the synergistic effect of the cave water and the Jinsha River played a great role in the formation of this cave. Flood backflush from the Jinsha River during the high water season has made the cave water more aggressive. Two large scallops on the entrance wall show that the speed of the water flow during the cave formation was very slow. Furthermore, it has a passage shape typical of epiphreatic conditions. This means that the backflush of the Jinsha River water fills the cave with water during the high water season; this has been so for a relatively long time.

On the right side of the entrance wall, under the scallops, there are some rock paintings. Because the rocks are throughly weathered, some of the paintings are broken in

156

pieces, or the colour is faded, and the content of the paintings can barely be made out. Parts of the paintings are buried by detritus sediments. Surprisingly, there are no paintings on the block rocks or inside the cave. One piece of stone is suspected to be a stone implement from the Paleolithic Age.

### 14.1.2 *Xiaodong Cave*

Xiaodong Cave (7) which is more or less like a rock shelter, is smaller than the Wanrendong Cave, only 14 m long, and half of it is unroofed. Because it is located on a platform (terrace) inclining towards the Jinsha River, the flat floor of the cave is suitable for a temporary residence, and the sediments of the inner cave have been changed by modern local people.

At the end of the cave there is a layer of half cemented, 0.4 m thick cave sediment. The components of the sediment are similar to that of the Wanrendong Cave, but they are a mixture of rock powders and pieces of stone, like the sediment at the end of the Wanrendong Cave. It is possible that this is the last sediment that surface percolating water had brought in before the solution fracture was blocked by the sediment itself. The sediments in the central part of the cave have been moved by people.
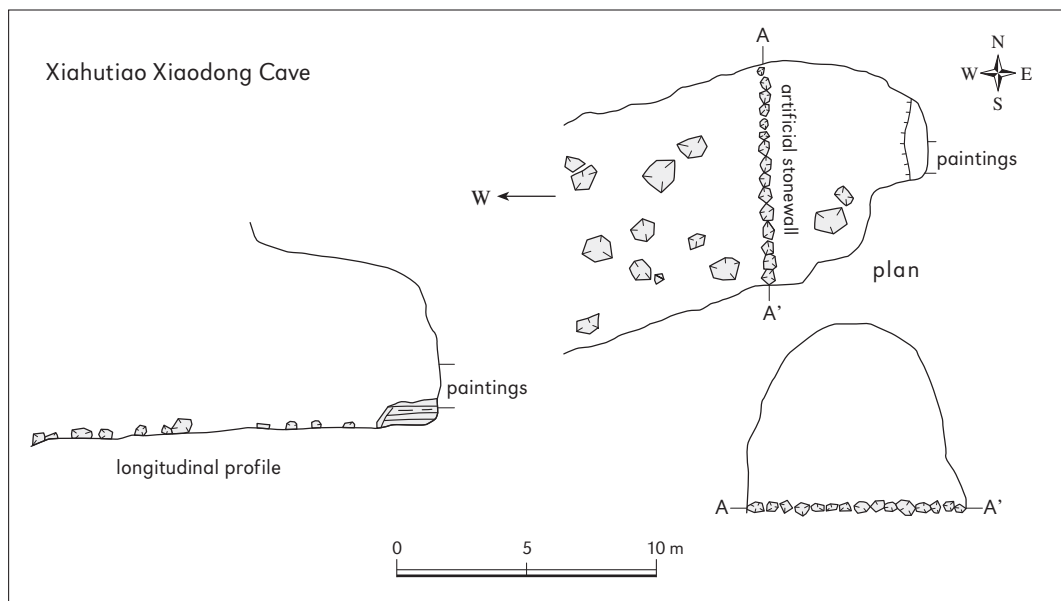
**7** Map of the *Xiaodong* Cave.

The Xiaodong Cave features rock art, too; however, for the same reasons as the Wanrendong Cave, the smoke blackened wall has made the paintings unrecognizable. There is no doubt that this cave was an ideal biding place for ancient people. Smoke marks on the wall have been partly buried by the remaining sediment, which suggests that ancient people once made fire in the cave.

### 14.2  ROCK SHELTERS AND ROCK ART

Caves and rock shelters were not only ideal place for ancient people to live, but also bearers of their resplendent cultures. Rock art is a shining example of human cultural heritage. It also continuously represents good material for studying anthropogenesis, national movements, environmental evolution, and so on. Jinsha River rock art has been known for a long time, but no detailed work has been done so far; most places have not even been recorded in detail. Widespread carbonate strata along the river provide fun-

The pilot study
of two caves,
rock shelters and
rock art along
the Jinsha River
(upstream of the
Yangtze)

damental conditions for the formation of caves and rock shelters. Along the river 52 rock art sites have been found, and it is believed that more new sites will be discovered in the remote areas with continuation of the studies. Seven of these sites (including the above mentioned two caves) have been recorded in detail, and two dating samples have been taken. Under increasing human impact and natural weathering, most of the content of the paintings is difficult to identify, especially in those sites that are easy to access.

### 14.2.1 *Huajizu rock art sites*

The Huajizu rock art sites, consisting of three rock art locations, surrounded by cliffs and located only 5 km away from the Xiazari village, remained undiscovered until 1988. On site 1, only a few paintings remained. It was not possible to identify the content of the paintings because they were mostly covered with a thin flowstone curtain (8). The paintings are located approximately 3–4 m above the ground.

**8** Maps of the *Huajizu* rock art site 1.
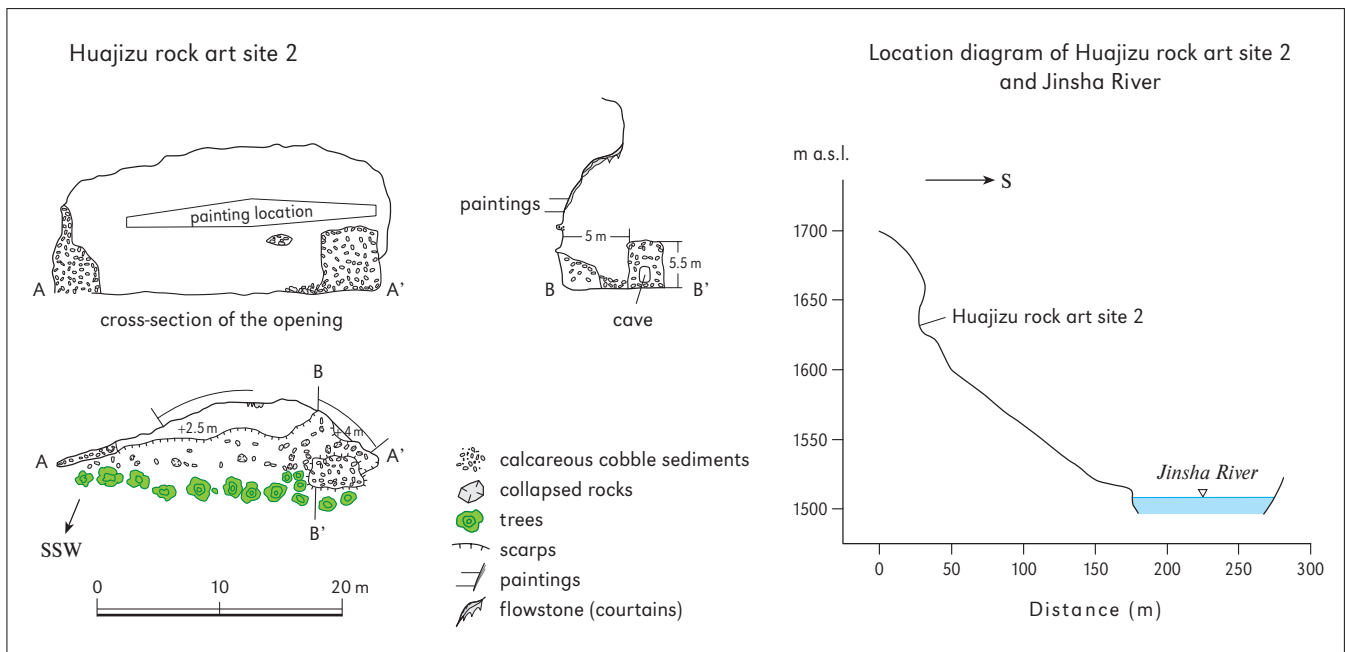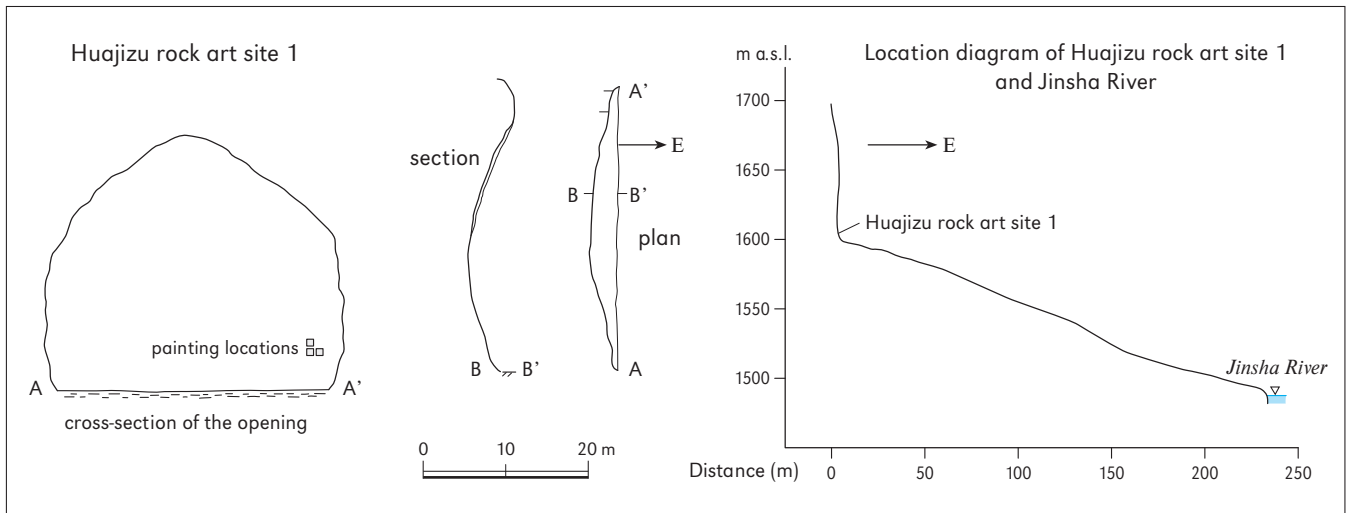


**9** Maps of the *Huajizu* rock art site 2.



Site 2, less than 150 m southwest from the site 1, features a painted area 24–25 m² in size, and 2.5–8 m above the ground (9). These paintings face the same problems – they are covered by thin flowstone curtains and natural weathering (10, 11).

**10** Paintings with several layers of overlay.



**11** Unknown features of animals.

One of the most interesting characteristics in this site are the remaining sediments in the rock shelter (12, 13). Measurements of the sediment position suggest that the paintings may have been drawn at the time when the lower part of the rock shelter was full of fluvial pebble sediment, which is solid calcareous cemented. One small cave formed in the calcareous cemented sediments in front of the shelter shows that those sediments were later washed away by the seasonal surface water. Since nearly 7 m of cemented sediments were washed away, it must have been a very long period.
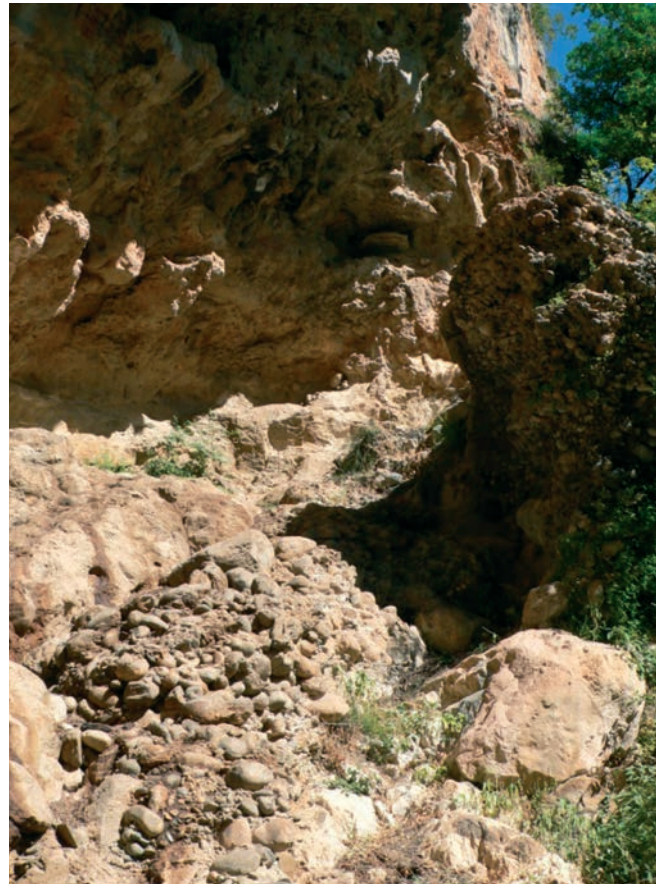
**12** Remaining sediments in a rock shelter.

**13** Remaining sediments in a rock shelter.

The temperature of the painting location is 30 °C and relative moisture 28 % in the afternoon when sunshine can reach the paintings. Judging from dry moss under the shrubs, it could be humid in winter.

### 14.2.2 *Lamazugu rock art site*

**14** Maps of the *Lama-zugu* rock art site.

This site is the only exception among the rock art sites; it is located one kilometre away from the main course of the Jinsha River and includes seven sites (14). GPS reading is 27°39.210'N, 100°16.087'E. The rock shelter is located on the banks of a small tributary



Lamazugu rock art site

Location diagram of Lamazugu rock art site and Jinsha River
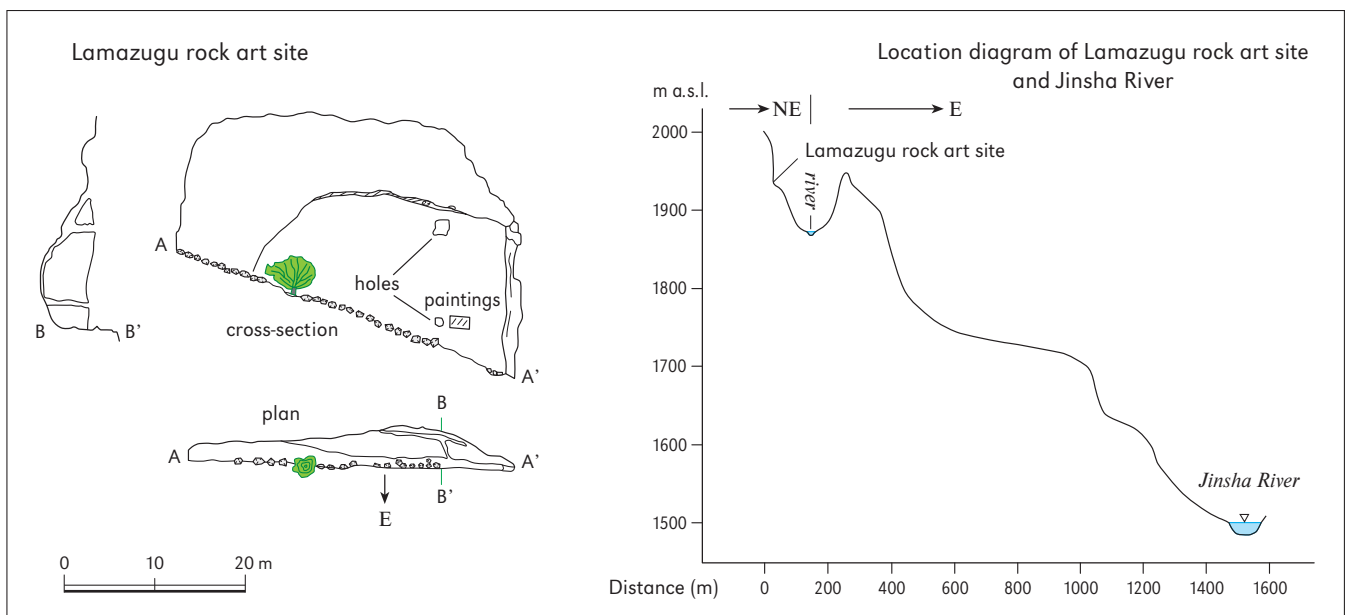
of the Jinsha River, almost 80 m higher than the river is. To a certain extent this rock shelter is still in the process of formation. One north striking fracture almost cuts the rocks in the central part of the shelter into two pieces. The wide open fracture provides percolating paths for water and rainfall, so there are two holes formed as water outlets. One is at the top, and another is close to the paintings on the same level. The fracture and the holes made the rocks more crashed. As a matter of fact, the outer layer of the rocks housing the paintings is gradually peeling off.

There were three species and 13 individual animals in total that could be identified at this site (15, 16). The paintings are concentrated in an area of 1.77 m (width) by 1.3 m (height), 2.13 m above the floor.

**15** Painting of a deer.



**16** Painting of a male goat.

The way animals are outlined suggests that the paintings might be very old. Unfortunately, the Liyuan hydropower station is under construction, and blasting for limestone nearby may have caused the paintings to be badly damaged, so the local cultural relic administration plans to excise the paintings and move them to the museum.

At the painting location, the temperature is 19 °C and relative moisture 35 % at noon. It is relatively benign microenvironment for preserving the paintings.

### 14.2.3  *Baiyun Bay rock art site*

Baiyun Bay rock art site lies about 5 km north of the Shangzari village, and is very difficult to access. GPS reading is 27°42.407'N, 100°16.600'E. The rock shelter faces south (17). Though a large area has been identified as a painted area, only a few characters can be recognized because of overlaying, fading and flowstone.

At noon, parts of the paintings are hidden in the shade, while parts lie in the sun. At the painting locations, the temperature and relative moisture readings in the sun and in the shade are completely different. The temperature is 51 °C and 23 °C, and relative moisture is 10 % and 39 %, respectively. The consequence of this difference is that the paintings in the sun are faded and the rock peeled; in the shade, higher moisture has enhanced the formation of flowstone curtains, so that the paintings are difficult to completely identify. The overgrowing flowstone offers a chance to establish a date. Two pieces of flowstone sample were taken. One sample contains two layers of painting material, which reveal that in the past some people kept coming to draw paintings on the wall.

**17** Maps of the *Baiyun* Bay rock art site.
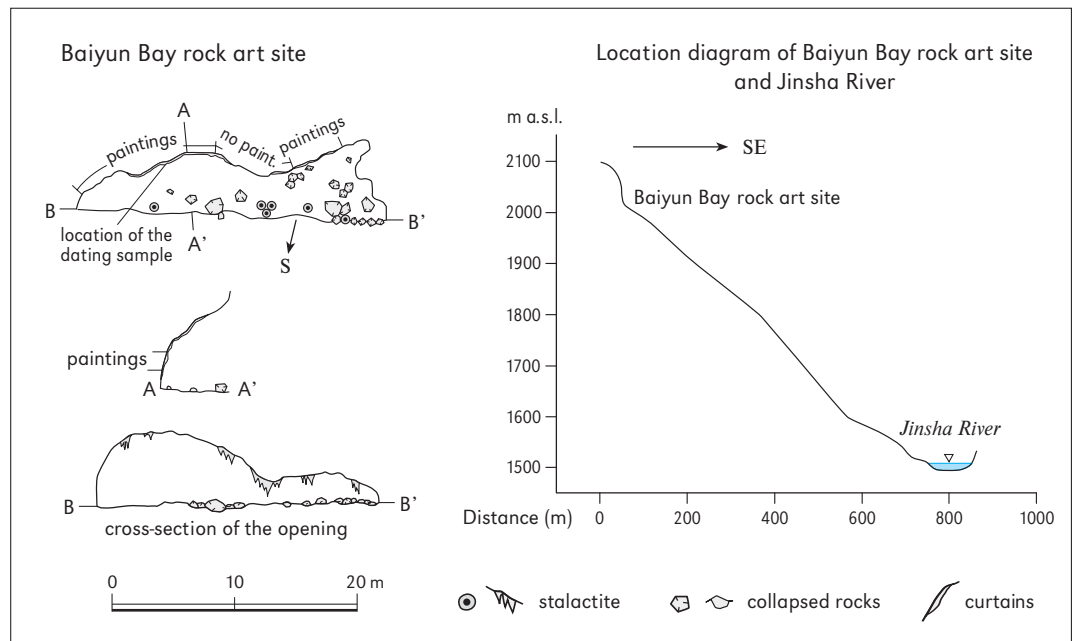
# LAOKUJING SHAFT AND ITS SEDIMENTS AT THE JIANGDONG MOUNTAIN – AN INDICATION OF THE HOLOCENE ENVIRONMENTAL CHANGE

HONG LIU, NINA G. JABLONSKI, XUEPING JI, ZHENG LI, LAWRENCE J. FLYNN, ZHICAI LI

The Laokujing shaft is located on the Jiangdong Mountain (1), a watershed area of the Minggang and Longjing rivers in Tengchong County, near the remarkable volcanic land-form distribution region (2), about 11 km northeast of the town of Gudong. GPS data are 25°23'24.6"N, 98°34'00.2"E and altitude is 2284 m. Jiangdong Mountain lies on the west side of the Gaoligong Mountain range (Gaoligong Shan) in southwestern China, which is of a considerable interest because of its unique geological, geographical, and environmental history and its high levels of biodiversity (*Chaplin*, 2005; *Jablonski et al.*, 2003). The study area is under the influence of the southwestern monsoon, with distinct dry and wet seasons. Since it lies on the windward side of the monsoon, the annual pre-cipitation reaches over 2000 mm; around 80 % of it occurs in the wet season. The annual temperature is 10–13 °C.

The shaft developed at the contact zone between the Permian Dadongchang group ($P_1dn$) and the Carboniferous upper section of the Kongshuhe group ($C_3k^2$). The former is a suite of grey to dark grey limestone with chert nodules or chert strips, grey to dark grey dolomitic limestone, with a medium to massive thickness reaching over 213.7 m, which is a disconformity over the stratum of the Kongshuhe group. The latter is car-neous to grey, medium to thick bioclastic limestone, crystallized limestone with a thick-



**1** Karst landscape of the *Jiangdong* Mountain area.

*Laokujing shaft
and its sediments
at the Jiangdong
Mountain – an
indication of the
holocene environ-
mental change*

ness 39–100 m. Their distribution is controlled by tectonics, surrounded by non-carbonate rocks. From the point of view of its geological structure, the shaft developed at the edge of the Dongshan syncline core (named for its location), where the core rock is the $P_1dn$, with an occurrence of W 10°. Outcrops of limbs are $C_3k^2$ and $C_3k^1$. The west flank has been destroyed by faults. In general, structural strikes are consistent with trends of strata extension, i.e. in N-S direction. Due to the underlying formation – Carboniferous
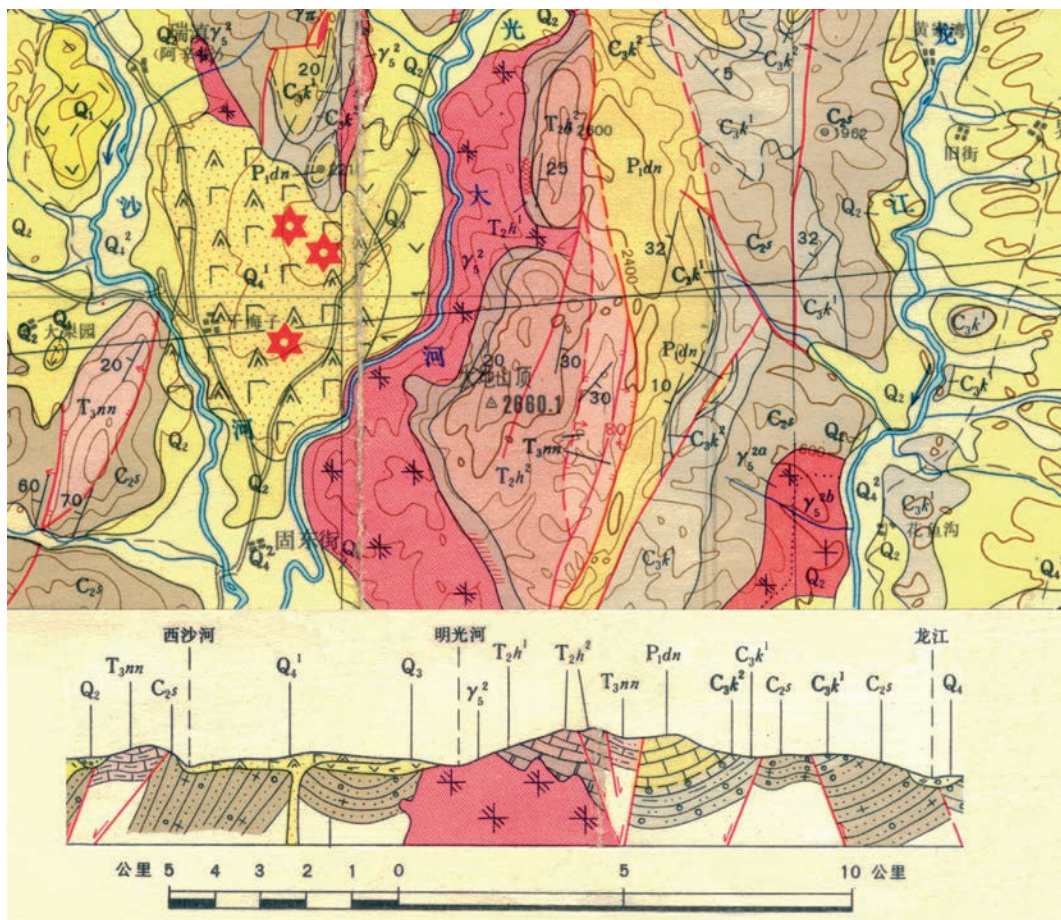


**2** Geological map of the study area.



**3** The cave entrance and its surroundings.

164

C$_3$k$^1$, a set of impermeable rock which prevents ground-water percolate down – there is a ground-water river system developed in the syncline. Along the path of the ground-water flow, a karst valley formed at the surface. The shaft formed right in the middle of the hillside towards the valley, around 50 m above the bottom.

As for vegetation, grass-land predominates; the forest surrounding the shaft has been destroyed. Only some shrubs cluster at the tops of the hills. At the entrance of the shaft several trees remain, influenced by moisture from the cave. Because of grazing and deforestation, there has been a serious soil and water loss (3).

## 15.1  LAOKUJING SHAFT CAVE

Laokujing shaft cave is a typical sinkhole with descending steps. In total, it is about 220 m long and 150 m deep. The entrance appears as an ellipse and is 2 m wide and 3 m long (4). The ranges of the width and height of cave passages are 0.5–12 m and 0.5–7 m,

*Laokujing shaft and its sediments at the Jiangdong Mountain – an indication of the holocene environmental change*

**4**  *Laokujing* shaft cave in the *Jiangdong* Mountain.
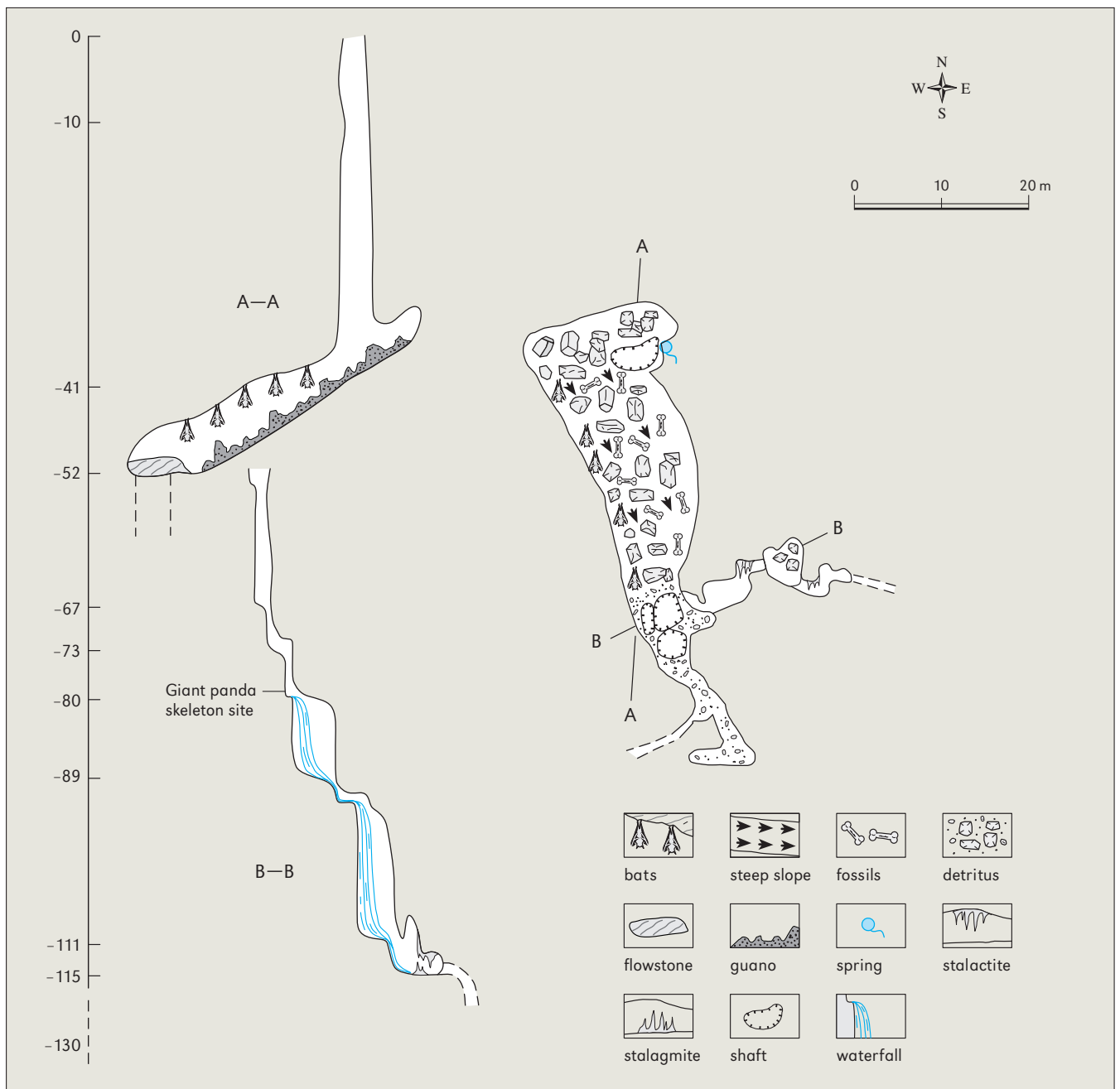
respectively. In general, the cave extends in the N-S direction, which coincides with tectonic bearing; from the third step of the shaft, the direction of cave passages is E-W. There are four steps in the cave, owing to the lithological variation. A few stairs can also be identified between the main steps. The steps are connected by very narrow passages.

The first stage from the entrance extends to −52 m, and is a regular shaft combined with a big chamber, which is 7–12 m wide and 5–7 m high. The bottom of the chamber, where fossils of giant pandas (*Ailuropoda melanoleuca*) and the Asian elephant (*Elephas maximus*) were discovered in 1997, declines to the south by 30 degrees. Owing to the rainfall before our expedition, a small brook with discharge of around 0.5 l/s flowed from the north end of the chamber to the south and disappeared. It is obvious that the discharge mainly depended on the quantity of precipitation; three days later, the water was reduced to 0.2 l/s. Judging from the size of the brook bed, the discharge could amount to 50 l/s in extremely wet conditions (1 m in width and 0.15 m in depth).

The second step, from −52 to −67 m, is a 15 m deep shaft. There is a branch cave in the N-S direction, 0.5–1.5 m wide, 1–2 m high, that developed at the −56 m level, with a 0.4 m thick layer of bat droppings. At the bottom of the shaft is a small room, 4 m long and 3 m wide. The flow reappears there. The cave room is sharply decrescent.

The third step, from −67 to −115 m, i.e. 48 m deep in total, is the combination of two substeps. Generally, the width of the passage is 1.5–4 m, and the height 3–5 m. Because of erosion and dissolution by the water flow, a few pits have developed on the floor and walls. Pieces of bones and animal fossils have been found on the floor or in the rock pits. In one pit on the wall, 1.2 m in diameter and 20 cm deep, a nearly complete weakly fossilized skeleton of a giant panda (*Ailuropoda melanoleuca*) was discovered during the exploration (5). Sediments, 15 cm thick, that were cemented by calcite were found in some parts of the pit. On the ground, through which the present flow passes, a few stalagmites grow.

**5**  A giant panda (*Ailuropoda melanoleuca*) skeleton, original site.

From −115 m downwards the fourth step is where the cave passage is narrow, fissure like, barely 0.5 m wide and from one to a few metres long. It declines towards the east where the karst valley is located. Another exploration of this cave in 2006 suggested that this narrow passage extended for at least another 40 m.

The profile of the Laokujing shaft indicates the cave has undergone at least two intermittent uplifts. The lowest step reveals that this area is still under the influence of a period of rapid uplift, which was validated by earthquake records of this region from 1502. During that period, 70 seisms over 5 on the Richter scale and more than 1000 weak temblors (less than 5 on the Richter scale) were recorded. All that evidence shows that the Jiangdong Mountain area is still under the influence of strong, distinct neotectonic movements.

## 15.2 SEDIMENTS

As an old sinkhole with relatively small passages, the Laokujing shaft has, owing to the impact of modern seasonal flows, little cave sediment, except for the large chamber at the bottom of the first shaft. Basically, according to their origin, the sediments can be divided into four types: speleothems, mechanical deposits, bio-sediments and cultural deposits.

In order to find more animal fossils, bones or relative dating materials, a 3.9 m long test trench was dug in the floor of the large chamber. The depth of the test trench varies from 0.35 m to 0.6 m, 0.45 m on average, because of the influence of the slope and sediment thickness.

In terms of differences of composition, texture and colour, the profile of the sediments could be divided into approximately four layers (6).

The top layer is 12–15 cm thick, grey to dark, and is thicker at the top than at the foot of the slope. It contains only a few pieces of rock and rotten wood. Apparently, those sediments came from the surface soil. Because they are located at the top, away from moisture, they are drier and harder than the layers below, and appear as a block structure.

The second layer, 24 cm thick and of dark grey colour, is similar to the top layer, except that the sediments are softer and tinier. It contains small pieces of rock and rotten wood, too, but is not as rocky as the top layer, and the pieces of rotten wood are big. Obviously, it has the same sources as the top layer.

*Laokujing shaft and its sediments at the Jiangdong Mountain – an indication of the holocene environmental change*
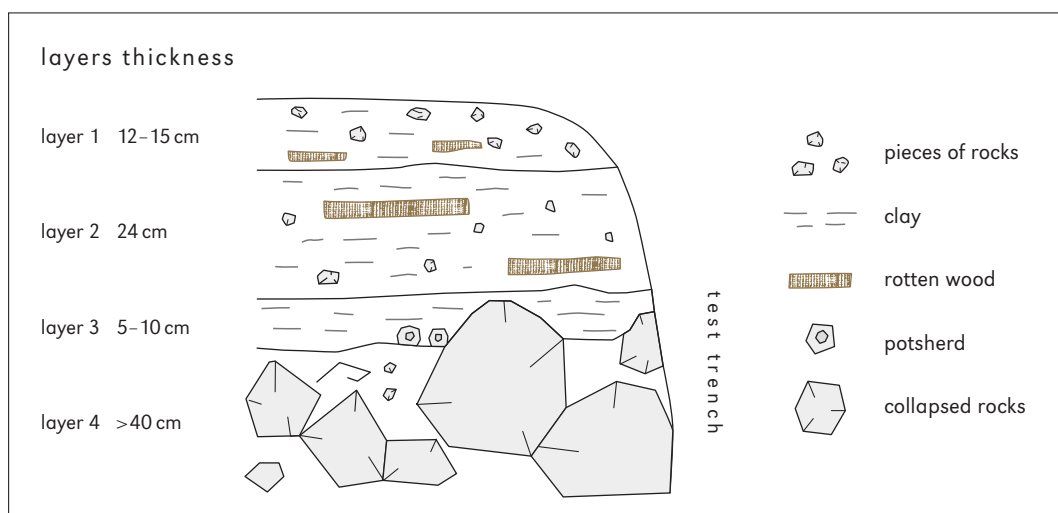


**6** The sediment profile of the test trench.

167

The third layer is thin, 5–11 cm thick, and uneven. The texture is firmer and clay is predominant. The top part is dark grey, below it the colour changes to yellowish. In some places, where there are big rock pieces underneath, this layer is absent. It is considered a transition layer to the second layer and the layer below.

The fourth layer is over 20 cm thick. It is composed of yellow detritus, coarse sand and lumps of rock. The moisture content of this layer is higher, due to the lower present seasonal ground-water course; water was exuded.

### 15.2.1  Speleothems

This cave is short of chemical sediments. Only individual stalagmites and stalactites developed, and these are small in size. The rock reliefs on the walls and ceiling of the large chamber suggest that this cave has been full of sediment. The location of the stalagmites on the ground indicates that most of them are located at places where the modern brook flows by. They could only grow in the dry periods or with very limited discharge of water. The pits on the ground and in the walls bear witness to a flood situation. All this implies that this area has suffered dramatic hydrological changes in the past.

### 15.2.2  Mechanical deposits

Mechanical deposits are the main sediments in this cave. They can be divided into collapse deposits and soil sediments. The collapse deposits are very common in the cave. The collapse of the ceiling is the main cause of the cave enlargement. Without exception, these deposits are distributed only in the large chamber. Beside the bottom of the entrance the shaft has some big collapsed rocks, in other parts rock fragments are small. This is related to the variation in the strata lithology. At the entrance, the rock ranges from thick to massive, while at the bottom it shifts to the medium thickness. In other passages of the cave few collapsed deposits are distributed.

The soil sediments are limited to the slope of the large chamber with an area measuring 30–35 m². They are composed of clay soil and rotten wood transported from the surface. The colour of the sediments ranges from grey to dark. The lower layers are slightly different. The lowest, yellow layer should be the early sediment on which the channel of the seasonal flow in the cave was created.

### 15.2.3  Bio-sediments

Though the Laokujing shaft cave is unremarkable, there are several bio-sediments preserved inside it. Exploration of the shaft in November 2005 yielded partial skeletons of two male giant pandas (*Ailuropoda melanoleuca*), as well as remains of lynx (*Lynx lynx*), Sumatran rhinoceros (*Dicerorhinus sumatraensis*), Yunnan horse (*Equus yunnanensis*), ibex (*Capra* sp.), Asian elephant (*Elephas maximus*), 11 other wild mammalian species and several cave dweller animal species (7, Table 1). The bones were not fossilized or were slightly fossilized and represented a natural accumulation of mostly large mammals (>30 kg) that had fallen accidentally into the sinkhole. The majority of the mammalian remains from the sinkhole complex were recovered from the large upper chamber, where they were found scattered on the sloping rocky floor and in small niches around the perimeter. The remains were not concentrated in any particular place nor were the remains from single individuals in any obvious association.

168

In order to find more animal bones and to establish their relative time sequences, around 50 kg samples were taken from each layer of the sediment. In the layer 1 only a few bone pieces from small animals were found.

**7** Parts of bones found in the shaft cave.

**Table 1**  Mammalian species from the *Laokujing* shaft cave on the *Jiangdong* Mountain.

| Order | Family | Species | Location within sinkhole | Nature of remains |
|---|---|---|---|---|
| Chiroptera | Rhinolophidae | *Rhinolophus* sp. indet. | test trench layer1 | 3 mandibles and assorted postcrania |
| Carnivora | Ailuropodidae | *Ailuropoda melanoleuca* | upper and lower chambers | 2 partial ♂ skeletons (one younger adult, one older adult) |
| Carnivora | Ursidae | cf. *Ursus* | lower steps passages | distal humerus |
| Carnivora | Felidae | *Lynx lynx* | upper chamber | radius |
| Carnivora | Felidae | cf. *Prionailurus* or *Pardofelis* | upper chamber | distal radius |
| Proboscidea | Elephantidae | *Elephas maximus* | upper chamber | associated teeth and postcrania |
| Perissodactyla | Rhinocerotidae | *Dicerorhinus sumatraensis* | upper chamber | lower molar and possibly associated postcrania |
| Perissodactyla | Equidae | *Equus yunnanensis* | upper chamber | associated rt. UI, lt. LM3, metacarpal, metatarsal, and manual phalanges |
| Artiodactyla | Cervidae | *Muntiacus gongshanensis* | upper chamber | partial mandible |
| Artiodactyla | Cervidae | *Cervus unicolor* | upper chamber | partial mandible |
| Artiodactyla | Bovidae | *Bos gaurus* | upper chamber | associated rt. and lt. UM2, rt. LM1-2, and assorted postcrania (upper chamber); rib (lower chamber) |
| Artiodactyla | Bovidae | *Naemorhedus* sp. indet. | upper chamber | partial mandible |
| Artiodactyla | Bovidae | *Capra* sp. indet. | upper chamber | associated maxillae and mandibles |
| Rodentia | Muridae | *Leopoldomys edwardsi* | test trench layer1 | molar and incisors |
| Rodentia | Muridae | *Mus musculus* | test trench layer1 | partial mandible |
| Rodentia | Rhizomyidae | Gen. et sp. indet. | test trench layer1 | rt. lower molar |

## 15.2.4 Cultural deposits

Only cultural deposits were recovered from the material taken from the test trench in the cave fill: a nearly complete ceramic bowl, which was found in four pieces dispersed in an area of 0.4 × 0.5 m in the third layer, approximately 0.5 m below the surface (8).

### 15.3 DATING RESULTS

In order to better understand when the large mammals fell into the cave, their bones and teeth were sampled for the accelerator mass spectrometry (AMS) radiocarbon dating at the laboratory of the Beijing University. AMS radiocarbon age determination of the bone samples from the upper chamber showed that they had been tightly clustered between 8470–8250 years BP, while an age of 5025 ± 35 years BP was determined for the giant panda bones from the pit of the third step (Table 2).

**Table 2**
AMS radiocarbon age determination for bones from the *Jiangdong* sinkhole.

| Level | Species | Corrected age (BP) | Radiocarbon years (BC) 1 σ (68.2 %) | Radiocarbon years (BC) 2 σ (95.4 %) |
|---|---|---|---|---|
| Upper chamber | *Ailuropoda melanoleuca* | 8470 ± 45 | 7575 BC (68.2 %) 7520 BC | 7590 BC (95.4 %) 7480 BC |
| Upper chamber | *Elephas maximus* | 8310 ± 45 | 7470 BC (68.2 %) 7320 BC | 7510 BC (88.8 %) 7240 BC 7230 BC (6.6 %) 7180 BC |
| Upper chamber | *Bos gaurus* | 8290 ± 50 | 7460 BC (61.3 %) 7300 BC 7220 BC (6.9 %) 7190 BC | 7490 BC (95.4 %) 7170 BC |
| Upper chamber | *Dicerorhinos sumatraensis* | 8370 ± 45 | 7520 BC (44.5 %) 7440 BC 7410 BC (23.7 %) 360 BC | 7540 BC (95.4 %) 7330 BC |
| Lower steps passages | *Ailuropoda melanoleuca* | 5025 ± 35 | 3940 BC (40.7 %) 3870 BC 3820 BC (26.6 %) 3760 BC 3730 BC (1.0 %) 3710 BC | 3950 BC (95.4 %) 3710 BC |

The broken bowl, recovered from the layer 3 of the test trench, was accurately dated based on its shape, glaze, and design by Prof. Qiyong Zhang from the Yunnan Provincial Museum. The bowl was a piece of common pottery from the early to the middle Ming Dynasty and most likely dates from the 1370s or 1380s.

### 15.4 IMPLICATIONS OF THE CAVE SEDIMENTS ON THE ENVIRONMENTAL CHANGE

The cave, especially its sediments, provides fundamental materials for studying the area's paleoenvironmental and landform evolution and neo-tectonic movement. The shape of the Jiangdongshan shaft, together with local temblor records and its two levels of step terraces, suggest that the study area has been suffering a strong, distinct uplift. The map of the cave reveals that the neotectonic movement has shifted the direction of the cave development. The old passages of the cave were oriented south, while the lower passages are turned to the east towards the bottom of the karst valley outside.

The dating results for the mammalian bones, which were tightly clustered between 8470–8250 years BP, show that a dramatic environmental change event may have occurred in that period. At least it suggests that the population number of the large mammalians declined sharply because not one piece of bone was found in the cave from the subsequent period of more than 3000 years. Or if we rephrase this: why did so many large mammals fall into the cave and die there? Though a few sites from the Neolithic Age have been found around this area, this does not seem to be a reasonable interpretation for the population decrease. Additionally, no bones of the large mammals have been found in the cultural sediments on those sites to date. What kind of event it could have been, remains unknown. Could it have been caused by a neotectonic movement?

The giant panda, *Ailuropoda melanoleuca*, is one of the best known symbols of China. Today it is found only in the small remnants of the bamboo forest in Sichuan and Shaanxi provinces. It has long been known that the giant panda inhabited a much larger range in the past, because panda fossils from the Pleistocene Age (1.6 million to 10,000 years ago) are relatively widespread in southern China. The discovery of the giant panda skeleton from 5025 ± 35 years BP suggests that the bamboo forest was widespread in this region until recently.

The finding of a Ming Dynasty bowl from the test trench highlights an important page of the environmental change in this area. The bowl under the bottom of soil sediment layers confirms that modern deforestation started with the early Ming Dynasty. Tengchong, located west of Yunnan, adjacent to Burma, was a very important town for economic and national security. Because of the strategic importance of Tengchong, a large number of forces in the garrison were dispatched by past dynasties, in particular by the Ming Dynasty. According to the Tengchong historical records, this dynasty stationed troops there after 1277. The soldiers had to do their own farming. From 1436 to 1449, Tengcong served as a strategic base for over 150,000 soldiers. It is coincident with the time of the bowl found in the cave, and suggests that these troops may have been the main cause of the deforestation and heavy soil erosion in the study area, in the remote karstic mountainous terrain. The thickness and composition of soil sediments in the areas around the cave show that they were clearly deforested in a short time. Since the sediments around 50 cm deep remained thick and contained many pieces of rotten wood, this suggests that this sedimentation occurred at the time of a shift in vegetation types from a dense forest to grass-land, or crop land. Therefore, the pattern of the modern environment in the study area is established by the significant human impact since the Ming Dynasty.

# EPIKARST FAUNA OF SELECTED CAVES IN YUNNAN PROVINCE

TANJA PIPAN, JANEZ MULEC, ANDREEA OARGA

Karst caves and other subterranean habitats share several key features. First, there is a permanent absence of light. Second, productivity is extremely limited, and except for rare cases, primary productivity is absent. Third, almost all systems of water- or air-filled cavities have biological activity. Fourth, there is reduced environmental variability relative to surface conditions. Thus, subterranean organisms must contend with complete darkness, limited food, and at least reduction in seasonal cues. Obligate subterranean species (stygobionts are aquatic and troglobionts are terrestrial cave dwelling species) share a convergent morphology of reduced or absent eyes and pigment, appendage lengthening, and an elaboration of extra-optic sensory structures (*Culver* and *Pipan*, 2009).

The subterranean domain includes both air- and water-filled underground habitats. China contains more than 500,000 km² of karst, mainly in the provinces of Yunnan, Guizhou and Guangxi (*Palmer*, 2007). Comprising approximately 15 % of the Earth's surface, karst represents 30 % of the land in three Chinese provinces (*Huang* and *Liu*, 1998).

In this contribution we review distinct communities of epikarst fauna in three geographically separate caves in Yunnan Province. The first investigation of epikarst communities in China was carried out in June 2006 when four sites in the cave Lao Huang Long Dong were sampled. Additional sampling of epikarst fauna was done in May 2009 when two caves were visited and six sites were sampled. In spite of many speleobiological expeditions and investigations in China in recent years (i.e. *Deharveng*, 2005; *Latella* and *Hu*, 2008), no previous work has included fauna from percolation water.

## 16.1 EPIKARST, COPEPODA (CRUSTACEA) AND THEIR ADAPTATION TO SUBTERRANEAN REALM

Epikarst is an uppermost layer of the karstic bedrock in the unsaturated zone, called the 'skin' of karst (*Bakalowicz*, 2004). It is typically 3–10 m deep, but its characteristics can vary considerably (*Ford* and *Williams*, 2007). Because of the position of the epikarst as the interface between soil and rock, epikarst is a transition zone between surface and subsurface (1). Seepage of water from many fractures and solution pockets that are constantly or periodically filled with water leads from the epikarst into the cave and brings with it particles as well as animals. Epikarst acts as a reservoir of water (*Petrič*, 2002; *Trček*, 2003) but unfortunately also for different kinds of pollutants from the surface. Epikarst is also the entry for most organic matter originating on the surface or in the soil.
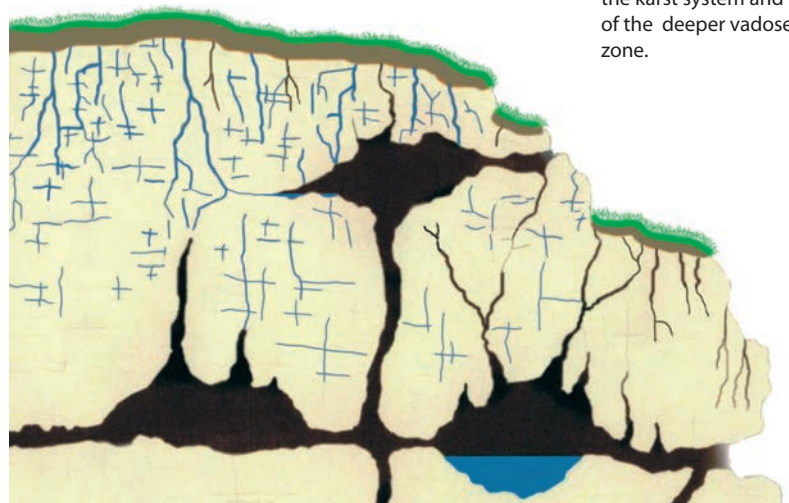
**1** Conceptual cross-sectional model of epikarst as the uppermost layer in the karst system and of the deeper vadose zone.

Epikarst fauna of
selected caves in
Yunnan Province

In this way percolating water entering into the underground ecosystem is crucial for the hypogean organisms in the caves as a source of nutrients (*Simon et al.*, 2007). From the ecological point of view, epikarst is both an exceptionally diverse and environmentally heterogeneous habitat (*Culver* and *Pipan*, 2009). It is a hotspot for ground-water animals, of which copepods (Crustacea) are the most abundant, but where other aquatic micro- and macroinvertebrates are also present (*Pipan*, 2005; *Pipan et al.*, 2006b).

The stygobiotic fauna from percolation water was first systematically investigated in Dinaric karst in Slovenia (*Pipan*, 2005). It was found out that epikarst is an important biological habitat with a diverse and specialized fauna. This specialized epikarst fauna, represented mainly by copepod crustaceans, has also been studied in Spain (*Camacho et al.*, 2006), Romania (*Moldovan et al.*, 2007; *Oarga*, 2008), West Virginia, U.S.A. (*Pipan* and *Culver*, 2005; *Pipan et al.*, 2006b; *Fong et al.*, 2007), as well as in patches of isolated karst in Slovenia (*Pipan et al.*, 2008).



**2** An oviferous female from the order Harpacticoida found in a pool with percolation water from the *Sigangli* Cave.

The subclass Copepoda belongs to the class Crustacea and comprises ten orders. Among them are four free-living copepod orders which representatives invaded subterranean waters: Calanoida, Cyclopoida, Gelyelloida, and Harpacticoida. In percolation water only specimens of Cyclopoida and Harpacticoida (2) have been found (*Pipan*, 2005).

Copepods are one of the most numerous metazoans and are adapted to all kinds of aquatic habitats (*Galassi*, 2001). The usual length of adults is 1–2 mm, but adults of some species may be as small as 0.2 mm and others may be as large as 10 mm. As do the other subterranean animals, stygobiotic copepods display various degrees of morphological and biological specialization to the underground environment. Depigmentation, thigmotaxis and miniaturisation occur in many species as a (pre)adaptation or exaptation which often determines the success of colonization to subterranean life (*Culver* and *Pipan*, 2009).

Frequent morphological adaptations of subterranean copepods are a lack of pigment and an absence of eyes, whilst their elongated and slim body shape indicates that the pore size of epikarst habitats is very small, like that of interstitial habitats. Pesce and Galassi emphasized the importance of reduction of spinulation on proximal segments of the body in Cyclopoida for movement in the sandy and muddy sediment (*Pesce* and *Galassi*, 1986). Another modification is the shortening of the swimming legs by oligomerisation in some ground-water copepods. Nevertheless, some stygobiotic harpacticoids have relatively long swimming legs. The differences in feeding and swimming behaviour between stygobiotic and epigean copepods are likely adaptations to subterranean habitats (*Galassi*, 2001; *Galassi et al.*, 2002), including epikarst.

Ground-water crustaceans such as Copepoda, Amphipoda and Isopoda produce, as a result of K-selection, fewer but larger eggs than epigean species. Large eggs ensure the food supply of nauplii in an oligotrophic environment. Ground-water copepods often lack true egg sacs (*Rouch*, 1977; *Dole-Olivier et al.*, 2000). Ground-water crustaceans show a general trend towards prolongation of the life cycle at various stages. Ground-water copepods develop slowly, with one or more generations per year (*Galassi*, 2001).

174

Our investigation was carried out in a dry period of the year in three caves in Yunnan Province: Lao Huang Long Dong, Lixin Cave and Sigangli Cave (3). In all investigated caves, epikarst fauna was sampled indirectly from pools filled with epikarst (percolation) water but not directly from trickles. Although it is recommended that epikarst fauna should be investigated by sampling of dripping water (*Pipan et al.*, 2006a), it is an investigation of pools fed by dripping water a reasonable surrogate for an inventory of epikarst fauna and is the only technique available when a cave is entered only once for speleobiological studies without possibilities of replications or long-term sampling.



**3** Locations of the studied caves in Yunnan.
1 – *Lao Huang Long Dong*;
2 – *Lixin* Cave;
3 – *Sigangli* Cave.

Pools filled by water that seeps down cave walls or drips from the cave ceiling form natural traps that harbour the epikarst fauna. After such suitable pool was located, basic physical and chemical parameters of water were measured (Table 1), using WTW Multiline P4. Each of these pools was sampled by filtering of different amount of water through the filtering bottle (4). It is a plastic bottle with openings on the sides covered with a net of mesh size 60 μm which allows water to pass through but retains organisms. Samples of organisms were preserved in 4 % formalin. After the completion of field collection, epikarst fauna was sorted under a dissecting microscope and stored in 70 % ethanol.



**4** Sampling of fauna from a pool filled by epikarst water.

| Pool number / Parameter | 1A | 1B | 1C | 1D | 1-drip | 2A | 3A | 3B | 3C | 3D | 3E |
|---|---|---|---|---|---|---|---|---|---|---|---|
| Temperature (°C) | 14.9 | 14.7 | | 14.7 | 14.2 | 15.5 | 12.6 | 12.5 | 12.6 | 12.7 | 12.8 |
| Conductivity (µs/cm) | 712 | 512 | | 236 | 446 | 306 | 328 | 312 | 248 | 393 | 262 |
| pH | 7.9 | 7.9 | | | | | | | | | |
| Discharge (ml/min) | | | | | | 8.4 | 2.2 | 0.2 | 6 | 12.2 | 8.2 |
| Volume (l) | 2 | 5 | 1 | 1 | | 0.2 | 0.3 | 2.5 | 0.3 | 1.5 | 2.5 |
| Total hardness (mg/l) | 364 | 274 | | | | | | | | | |
| Ca/Mg | 6.6 | 1.4 | | | | | | | | | |

## 16.2.1 *Lao Huang Long Dong*

In the cave Lao Huang Long Dong four pools (1A–1D) were sampled at a distance of 115 m between the first and the last pool while the distance from the entrance and the first sampled pool was 150 m. While the pool 1A was deepest in the cave, fed also by water from a small cave stream formed from percolation water, the pool 1B was composed from the network of pools (5, 6). The pool 1C was the largest one among the sampled pools. The first two were contaminated with guano and with many Diptera larvae, indicating the presence of bats in the cave during some parts of the year. The pool 1D was above the system of the pools, on a stalagmite, close to the entrance.



**5**  Sketch of sampled pools in the *Lao Huang Long Dong*.
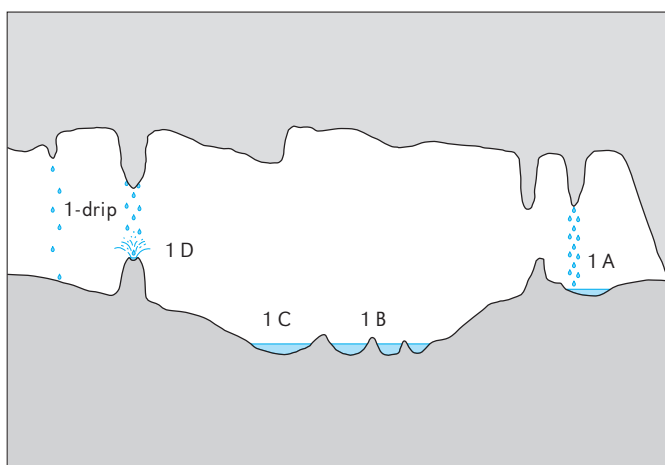


**6**  Sampling of fauna from the pool 1B in the *Lao Huang Long Dong*. Water is filtered through a bottle with netting (photo M. Petrič).

### 16.2.2 *Lixin Cave*

Lixin Cave has a large entrance (30 m × 30 m) with an active water flow during the rainy period. Due to speleothems found inside the cave, it has become an attraction for local people, but not yet equipped as a show cave (7). In the cave bats were observed. For the epikarst fauna one pool (2A) with percolation water 150 m inside the cave was sampled (8).
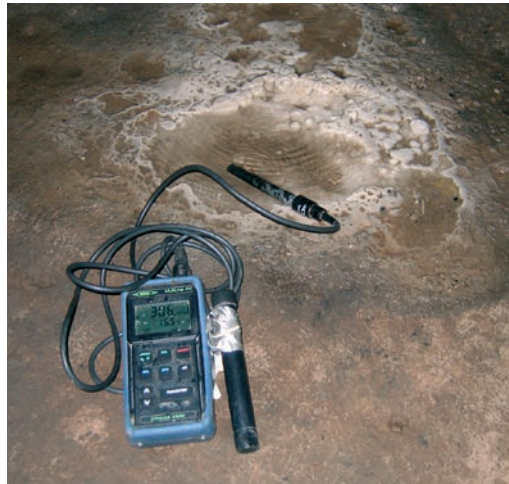


**8** A sampled pool in the *Lixin* Cave.

### 16.2.3 *Sigangli Cave*

Sigangli Cave is partially equipped for tourist visits. Stairs, a fence and paths are built, besides lamps and colourful lighting are installed (9). Along the tourist path in the cave five distinctive sampling sites were chosen (3A-3E) (10). The first two sampling pools (3A, 3B) were chosen close to the entrance, both with sandy sediment and detritus. The type of the third sampling pool (3C) corresponds to the pool 1D from Lao Huang Long Dong as was selected on the top of a stalagmite. Samples from such types of the pools are usually very clean and epikarst water with fauna from usually only one drip is collected there. The fourth sampling site (3D) consisted from several pools bounded by the flowstone formation. A morphological similar site was chosen in Lao Huang Long Dong as the pool 1B (6). The last pool (3E) was sampled at the end of the tourist part and was a pool in the armpit of a stalagmite. In the cave a colony of bats was seen.

**9** The huge entrance of the *Sigangli* show cave.

## 16.3 RESULTS AND DISCUSSION

The measured temperature in the pools in Lao Huang Long Dong was quite similar to the temperature in one drip (14.2 °C) (Table 1) what suggests that the pools were indeed permanently fed by the epikarst water. The temperature of percolation water from the Lixin and Sigangli caves was lower than in Lao Huang Long Dong. What is interesting, is a big difference in conductivity among the caves and within them. Kogovšek reported similar differences in conductivity of percolation water in caves in the Naigu stone forest (*Kogovšek*, 1998). In these caves conductivity of percolation water was in general higher than 400 µS/cm, what is similar to conductivity of percolation water in the cave Lao Huang Long Dong (487 ± 239 µS/cm), but in the Lixin (306 µS/cm) and Sigangli
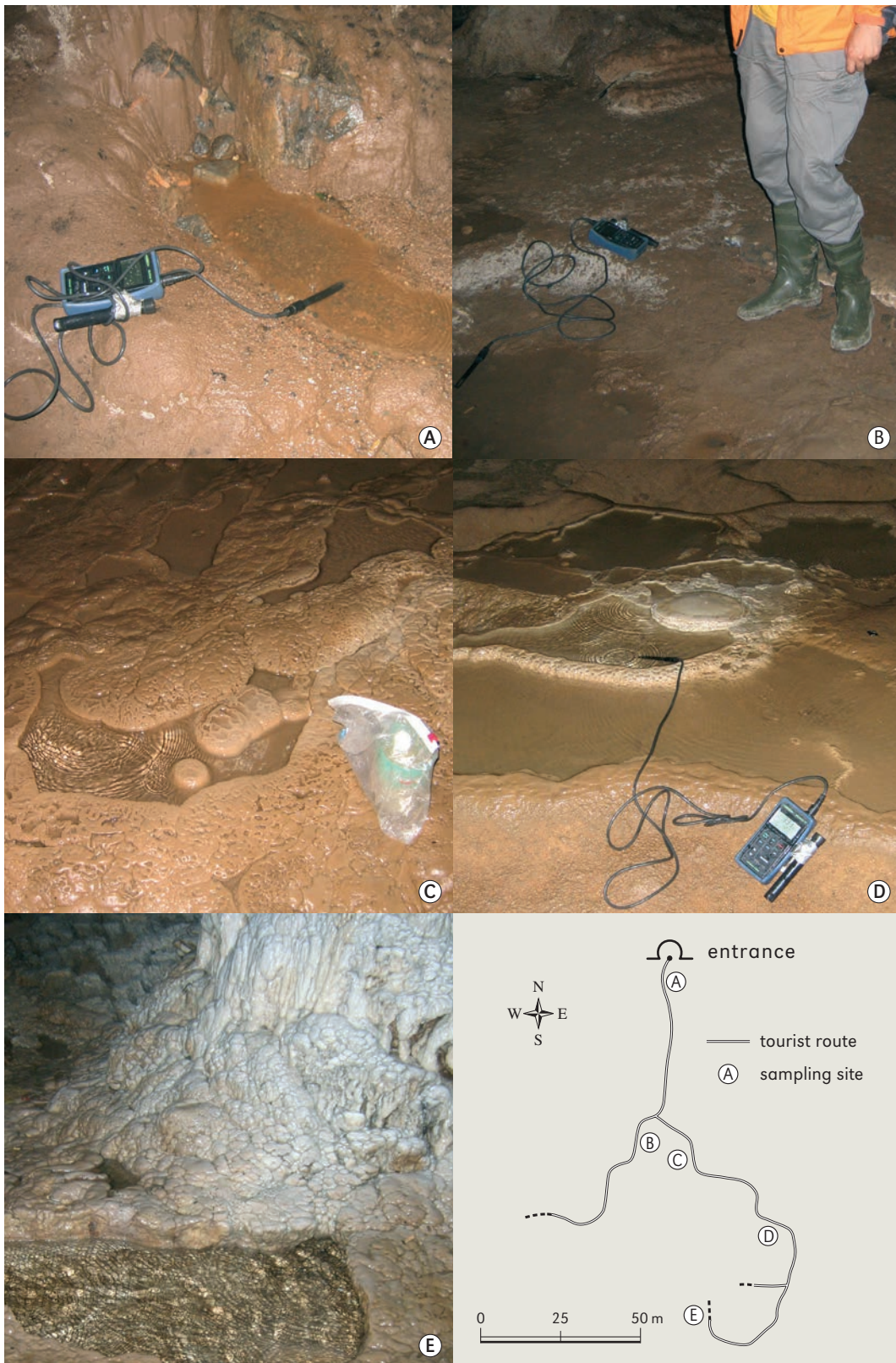
**10** Ground map of the *Sigangli* Cave and sampling sites (A–E).

(309 ± 58 µS/cm) caves conductivity was lower (Table 1). It is known that chemistry of percolation water varies considerably and higher values of conductivity are due to longer retention time of water in the epikarst and dissolution of carbonates (*Knez et al.*, 2009). Looking differences within the cave, they were higher in Lao Huang Long Dong than in the Sigangli Cave. Usually smaller discharge of percolation water resulted in higher values of conductivity and hardness (*Kogovšek*, 1998).

179

The chemical composition of percolation water in Lao Huang Long Dong shows that the ratio between the carbonate and magnesium content in the pool 1A was much higher than in the pool 1B which indicates a lower proportion of magnesium dissolution (dolomite) compared to calcium (limestone). In the pool 1A total hardness and calcium hardness were higher than in the pool 1B. In fauna composition there were no significant differences between these two pools, as both were not rich in fauna (Table 2).

**Table 2**
List of taxa and abundance of individuals found in drip pools in three caves in China, sampled in June 2006 and May 2009. Abbreviations are as follow:
1 – *Lao Huang Long Dong*;
2 – *Lixin* Cave;
3 – *Sigangli* Cave;
capital letters indicate sampled pools.

| Pool number / Higher group | 1A | 1B | 1C | 1D | 2A | 3A | 3B | 3C | 3D | 3E |
|---|---|---|---|---|---|---|---|---|---|---|
| Turbellaria | | | | | | | | | 1 | |
| Nematoda | | 1 | | | 1 | | 1 | | | |
| Gastropoda | | | | | | | | 1 | 1 | |
| Oligochaeta | | 3 | | 1 | 2 | | | 6 | | |
| Acarina | | 4 | 1 | 5 | | | | 2 | 2 | 1 |
| Ostracoda | | 4 | 2 | 13 | | | | | | |
| Copepoda – Harpacticoida | | | | 220 | 16 | 18 | 1 | 25 | 14 | 3 |
| Copepoda – Cyclopoida | | | | | | 1 | | | | |
| Copepoda – nauplia | | | | 4 | 1 | 4 | 1 | | | 1 |
| Cladocera | | | | 4 | | | | | | |
| Cladocera – ephippium | | | | 1 | | | | | | |
| Collemboia | | | | 1 | | | | | | |
| Insecta – larvae | 3 | 2 | 17 | >36 | | | | | | |
| Total number | 3 | 14 | 20 | >284 | 19 | 25 | 3 | 34 | 18 | 5 |

In all ten sampled pools from the three caves we found ten groups of invertebrates. The highest abundance was found in the pool 1D of Lao Huang Long Dong. Conductivity in this pool was lower (236 µS/cm) than in the first two pools and similar to conductivity in the Sigangli Cave (mean 309 µS/cm). The pool 3C in the Sigangli Cave was structurally and chemically similar to the pool 1D of Lao Huang Long Dong. Both were developed at the top of a stalagmite. Fauna was the most abundant and diverse in these two pools (11, Table 2). Conductivity in both pools was almost equal and lower than in all the other pools.

**11** Proportion of a different number of taxa in ten sampled pools in south China (see the text and Tables 1 and 2 for abbreviations).
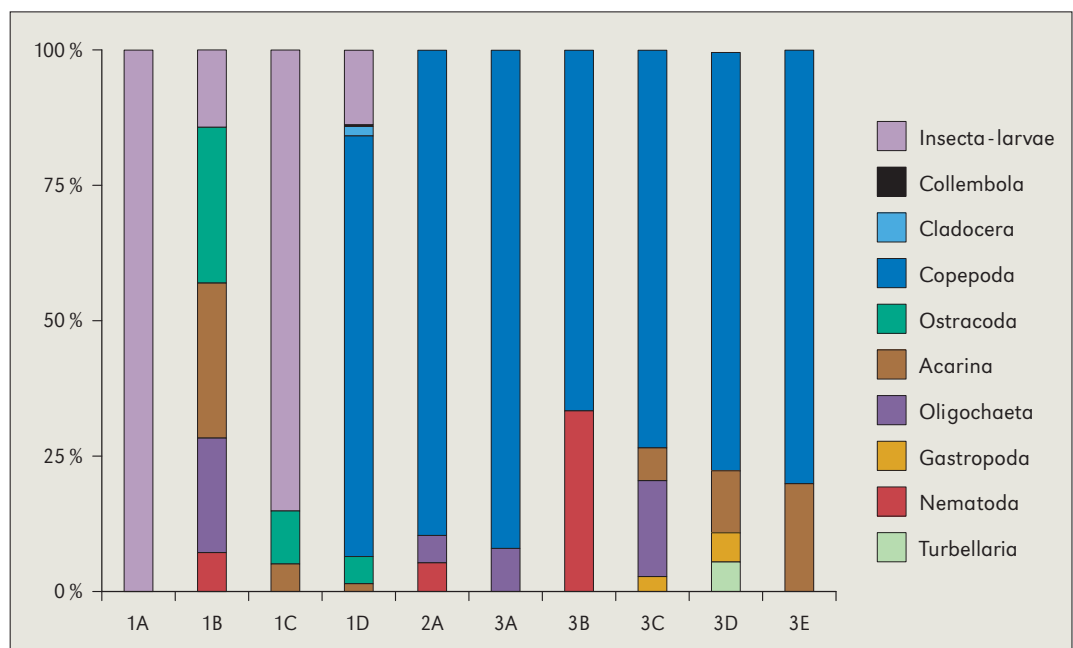
Some of the animals found in the pools, such as Gastropoda, Acarina and Collembola, are terrestrial species and presumably washed from the surface, soil or dry parts of the epikarst as is certainly also the case for larvae of Insecta. Oligochaeta and Nematoda were not abundant although in other sites they have been reported as dominant groups in the pools (*Pipan*, 2005; *Pipan et al.*, 2006b; *Moldovan et al.*, 2007).

The most numerous group were Copepoda. The number of individuals and taxa does not depend on the quantity of filtered water (Tables 1, 2) but may be related to differences in microhabitat in different pools. The best example is the pool 1D from Lao Huang Long Dong where Harpacticoida in the pool represented 74 % of all Copepoda found in all sampled pools. In this pool Harpacticoida represented 77 % of all individuals found in a drip pool, and in the pool 3C of the Sigangli Cave 74 %, respectively. Washed copepods from the epikarst captured in the pool, enriched with organic matter but not contaminated with bat guano, was the habitat that best enabled Copepoda for an extended period of time.

Other common animals found in the cave Lao Huang Long Dong were Ostracoda. An interesting finding were individuals of Cladocera (water fleas), and one cladoceran ephippium. Ephippium is the resting stage of animals, resistant to the change of temperature and loss of water. Although identification to species was not done, we assume at least for some species of the three crustacean groups (Copepoda, Ostracoda, Cladocera) they can be aquatic obligate subterranean dwellers – stygobionts.

## CONCLUSION

This study provides preliminary results about fauna in the epikarst waters from selected caves in South China. Although sampling was not long-term and not systematic, some common characteristics of the epikarst fauna composition and its primary (epikarst) and secondary (pools) habitat were obtained. Epikarst acts as a source for populations, mostly copepods, found also in the caves and it connects them with the other caves. Epikarst is also an important source of organic carbon and other nutrients that enter the caves via dripping water (*Simon et al.*, 2007). This is especially important for the caves without streams what the situation in our study was.

Drip-water fauna and other findings from this investigation provided also some other useful information such as the observation that part of the epikarst must be sufficiently saturated year-round to sustain communities. It is epikarst and its communities are highly vulnerable to any pollution on the surface. The presence of many copepods and animals from other groups is the best indicator to show that the investigated subterranean habitats and the surface area above are rather intact and not subject to pollution. More profound ecosystem conditions in the studied area can be assessed with the epikarst sampling that is both spatially and temporarily extensive.

# CHARACTERISTICS OF THE UNDERGROUND WATER FLOW IN THE TIANSHENGAN AREA AT HIGH WATER LEVEL

JANJA KOGOVŠEK, HONG LIU

As part of a three-year international scientific co-operation project between the Republic of Slovenia and the People's Republic of China, we conducted hydrogeological research. Its purpose was to carry out water tracing tests of underground water in the area of Tianshengan (Lunan, Yunnan) during different water levels (*Kogovšek et al.*, 1997; 1998; *Kogovšek* and *Liu*, 1999). The following are the results of water tracing made during high water level in September 1997.

The area in which the research on underground water drainage was conducted lies near the town of Tianshengan and is predominantly agricultural. The rainy season lasts from May to October, when most of the annual precipitation falls, followed by a long dry period. As a great amount of water is required for irrigation during the dry season, the capacity of the existing reservoirs is insufficient. In an attempt to solve this problem, new above- and underground reservoirs were constructed. Our study, which included water tracer tests, became part of a new underground reservoir construction (*Kogovšek et al.*, 1997; 1998). With water tracer tests, we tried to establish the direction of the underground drainage and its velocity at single sections under different hydrological conditions. The following are the results of a combination tracer test conducted during the high water level.

## 17.1  BASIC PROPERTIES OF THE AREA

The Lunan climate is subtropical; total annual precipitation averages 796 mm, average relative humidity is 75.3 % and an average annual temperature 15.6 °C (for the period 1980–1992). The amount of annual precipitation varies a lot. Over the same period it ranged from 542 mm in 1992 to 1066 mm in 1991. A wet season from May to October is followed by a dry season, when there is only 12–20 % of the annual rainfall. The area where ground-water tracing tests were conducted (1) covers 50 km². It lies in the immediate vicinity of Shilin, at an altitude of 1920 m in the east and 1750 m in the west, an area known for the Dalongtan karst spring (*Kogovšek et al.*, 1997; 1998).

The central part of the area consists of Carboniferous and Permian carbonate rocks interbedded by a narrow belt of less permeable quartz sandstone and shale marls, dividing the aquifer into the eastern and western parts. The thickness of this belt is between 20 and 30 m. The rocks are poorly permeable, but as they are fissured and not exceedingly thick, they do not act as an impermeable barrier. Among carbonate rocks, well karstified and permeable limestone and oolitic limestone prevail. Karst fissure porosity is typical of these rocks. The main drainage is thus provided by underground channels in combination with a network of fissures, creating a heterogeneous karst-fissure aquifer. At low water level, the passages are only partly filled with water, and during drought

**1** Hydrogeological map (based on *Kogovšek et al.*, 1997).

1 – Precambrian non-carbonate rocks,
2 – Carboniferous and Permian carbonate rocks,
3 – Lower Permian clastic rocks,
4 – a fault,
5 – a cave or a shaft with the underground water flow (the sampling point),
6 – a cave or a shaft with the underground water flow,
7 – a karst spring (the sampling point),
8 – a small spring,
9 – a surface stream,
10 – a lake or a water reservoir,
11 – the weather station,
12 – the proved direction of the underground water flow (red – Uranine, September 1997; blue – NaCl, September 1997),
13 – the uncertain direction of the underground water flow (red – November 1997),
14 – the possible direction of the underground water flow,
15 – a road,
16 – a village,
17 – the *Shilin* stone forest.
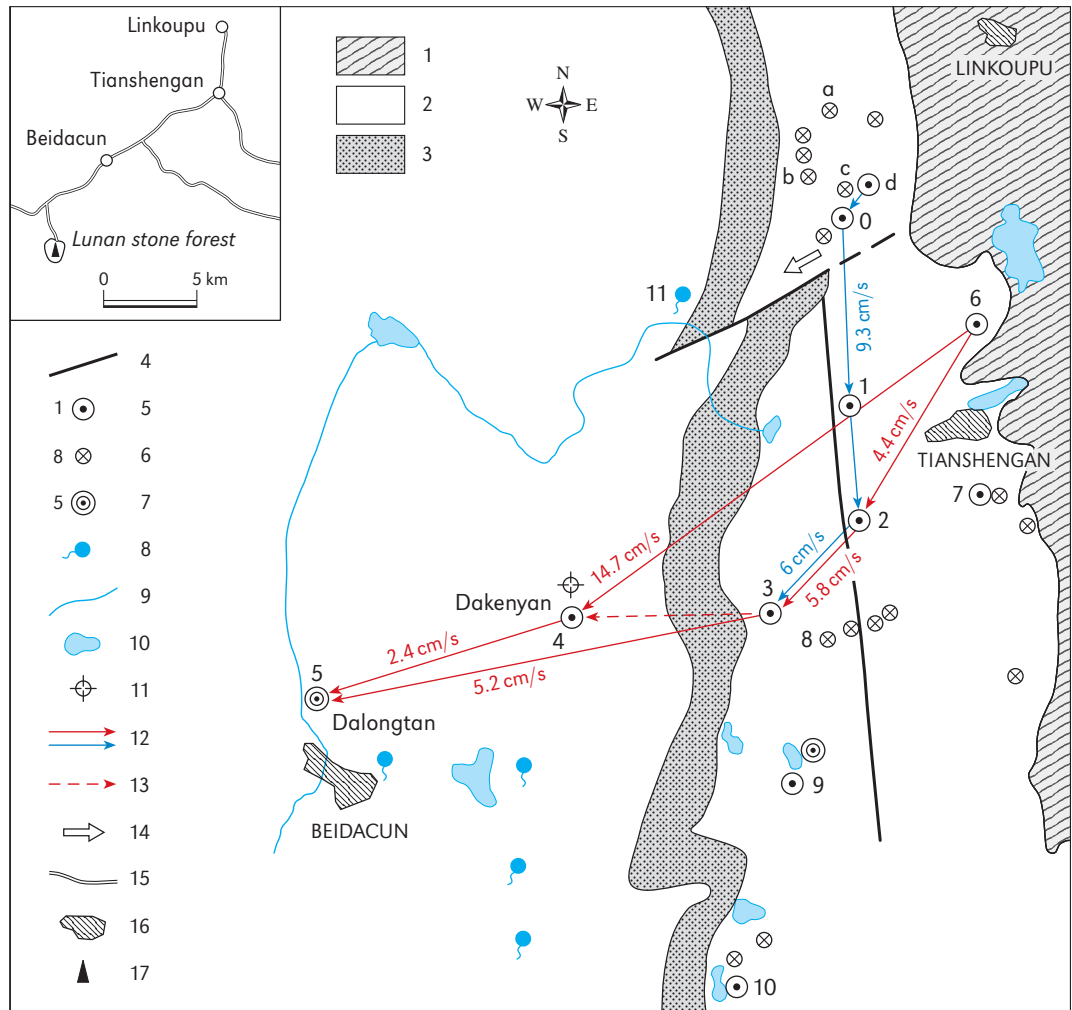
the water table is only 30 m below the surface. In the wet season water may flood the passages and even the lower lying fields.

Two faults are important in this area: the Tianshengan fault, trending N-S, and the Shibanshou fault, trending NE-SW. Numerous shafts and caves with underground water flow that we observed during the water tracer test are distributed along the Tianshengan fault (*Kogovšek et al.*, 1998).

## 17.2 THE TRACER TEST

### 17.2.1 *Hydrological conditions*

In September 1997 the water tracer test was carried out at relatively high water level with maximum discharge 2.24 m³/s. The discharge was several times higher than during the medium water level test in July 1996, but still lower than the maximum discharges in the years 1993–1995 (2). During the tracer injection the discharge at Point 6 was about 15 l/s and an abundant trickle even percolated through a thin roof. At Point d the discharge was judged to be close to 100 l/s; during the tracer tests at medium (July 1996) and low (November 1998) water levels it was around 30 l/s. The discharge measurements of the underground flow in the area of the water tracer test were made at the hydrological station Dakenyan only (Point 4). The artificial passage leading to the water flow was partly blocked during our test and because of the intensive rain part of the ceiling collapsed making access to the water flow even more difficult.
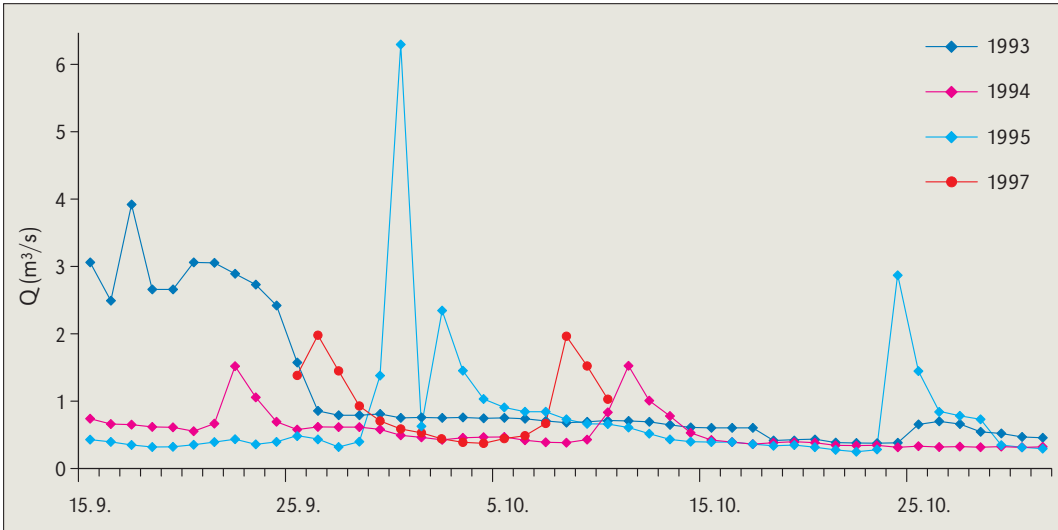
**2** Comparison of the underground water flow discharge at *Dakenyan* (Point 4) at the end of the dry period (at the end of September and at the beginning of October) between 1993 and 1995 and in 1997.

During the test we measured the discharge at Point 4 with the same dynamics as we sampled the water flow. The discharge, which measured 1.38 m³/s on 26 September at the time of injection, increased and reached its maximum value on 27 September (2.24 m³/s); later it decreased rather regularly until 3 October when it started to increase again. On 8 October it reached its maximum value of 1.96 m³/s and then decreased again.

### 17.2.2  *Injection, sampling and methodology*

The first tracer (1 kg of Uranine) was dissolved in 50 l of water and injected at Point 6 (Wayaodong) on 26 September 1997 from 16.30 to 16.40 (3). On the same day, from 15.00 to 15.15, 200 kg of sodium chloride was injected (4, 5) at Point d as the second tracer.



**3** Injection of Uranine into the water flow at Point 6 (*Wayaodong*).

185

**4** Preparation of solution of sodium chloride (NaCl) for injection at Point d.



**5** Injection of NaCl solution at Point d.

Sampling was organized at the following points: 1 – Maoshuidong, 2 – Shihuiyao, 3 – Xiangshuidong, 4 – Dakenyan, 5 – Dalongtan, 7 – Guanyindong, 9 – Changshuitang, and 10 – Xiniutang. At the points 2, 3, 4, 5, 9, and 10, where we expected the appearance of tracers, the sampling was more frequent during the foreseen flood events and later less frequent. Sampling frequency is shown on Table 1. The samples were stored in plastic bottles.

The sample analyses related to the chloride level were done by Wenqing Wu from the Geographic Institute in Kunming. The fluorescence analyses on Uranine by a luminiscent spectrometer LS 30 ($E_{ex}$ = 492 nm, $E_{em}$ = 515 nm) of water samples from the points 3, 4, 5, 9, and 10 were done at the Karst Research Institute in January 1998, while the sample analyses from Point 2 only in July 2000. We envisaged that the analyses of samples from the points 3, 4, 5, 9, and 10 would provide the expected information relat-

**Table 1**
The plan of water sampling (frequency by hour).

| Place of sampling | 1. day | 2. day | 3. day | 4. day | 5. day | 6. day | 7. day | 8. day | 9. day |
|---|---|---|---|---|---|---|---|---|---|
| Point 1 | 4 | 2 | 4 | 6 | 12 | | | | |
| Point 2 | 4 | 2 | 2 | 4 | 6 | 12 | | | |
| Point 3 | 4 | 2 | 2 | 4 | 4 | 6 | 12 | | |
| Point 4 | 6 | 2 | 2 | 2 | 4 | 6 | 6 | 12 | |
| Point 5 | 12 | 6 | 4 | 4 | 4 | 6 | 6 | 6 | 12 |
| Point 7 | 4 | 2 | 4 | 4 | 6 | 12 | | | |
| Point 9 | 6 | 4 | 4 | 4 | 4 | 6 | 6 | 12 | |
| Point 10 | 12 | 6 | 4 | 4 | 4 | 6 | 6 | 6 | 12 |

186

ing to flow velocity, yet the results showed additional directions of the flow at high water level compared to low and medium water level; this required additional checking.

The velocity of water flow was calculated relative to the linear distance between the point of injection and the point where the tracer appeared and relative to the time after injection when the tracer reached its maximum value (apparent dominant velocity).

## 17.3 THE RESULTS

### 17.3.1 *Transport of sodium chloride*

Because of high dilution levels only a slight increase in sodium chloride (NaCl) concentration was recorded at the points 2 and 3. The maximum concentration of 3.4 mg $Cl^-/l$ appeared 10 hours after the injection at Point 2 and after 16 hours (5.1 mg $Cl^-/l$) at Point 3 (6). The apparent flow velocity calculated on this basis from the injection Point d to Point 2 was about 9 cm/s and from Point 2 to Point 3 almost 6 cm/s. In July 1996, at medium water level, water flowed to Point 2 twice as slowly, by 4.7 cm/s, and from Point 2 to Point 3 even more slowly, 2.2 cm/s (Table 2).
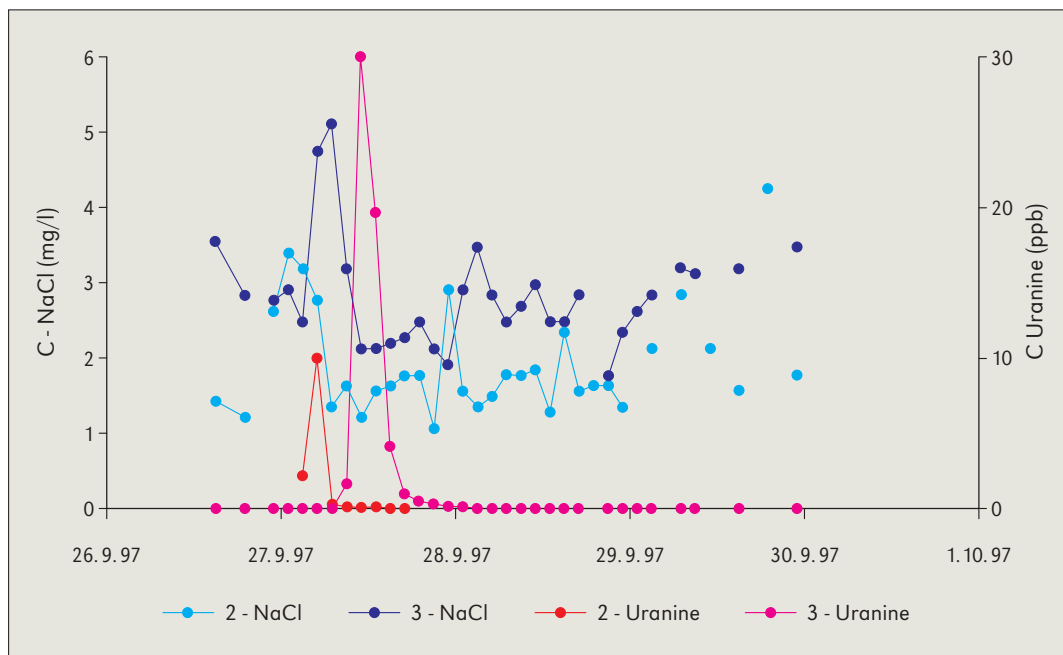
**6** Breakthrough curves of NaCl and Uranine at the points 2 and 3.

| Relation | l (m) | $t_{dom}$ (h) | $v_{dom}$ (cm/s) | $v_{dom\ 96}$ (cm/s) |
|---|---|---|---|---|
| d-2 | 3350 | 10.0 | 9.3 | 4.7 |
| d-3 | 4600 | 16.0 | 8.0 | 3.6 |
| 6-2 | 2000 | 12.5 | 4.4 | 3.3 |
| 6-2-3 | 3250 | 18.5 | 4.9 | |
| 2-3 | 1250 | 6.0 | 5.8 | 2.2 |
| 3-5 | 4100 | 22.0 | 5.2 | 2.7 |
| 4-5 | 2450 | 28.0 | 2.4 | 3.1 |
| 6-4 | 4500 | 8.5 | 14.7 | 3.0 |
| 6-2-3-5 | 7350 | 40.5 | 5.0 | 2.7 |
| 6-9 | 4050 | 72.0 | 1.6 | 0.6 |
| 6-10 | 6100 | 62.5 | 2.7 | |

**Table 2**
Air distances (l), time of tracer flow ($t_{dom}$), dominant velocities ($v_{dom}$), and velocities at medium water level – the tracing experiment in July 1996 ($v_{dom\ 96}$).

The minimal chloride level increase at Point 4 was recorded slightly earlier than at Point 3. This fact and also the highest concentration of chlorides recorded at Point 3 compared to Point 2 during high water level indicate the possibility of a many-sided water flow by the conduits lying higher than the permanently active channels. The flow velocities from Point d (NaCl) to the points 2 and 3 were higher as the flow velocities from Point 6 (Uranine) to these points (1, Table 2).

### 17.3.2  *Transport of Uranine*

At Point 2 Uranine reached its maximum value (10 ppb) 12.5 hours after the injection at Point 6. The calculated apparent water flow velocity to Point 2 was 4.4 cm/s (7, Table 2).

At Point 3 a distinctive Uranine breakthrough curve was formed; the first appearance of Uranine in concentrations of 1.64 ppb was recorded 16.5 hours after the injection, and in the following two hours the maximum value (30 ppb) in this breakthrough curve was reached. Then the Uranine concentration decreased only to increase again 18 hours after the maximum to 0.05 ppb and then decreased quickly below the limit of detection. The calculated velocity of the water flow from Point 6 to Point 3, related to the maximum Uranine concentration (flow direction 6-2-3), was 4.9 cm/s, and 5.8 cm/s in the sections 2-3 (6, Table 2).

The maximum concentration at Point 2 is noticeably lower than at Point 3. The sodium chloride that was injected at Point d showed lower concentration at Point 2 in comparison with Point 3. Yet fluorescence analyses of these samples were made more than two years later. Samples were kept in plastic bottles and in the dark. Thus adsorption to the bottle and solid particles in the sample was possible, as in this time the water transported a great amount of solid particles which may have been the cause of the fluorescence decrease over time. On the basis of the water tracing curve at the points 2 and 3 we may suggest a probable route for the tracer with water from Point 2 to Point 3 (7).

The highest concentration of 1.95 ppb at Point 4 was recorded 10.5 hours after the injection. Figures 7 and 8 show that it lies in a steep part of the breakthrough curve. On the basis of the water tracing from 1996, we presumed consecutive water flow through the points 2 and 3 to 4 and thus the later appearance of Uranine; this is why the preliminary sample was taken 6 hours in advance. This sample showed no traces of Uranine.
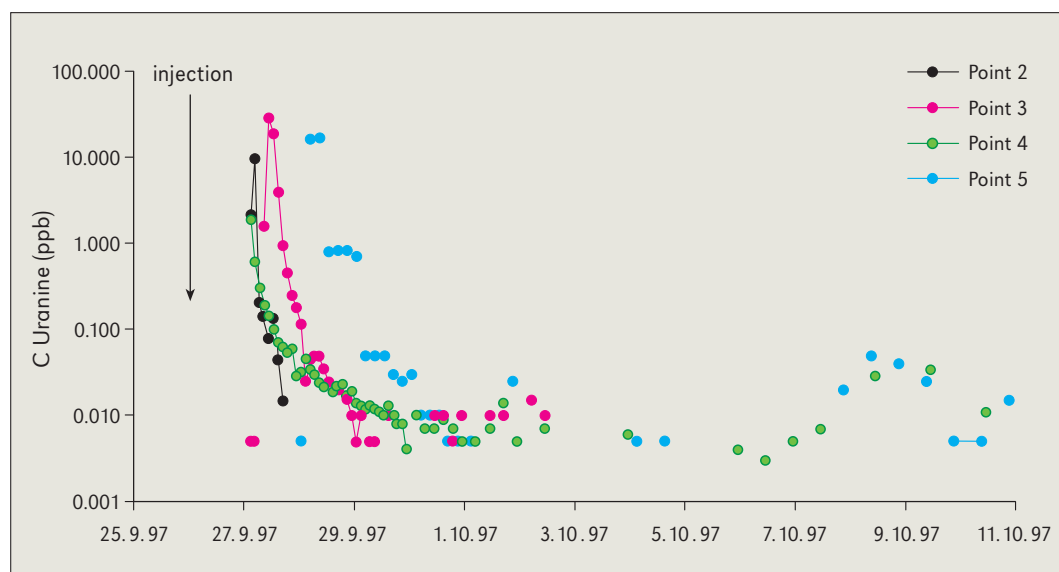


**7**  Uranine breakthrough curves at the points 2, 3, 4, and 5.

Thus we presume that the highest concentration occurred one or two hours before the recorded highest value and that the virtual highest value was higher.

The calculated water flow velocity from Point 6 to Point 4 was almost 14.7 cm/s. Since Uranine from Point 6 appeared at Point 4 earlier than at the points 2 and 3, the only possible explanation lies in fast, direct high water outflow from Point 6 towards Point 4 and slower flow in the already known direction through Point 3. However, it is surprising that the tracing curve was not more distinctive at Point 4 as one might expect on the basis of the results from the medium- (*Kogovšek et al.*, 1997) and low- (*Kogovšek* and *Liu*, 1999) water tracing tests.

It seems likely that at high water level water discharges both from Point 3 towards Point 4 and also directly towards the Dalongtan spring (Point 5); two distinctive, consecutive, proportionate breakthrough curves at these two points (3 and 5) confirm this. The flow velocity from Point 3 directly to Point 5 would be 5.2 cm/s (Table 2).

In any case these are established connections. However, it remains unclear why the water flow during high water level essentially deviates from the water flow during medium and low water levels. This will have to be checked in the future.

At the Dalongtan spring (Point 5) we succeeded in taking the entire breakthrough curve (7). The first Uranine appearance was recorded on 28 September at 1.00. The concentration increased in 8 hours to the maximum value 17.4 ppb; the peak of the pulse lasted for 4 hours. The Uranine concentration decreased fast and persisted at a level between 0.81 to 0.72 ppb for 16 hours and then started to decrease slowly. On 1 October the concentration decreased below the detection limit. A smaller tracer pulse was recorded again on 7 to 9 October when the maximum value was 0.035 ppb in the decreasing part of the breakthrough curve. This repeated intensive Uranine rinsing was due to abundant rain at the beginning of October; this rain caused the first visible increase in discharge after the first water pulse that followed the injection. However, we recorded lower Uranine concentration variations during the whole decreasing part of the first breakthrough curve which was probably due to the rain contributing to Uranine rinsing but not to a distinctive increase in discharge.

If in the first peak of the breakthrough curve at Point 5 Uranine from Point 3 was reflected, which seems more probable according to the shape of the curve, then the flow velocity from Point 3 to Point 5 was 5.2 cm/s; if, however, the peak reflected Uranine from Point 4, the flow velocity between the points 4 and 5 was at the most 2.4 cm/s; it seems that high water level slowed down the drainage through this passage.

We can confirm for certain that the flow velocity from Point 6 to Point 5 with regard to the maximal achieved Uranine concentration was 5.0 cm/s if we assume that the consecutive flow over the points 2, 3 to 5 compared to the drainage at medium water level (water tracing in July 1996) was twice as fast.

By sampling at the points 9 and 10 we tried to establish a potential underground water connection with Point 6. The water tracing test in July 1996 had indicated the possibility of such a link (*Kogovšek et al.*, 1997; 1998). In September 1997 we recorded at Point 9 a minimally increased signal of fluorescence. The Uranine signal was so faint that it could not be attributed to the injected Uranine for certain. We may conclude that even if a connection between the points 6 and 9 exists, it is insignificant at both, medium and high water levels.

Slightly more distinctive was the Uranine appearance at the spring 10 where on 29 September a slightly increased Uranine value (0.035, 0.040 and 0.175 ppb) was recorded three times in 10 hours. The flow velocity calculated on this basis would be 2.7 cm/s

*Characteristics of
the underground
water flow in the
Tianshengan area
at high water level*

(Table 2). Later, a single Uranine level increase was recorded. Thus we think that during high water level a weak connection between the points 6 and 10 exists but is not significant.

### 17.3.3 Returned Uranine quantity

The tracer analysis at Point 4 – where the peak of the tracing curve is missed – and measurements of discharge at the same point at high water level in September 1997 allowed us to calculate the returned quantity of the injected Uranine. Figure 8 shows how Uranine passed Point 4. During the first tracing pulse (6 days) only 60 g of Uranine reached this point, which is only 6 %. If we add the estimated Uranine quantity reaching the supposed peak of the tracing curve, the returned quantity may be two or even three times greater. Nevertheless, it is obvious that most of Uranine did not reach Point 4 but flowed to Point 5. Of course, rinsing continued. In the case of water tracing at medium water levels in July 1996, more than 50 % of the injected tracer came through Point 4 in one week. This also shows that part of Uranine avoided Point 4; the calculation of the returned Uranine quantity for Point 5 would yield this maximal value, but alas, we do not have data about discharge at this point. This shows the limited permeability of lower underground water passages from Point 3 to Point 4, which was already indicated by the smallest velocity of the flow in this section at medium water level.

Obvious, fast water flow in the treated area of karst during high water level demands a more detailed calculation of the returned tracer and also more complete curves, more frequent sampling that would have to take place every hour or even every half an hour. Newly established water flow directions at high water level with extremely high velocities conditioned the transport of the tracer during the time when we did not expect the tracer to appear, and we were sampling at longer intervals as recommended. Thus, in the future organized water tracing at high water level would give a more detailed notion of a very complex water flow and would answer the questions raised by the water tracing.

**8** The discharge curve, breakthrough curve of Uranine and returned Uranine at *Dakenyan* (Point 4).
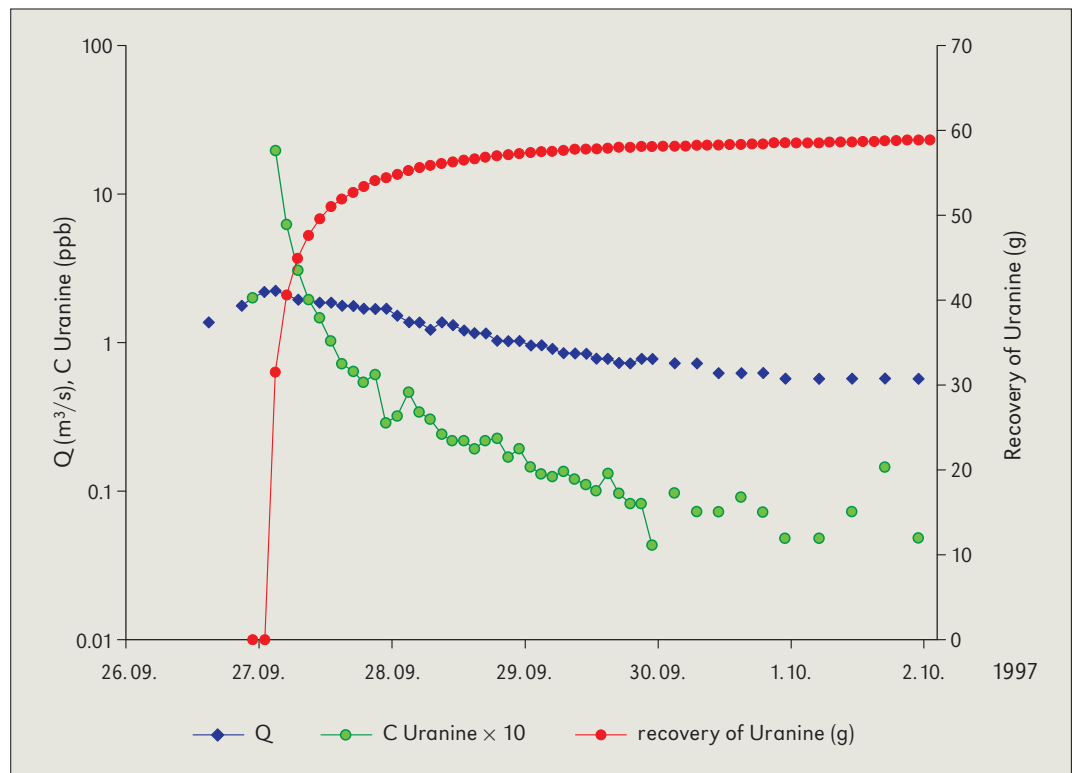
The tracer test by sodium chloride injected at Point d gave useful results only in the initial part of the water flow. Up to Point 2 and further on to Point 3 water flowed 2 to 3 times faster at high water level than at medium level and almost 10 times faster than at low water level at the end of November 1998 (see Chapter 18).

The tracer test using Uranine showed a poor connection of the underground water from Point 6 to Point 10, while the connection with Point 9 is questionable and may be neglected. The water tracing showed that at high water level there is, besides the water drainage towards the points 2, 3, 4, and 5, also a direct connection from Point 6 to Point 4 and from Point 3 to Point 5 along the higher lying channels. The determined flow velocity from Point 6 to the Dalongtan spring – Point 5 (6-2-3-5) was 5 cm/s, which is twice faster (maximum discharge 2.24 m³/s) than at medium water level (maximum discharge 0.902 m³/s). The direct connection from Point 6 to Point 4 allows faster water flow (14.7 cm/s) as was recorded during the medium water level in the section d-0. The established water flow velocities correspond to the values given for the underground waters of southern China (*Yuan*, 1991; *Song et al.*, 1993) ranging from several mm/s to more than tens of cm/s.

The returned Uranine quantity at Point 4, estimated as slightly more than 10 %, is low as probably most of Uranine flowed directly over Point 3 into the Dalongtan spring (Point 5). Only additional, well-organized tracer tests with discharge measurements at high water level can answer the questions raised by these findings.

*Characteristics of the underground water flow in the Tianshengan area at high water level*

191

# CHARACTERISTICS OF THE UNDERGROUND WATER FLOW IN THE TIANSHENGAN AREA AT LOW WATER LEVEL

JANJA KOGOVŠEK, HONG LIU

As part of an international scientific co-operation project between the Republic of Slovenia and the People's Republic of China that took place from 1996 to 1998, we studied the basic physico-chemical properties of karst waters and the properties of karst water drainage in the region of Lunan in Yunnan Province. The project was supported by the then Slovene Ministry of Science and Technology and the corresponding ministry of China.

The area in which our research took place lies near the town of Tianshengan (*Kogovšek et al.*, 1997). The dry period in this part of Yunnan lasts from November to May when only up to 20 % of annual precipitation falls. Because the area is predominantly agricultural, a lot of water is required in the dry period. By building reservoirs, people try to provide enough water for the dry season. Essential for such interventions in karst is good knowledge of underground water drainage.



**1** Hydrogeological map (based on *Kogovšek et al.*, 1997).

1 – Precambrian non-carbonate rocks,
2 – Carboniferous and Permian carbonate rocks,
3 – Lower Permian clastic rocks,
4 – a fault,
5 – a cave or a shaft with the underground water flow (the sampling point),
6 – a cave or a shaft with the underground water flow,
7 – a karst spring (the sampling point),
8 – a small spring,
9 – a surface stream,
10 – a lake or a water reservoir,
11 – the weather station,
12 – the proved direction of the underground water flow (red– Uranine, November 1998),
13 – the possible direction of the underground water flow,
14 – a road,
15 – a village,
16 – the *Shilin* stone forest.

Characteristics of
the underground
water flow in the
Tianshengan area
at low water level

Basic knowledge about the underground water drainage in this karst area may be provided by tracing tests. In three years we carried out three water tracing tests of underground water in the area of Tianshengan during different water levels. The first water tracing was performed in July 1996 at medium water level (*Kogovšek et al.*, 1997; 1998), the second one in September 1997 at high water level (*Kogovšek* and *Liu*, 2000) and the third one in November 1998 at low water level (*Kogovšek* and *Liu*, 1999). The following are the results of the water tracing that took place at low water level in November 1998. This water tracing complemented the knowledge gained by the water tracing during the middle and high water levels.

## 18.1  BASIC NATURAL PROPERTIES OF THE AREA

The Lunan climate is subtropical; total annual precipitation averages 796 mm, average relative humidity is 75.3 % and an average annual temperature 15.6 °C (for the period 1980–1992). The amount of annual precipitations varies a lot. In the study period it ranged from 542 mm in the year 1992 to 1066 mm in the year 1991. A wet season from May to October is followed by a dry season when there is only 12 to 20 % of the annual rainfall.

The area where the ground-water tracing test was conducted (1) covers 50 km² and lies in the immediate vicinity of Shilin, at an altitude of 1920 m in the east where the tracers were injected and 1750 m in the west where the important Dalongtan spring (*Kogovšek et al.*, 1998) lies. The basic natural properties of the area are presented in Chapter 17.

## 18.2  THE TRACING TEST

### 18.2.1  *Hydrological conditions during the test*

The hydrological station is located at Dakenyan (Point 4). At the time of the water tracing test in November 1998 an access to the water flow at Point 4 through the artificial channel was not possible. Owing to intensive rainfall during the summer, part of the ceiling had collapsed and filled up the passage; it was only possible to reach the water flow by a more difficult access through a deep valley.

In this part of the karst the dry season usually starts in November with minimal rainfall and low discharges and lasts to May. But this changes from year to year. In Figure 2 the discharges at Point 4 for two hydrological years are presented: the first one



**2**  Daily precipitation and discharge at the *Dakenyan* station in the hydrological years 1994–1995 and 1995–1996.
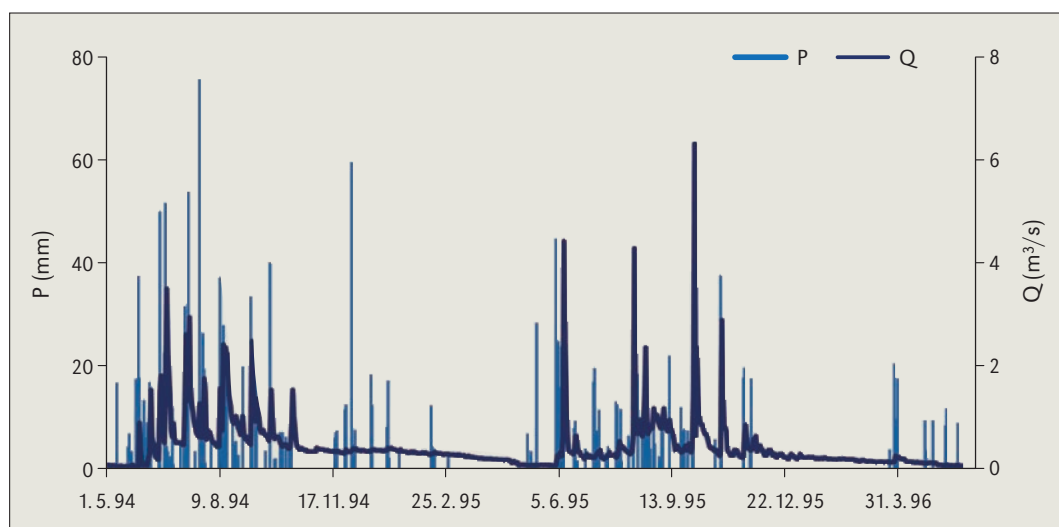
from 1 May 1994 to 30 May 1995 and the second one from 31 May 1995 to 22 May 1996. Great differences were noticed between them. The total amount of annual precipitation in the first hydrological year was 1153 mm, with maximum annual discharge of the underground water flow of 3.48 m³/s, and in the second year only 741 mm, but with maximum discharge of 6.28 m³/s.

The amount of precipitation in the dry season from November to May in the first year was 234 mm and in the second one 163 mm. The amount of rain in November 1994 was 43 mm with mean discharge of the underground water flow of 0.34 m³/s and 60 mm in November 1995 with mean discharge of 0.39 m³/s.

Figure 3 represents discharges for the period from the end of November to the beginning of December for the years 1993, 1994, 1995, and 1998 (daily values). Thus, the water tracing test in November 1998 was achieved at relatively low, slightly decreasing discharge. In 1993 the discharge in this period of time was even lower. It is hard to define the minimum discharge, because in the dry period it largely depends on the quantity of water pumped by different pumping stations for irrigation.



*Characteristics of the underground water flow in the Tianshengan area at low water level*
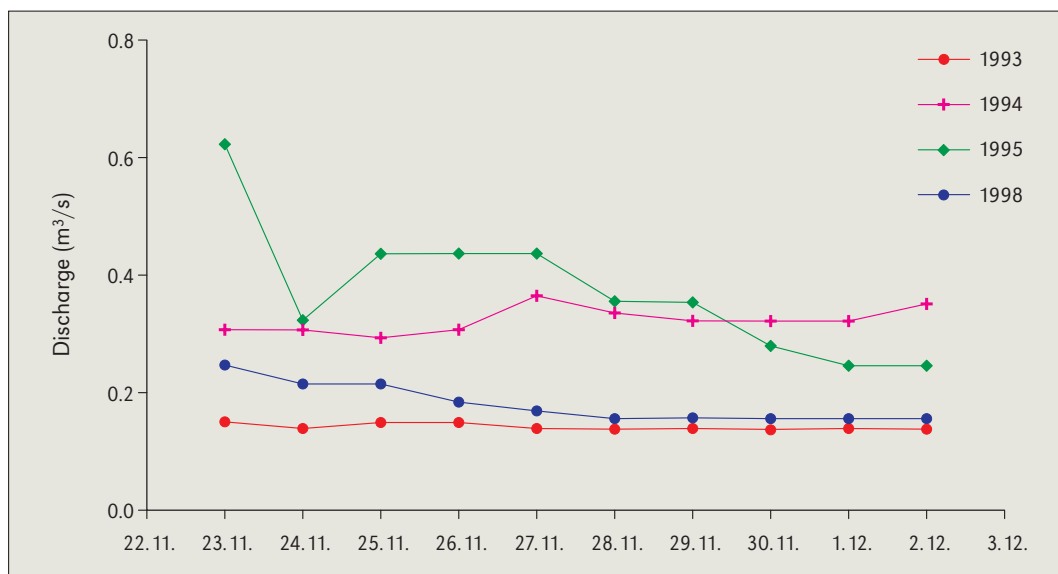
**3** Comparison of the underground water flow discharge at *Dakenyan* (Point 4) at the beginning of the dry period (at the end of November and at the beginning of December) between 1993 and 1995 and in 1998.

After the injection on 23 November 1998 measurements of the discharge at Dakenyan were carried out at shorter time intervals that were in accordance with water sampling at this site. The results of discharge measurements are shown in Figure 4.
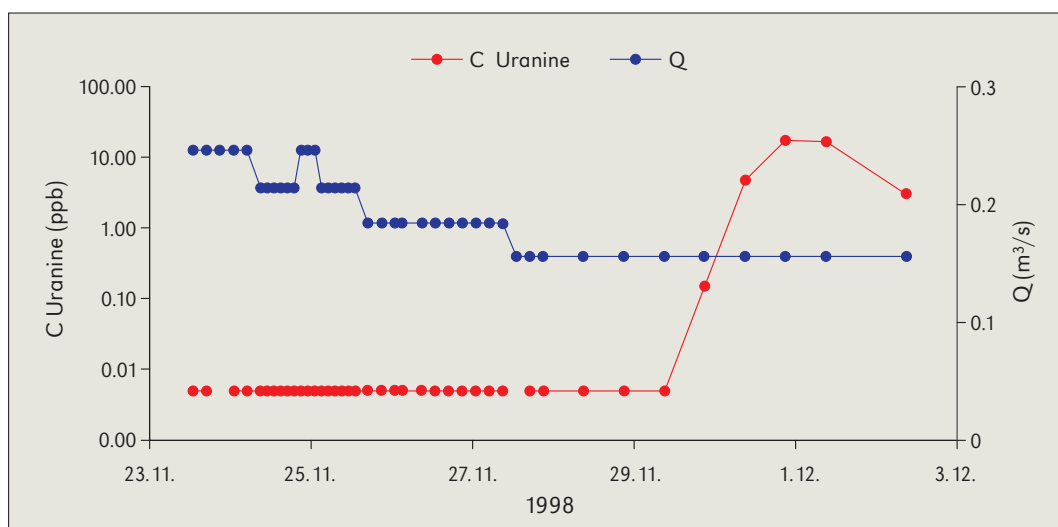


**4** The course of discharge and the breakthrough curve of Uranine at *Dakenyan* (Point 4) after the injection on 23 November 1998.

The outflow discharge during the injection was 0.246 m³/s at Point 4. In the following ten days when the samples for fluorescence analyses were taken discharge evenly decreased and on 28 November reached 0.156 m³/s. It slightly increased only in the night from 24 to 25 November without having any influence on tracer transport in the middle and lower part of the underground water flow, and it can be said that the water tracing was carried out at low, steady discharge in a slight decrease.

### 18.2.2  *Injection of the tracer and its sampling*

On 23 November 1998, at 11.00, we injected 0.8 kg of Uranine dissolved in 50 l of water at Point d where we had injected Uranine in July 1996 and sodium chloride in September 1997. The injection was practically instantaneous. At that time the discharge at this point was from 30 to 40 l/s (5).

**5**  Injection of Uranine solution at Point 4.



We made a detailed plan for sampling. We organized sampling (6) at Point 11 – a small spring, Point 2 – Shihuiyao, Point 3 – Xiangshuidong, and Point 4 – Dakenyan (1). At Point 2 we sampled at first every 4 hours and on 24 November we started to sample every 2 hours (for 28 hours) then every 4 hours and later every 6 and 12 hours. At the end of the sampling, on 1 December, we sampled once a day.

At Point 3 we sampled at first every 4 hours, at 11 p.m. on 24 November we started to sample every 2 hours (for 28 hours). We continued sampling on a 4-hour basis and later every 6 and 12 hours. At the end of sampling, which was on 1 December, we sampled once a day.

At Point 4 we sampled at first every 4 hours, on 24 November we started to resample every 2 hours and on 25 November every hour. In the afternoon we restarted by sampling on a 2-hour basis (for 20 hours) and then every 4 hours and on 28 November every 6 hours. For the next two days we sampled twice and later once a day. The sampling was finished on 2 November.

## 18.3 THE RESULTS

### 18.3.1 *Uranine transport through the observed points*

As the quantity of the returned tracer at Point 4 during the water tracing in July 1996 was relatively low (55 %) and at Point 11 we did not sample at that time, we wanted to establish whether Point 11 was connected with Point d. The water tracing in September 1997 when we injected sodium chloride at Point d and also observed Point 11 did not yield good results, probably because of heavy dilution. The detailed sampling at spring 11 during the water tracing in November 1998 showed that at low water level this connection did not exist, as Uranine did not appear at Point 11.

As expected, Uranine consecutively appeared at the points 2, 3, and 4 (7). At Point 2 the most distinctive breakthrough curve was formed, having a quick increase in the Uranine concentration (on 24 November) without major variations; its maximum value
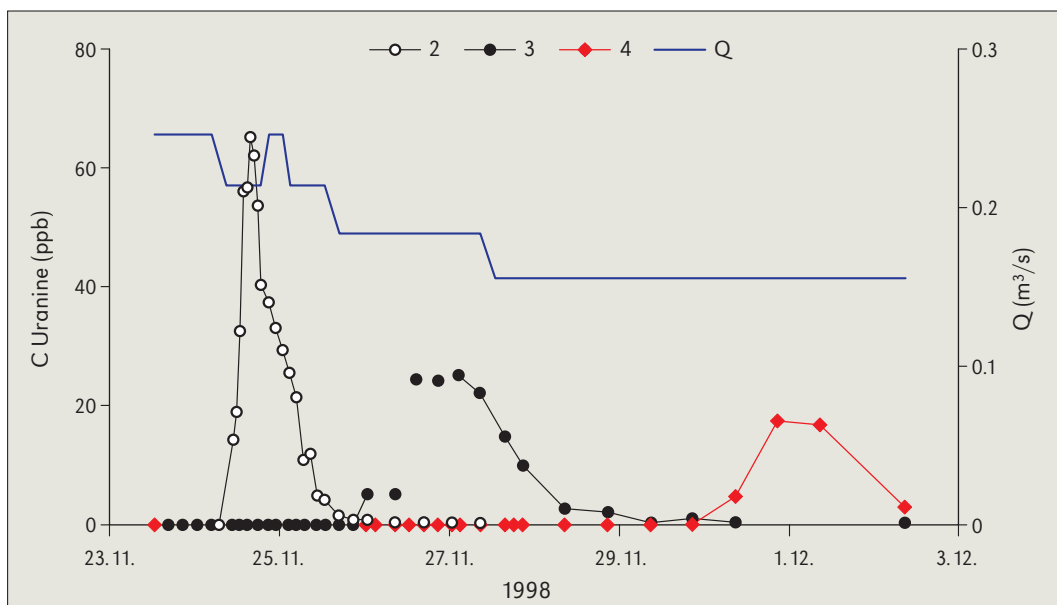


**7** Breakthrough curves of Uranine at the consecutive points 2, 3 and 4 of the underground water flow.

197

was 65 ppb. Uranine concentrations higher than 50 ppb were recorded for 5 hours, and then they started to decrease, at first fast and later slowly to reach the value of 0.065 ppb on 30 November, which is 1000-times lower than the maximum recorded concentration. Certainly more intensive transport of Uranine continued for at least one week, and complete restoration of the state before the injection took even more time; this depended on the rainfall that washed off the remaining Uranine.

At Point 3, like at Point 2, the Uranine concentration reached its maximum value (25.2 ppb) rapidly, yet later the transport of Uranine showed a flattened and lengthened breakthrough curve. The start of the breakthrough curve at Point 3 lags behind Point 2 by only 40 hours (its maximum values already for 58 hours) and the only smaller increase in the Uranine concentration in a decreasing part of the breakthrough curve took four days.

At Point 4 the tracer appeared four days after its first appearance at Point 3 and the breakthrough curve was even more flattened. Since, unfortunately, at the time of planning the water tracer test and during the injection we lacked data about the actual discharge, we anticipated according to an estimate of the discharge rate at injection Point d, slightly faster Uranine transfer than was actually the case. This is why the sampling at Point 4 (Dakenyan) was already less frequent, every 12 hours, when Uranine appeared and reached its maximum concentration. Later we finished the sampling. Nevertheless, we did succeed in recording the initial part and the breakthrough curve with the maximum Uranine concentration of 17.4 ppb but not its decreasing part. According to the breakthrough curve at Point 2 and the results of water tracing in July 1996, we concluded that the curve at Point 4 must be rather flattened and lengthened. We anticipated that Uranine transport through Point 4 would last at least one month with gradual decrease in the Uranine concentrations. This transport depends on rinsing by the rainfall that followed. Based on measurements, we calculated the velocity of the through flow, but unfortunately we were not able to calculate the precise amount of the returned tracer at Point 4.

### 18.3.2 *Velocity of the underground flow*

On the basis of the known distances between the injection point and successive sampling points and the travel time of tracers to these points (measurements of fluorescence), we were able to calculate the underground flow velocities for single sections. In Table 1 the maximum ($v_{max}$) and in Table 2 the dominant ($v_{dom}$) apparent velocities of the underground flow are presented for sections d-2, 2-3, 3-4, and d-3, d-4. Maximum apparent velocities are calculated by considering the first appearance of the tracer, and dominant velocities by the maximum concentration of the tracer.

**Table 1**
Maximum apparent underground flow velocities ($v_{max}$).

| Relation | Distance (m) | Time (h) | Velocity (cm/s) |
|---|---|---|---|
| d – 2 | 3350 | 22 | 4.2 |
| 2 – 3 | 1250 | 40 | 0.87 |
| 3 – 4 | 1850 | 90 | 0.57 |
| d – 3 | 4600 | 62 | 2.1 |
| d – 4 | 6450 | 152 | 1.2 |

**Table 2**
Dominant apparent underground flow velocities ($v_{dom}$).

| Relation | Distance (m) | Time (h) | Velocity (cm/s) |
|---|---|---|---|
| d – 2 | 3350 | 28 | 3.3 |
| 2 – 3 | 1250 | 58 | 0.60 |
| 3 – 4 | 1850 | 90 | 0.57 |
| d – 3 | 4600 | 86 | 1.5 |
| d – 4 | 6450 | 176 | 1.0 |

The results show that the velocity of the underground flow in that area at low water level is substantially lower than at medium or high water level. The maximum velocities

($v_{max}$) at low water level calculated by the first appearance of the tracer were much higher for the initial part of the flow compared to the dominant apparent velocities ($v_{dom}$). Equal values in section 3-4 are due to sparse sampling and less precise determination of the beginning and peak of the concentration curve.

We discovered out that the water velocity is highest in the section from injection Point d to Point 2 ($v_{dom}$ = 3.3 cm/s). In sections 2-3 and 3-4 the drainage is slower ($v_{dom}$ = 0.6 cm/s). Obviously, the water flow is not slowed down by a non-carbonate barrier between points 3 and 4 only, but also by the Tianshengan fault, trending N-S, which is crossed by the underground water flow behind Point 2. Upstream, water flows almost parallel to the fault. The Shibanshou fault, trending NE-SW, obviously does not control the conduit network to a parallel flow and it does not cross the non-carbonate belt of rocks in the direction of Point 11; we can affirm this at least for the period of low water level.

If we had not observed the Uranine appearance at so many points, our information about the water flow velocity would be less precise. At the section d-3 the average dominant velocity was 1.5 cm/s, while at the section d-4 – this means the average velocity of the entire observed way – it was 1 cm/s.

### 18.3.3 *Recovery of the tracer*

Calculation of the returned tracer was possible only at Point 4, as this was the point where the measured discharge data were available.

The water tracing test in July 1996 and the dynamics of the quantity tracer transport showed that most of the tracer crossed Point 4 in the central part of the breakthrough curve. In the beginning a sharp increase of the Uranine concentration was recorded; however, it also decreased rapidly and later asymptotically slowly approached the initial value. The subsequent washing of Uranine was generated by the rainfall that followed.

The water tracing test in November 1998 at low water level shows a more flattened and lengthened tracing pulse. Compared to previous tracings at medium and high water levels when the water flow and transport of the tracer were much faster, we can expect much longer Uranine retention time in the case of low water levels when the flow velocity is substantially lower. Figure 8 shows the dynamics of the Uranine travel in the central part of the breakthrough curve at Point 4 when 40 % of the injected Uranine passed in the course of three days. However, the transport of Uranine lasted longer even
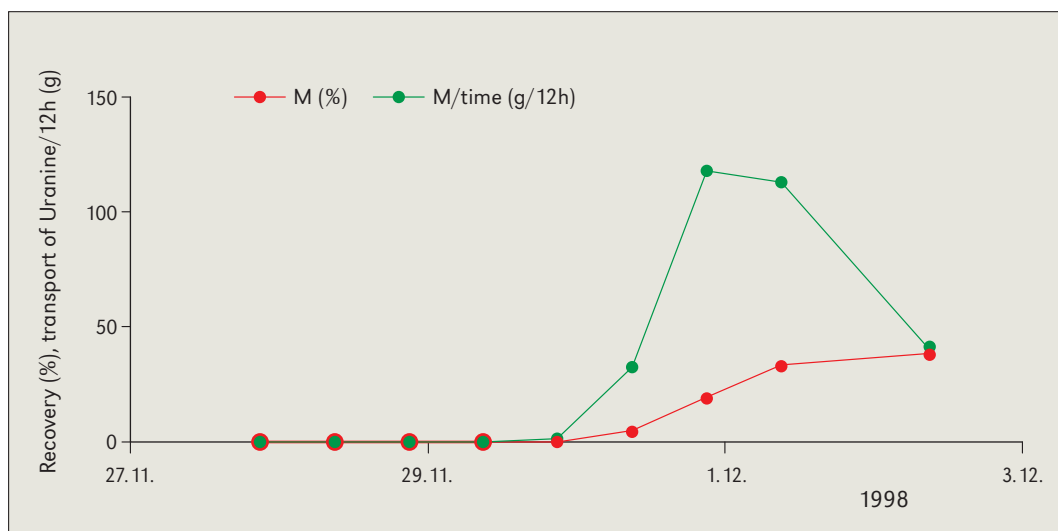


**8** Temporal course of the Uranine transport (M) and returned Uranine at Point 4 (*Dakenyan*).

when we were no longer sampling. According to the experience from previous tracings, we assumed that further intensive washing of the tracer followed after every rainfall. If there was no rainfall for an extended period – the water tracing test was done at the beginning of the dry period which usually lasts to May – we assume that all the remaining tracer would be washed out only during the following rain period.

## CONCLUSION

The tracing test at low water level showed the same directions of underground drainage from Point d as the tracing test at medium water level.

Based on the results of the water tracing test, we concluded that water from Point d does not flow into the direction of Point 11 parallel to the Shibanshou fault; we can ascertain this at least for low water periods.

The velocities of water drainage at low water level are considerably lower than at high water level, yet they differ in particular sections from Point d to Point 4, in a manner similar to what we stated for water drainage at medium water level. At different water levels the water flow is the fastest in its initial stage. The highest velocity at low water level from the injection point to Point 2 is 3.3 cm/s, and the slowest one in the section between the points 3 and 4 only 1 cm/s. The researchers cite the lowest values for the underground water in southern China of several mm/s (*Yuan*, 1991; *Song et al.*, 1993).

Owing to the low water velocity, the water tracing breakthrough curve was flattened and lengthened, and thus the majority of Uranine was flowing by the observation points for a longer time than during medium water level. At Point 4, only three days after its first appearance, we recorded 40 % of the tracer. The washing of the remaining tracer continued in the following days and probably after every subsequent rainfall. Since the injection started at the beginning of the dry period, we assume that the complete passage of Uranine was achieved in the following wet period in spring 1999. Such a conclusion is based on our previous water tracing test in the Slovene karst (*Kogovšek* and *Petrič*, 2002).

We think that in such conditions the transport of soluble substances, including pollution, is relatively slow but longer-lasting.

# HYDROCHEMICAL CHARACTERISTICS OF SPRINGS AND THEIR POSITION IN RELATION TO TECTONIC SITUATION (CENTRAL AND NORTHWEST YUNNAN)

JANJA KOGOVŠEK, STANKA ŠEBELA

19

Exposed karst areas in China comprise about 900,000 km² and the karst area in Yunnan includes 110,900 km². The Yunnan region in southwest China is located in the boundary area between the active Tibetan plateau to the west and the stable South China platform to the east. This region is characterized by the complex Cenozoic structures and active seismotectonics.

The studied area is part of the Three Parallel Rivers of the Yunnan protected areas which are inscribed in the Unesco World Heritage List. The area represents geological history of at least 50 million years associated with the collision of the Indian plate with the Eurasian plate, the closure of the ancient Thethys Sea, and the uplifting of the Himalayan range and the Tibetan plateau.

The site consists of 15 protected areas in the mountainous northwest of Yunnan Province and extends over a total area of 1,698,400 ha, encompassing the watershed areas of the Jinsha (Yangtze), Lacang (Mekong) and Nujiang (Salween) rivers. The rivers pass through steep gorges, in places up to 3000 m deep. At their closest the three gorges are 18 km and 66 km apart.

The research work in this region was performed within the Slovene-Chinese project with Yunnan Institute of Geography from 18–29 October 2004 (*Šebela* and *Kogovšek*, 2006). In the previous years most researches were oriented to the area around Kunming (Lunan) and southeast from there (Xichou, Qiubei, Guangnan) (1). Shilin, fengcong, fenglin, karst caves were studied (*Knez* and *Slabe*, 2002; *Šebela et al.*, 2004) and water tracing tests were performed (*Kogovšek et al.*, 1997; *Kogovšek* and *Liu*, 2000). In the year 2004 it was the first time that the areas of the northwestern Yunnan were visited and some thermal and non-thermal springs with tufa deposits related to active tectonics were studied.

## 19.1 TECTONIC SITUATION

Tectonic development of the southeast Asia includes the Indian subcontinental collision which represents the penetration of a rigid block (representing India) into layers of plasticine in a partly confined block (Asia) (*Tapponnier et al.*, 1982). The Red River fault zone (1) is the major geological discontinuity that separates South China from Indochina. Today it corresponds to a great right-lateral fault, following for over 900 km the edge of four narrow (<20 km wide) high-grade gneiss ranges that together form the Ailao Shan-Red River metamorphic belt (*Leloup et al.*, 1995).

The movement along the Red River fault has been dominantly right lateral since the close of the Tertiary. The best evidence comes from offsets of tributary streams of up to 5–6 km in the last 2–3 Ma (amounting to slip rates of 2–5 mm/yr). No significant earthquake has occurred along the fault in the last 2000 years (*Allen et al.*, 1984).

Tapponnier with the others surmise reversal of the movement on the Red River fault from the initial left-lateral sense during the first 20–30 Ma following the onset of the Indian collision. A different regional stress pattern now favours adjustment by a dextral slip. The orientation of the fault is consistent with N-S shortening and E-W extension.

Geological relations near the NW termination of the Ailao Shan suggest the Red River fault had a minimum of 14–48 km of right-lateral displacement in pre-Pliocene (and presumably post-17 Ma) time and only 5–6 km of displacement in Quaternary time (*Allen et al.*, 1984; *Wang et al.*, 1998).

Active right-lateral displacement on the eastern part of the Red River fault zone is interpreted to be caused by a segment of the fault zone being rotated counterclockwise by a shear related to the left-lateral Xiaojiang fault system (*Wang et al.*, 1998).

Stating that the Red River fault has been displaced by the Xiaojiang fault, it can be concluded that with respect to its present kinematics, the eastern part of the Red River fault does not accommodate large motions nowadays (*Michel et al.*, 2000).



**1** Tectonic situation of *Yunnan* (after *Burchfiel* and *Wang*, 2003):
1 – *Yulong* Snow Mountain, 5596 m a.s.l., and lakes;
2 – faults:
ZF = *Zhongdian* fault,
JF = *Jianshui* fault,
QF = *Quijiang* fault;
3 – studied areas:
1 = *Tianshengqiao* and *Xiageiwenquan* springs,
2 = *Baishuitai* tufa deposits,
3 = springs north of *Kunming*;
4 – right-lateral slip along the fault;
5 – left-lateral slip along the fault.
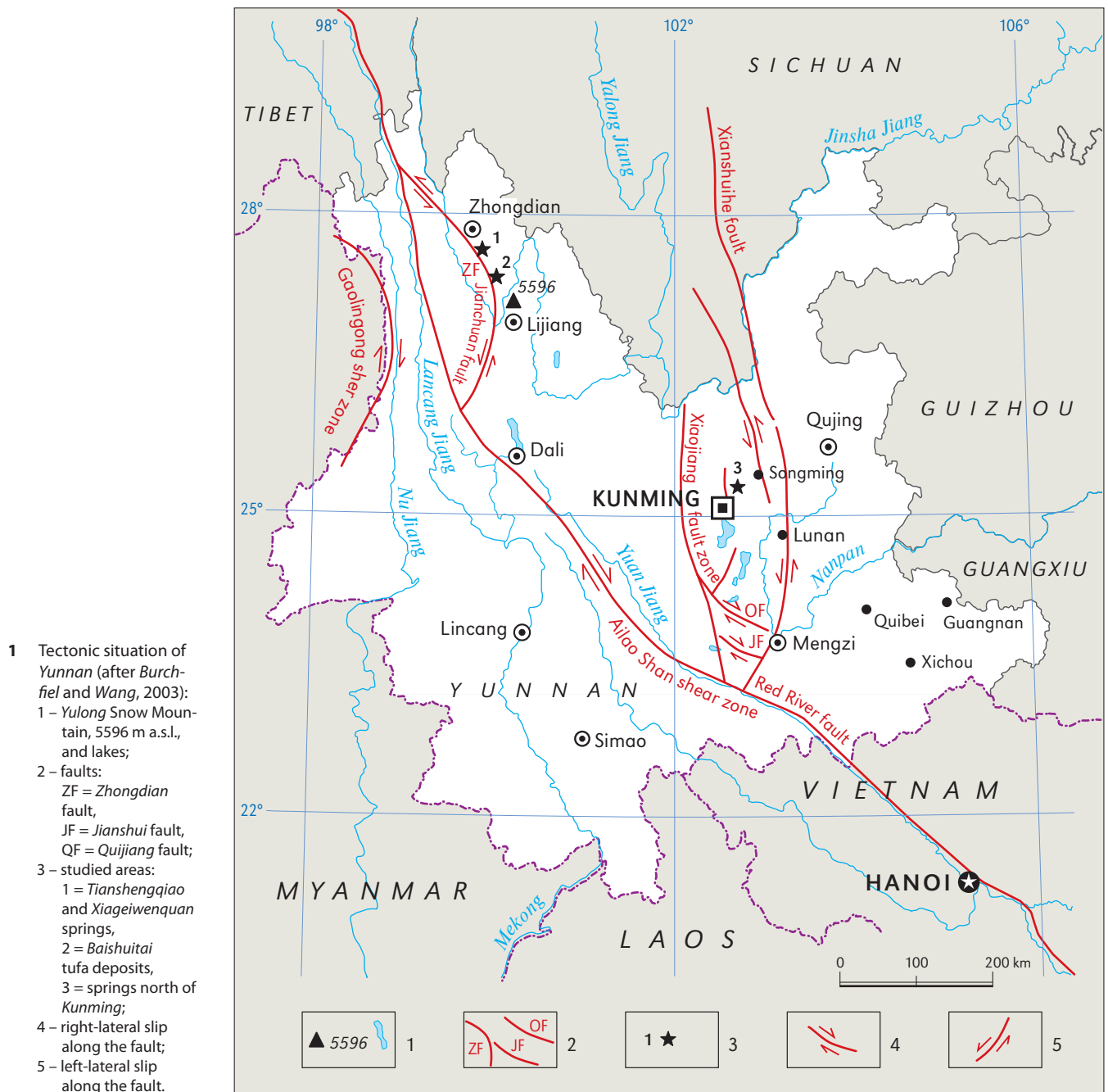
The northwest-striking Jianshui and Qujiang faults (1) and probably the Zhongdian fault show evidence for different amounts of Middle Cenozoic (pre-Pliocene and post-early Paleogene) left-lateral displacement that range from 6–25 km. The age and orientation of the left-lateral faults suggest that the faults are related to a regional deformational event associated with important left-lateral shear on the Ailao Shan shear zone (*Burchfiel* and *Wang*, 2003).

The Zhongdian fault (1) appears to have undergone only left-lateral displacement, some of which may be Middle Cenozoic and some post-Miocene in age. Active displacement on the Zhongdian fault is interpreted to mark the eastern boundary for a small crustal fragment that rotates clockwise around the eastern Himalayan syntaxis (*Burchfiel* and *Wang*, 2003).

Active right-lateral movement on the Jianshui fault (1) can be documented by numerous geological (offset structures) and geomorphic (deflected rivers and pull-apart basins) features. Active right-lateral displacement of the Quijiang fault is demonstrated by numerous scarps and offset Holocene feature and seismic activity (*Burchfiel* and *Wang*, 2003).

Southeast of Zhongdian the Zhongdian fault passes through a series of basins filled with Quaternary sediments and the analysis suggests left-lateral stream deflections indicating the fault is active. The fault bends south at the Jinsha River and merges with the active left-lateral Jianchuan fault (*Burchfiel* and *Wang*, 2003).

Quaternary basins and lakes north of Dali and within the southern part of the Xiaojiang fault zone are areas of local active extension (*Wang* and *Burchfiel*, 2000).

Only the Jianshui fault and possibly the Quijiang fault contain evidence for right-lateral reactivation of older left-lateral faults (*Burchfiel* and *Wang*, 2003).

The Xiaojiang fault system is at least 2–4 Ma old, and possibly as old as 6–8 Ma, which suggests that rapid right-slip did not begin on the Quaternary Jianshui and Quijang faults until left-lateral shear within the Xiaojiang fault system was well underway (*Burchfiel* and *Wang*, 2003).

The Pliocene-Quaternary sedimentary fill in pull-apart basins associated with left-lateral Xianshuihe-Xiaojiang fault system indicates that this fault system was initiated by at least 2–4 Ma (*Wang et al.*, 1998).

Kunming is moving due south with respect to Sundaland-South China indicating sinistral movement along the Xiaojiang fault system with a rate of 11 ± 4 mm/yr. The Xianshuihe-Xiaojiang fault system suffers pure sinistral strike slip faulting in its central part with respect to South China (*Michel et al.*, 2000).

## 19.2 SEISMICITY

In the broad sense, strike-slip faults and earthquakes in southwest China result from the eastward motion of the Earth's crust that is driven by the collision of the Indian and Eurasian continental plates beneath the Himalaya Mountains and the Tibetan plateau to the west.

There is an obvious difference between the southern and northern segment of the Red River fault from the viewpoint of modern seismicity. The most disastrous earthquakes occurred in the northern segment. Feigl and others report that the Red River fault did not slip faster than 1 or 2 mm/yr between 1994 and 2001 near Thác Bà, Vietnam (*Feigl et al.*, 2003).

A strong earthquake occurred in the Lijiang area in Yunnan Province on 3 February

1996 (M = 7.0). The epicenter was determined to be in the seismically active region of the Hengduan Mountains, which belong to the Alpine-Himalaya seismic belt.

Kunming is situated in the middle and southern part of seismically active Xiaojiang fault. In the year 1833 earthquakes (M = 8.0) were located in the area of Songming (1).

The focal mechanisms of the 1966 earthquakes on the N-S-striking Xiaojiang fault imply left-lateral slip along it. A normal component of the slip on the roughly N-S faults south from Kunming has created several Quaternary half-grabens, some of them filled by lakes (*Tapponnier* and *Molnar*, 1977).

An earthquake of M = 7.7 occurred on the Quijiang fault in 1970 (Tunghai earthquake). The event produced a 60 km long surface break with a maximum right-lateral displacement of 2.7 m (*Liu et al.*, 1988; *Ma*, 1990).

In southern Yunnan (south of the Red River fault, between Pu'er and Simao) there was an earthquake with M = 6.3 (depth 10 km) on 2 June 2007, showing that the fault is very active.

## 19.3 SPRINGS NORTH FROM KUNMING

Upper Devonian, Carboniferous and Permian shallow-water carbonates build south China tower karst, south from Kunming. Near Kunming basalt rock is interbedded with Upper Permian limestones.

Within the frame of the fieldwork the Songhuaba accumulation lake and Quinglongtan springs north from Kunming (2) were studied in October 2004 and June 2006. The water from springs is led to a common channel that runs into the accumulation lake that was made for irrigation and water supply of Kunming. The springs are located in the wider zone of Xiaojiang fault (1) which is still tectonically active.

The measured temperature and conductivity (EC) of the three main springs on 21 October 2004 showed that the water from the springs belonged to the same source (temperature 14.7 °C and conductivity 277 µS/cm). The water in the accumulation lake was

**2** One of the *Quinglongtan* springs north from *Kunming*.

warmer (19.4 °C) while the EC measurement was within the values of the Quinglongtan spring (268 μS/cm). Measurement of conductivity of drinking water in Kunming showed the value 256 μS/cm. Carbonate concentration in the springs and in the accumulation lake was low; just 135 mg CaCO₃/l (2.7 meq/l) what means it was a little bit lower than total hardness (146 mg CaCO₃/l or 2.92 meq/l). In June 2006 in rainy period we sampled the Quinlongtan spring again (Table 1). The temperature was a little warmer, conductivity and total hardness were lower as in October 2004. Calculation of Ca/Mg ratio gave us the value 3.3. The water flow from the nearby cave with temperature of 15.2 °C had conductivity 291 μS/cm. In the Tianshengan area we measured higher values of hardness in karst springs (*Kogovšek*, 1998).

| Spring | Date | T (ºC) | SEC (μS/cm) | pH | Carb. | Ca+Mg (meq/l) | Ca | Ca/Mg |
|---|---|---|---|---|---|---|---|---|
| Quinglongtan spring | 21.10.2004 | 14.7 | 277 | 7.7 | 2.71 | 2.92 | | 3.3 |
| Quinglongtan spring | 9.6.2006 | 15.1 | 247 | 7.6 | | 2.71 | 2.08 | |
| Water flow from the cave | 9.6.2006 | 15.2 | 261 | 7.6 | | | | |
| Acumulation lake | 21.10.2004 | 19.4 | 268 | 7.6 | 2.40 | 2.81 | | |
| Huolongtan spring | 9.6.2006 | 20.5 | 284 | 7.6 | | 2.95 | 2.08 | 2.4 |
| Heilongtan spring | 9.6.2006 | 15.9 | 263 | 7.6 | | 2.79 | 2.16 | 3.4 |

**Table 1**
Physico-chemical characteristics of sampled waters.

On 9 June 2006 we sampled also the Huolongtan and Heilongtan springs (Table 1). Also these two springs were characterized by low values of EC and total hardness, but higher than the Quinglongtan spring. Heilongtan had temperature of 15.9 °C, Huolongtan was warmer, we measured 20.0 °C.

In the Tianshengan area (*Kogovšek*, 1998) we measured such low values of conductivity and hardness in karst springs only at high hydrological conditions. The highest measured values in the year 2004 (3) characterize oversaturated water of Baishuitai.

The phosphate concentration in the Songhuaba accumulation lake and in the Quinlongtan spring (October 2004) was under the detection limit of the method (<0.01 mg $PO_4^{3-}$/l), the nitrate concentration was 4.6 or 4.4 mg $NO_3^-$/l, what shows good water quality.
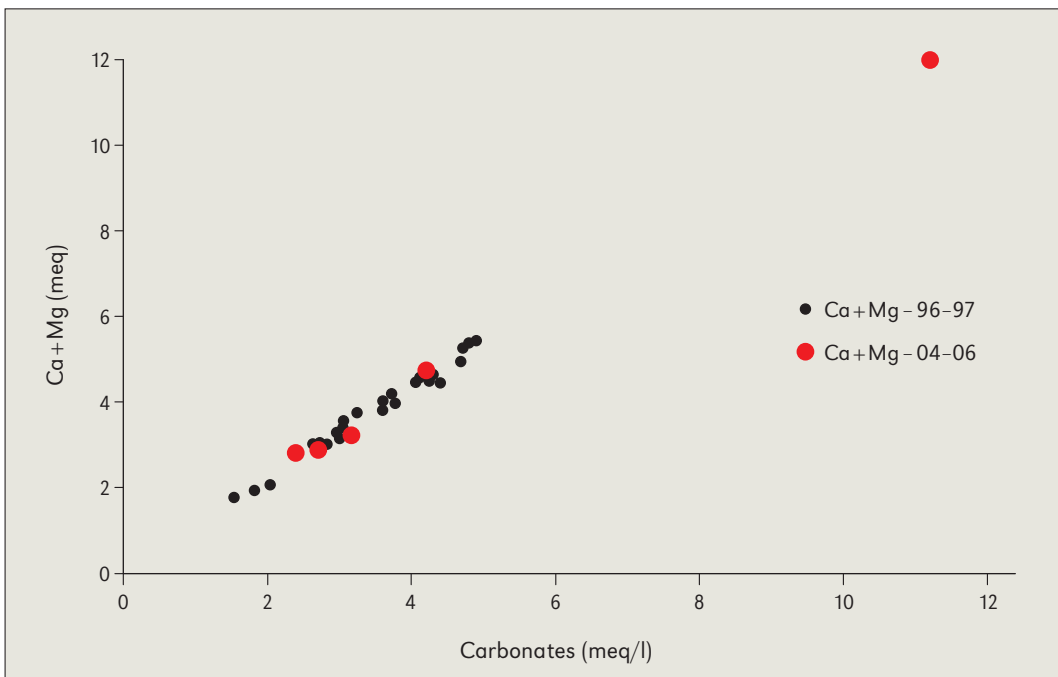


**3** Total and carbonate hardness of sampled springs north from *Kunming* in the years 2004– 2006 in comparison with karst waters in the *Tianshengan* area in the years 1996–1997 at low and high water conditions.

205

The water supply for Lijiang derives from the nearer Zhenzhuquan spring (4) where the water is cached in a smaller lake (5) that is regulated for tourism. Part of the water is accumulated into the channels that run through the Lijiang town. On the principal spring there is a pumping area that is still used for water supply of Lijiang. During our visit on 24 October 2004 we met many natives who came to take the water from the spring. The water temperature was 14.8 °C, EC 370 µS/cm, carbonate hardness 158 mg CaCO$_3$/l (3.16 meq/l), and total hardness 162 mg CaCO$_3$/l (3.24 meq/l). These measurements fall well with characteristics of ground-water and karst springs in the Tianshengan area near the Stone Forest (*Kogovšek*, 1998; *Kogovšek et al.*, 1997). The water had good quality regarding the low chloride concentration (1 mg Cl$^-$/l), the nitrate concentration (1.3 mg NO$_3^-$/l), and the o-phosphates (<0.01 mg PO$_4^{3-}$/l).

Yulong Snow Mountain (5596 m) consists of Paleozoic carbonate rocks and in the eastern area of Tertiary clastic rocks with marlites and calcareous rocks (*Huang*, 2004). Bai Shui He River that runs



*Hydrochemical characteristics of springs and their position in relation to tectonic situation (central and northwest Yunnan)*

**4**  *Zhenzhuquan* spring north from *Lijiang*.

**5**  An accumulated lake at the *Zhenzhuquan* spring.

on the northern slope of the mountain showed the temperature of 9.6 °C (23 October 2004), low EC (196 µS/cm) and low carbonate hardness (109 mg CaCO$_3$/l or 2.17 meq/l). The pH measurement showed 8.2 with water containing just 1 mg NO$_3^-$/l.

## 19.5 SPRINGS SOUTH FROM ZHONGDIAN

About 42.2 % of Zhongdian County represents carbonate surface. Most of carbonate rocks are from the Devonian and Cretaceous. Some are from the Lower Permian and the Middle and Lower Triassic (*Huang*, 2004).

In the wider zone of the Zhongdian fault near the town of Zhongdian and Jinsha River there are more tectonic depressions that are developed inside carbonate rocks but border also to other rocks as magmatic, sandstones and marbles. In such cases we do not deal with true karst poljes. All depressions are related to the active tectonic faults that are NW-SE oriented with active sinistral horizontal movements.

In the area of the active Zhongdian fault there are more springs (1). Some are thermal springs, others have lower temperature and many of them precipitate tufa deposits. The spring waters are supposed to come from the depths.

During our field studies we visited the Xiageiwenquan thermal springs, Tianshengqiao thermal spring and Baishuitai tufa deposits. All three locations are tourist attractions.

Xiageiwenquan (6) is situated about 10 km east from the Zhongdian town and represents about 10 smaller and bigger thermal springs in the distance of 300 m. In the area there are older and younger still active tufa deposits. The area is built of Triassic limestones, sandstones and mudstones.

**6** *Xiageiwenquan* thermal spring.

There are 9 springs with discharges between 0.5 to 1 l/s and temperature between 36.6 and 67.4 °C. The EC values of the springs were between 1676 and 2660 µS/cm.

Our measurements taken on 26 October 2004 detected the temperature being between 48.3 and 66.8 °C, and minimal discharges. The EC values were from 1260 to 1510 µS/cm (LF 90 instrument, ref. temperature 20 °C).

Tianshengqiao is situated a few kilometres south from Xiageiwenquan, along the active sinistral horizontal Suoge-Xuejiping fault on the western side of the Jinsha River. The fault is deep and wide formed in the early stage of Permian but still active today. A hot liquid of the gabbro plasma effuses up through this fault. And it is the precondition to form tufa landscapes (*Huang*, 2004).

The attraction of Tianshengqiao is a natural bridge with the Shuodugang River running below it (7). The limestone natural bridge is 40 m high, 10 m wide and 15 m long. In the area there is also the Tianshengqiao thermal spring with tufa deposits. C. Huang (2004) speaks about sulphur springs formed in different stages. The east side is from the earlier stage and the west side from the later stage. Calcium carbonate deposits at a relatively high speed with the estimated sedimentation 1–5 cm/yr. By comparison with other tufas in the surrounding areas the tufa of Tianshengqiao did not form earlier than 5000 years ago.

The thermal water of the Tianshengqiao spring is accumulated into the thermal pools (8) used by tourists. On 25 October 2004 the Shuodugang River had temperature of 10 °C and low EC (115 µS/cm). The water of the thermal spring had temperature of 57.5 °C and high EC (1805 µS/cm), high carbonate concentration (20 meq/l), higher chloride values (27 mg $Cl^-$/l) and sulphate values of 26 mg $SO_4^{2-}$/l. High EC value means high concentration of dissolved substances. The water probably contains other substances but our analyses were limited to the analyses mentioned above.

The scenic spot is a gathering place between the surface and underground water, and also a converging place of the N-S trending Suoge-Xuejiping fault and another E-W trending fault (*Huang*, 2004).



**7** The natural bridge of *Tianshengqiao.*

**8** Thermal spring of *Tianshengqiao* is accumulated into the pools.

The Baishuitai springs contain high mineralized waters with regular temperatures. They are situated about 20–30 km north from the Jinsha River. The area is built of Triassic rocks (limestones and sandstones) as well as of Permian and Quaternary (delluvium) rocks.

Because the spring water is oversaturated, it deposits dissolved mineral substances. In this sense the slopes are covered mostly with white tufa. Tufa dams (9, 10) are covering the areas of Lower and Middle Triassic limestones. The water resurges from different springs. The spring area is covered by deciduous trees which are the source for pollution and also the food for algae growth. The springs are decorated with Buddhist symbols. Many people visit the spring area and walk over the tufa deposits what causes destruction of the dams. The park administration is trying to protect the area.

The temperature of the springs is between 11.1 and 13.3 °C. The EC measurements showed a little bit over 1000 µS/cm what means that the water has a lot of dissolved carbonates. Total hardness was 600 mg $CaCO_3$/l (12 meq/l), 560 mg belonging to $CaCO_3$/l (11.2 meq/l). The ratio Ca/Mg of the water was equal to 4.4 what shows that the Mg values are 4.4-times lower then the Ca and that the water is coming from the hinterland with these characteristics. The water had lower nitrate and phosphate concentrations and 40 mg $SO_4^{2-}$/l of sulphates.

The water temperature in the dams showed warming of the water and lowering of the EC values what is typical for intensive carbonate precipitation. At the bottom of the slope water is led into the channel that runs to the nearest village where it is used for water supply and irrigation. Total hardness of that water was only 240 mg $CaCO_3$/l (4.8 meq/l), with 210 mg belonging to $CaCO_3$/l (4.2 meq/l). The ratio Ca/Mg was 3 what suggests the calcium carbonate precipitation. The lower concentration of sulphates (5 mg/l) comparing with the values of the higher spring is showing the sulphate precipitation. These are the first results which should be expanded, because the dams need to be protected from numerous visitors.

Baishuitai tufa deposits in Yunnan are comparable with the Plitvice travertine dams

in Croatia. Baishuitai site is the largest in the province near Chungtien, with a series of dams depositing over 1 km² at 3000 m a.s.l. They are probably thermogene (*Pentecost* and *Zhang*, 2001).

## 19.6 TUFA DEPOSITS

Tufa as a general name covers a wide variety of calcareous freshwater deposits which are particularly common in the late Quaternary and recent successions. Tufa is the product of calcium carbonate precipitation under a cool water regime and typically contains remains of micro- and macrophytes, invertebrates and bacteria. The term travertine is restricted to all 'freshwater' thermal and hydrothermal calcium carbonate deposits dominated by physico-chemical and microbial precipitates, which invariably lack *in situ* macrophyte and animal remains. Tufas are usually distinguishable from travertines, even in ancient deposits, by the comparatively high diversity of contained plants, including macrophytes, and animals (*Ford* and *Pedley*, 1996).

In China's vast karst landscapes there are many tufa deposits. They are known in the Sichuan, Guizhou, Guangxi and Tibet provinces. Some of the tufa cascades in Guizhou are broadly comparable with the Plitvice barrages (*Ford* and *Pedley*, 1996). Frančišković-Bilinski with others analysed the tufa from Guangxi (*Frančišković-Bilinski et al.*, 2003). One tufa sample originated from the Pleistocene and others from the Holocene.

The travertines in China are divided into two major geochemical groups: the meteogenes and thermogenes. The thermogenes are essentially hydrothermal deposits where

**9** Tufa dams of *Baishui-tai.*

$CaCO_3$ is precipitated from high-$CO_2$ ground-waters. Most of this $CO_2$ comes from deep within the crust as a result of magmatic degassing or limestone decarbonation with DIC (dissolved inorganic carbon) values typically >>10 mM/l. They are usually found in tectonically and/or volcanically active regions (*Pentecost* and *Zhang*, 2001).

Tibet, in spite of its cold dry climate and high altitude, has a scatter of tufa deposits, mostly either calcareous crusts on colluvium or associated with geothermal springs (*Waltham*, 1996).

### CONCLUSION

Yunnan Province lies on the eastern rim of the collision zone between the Indian plate and Eurasia. This region is characterized by the complex Cenozoic structures and active seismotectonics.

The Quinglongtan springs (T = 14.7 °C and low values of EC, carbonate and total hardness) are situated north from Kunming. Similar values were detected in the area of Tianshengan in Yunnan. The Zhenzhuquan spring near Lijiang had the same temperature but higher values of the EC and hardness.

The Zhenzhuquan spring, Quinglongtan springs and the Songhuaba accumulation lake had lower phosphate values (under 0.01 mg $PO_4^{3-}$/l) and low nitrate concentrations (from 1.3 to 4.6 mg $NO_3^-$/l) and are showing good water quality. The springs are situated inside the Xiaojiang fault zone along which sinistral horizontal movements are still active (1). Most probably they are karst springs.

**10** Tufa dams of *Baishuitai*.



211

In the wider zone of the Zhongdian fault between Zhongdian town and Jinsha River there are more tectonic depressions (11) which are developed inside carbonate and non-carbonate rocks. In this sense they are not true karst poljes. All depressions are developed inside NW-SE and N-S oriented active fault zone with sinistral horizontal movements.

There are also more springs related to active tectonics. The Tianshengqiao (T = 57.5 °C) and Xiageiwenquan springs (T = 48.3–66.8 °C) are thermal springs with tufa deposits. Baishuitai is a very strongly mineralized spring but shows lower temperature (T = 11.1–13.3 °C) and deposits mostly calcium carbonate while Mg remains in dissolution what means that the ratio of Ca/Mg decreases along the precipitation path. Also the sulphates are partly precipitating.

Baishuitai travertines are probably thermogene (*Pentecost* and *Zhang*, 2001). Because carbonate tufas are very sensitive to water and climate, C. Huang performed the geomorphological investigations to provide a scientific basis for the protection of tourist tufa resources at Tianshengqiao (*Huang*, 2004).
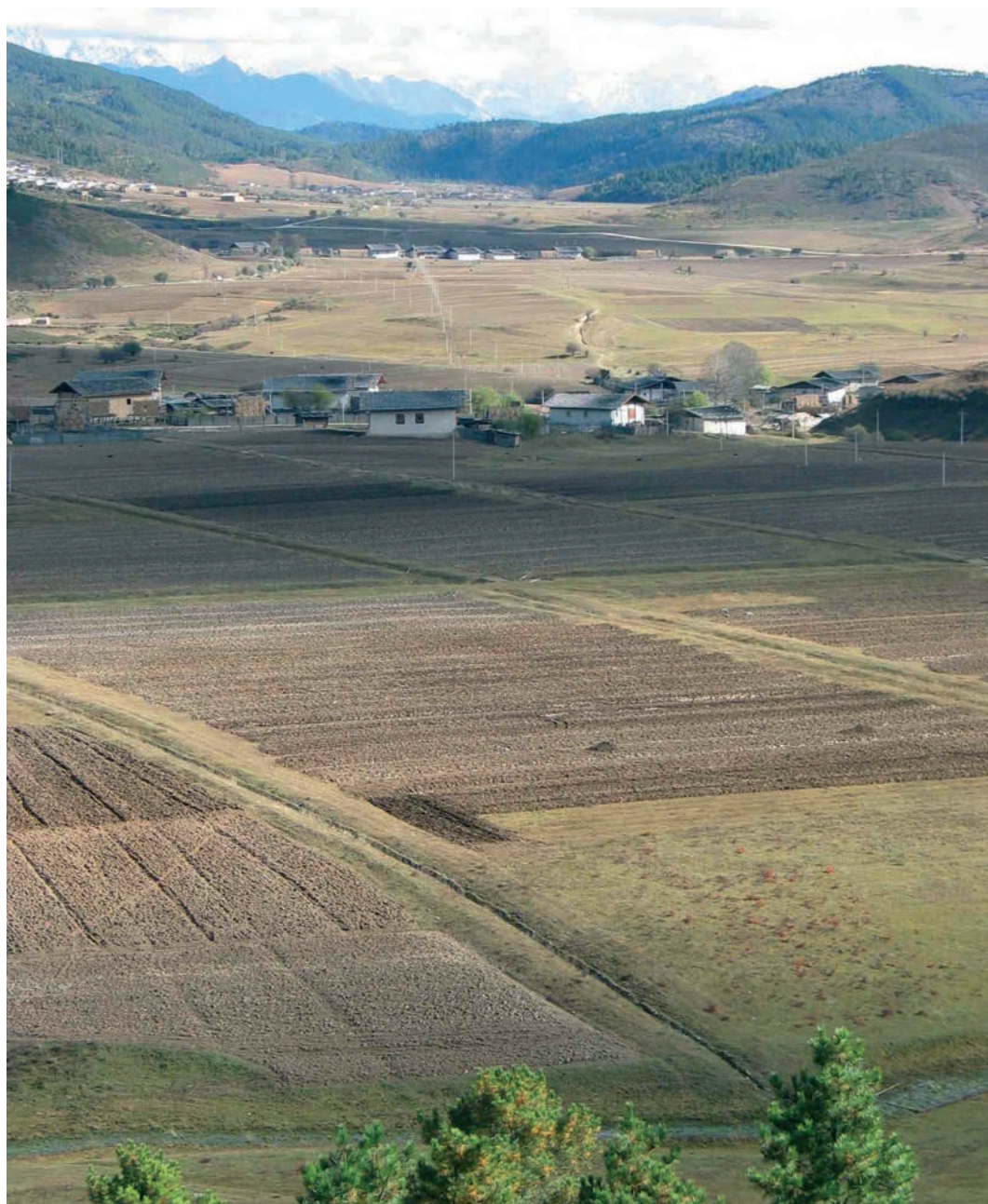


**11** Tectonic depression south from *Zhongdian*.

# CALCULATION OF CARBON SINK OF A TYPICAL GRANITE AREA (YUNNAN WEIXI) AND THE STUDY OF THE INFLUENCE FACTORS

YU LIU, DESHEN LIU, LICHENG SHEN

The weathering process of granite which represents about 15 % of the bedrock outcrop in China (*Song* and *Zhang*, 1999) is a carbon consumption process. Its importance in the carbon cycle was not realized until the presumption of its relation to the Cenozoic global cooling and $CO_2$ missing sink in the modern carbon cycle model (*Raymo* and *Ruddiman*, 1992). Velbel estimated (1993) that the $CO_2$ sink by silicate weathering accounts for 58 % of the global $CO_2$ sink of weathering while Sarin (2001) estimated it was 41 % and about 1/6 took place in the area of the Himalayas. However, scientists hold different opinions about the influence factor of silicate weathering (*Meybeck*, 1987; *Blum*, 1997; *Jacobson et al.*, 2002; 2003; *White* and *Blum*, 1995). Therefore, further study on the role of the $CO_2$ consumption and controlling factors has significance for observing the character of the $CO_2$ exchange at the interface of atmosphere and lithosphere, for investigation of the $CO_2$ missing sink and modification of the global carbon cycle model (*Amiotte-Suchet et al.*, 2003).

At present, the study of silicate weathering is mainly focused on river dissolved material based on a large spatial scale (hundred – several million km$^2$) (*Jacobson et al.*, 2003; *Meybeck*, 1987), such as the study in the Gangal Brahmaputra River (*Sarin et al.*, 1989), Indus River basin (*Ajaz* and *Veizer*, 2000), White River in Vermont, USA (*Thomas*, 2006),



**1** *Weixi* granite moutains.

Amazon River (*Gaillardet et al.,* 1997), Congo River basin (*Gaillardet et al.,* 1995), Bengal drainage basin, Bangladesh (*Datta* and *Subramanian,* 1997), Niger basin (*Boeglin* and *Probst,* 1998) and Chinese rivers (*Chen et al.,* 1999; *Zhang,* 1996; *Li* and *Zhang,* 2002). The result shows that silicate weathering shows enormous global differences. Chang Jiang has the highest hydrochemical weathering, which is 271 mm/ka while it is 1 mm/ka in the Niger and in the Bangladesh basins. Therefore, further study on silicate weathering on a smaller spatial scale should be carried on to understand the silicate weathering equation.

This study chose, as its target, a small typical granite area, Yunnan Weixi, analysed its major hydrochemical indexes, calculated its carbon sink caused by granite weathering and discussed carbon sink characteristics and influencing factors.

**Table 1**
Major hydro-chemical components of springs in August and December 2005 in *Weixi* (mg/l).

| Spring category | | Spring no. | Season | pH | $K^+$ | $Na^+$ | $Ca^{2+}$ | $Mg^{2+}$ | $Cl^-$ | $SO_4^{2-}$ | $HCO_3^-$ | Solid $CO_2$ | Free $CO_2$ | $SiO_2$ |
|---|---|---|---|---|---|---|---|---|---|---|---|---|---|---|
| Granite pore water (A) | | WX19 | Summer | 4.78 | 0.64 | 0.73 | 0.94 | 0.15 | 1.86 | 0.74 | 10.46 | 3.76 | 42.22 | 6.98 |
| | | | Winter | 4.93 | 0.77 | 0.66 | 1.10 | 0.48 | 1.86 | 0.31 | 6.97 | 2.51 | 39.33 | 6.11 |
| | | WX21 | Summer | 4.93 | 0.77 | 0.66 | 1.10 | 0.48 | 1.86 | 0.31 | 6.97 | 2.51 | 39.33 | 6.11 |
| | | | Winter | 4.93 | 0.77 | 0.66 | 1.10 | 0.48 | 1.86 | 0.31 | 6.97 | 2.51 | 39.33 | 6.11 |
| Shallow fracture water | Fracture water in the surface weathering zone (B₁) | WX03 | Summer | 7.03 | 0.62 | 2.37 | 3.23 | 1.58 | 1.86 | 0.80 | 27.89 | 10.05 | 4.97 | 17.06 |
| | | WX06 | Summer | 6.83 | 1.15 | 3.01 | 1.51 | 0.17 | 2.79 | 1.26 | 19.18 | 6.91 | 4.97 | 19.22 |
| | | WX11 | Summer | 6.69 | 0.68 | 2.44 | 3.13 | 0.62 | 2.79 | 0.74 | 22.66 | 8.16 | 7.45 | 11.97 |
| | | WX12 | Summer | 6.89 | 0.61 | 2.24 | 4.57 | 0.70 | 1.86 | 3.16 | 24.41 | 8.80 | 6.21 | 10.73 |
| | | WX13 | Summer | 6.36 | 0.93 | 1.41 | 1.07 | 0.56 | 1.86 | 0.33 | 12.20 | 4.40 | 9.93 | 11.30 |
| | | | Winter | 7.02 | 0.94 | 4.21 | 7.07 | 1.43 | 2.34 | 7.53 | 28.88 | 10.41 | 3.40 | 15.72 |
| | | WX18 | Summer | 6.86 | 0.53 | 3.10 | 6.98 | 1.22 | 1.86 | 1.61 | 38.35 | 13.82 | 4.97 | 13.47 |
| | | WX20 | Summer | 6.81 | 0.45 | 2.72 | 2.79 | 0.69 | 1.86 | 0.36 | 24.41 | 8.80 | 6.21 | 13.76 |
| | Fracture water in the medium weathering zone (B₂) | WX01 | Summer | 7.03 | 0.70 | 4.16 | 6.67 | 1.82 | 5.57 | 0.70 | 31.38 | 11.31 | 7.45 | 14.37 |
| | | | Winter | 6.93 | 0.54 | 4.50 | 7.86 | 2.86 | 4.68 | 3.77 | 34.65 | 12.50 | 5.10 | 14.76 |
| | | WX04 | Summer | 7.34 | 0.41 | 2.96 | 3.98 | 0.96 | 1.86 | 1.05 | 33.12 | 11.95 | 6.21 | 13.09 |
| | | | Winter | 7.16 | 0.23 | 2.78 | 6.28 | 1.19 | 2.34 | 0.00 | 34.65 | 12.50 | 3.40 | 15.72 |
| | | WX05 | Summer | 6.80 | 0.45 | 2.95 | 3.90 | 0.99 | 1.86 | 1.12 | 31.38 | 1.10 | 4.97 | 12.74 |
| | | | Winter | 7.53 | 0.36 | 2.88 | 5.50 | 3.34 | 3.51 | 0.00 | 28.88 | 10.41 | 3.40 | 13.88 |
| | | WX09 | Summer | 6.75 | 1.49 | 6.22 | 5.96 | 2.16 | 2.79 | 3.20 | 31.38 | 11.31 | 7.45 | 19.80 |
| | | | Winter | 7.23 | 1.39 | 11.82 | 13.35 | 4.76 | 5.85 | 3.77 | 80.86 | 29.15 | 3.40 | 23.70 |
| | Fracture water influenced by the mineral zone (B₃) | WX10 | Summer | 6.71 | 2.92 | 10.57 | 7.11 | 2.12 | 4.05 | 6.44 | 47.07 | 16.96 | 8.69 | 39.98 |
| | | | Winter | 7.32 | 2.84 | 8.54 | 18.07 | 10.01 | 11.69 | 1.88 | 119.36 | 43.03 | 3.40 | 21.36 |
| Deep bearing tectonic fracture water (C) | | WX02 | Summer | 7.34 | 0.61 | 6.03 | 11.34 | 2.68 | 1.86 | 3.55 | 66.25 | 23.89 | 3.73 | 16.77 |
| | | | Winter | 7.76 | 0.59 | 7.48 | 15.71 | 1.43 | 3.51 | 5.65 | 63.53 | 22.90 | 3.40 | 17.52 |
| | | WX14 | Summer | 7.36 | 0.90 | 6.96 | 10.94 | 2.75 | 1.86 | 1.12 | 73.22 | 26.40 | 3.73 | 20.65 |
| | | WX22 | Summer | 7.52 | 0.73 | 3.26 | 19.96 | 3.68 | 1.86 | 2.10 | 94.14 | 33.95 | 3.73 | 13.72 |
| | | | Winter | 7.98 | 0.66 | 4.27 | 22.78 | 2.86 | 2.34 | 3.77 | 82.78 | 29.85 | 1.70 | 15.24 |
| Water at the interface of granite and Quaternary deposit (D₁) | | WX23 | Summer | 6.69 | 0.56 | 1.06 | 14.90 | 1.54 | 1.86 | 0.53 | 66.25 | 23.89 | 7.45 | 9.53 |
| | | WX08 | Summer | 6.55 | 2.14 | 5.27 | 9.60 | 2.39 | 4.65 | 3.60 | 55.79 | 20.11 | 14.9 | 13.05 |
| | | | Winter | 6.71 | 1.66 | 4.07 | 11.00 | 3.57 | 4.68 | 7.53 | 50.05 | 18.04 | 3.40 | 11.52 |
| | | WX15 | Summer | 6.70 | 1.31 | 5.04 | 8.55 | 2.00 | 1.86 | 0.61 | 52.30 | 18.85 | 8.69 | 15.87 |
| | | WX16 | Summer | 6.83 | 1.24 | 3.47 | 7.80 | 1.39 | 0.93 | 1.24 | 48.81 | 17.60 | 6.21 | 14.20 |
| | | WX17 | Summer | 6.80 | 1.01 | 4.65 | 6.79 | 2.00 | 1.86 | 0.37 | 48.81 | 17.60 | 6.21 | 25.45 |
| | | WX24 | Summer | 6.14 | 2.97 | 4.57 | 7.89 | 1.58 | 3.72 | 3.86 | 36.61 | 13.20 | 14.90 | 13.06 |
| | | | Winter | 6.73 | 2.27 | 3.71 | 7.85 | 2.38 | 2.34 | 7.53 | 28.88 | 10.41 | 10.20 | 13.12 |
| | | WX25 | Summer | 6.32 | 6.81 | 5.34 | 10.65 | 2.05 | 1.86 | 4.19 | 45.33 | 16.35 | 11.18 | 12.85 |
| Water at the interface of granite and carbonate (D₂) | | WX07 | Summer | 7.34 | 1.94 | 5.11 | 27.21 | 5.11 | 1.86 | 15.82 | 115.06 | 41.49 | 3.73 | 25.52 |
| | | | Winter | 7.27 | 1.76 | 5.39 | 31.42 | 4.76 | 3.51 | 9.41 | 123.21 | 44.42 | 3.40 | 25.80 |

Weixi, situated in northwest Yunnan Province, southeast of the Tibetan plateau, is a typical granite area. Analysis of its granite weathering helps us to understand the influence of the Tibetan plateau uplift on the global climate change.

The study area of Weixi occupies 230 km². It is mainly composed of biotite adamellite which was formed during the Indo-Chinese epoch (1). Fractures develop very well.

This study analysed the chemical characteristics of 38 granite springs, from samples collected between May 2004 and December 2005. Those chemical characteristics include pH, $K^+$, $Na^+$, $Ca^{2+}$, $Mg^{2+}$, $HCO_3^-$, $Cl^-$, $SO_4^{2-}$ (Table 1). Springs are divided into five categories (2) based on combination of study yield and mathematical calculation:

*Calculation of carbon sink of a typical granite area (Yunnan Weixi) and the study of the influence factors*



parent rock
fracture
clay
ascending spring
fountain
quaternary deposits
limestone

**2** Major categories of a granite spring:

1 – water at the interface of granite and carbonate;
2 – shallow fracture water;
3 – granite pore water;
4 – deep bearing tectonic fracture water;
5 – water at the interface of granite and Quaternary deposit.

**3** Granite pore water (Spring WX19).



215
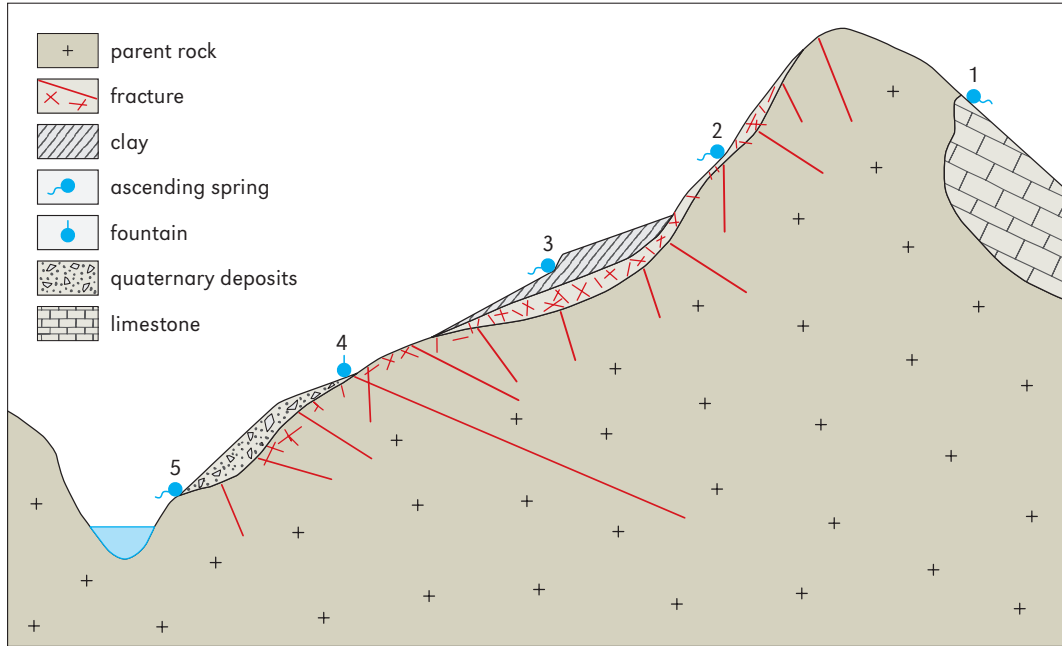
**4** Shallow fracture water (Spring WX04).



**5** Deep bearing tectonic fracture water (Spring WX22).

granite pore water (3), shallow fracture water (4), fracture water influenced by mineral zone, deep bearing tectonic fracture water (5), water at the interface of granite and Quaternary deposit (6), and water at the interface of granite and carbonate.

**6** Water at the interface of granite and Quaternary deposit (Spring WX15).

## 20.2 THE CALCULATION METHOD

The weathering process of granite is a carbon consumption process during which it is characteristic that water acts as a reactant and output medium as well. The main minerals in the process are potash feldspar, lime feldspar and biotite:

- Feldspar
  $7NaAlSi_3O_8$ (soda feldspar) + $6CO_2$ + $26H_2O$ → $6Na^+$ + $6HCO_3^-$ + $10Si(OH)_4$ + $3Na0.33Al_2.33Si_3.67O10(OH)_2$ (montmorillonite)

  $2NaAlSi_3O_8$ (soda feldspar) + $2CO_2$ + $11H_2O$ → $2Na^+$ + $2HCO_3^-$ + $4H_4SiO_4$ + $Al_2Si_2O_5(OH)_4$ (kaolinite)

  $3KAlSi_3O_8$ (potash feldspar) + $2H_2CO_3$ + $12H_2O$ → $2K^+$ + $2HCO_3^-$ + $6H_4SiO_4$ + $KAl_3Si_3O10(OH)_2(s)$

  $CaAl_2Si_2O_8$ (lime feldspar) + $2CO_2$ + $3H_2O$ → $Al_2Si_2O_5(OH)_4$ (kaolinite) + $Ca^{2+}$ + $2HCO_3^-$
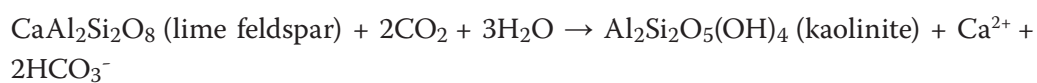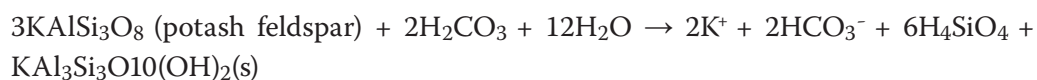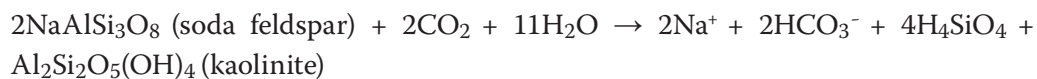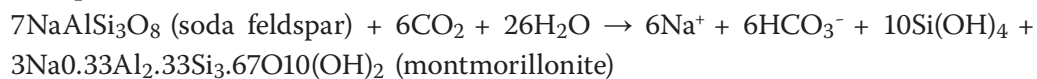
  Potash feldspar may be changed by entering $Na^+$: $KAlSi_3O_8 + Na^+ = K^+ + NaAlSi_3O_8$
  Therefore, the weathering of feldspar can be written as:
  (Na, K, Mg, Ca) silicates + $3CO_2$ + $H_2O$
  $10Si(OH)_4$ + $3HCO_3^-$ + $Na^+$ + $K^+$ + $0.3Mg^{2+}$ + $0.2Ca^{2+}$ solid products

- Biotite
  $KMg_3Al_3Si_3O10(OH)_2$ + $7H_2CO_3$ + $1/2H_2O$ → $K^+$ + $3Mg^{2+}$ + $7HCO_3^-$ + $2H_4SiO_4$ + $1/2Al_2Si_2O_5(OH)_4$

217
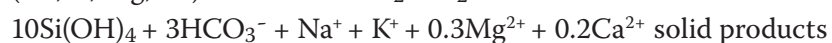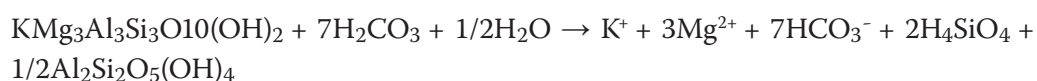
It should be noted that 1 mol $CO_2$ in air or soil will be changed to 1 mol $HCO_3^-$ during granite weathering, which shows that granite weathering is a process of carbon consumption on any time scale.

The following hydrochemical method can be used to calculate $CO_2$ sink:

quantity of carbon sink = unit area carbon sink * basin area

unit area carbon sink = ($CO_2$ sink rate* Q) / basin area

The $CO_2$ sink rate can be calculated with the following two methods:

- Anion method
  $CO_2$ sink rate = ($[HCO_3^-]s + [CO_3^{2-}]s + [H_2CO_3]s − [C]R$)*44
  $[HCO_3^-]s$, $[CO_3^{2-}]s$, $[H_2CO_3]s$ are $[HCO_3^-]$, $[CO_3^{2-}]$, $[H_2CO_3]$ in spring.
  $[C]R$ is the rain source $[C]$ in spring.

- Cation method
  The process of granite carbon sink is accompanied by the release of $SiO_2$ and by some cations such as $K^+$, $Na^+$, $Ca^{2+}$. Therefore, the analysis of those major components helps us understand carbon sink capacity and the process caused by granite weathering. The steps are as follows: a) analyse the original mineral and last reaction product under a polarizing microscope; b) analyse the main geo-hydro chemical process by taking advantage of observed hydrochemistry data and plot them on a mineral stability graph to study what hydrochemical reaction has taken place; c) calculate how much $CO_2$ would be consumed to produce the cations and $SiO_2$ obtained in step b.

The two methods emphasize different aspects. The anion method acts as a black box that is only concerned with the in-system C and the out-system C. It has the advantage of simplicity. However, the out-system C may contain other sources of C, such as C coming from vegetation aspiration, which may affect the accuracy of the result. The cation method acts as a grey system which is based on a chemical function. Therefore, it can better indicate the carbon sink character. But this method is much more complicated, and some weathering information may be concealed because some ions may be influenced greatly by the multi-hydrochemical process and multi-source ions, such as $K^+$ which may come from other minerals besides potash, feldspar and biotite.

In conclusion, the extraction of the rain source C is the basis of the accurate calculation of carbon sink caused by granite weathering.

## 20.3 CALCULATION OF THE CARBON SINK CAUSED BY GRANITE WEATHERING IN WEIXI

In order to analyse the contribution of rain to dissolved materials, this study calibrated spring major components by combining the method of local rain calibration and sea water calibration. The calibration indexes are listed in Table 2.

**Table 2**
Values of major calibration components.

| | Major components | | | | | |
|---|---|---|---|---|---|---|
| | $K^+/Cl^-$ | $Na^+/Cl^-$ | $Ca^{2+}/Cl^-$ | $Mg^{2+}/Cl^-$ | $SO_4^{2-}/Cl^-$ | $HCO_3^-/Cl^-$ |
| Local rain calibration indexes | 0.42 | 0.25 | 0.75 | 0.17 | 3.50 | 0.833 |
| Sea water calibration indexes | 0.02 | 0.36 | 0.02 | 0.05 | 0.38 | |
| Combination of two methods | 0.22 | 0.31 | 0.39 | 0.11 | 1.94 | 0.833 |

Taking a summer spring as a case study, its calibration result can be seen in Table 3. The result shows that on the whole, the contribution of rain to the major spring cations is about 20 % which indicates that springs in the study area cycle shallowly and they are greatly influenced by precipitation as well. The contribution of rain to different ions is quite diverse. 40 % of $K^+$ comes from rain while it is only 4.62 % of $HCO_3^-$. The calibrated result of $K^+$, $SO_4^{2-}$ appears as a negative value under some conditions which shows that the adsorption function cannot be neglected in granite weathering.

| Category | Num | K⁺ Observed | K⁺ Calibrated | K⁺ Rain source | Na⁺ Observed | Na⁺ Calibrated | Na⁺ Rain source | Ca²⁺ Observed | Ca²⁺ Calibrated | Ca²⁺ Rain source | Mg²⁺ Observed | Mg²⁺ Calibrated | Mg²⁺ Rain source | HCO₃⁻ Observed | HCO₃⁻ Calibrated | HCO₃⁻ Rain source |
|---|---|---|---|---|---|---|---|---|---|---|---|---|---|---|---|---|
| A | WX19 | 0.64 | 0.23 | 0.41 | 0.73 | 0.15 | 0.58 | 0.94 | 0.21 | 0.73 | 0.15 | -0.05 | 0.20 | 10.46 | 8.91 | 1.55 |
| A | WX21 | 0.77 | 0.36 | 0.41 | 0.66 | 0.08 | 0.58 | 1.10 | 0.37 | 0.73 | 0.48 | 0.28 | 0.20 | 6.97 | 5.42 | 1.55 |
| B₁ | WX03 | 0.62 | 0.21 | 0.41 | 2.37 | 1.79 | 0.58 | 3.23 | 2.50 | 0.73 | 1.58 | 1.38 | 0.20 | 27.89 | 26.34 | 1.55 |
| B₁ | WX06 | 1.15 | 0.54 | 0.61 | 3.01 | 2.15 | 0.86 | 1.51 | 0.42 | 1.09 | 0.17 | -0.14 | 0.31 | 19.18 | 16.86 | 2.32 |
| B₁ | WX11 | 0.68 | 0.07 | 0.61 | 2.44 | 1.58 | 0.86 | 3.13 | 2.04 | 1.09 | 0.62 | 0.31 | 0.31 | 22.66 | 20.34 | 2.32 |
| B₁ | WX12 | 0.61 | 0.20 | 0.41 | 2.24 | 1.66 | 0.58 | 4.57 | 3.84 | 0.73 | 0.70 | 0.50 | 0.20 | 24.41 | 22.86 | 1.55 |
| B₁ | WX13 | 0.93 | 0.52 | 0.41 | 1.41 | 0.83 | 0.58 | 1.07 | 0.34 | 0.73 | 0.56 | 0.36 | 0.20 | 12.20 | 10.65 | 1.55 |
| B₁ | WX18 | 0.53 | 0.12 | 0.41 | 3.10 | 2.52 | 0.58 | 6.98 | 6.25 | 0.73 | 1.22 | 1.02 | 0.20 | 38.35 | 36.80 | 1.55 |
| B₁ | WX20 | 0.45 | 0.04 | 0.41 | 2.72 | 2.14 | 0.58 | 2.79 | 2.06 | 0.73 | 0.69 | 0.49 | 0.20 | 24.41 | 22.86 | 1.55 |
| B₂ | WX01 | 0.70 | −0.53 | 1.23 | 4.16 | 2.43 | 1.73 | 6.67 | 4.50 | 2.17 | 1.82 | 1.21 | 0.61 | 31.38 | 26.74 | 4.64 |
| B₂ | WX04 | 0.41 | 0.00 | 0.41 | 2.96 | 2.38 | 0.58 | 3.98 | 3.25 | 0.73 | 0.96 | 0.76 | 0.20 | 33.12 | 31.57 | 1.55 |
| B₂ | WX05 | 0.45 | 0.04 | 0.41 | 2.95 | 2.37 | 0.58 | 3.90 | 3.17 | 0.73 | 0.99 | 0.79 | 0.20 | 31.38 | 29.83 | 1.55 |
| B₂ | WX09 | 1.49 | 0.88 | 0.61 | 6.22 | 5.36 | 0.86 | 5.96 | 4.87 | 1.09 | 2.16 | 1.85 | 0.31 | 31.38 | 29.06 | 2.32 |
| B₃ | WX10 | 2.92 | 2.03 | 0.89 | 10.57 | 9.31 | 1.26 | 7.11 | 5.53 | 1.58 | 2.12 | 1.67 | 0.45 | 47.07 | 43.70 | 3.37 |
| C | WX02 | 0.61 | 0.20 | 0.41 | 6.03 | 5.45 | 0.58 | 11.34 | 10.61 | 0.73 | 2.68 | 2.48 | 0.20 | 66.25 | 64.70 | 1.55 |
| C | WX14 | 0.90 | 0.49 | 0.41 | 6.96 | 6.38 | 0.58 | 10.94 | 10.21 | 0.73 | 2.75 | 2.55 | 0.20 | 73.22 | 71.67 | 1.55 |
| C | WX22 | 0.73 | 0.32 | 0.41 | 3.26 | 2.68 | 0.58 | 19.96 | 19.23 | 0.73 | 3.68 | 3.48 | 0.20 | 94.14 | 92.59 | 1.55 |
| C | WX23 | 0.56 | 0.15 | 0.41 | 1.06 | 0.48 | 0.58 | 14.90 | 14.17 | 0.73 | 1.54 | 1.34 | 0.20 | 66.25 | 64.70 | 1.55 |
| D₁ | WX08 | 2.14 | 1.12 | 1.02 | 5.27 | 3.83 | 1.44 | 9.60 | 7.79 | 1.81 | 2.39 | 1.88 | 0.51 | 55.79 | 51.92 | 3.87 |
| D₁ | WX15 | 1.31 | 0.90 | 0.41 | 5.04 | 4.46 | 0.58 | 8.55 | 7.82 | 0.73 | 2.00 | 1.80 | 0.20 | 52.30 | 50.75 | 1.55 |
| D₁ | WX16 | 1.24 | 1.04 | 0.20 | 3.47 | 3.18 | 0.29 | 7.80 | 7.44 | 0.36 | 1.39 | 1.29 | 0.10 | 48.81 | 48.04 | 0.77 |
| D₁ | WX17 | 1.01 | 0.60 | 0.41 | 4.65 | 4.07 | 0.58 | 6.79 | 6.06 | 0.73 | 2.00 | 1.80 | 0.20 | 48.81 | 47.26 | 1.55 |
| D₁ | WX24 | 2.97 | 2.15 | 0.82 | 4.57 | 3.42 | 1.15 | 7.89 | 6.44 | 1.45 | 1.58 | 1.17 | 0.41 | 36.61 | 33.51 | 3.10 |
| D₁ | WX25 | 6.81 | 6.40 | 0.41 | 5.34 | 4.76 | 0.58 | 10.65 | 9.92 | 0.73 | 2.05 | 1.85 | 0.20 | 45.33 | 43.78 | 1.55 |
| D₂ | WX07 | 1.94 | 1.53 | 0.41 | 5.11 | 4.53 | 0.58 | 27.21 | 26.48 | 0.73 | 5.11 | 4.91 | 0.20 | 115.06 | 113.51 | 1.55 |
| Contribution of precipitation (%) | | 39.79 | | | 18.96 | | | 12.18 | | | 15.66 | | | 4.62 | | |

### 20.3.1 Calculation of the CO₂ sink rate

The minerals that are produced in the process of granite weathering can be analysed on a mineral stability graph (7). It can be observed that lime feldspar and biotite have changed into kaolinite. Soda feldspar has mainly changed into Na-montmorillonite, but some into kaolinite. To simplify the calculation process, this study treated them all as having been changed into Na-montmorillonite. The result of the calculation of the $CO_2$
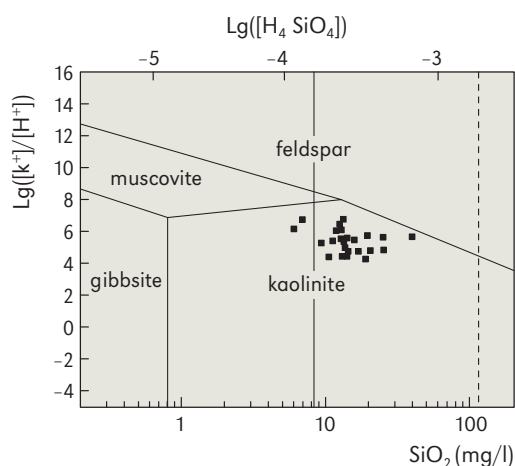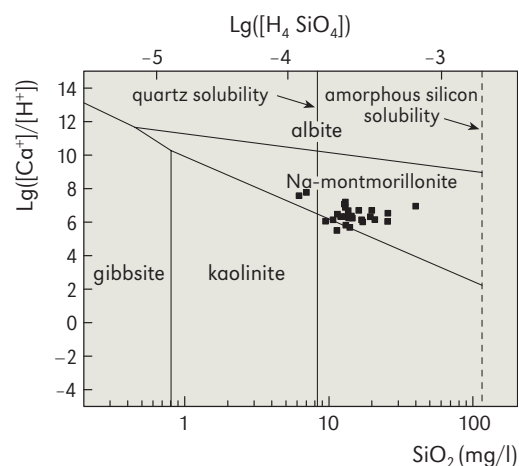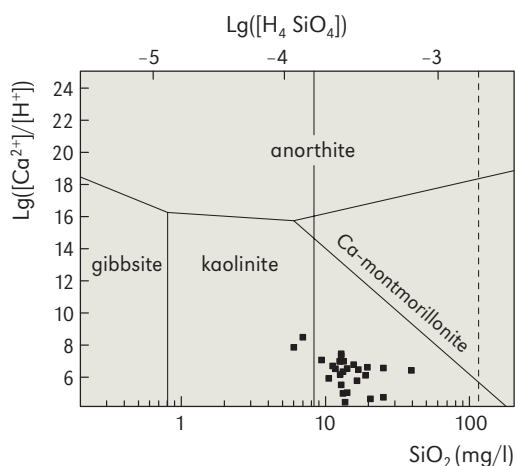
**7** Stability diagram of granite spring major ions (a) Ca-Stability diagram; (b) Na-Stability diagram; (c) K -Stability diagram.

sink rate is listed in Table 4. It has been established that the closer the spring is to the land surface, the more errors appear in the calculation. Table 4 shows that both the cation and the anion methods act well, and that there is little difference in deep cycling springs. The reason may be that other functions such as physical absorption and biological function are greater in a shallow granite weathering zone.

The granite carbon sink rate is quite different for various degrees of rock weathering. Generally speaking, the lower the degree of granite weathering, the greater the carbon sink rate. According to the results, the complete weathering zone shows the characters of carbon source instead of carbon sink. The reasons may lie in the following features of the sample area: a) there is almost no feldspar or mica left, minerals which cause carbon

**Table 4**
Carbon sink rate of each category of springs in summer and winter (mg/l).

| Category | Summer | | | | Winter | | | |
|---|---|---|---|---|---|---|---|---|
| | Carbon sink rate (mg/l) | | Average | Error (%) | Carbon sink rate (mg/l) | | Average | Error (%) |
| | Anion method | Cation method | | | Anion method | Cation method | | |
| A | 5.17 | 1.61 | 3.39 | -101.14 | 6.43 | 0.83 | 3.63 | -154.46 |
| $B_1$ | 16.15 | 11.28 | 13.71 | -42.63 | 19.42 | 24.99 | 22.21 | 25.07 |
| $B_2$ | 21.13 | 19.02 | 20.08 | -14.30 | 29.82 | 31.89 | 30.86 | 6.16 |
| $B_3$ | 31.52 | 38.42 | 34.97 | 19.73 | 79.07 | 71.42 | 75.24 | -10.17 |
| C | 52.96 | 46.35 | 49.65 | -13.80 | 51.01 | 56.00 | 53.50 | 9.16 |
| $D_1$ | 33.09 | 32.51 | 32.80 | -2.31 | 26.36 | 33.92 | 30.14 | 27.97 |
| $D_2$ | 81.88 | 86.65 | 84.26 | 5.67 | 86.76 | 91.49 | 89.13 | 5.31 |

sink, because of their long-time leaching effect in the surface weathering zone; b) the rock particles in the surface weathering zone are small and the particular surface area is comparatively large. This makes the absorption function of the rock particles greater; c) plants in the surface weathering zone are more active, and they absorb more cations from underground water and rock surface. The latter two may be the main reasons for carbon sources in the surface weathering zone; d) as for the same zone, the $CO_2$ consumption capability differs greatly. For example, particular minerals can enhance the $CO_2$ sink by 1.5–2.5 times in the medium weathering zone. Therefore, special attention should be paid to study $CO_2$ consumption in the mineral zones.

### 20.3.2 Calculation of the unit area carbon sink of Yunnan Weixi

The unit area carbon sink of the Yunnan Weixi granite area is calculated in Table 5. It can be seen that the deeper the water cycle, the greater the unit area carbon sink. Take summer as an example: the unit area carbon sink of the complete granite weathering zone (A) is 6.81 mgs$^{-1}$km$^{-2}$ while the shallow fracture zone (B1, B2) is 1.6 times greater. The unit area carbon sink of deep bearing tectonic fracture water (C) is 56.61 mgs$^{-1}$km$^{-2}$, five times that of shallow fracture water. Seasonal changes in the carbon sink rate are smaller then the change in the unit area runoff. Generally speaking, the carbon sink rate in summer is usually 0.7–1 times that in winter, while the unit area runoff is 2–3.5 times higher. Therefore, the unit area carbon sink is determined by the unit area runoff to some extent. The unit area carbon sink rate of the strong weathering zone is lower in summer than in winter because of increasing precipitation, the diluting function of which reduces the density of the granite spring.

**Table 5**
Calculation of the unit area carbon sink of *Yunnan Weixi* granite area (mg/l).

| Category | Summer | | | Winter | | | Summer / Winter | | |
|---|---|---|---|---|---|---|---|---|---|
| | Unit area runoff | Carbon sink rate | Unit area carbon sink | Unit area runoff | Carbon sink rate | Unit area carbon sink | Unit area runoff | Carbon sink rate | Unit area carbon sink |
| | (l/skm²) | (mg/l) | (mgs$^{-1}$km$^{-2}$) | (l/skm²) | (mg/l) | (mgs$^{-1}$km$^{-2}$) | (l/skm²) | (mg/l) | (mgs$^{-1}$km$^{-2}$) |
| A | 1.94 | 3.39 | 6.81 | 0.09 | 3.63 | 0.31 | 22.59 | 0.94 | 21.90 |
| B$_1$ | 0.67 | 13.71 | 11.05 | 0.59 | 22.21 | 13.07 | 1.13 | 0.75 | 0.85 |
| B$_2$ | 0.54 | 20.08 | 11.22 | 0.18 | 30.86 | 7.16 | 2.92 | 0.65 | 1.57 |
| B$_3$ | 0.99 | 34.97 | 34.48 | 0.17 | 75.24 | 12.79 | 5.80 | 0.46 | 2.70 |
| C | 1.16 | 49.65 | 56.61 | 0.74 | 53.51 | 36.75 | 1.58 | 0.98 | 1.54 |
| D$_1$ | 1.09 | 32.80 | 36.59 | 0.46 | 30.14 | 13.32 | 2.35 | 1.09 | 2.75 |
| D$_2$ | 0.79 | 84.26 | 66.90 | 0.37 | 89.13 | 33.26 | 2.13 | 0.95 | 2.01 |

### 20.3.3 Calculation of the total carbon sink of Yunnan Weixi

According to the calculation method in Part 2, the total carbon sink of different springs is listed in Table 6. The result shows that granite weathering consumes $CO_2$ at 14.33 mgs$^{-1}$ km$^{-2}$ based on the hydrochemical calculation, including the anion and cation methods, and it is estimated that 55 % $CO_2$ sink occurs in summer. What is more, the $CO_2$ consumption rate in summer is lower than that in winter, which hints that rainfall plays a more important role than temperature. The thickness of the shallow fracture zone and the degree of denudation in the shallow weathering zone (A, B, D) determined the $CO_2$ consumption budget because they account for 90 % of it while only 7 % and 14 % of $CO_2$ consumption take place in the deep circular zone (C) in summer and winter, respectively.

| Category | Percent of runoff in study area (%) | | Unit area carbon sink ($mgs^{-1}km^{-2}$) | | Total carbon sink ($mgs^{-1}km^{-2}$) | | Percent of total carbon sink in study area (%) | |
|---|---|---|---|---|---|---|---|---|
| | Summer | Winter | Summer | Winter | Summer | Winter | Summer | Winter |
| A | 50.38 | 10.40 | 6.81 | 0.31 | 3.95 | 0.03 | 25.07 | 0.25 |
| $B_1$ | 29.84 | 49.58 | 11.05 | 13.07 | 1.53 | 6.48 | 9.71 | 50.27 |
| $B_2$ | 1.45 | 1.00 | 11.22 | 7.16 | 0.08 | 0.07 | 0.51 | 0.56 |
| $B_3$ | 1.07 | 6.63 | 34.48 | 12.79 | 3.28 | 0.85 | 20.77 | 6.57 |
| C | 2.50 | 4.88 | 56.61 | 36.75 | 1.08 | 1.79 | 6.84 | 13.91 |
| $D_1$ | 14.78 | 27.52 | 36.59 | 13.32 | 5.85 | 3.67 | 37.09 | 28.43 |
| $D_2$ | 0.00 | 0.00 | 66.90 | 33.26 | 0.00 | 0.00 | 0.00 | 0.00 |
| Total | | | | | 15.77 | 12.89 | 100.00 | 100.00 |
| Average | | | | | 14.33 | | | |

**Table 6**
Calculation of the total carbon sink of *Yunnan Weixi* granite area (mg/l).

## CONCLUSION

We studied the $CO_2$ consumption equation for granite weathering in Weixi, Yunnan Province, from the angle of the mineral analysis and hydrochemical characteristics in the study period. The results can be summarized as follows.

The study put forward two methods, the anion and the cation method, to calculate carbon sink in Yunnan Weixi. The result shows that the two methods are simple and act well.

On the whole, the contribution of rain to major spring cation components is about 20 %; thus, the contribution of rain cannot be neglected in the calculation.

Granite weathering consumes $CO_2$ at 14.33 $mgs^{-1}km^{-2}$ based on the hydrochemical calculation including the anion and cation methods, and it is estimated that 55 % $CO_2$ sink occurs in summer. What is more, the $CO_2$ consumption rate in summer is lower than in winter which hints that rainfall plays a more important role than temperature.

The thickness of the shallow fracture zone and the degree of denudation in the shallow weathering zone (A, B, D) determined the $CO_2$ consumption budget because they accounted for 90 % of it while only 7 % and 14 % of $CO_2$ consumption took place in the deep circular zone (C) in summer and winter, respectively.

A special attention should be paid to study $CO_2$ consumption in the mineral zone because even for the same zone $CO_2$ consumption capacity differs greatly. For example, particular minerals can enhance $CO_2$ sink by 1.5–2.5 times in the medium weathering zone.

# LUNAN SHILIN (STONE FOREST), HUMAN IMPACT AND PROTECTION OF THE WORLD NATURAL HERITAGE SITE

ANDREJ KRANJC, HONG LIU

The Chinese expression 'shilin' (shi = stone, lin = forest = 石林) is slowly becoming an international term meaning a kind of 'megakarren', that is a 'forest' of intensively corroded limestone pinnacles up to some ten metres high. D. Yuan defined it as: "a complex landscape consisting of dense rock spires having a variety of shapes separated by numerous dissolution widened fractures. The surfaces of the spires and walls of the grikes exhibit vertical flutes (karren). The spires are commonly about 20 m high although the highest reach 50 m. The upper surfaces of the spires are modified by dissolution by rain water" (*Yuan*, 1988). According to T. Waltham, there are two types of pinnacle karst, so-called 'pinnacle (normal) karst' and 'shilin' or 'stone forest karst' (*Waltham*, 1997). While the first one is typical of steep slopes of high limestone mountains, the second one developed on single beds of gently dipping, solid limestone on the leveled top plateau of southern China. The Dictionary of Modern Geography (*Zu*, 1990) defined shilin as a special kind of high stone teeth with vertical solutional troughs paralleling the vertical rock surface, where columns, commonly 20 m and even 50 m high, were formed by the water within the loose sediments (*Song* and *Li*, 1997).

**1** *Lunan Shilin*, carvings in the rock mean *Shi lin*, that is Stone forest.
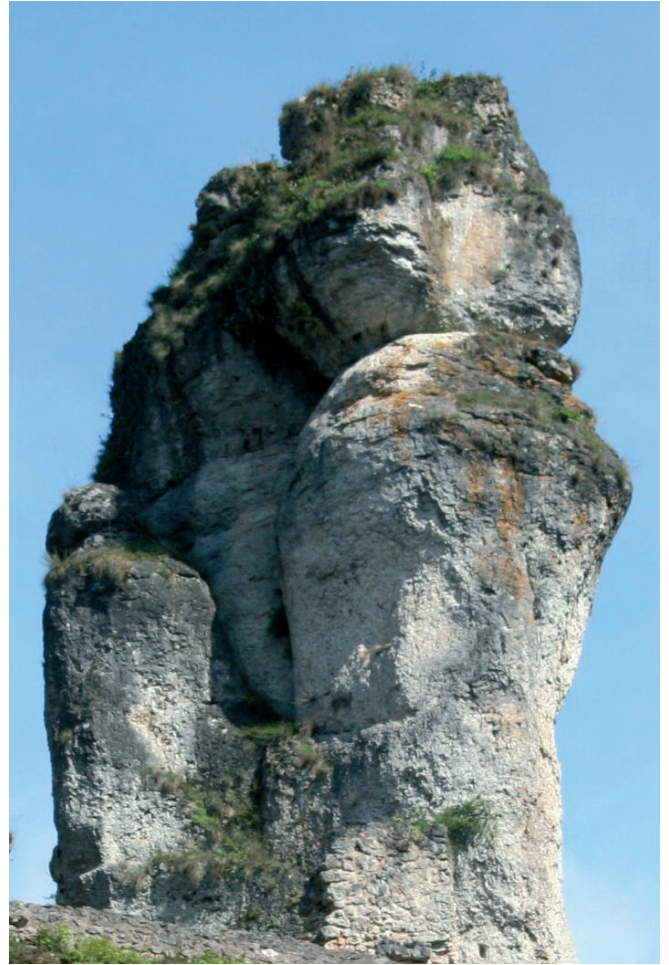
The best and the first known (in literature) shilin is that one near the town of Lunan (1). But there are several shilins round Lunan and they can be found not only in Yunnan but also in the other provinces of China, as Guizhou, Hubei, Hunan and Sichuan shilins are known (altogether they cover about 900 km²). In the karstological literature in Central Europe the term 'Steinwald' (i.e. stone forest in German language) is mentioned in Denes Balazs's report of his visit to karst in China in the years 1958 and 1959. He included pictures of a natural bridge in Lunan (Tienschengtschiao) and a map of the Zhiyun Cave, and he writes about "the world famous Schiling (Steinwald)" in Lunan County (*Balazs*, 1960). The first detailed description of Lunan Shilin in Slovene karstological literature was written by P. Habič (1980).

Later, due to the bilateral projects between Yunnan Geographical Institute and Karst Research Institute, Postojna, more reports on this and other shilins have been published in the Slovene karst literature (*Šebela*, 1996; *Knez*, 1997; *Zupan Hajna*, 1997; *Chen et al.*, 1998). From some other karst landscapes in the world features similar to shilin (or sometimes even the same as shilin) were described. At some places we can speak about a real shilin; some described features are similar but different and have different names (i.e. tsingy in Madagascar; *Salomon*, 1997). More and more as we are acquainted with karst regions of the world, more examples of pinnacle or similar karst features are known. There are examples from America (Sierra de San Luis Potosi in Mexico, Sierra de los Organos in Cuba), Africa (Kouilou near Mombasa), and Asia (Mulu in Sarawak, Mt. Kaijende in Papua New Guinea) (*Ford et al.*, 1997). In Europe the most often cited are Montpellier-le-Vieux in France ('relief ruiniforme' in dolomites), Ciudad Encantada (2) and El Torcal (3) in Spain, and 'rocks' (more the result of erosion in different rocks) in the Jura Mountains (4). These are similar features in appearance but they are different in origin and evolution. So we fully agree with the statement of H. Trimmel (1997), that "the term stone forest should be restricted to the classical sites within southern China".

The best known and we can say classical shilin is Shilin near the town of Lunan (former 'xian' – county of Lunan, renamed into Shilin), 90 km southeast from the Yunnan capital Kunming, designating the geographical name. Its geographical position is 24°30'N and 103°20'E, at 1750 m above sea level. Mean temperature is 16.3 °C with 936 mm of precipitation per year (*Zhang*, 1984). This shilin is the best known and usually when referring to shilin one thinks of Lunan Shilin. The word



**2** Pinnacle "Mushroom" in *Ciudad Encantada* (*Cuenca, Castilla – La Mancha*, Spain). The influence of lithology upon the shape is clearly visible (photo K. Kranjc).

shilin was first written down by the ancient great Chinese poet Qu Yuan (about 340–278 BC) in his poem Ask Heaven (*Pan* and *Ji*, 1997). The well known description of Shilin is from 1382 (*Wang et al.*, 1994). According to Lu Lian Zhou Zhi (1573–1619) there was a temple on a karst hill nearby the HEMO station of the Naigu Shilin ancient paths, which had become the site of Buddha worship for the local people. Man began to excavate the Ziyun Cave in 1614 and placed a stele at the entrance. In this period also the tourist path was constructed round Shilin (*Song*, 1995). Xu Xiake (1587–1641), a famous geographer and karst researcher, travelled to Yunnan in 1638. Because his Yunnan Travel Diary I is lost, it is impossible to recognise his route and his impressions in detail. From the remnants of his travel notes it is possible to presume that Xu Xiake visited Shilin. The great philosopher and scholar Gu Yanwu (1613–1682) gave the first convincing description of Shilin. This period can be called the early discovery phase.

The second phase can be called the early tourism development phase during which exploitation, protection and scientific research have developed. In 1931, the chairman of Yunnan Province, Yun Long visited the Dadeishui waterfall with the government officials and his family and enjoyed the Shilin landscape on the way home. He wrote 'shilin' to describe the unique and magical stone forest landscape. He set up a special fund for pavilions, paths and villa construction there, and appointed regional staff to manage them. These were the earliest tourism facilities in the Shilin scenic area. In the 30's of the twentieth century, the universities from Beijing, Qinghua and Nankai moved to Kunming, due to the war against Japan; there many scholars have made the research of Yi nationality culture in this area and also of Shilin (*Ma*, 1936) (5). In 1941 Shilin was used for grazing (6), in 1944 the provincial government set aside a sum of money to

**3** View of *El Torcal de Antequera* (*Andalusia*, *Malaga*, Spain). The height of the central pillar is about 20 m.

**4** The Malm limestone pillar *Tüchersfeld* (Franconian Switzerland, Bavaria) is due mostly to the erosion process (photo K. Kranjc).

225

build a villa, and assigned a fulltime officer and 20 staff to manage house property and reforestation. At that time, Shilin was not opened to the public yet. The visitors were all government officials and rich men, the sightseers were few, but have left many art works of carved stone behind. The Shilin management office was set up in 1951 under the leadership of Yunnan Province and Lunan County government. In the next year the Shilin management department was set up, which was responsible for the management of Shilin. In 1953, Shilin got the first international visitor, a Soviet delegation, and premier Zhou Enlai made a special trip to Shilin and gave his approval for its exploitation. Since that time the government has invested in building a tourist route, making stone tables, planting flowers and trees, allowing Shilin to receive more tourists. From 1961 to 1965, different levels of administration have paid attention to the exploitation of Shilin. Sooner or later state leaders have visited Shilin giving the area a high reputation, and the number of visitors to the Shilin landscape was increasing.

Unfortunately, the culture revolution, from 1966 to 1976, caused a lot of damage to tourism of Shilin. Not only the buildings were demolished, but also some scenery stones were damaged. Deforestation occurred in some places.

Since 1979, the scenic area of Shilin has stepped into a quick development phase, the first development and protection promoted phase, which can be called the modern tourism phase. The government has recognised the scientific value of the Shilin landscape, assuming that its exploitation will have a great influence on local economy and culture, so they began to look to strengthen the protection of Shilin and its envi-

**5**   *Shilin* in 1938 (photo Chunzou Yang).



226

6   *Shilin* in 1941, used
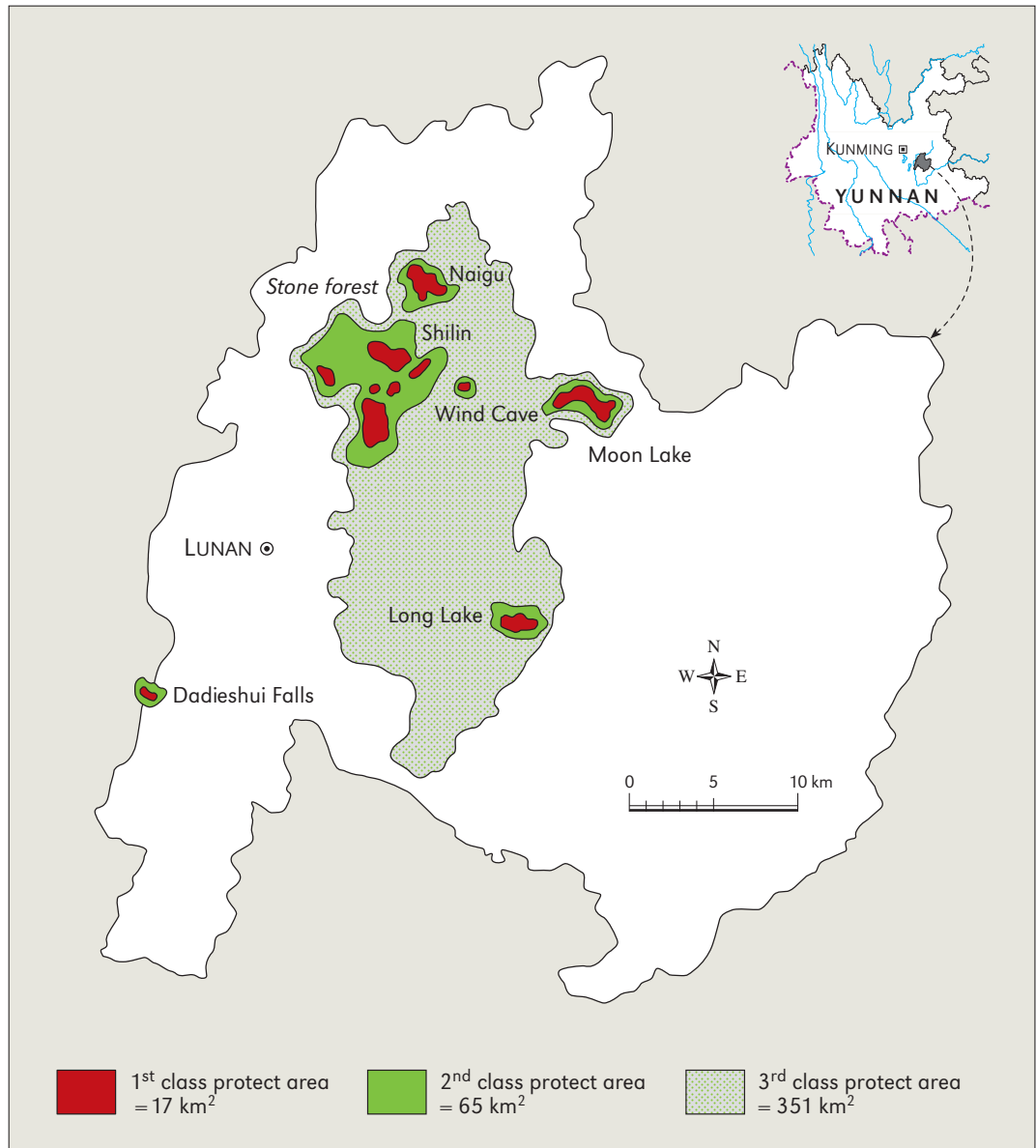for grazing (photo
Chunzou Yang).

ronment, including its restoration. In 1980, the Administrative Office of Shilin Scenery
(Bureau of Shilin Management) was set up; it was divided into five different depart-
ments. There were garden and forestry, agrarian pre-plan, tourist service, environment
protection, and publicity departments. It has organized experts to carry out the work
of fully systematic investigation and estimation. In 1981 Shilin was listed as a province
natural protected area covering 350 km², mainly protecting the Shilin landscape and its
geological phenomena and in 1982 it became a National Park.

In 1987 the state Ministry of Construction formally approved The Overall Plan of Lu-
nan Shilin Scenic Area. It defines the extent of the Shilin protected area (350 km²), and
the whole region was divided into three zones with different protection levels. The first
level includes the Major and Minor Shilin scenic areas (7), Naigu Shilin area, Ziyundong
Cave area, Qifongdong Cave area, Changhu Lake area, Yuehu Lake area and Dadeishui
waterfall area. The whole surface of the first level has 15.76 km² (later it was adjusted to
18.5 km²). The second level areas are the first levels' buffer zone, or we can say it is an en-
vironmental transition zone, occupying 28.14 km². The third protection level, similarly,
is the buffer zone of the second level areas, covering 306.1 km². Since then, they have
made the detailed plan of scenic areas, which let the management of the Shilin Scenic
Area move into a next phase. By the Protection Act of Lunan Shilin Scenic Area the ex-
ploitation and protection of Shilin was set into the legal system (*Wang et al.*, 1994).

In 1988 Shilin was listed as a State-level scenic area. Common people little by little
understood the value of the Shilin landscape and its scenery was becoming more and
more known. From 1990 to now, the Shilin Management Bureau has paid more attention
to the protection of the Shilin landscape and its environment. A lot was done to expand
and to improve tourist facilities, too. In 1986 Naigu shilin was opened to the public and
in the same year already it had over 46,900 visitors. Later on their number declined. In
the same year also Dadeishui waterfall area was opened to the public and had 55,000

227

*Lunan shilin (stone forest), human impact and protection of the world natural heritage site*

**7** Map of the *Shilin* National Park (Ford et al., 1996).

1st class protect area = 17 km$^2$

2nd class protect area = 65 km$^2$

3rd class protect area = 351 km$^2$

visitors that year. In 1988 Ziyundong Cave was opened and there were 64,500 visitors. In the period 1980–1990 Shilin scenic area has been visited by 10 million tourists and in 1999 alone by more than 2 million.

Therefore safeguarding and protecting of Shilin is becoming more and more important. Under the auspices of the National Ministry of Construction they began to collect material for the preparation of an application to inscribe Shilin into the list of World's Natural Heritage at UNESCO. The task was in charge of Prof. Rouwei Xiong from Yunan Normal University and Prof. Lingao Xie from Beijing University within the co-operation of Yunnan Normal University, Government of Shilin County, and Beijing University. In 1995 the International Symposium for Lunan Shilin to Apply for World Natural Heritage Status with the aim to confirm the justification of Shilin's inscription into the World Heritage list was organized (*Song et al.*, 1997). During this event a number of Chinese and most eminent western karstologists evaluated Shilin from very different points of view. The concluding remark by Zhang Yaoguang, the member of Chinese Academy of Sciences, was: "Lunan Shilin therefore has high values both to science and economy. It must be designated as a World Natural Heritage Site" (*Song et al.*, 1997, 95). But the task was not so easy and simple. The members of IUCN, International

Union for Conservation of Nature, who were asked to give the opinion to the UNESCO regarding the inscription of Shilin, had serious remarks why not to include Shilin on the list of UNESCO. So it lasted till 2007 that Shilin was finally put on the UNESCO list of the World Natural Heritage. On 27 June 2007 natural sites in Madagascar, China and Korea were inscribed on the UNESCO World Heritage List. Shilin is not on the list of UNESCO itself, but as a part of South China Karst. It includes also the karst of Guizhou Province (the cone and tower karsts of Libo) and Chongqing Municipality (giant dolines, natural bridges and caves of Wulong karst). By UNESCO the stone forests of Shilin are considered superlative natural phenomena and a world reference with a wider range of pinnacle shapes than other karst landscapes with pinnacles, and a higher diversity of shapes and changing colours.

It is self-evident that such a site needs protection and safeguarding measures. Some have been shown in the previous text already. With the increase of the number of visitors human impact problems are growing, too. The most important are:

– quarrying,
– growth of population (urban growth),
– agriculture and stock breeding (pollution),
– soil and water loss (pressure on local water supply),
– mass tourism.

Quarrying has been a knotty problem of long standing in the management of Shilin. Although the Management Bureau has repeatedly forbidden the exploitation (destruction) of limestone pinnacles as a source of rock material (8), it could not stop it completely. In 1999, the county government and Shilin authorities made the big decision to stop it. They not only forbid quarrying activities inside the protected area, but ask the people who previously quarried to reforest the land and to carry out ecological restoration works in those areas.

The second important threat is the pressure of population towards the protection zone, due to its increase. This can be seen through the pressure for new building plots (the inhabitants inside the protected area occupied more and more land) and through



**8** Traces of human activity in the *Shilin* surroundings.

*Lunan shilin (stone forest), human impact and protection of the world natural heritage site*

229

the intensification of agriculture and its needs (farming and stockbreeding). The soil and water loss phenomena were becoming serious, the fertilisers used were also a potential pollution source of underground water (*Zhang et al.*, 2003).

The third impact is directly by mass tourism, due to the fast growth of the visitors' number which certainly makes a great pressure on environment and landscape protection work. In order to adapt the requirement of tourism, there have been built some tourist service facilities around the outer ring of Shilin scenic spots, which was partially in contradiction to protection of the original Shilin landscape panorama. The relationship between protection and exploitation still needs further harmonization. In order to adapt the application work, the Shilin Management Bureau and the government of Shilin County have decided to demolish some buildings and facilities which are inside the scenic area and to construct new tourist facilities out of the core zone, which help a lot towards the positive opinion of the IUCN members.

The Management Bureau and Shilin Administration prepared special protection plans and measures, including special organization of human resources, too. Besides the delimitation of sectors with different steps of protection (core zone, buffer zone,…), the Shilin Administration introduced different protection measures (*Zhang* and *Day*, 2002; *Zhang et al.*, 2005). They have set up a special Environmental Protection Department under the Shilin Management Bureau. It consists of 18 persons, specially engaged in landscape resources and environmental resources protection. This department is under the leadership of a deputy director of the Bureau. Each of the team is in charge of the protection work of certain areas. They all have the high school education. Moreover, the head or a person with high reputation of every village or township in the region is also engaged as a special ranger (volunteer), who is responsible for preventing the inhabitants damaging stone and nature resources. When they find out or hear something happening in the protected area, they go there to check it out and report to the leader of the Management Bureau. Interdiction of rock (limestone pinnacles) exploitation in the protection zone has been mentioned already. These special rangers are entitled to give an advice to stone pillars destroyers. If the advice is not respected, they have the right to confiscate their transport tools and equipment. And even more, they have the authority to fine the destroyers up to 5000 yuan. But for the bigger affairs all the leaders of the Shilin Directorate need to deal with and to harmonize it.

For the conclusion it can be said that all the suggestions of the IUCN members have been observed, the organization of the protection, regarding the terrain as well as the personnel was well organized and adequate, the protection measures observed – and in June 2007, during the UNESCO Committee meeting in Christchurch, New Zealand, Shilin attained the wish from long ago, to become the member of the UNESCO World Natural Heritage.

# References

AJAZ, K., J. VEIZER, 2000: Weathering processes in the Indus River Basin: implications from riverine carbon, sulfur, oxygen, and strontium isotopes. *Chemical Geology* 170/1–4, 153–177.

ALLEN, C. R., A. R. GILLESPIE, Y. HAN, K. E. SIEH, B. ZHANG, C. ZHU, 1984: Red River and associated faults, Yunnan Province, China: Quaternary geology, slip rates and seismic hazard. *Geological Society of America Bulletin* 95/6, 686–700.

AMIOTTE-SUCHET, P., J.-L. PROBST, W. LUDWIG, 2003: Worldwide distribution of continental rock lithology: implications for the atmospheric/soil $CO_2$ uptake by continental weathering and alkalinity river transport to the oceans. *Global Biogeochemical Cycles* 17/2, 1038.

BAKALOWICZ, M., 2004: The epikarst. The skin of karst. In: Jones, W. K., D. C. Culver, J. S. Herman (Eds.), *Epikarst. Proceedings of the Symposium held October 1–4, 2003, Sheperdstown, West Virginia, USA*. Karst Waters Institute Special Publication 9, Charles Town, WV, 16–22.

BALÁZS, D., 1960: Beiträge zur Speläologie des südchinesischen Karstgebietes. *Karszt-és barlang-kutatás* 2, 3–82.

BLUM, J. D., 1997: The effect of Late Cenozoic Glaciation and Tectonic Uplift on silicate weathering rates and the marine 87Sr/86Sr record. In: Ruddiman, W. F. (Ed.), *Tectonic Uplift and Climate Change*. Plenum Press, New York, 259–288.

BOEGLIN, J. L., J. L. PROBST, 1998: Physical and chemical weathering rates and $CO_2$ consumption in a tropical lateritic environment: the upper Niger basin. *Chemical Geology* 148, 137–156.

BÖGLI, A., 1980: *Karst Hydrology and Physical Speleology*, Springer-Verlag, Berlin, 284 p.

BRIAIS, A., P. PATRIAT, P. TAPPONIER, 1993: Updated interpretation of magnetic anomalies and seafloor spreading stages in the South China Sea: implications for the Tertiary tectonics of Southeast Asia. *Journal of Geophysical Research* 98, 6299–6328.

BURCHFIEL, B. C., E. WANG, 2003: Northwest-trending, middle Cenozoic, left-lateral faults in southern Yunnan, China, and their tectonic significance. *Journal of Structural Geology* 25/5, 781–792.

CAMACHO, A. I., A. G. VALDECASAS, J. RODRÍGUEZ, S. CUEZVA, J. LARIO, S. SÁNCHEZ-MORAL, 2006: Habitat constraints in epikarstic waters of an Iberian Peninsula cave system. *Annales de Limnologie/International Journal of Limnology* 42/2, 127–140.

CHAPLIN, G., 2005: Physical Geography of the Gaoligong Shan Area of Southwest China in Relation to Biodiversity. *Proceedings of The California Academy of Sciences, Fourth Series*, 56/28, 527–556.

CHEN, B., Y. LI, J. QU, 1992: On the main geotectonic problems in the Sanjiang Region and their relations to metallization. *Geological Memoirs* 5/11, 47–50.

CHEN, J. H., XING-HUI, L. ZHANG, 1999: The tendency of water quality of Changjiang, Huanghe, Songhuajiang and its relation between social economy development between 60's and 90's, *Journal of Environment Science* 19/5, 500–505 (in Chinese with English abstract).

CHEN, X., F. GABROVŠEK, C. HUANG, Y. JIN, M. KNEZ, J. KOGOVŠEK, H. LIU, A. MIHEVC, B. OTONIČAR, M. PETRIČ, M. SHI, T. SLABE, S. ŠEBELA, W. WU, S. ZHANG, N. ZUPAN HAJNA (Eds.), 1998: *South China Karst 1*, Zbirka ZRC 19, Publishing ZRC, Ljubljana, 247 p.

CHEN, Z., L. SONG, M. M. SWEETING, 1986: The Pinnacle Karst of the Stone Forest, Lunan, Yunnan, China: an example of a subjacent karst. In: Paterson K., M. M. Sweeting (Eds.), *New Directions in Karst*, Geobooks, Norwich, 597–607.

CLTGI, 1991: *Chenanzhe Luyunting Travelling Geoscience Introduction*, Beijing University Press.

CNST, 1993: *Chenshicai Natural Scenery Travelling*, Earthquake Press.

CULVER, D. C., T. PIPAN, 2009: *The Biology of Caves and Other Subterranean Habitats*. Oxford University Press, Oxford, 256 p.

DATTA, D., V. SUBRAMANIAN, 1997: Nature of solute loads in the rivers of Bengal Basin, Bangladesh. *Journal of Hydrology* 198, 196–208.

DEHARVENG, L., 2005: Diversity patterns in the tropics. In: Culver, D. C., W. B. White (Eds.), *Encyclopedia of caves*, Elsevier/Academic Press, Amsterdam, 166–170.

DOLE-OLIVIER, M.-J., D. M. P. GALASSI, P. MARMONIER, M. CREUZÉ DES CHÂTELLIERS, 2000: The biology and ecology of lotic microcrustaceans. *Freshwater Biology* 44, 63–91.

DONG, H., 1996: *Study of developing strategy on the karst area*. Yunnan Science and Technology Publishing House, Kunming, 29–32.

DU, X. (Ed.), 2007: *Atlas of China*. SinoMaps Press, Beijing, 283 p.

DUN, J., 1999: Neogene's transform structure feature in Three Parallel Rivers Region, West of Yunnan Province. *Yunnan Geology*, 2–5.

FEIGL, K. L., C. C. DUONG, M. BECKER, D. T. TRAN, K. NEUMANN, Q. X. NGUYEN, 2003: Insignificant horizontal strain across the Red River Fault near Thác Bà, Vietnam, from GPS measurements 1994–2000. *Geophysical Research Abstracts* 5, 4707.

FONG, D. W., D. C. CULVER, H. H. HOBBS III, T. PIPAN, 2007: *The Invertebrate Cave Fauna of West Virginia (2nd Ed.),* West Virginia Speleological Survey Bulletin 16, Barackville, 167 p.

FORD, D. C., P. W. WILIAMS, 2007: *Karst Hydrogeology and Geomorphology.* Wiley, Chichester, 576 p.

FORD, D., J.-N. SALOMON, P. WILLIAMS, 1996: Les "Forêts de Pierre" ou "Stone forests" de Lunan (Yunnan, Chine). *Karstologia* 28/2, 25–40.

FORD, D., J.-N. SALOMON, P. WILLIAMS, 1997: The Lunan Stone forest as a potential world heritage site. In: *Song et al.*, 1997, 107–123.

FORD, T. D., H. M. PEDLEY, 1996: A review of tufa and travertine deposits of the world. *Earth-Science Reviews* 41/3–4, 117–175.

FORNÓS, J. J., A. GINÉS (Eds.), 1996: *Karren landforms.* Servei de Publicacions, Universitat de les Illes Balears, Palma de Mallorca, 450 p.

FRANČIŠKOVIĆ-BILINSKI, S., H. BILINSKI, D. BARIŠIĆ, N. HORVATINČIĆ, 2003: Analysis of Tufa from Guangxi (China). *Acta Geologica Sinica (Engl. Ed.)* 77/2, 267–275.

FUYUAN, L., 2000: *Genesis of Lunan Stone Forest Landscape and Subsoil Dissolution.* MSc Thesis, Institute of Geographic Sciences and Natural Resources Research, Chinese Academy of Sciences, Beijing.

GAILLARDET, J., B. DUPRÉ, C. J. ALLÈGRE, 1995: A global geochemical mass budget applied to the Congo basin rivers: Erosion rates and continental crust composition. *Geochimica et Cosmochimica Acta* 59/17, 3469–3485.

GAILLARDET, J., B. DUPRÉ, C. J. ALLÈGRE, P. NÉGREL, 1997: Chemical and physical denudation in the Amazon River Basin. *Chemical Geology* 142/3–4, 141–173.

GALASSI, D. M. P., 2001: Groundwater copepods: diversity patterns over ecological and evolutionary scales. *Hydrobiologia* 453–454/1, 227–253.

GALASSI, D. M. P., P. MARMONIER, M.-J. DOLE-OLIVIER, S. D. RUNDLE, 2002: Microcrustacea. In: Rundle, S. D., A. L. Robertson, J. M. Schmid-Araya (Eds.), *Freshwater Meiofauna: Biology and Ecology,* Backhuys Publishers, Leiden, 135–175.

GDR, 1989: *Genghong development research of travelling geoscience resources in Yunnan Province*, Bureau of Geology and Mineral Resources of Yunnan Province.

GENG, H., 1989: *Geological Resources for Tourism in Northwest of Yunnan.* Yunnan Bureau of Geology and Mineral Resources, 295 p.

GU, J., X. ZHANG, H. FANG, 2002: Characteristics and Genetic Analysis of the Deep-buried Weathered-crust Karst Hydrocarbon Reservoirs of the Lower Paleozoic Group in the Tarim Basin. *Acta Geologica Sinica (Engl. Ed.)* 76/4, 494–502.

HABIČ, P., 1980: S poti po kitajskem krasu. *Geografski vestnik* 52, 107–122.

HANTOON, P. W., 1997: Definition and characteristics of Stone forest epikarst aquifers in south China. *Proceedings of the 12th International Congress of Speleology* 1/8, 311–314.

HE, K., C. LIU, S. WANG, 2001: Karst collapse mechanism and criterion for its stability. *Acta Geologica Sinica (Engl. Ed.)* 75/3, 330–335.

HUANG, C., 2004: *Characteristics and formation mechanism of tufa landscape at Tianshengqiao, Zhongdian County, Yunnan Province, China.* Unpublished report, 8 p.

HUANG, C., H. LIU, 1998: Karst of Yunnan. In: *Chen et al.*, 1998, 11–17.

HYDROGEOLOGICAL TEAM, 1977: Hydrogeological and Engineering Geological Survey Team of the Yunnan Geological Bureau.

INFORMATION COLLECTION, 1984: *Information collection on Agriculture Climate of Yunnan Province.* Yunnan People's Press, Kunming.

JABLONSKI, N. G., X. JI, G. CHAPLIN, L. WANG, S. YANG, Z. LI, G. LI, 2003: A preliminary report on new and previously known vertebrate paleontological sites in Baoshan Prefecture, Yunnan Province, China. *Proceedings of The California Academy of Sciences, Fourth Series*, 54, 209–224.

JACOBSON, A. D., J. D. BLUM, L. M. WALTER, 2002: Reconciling the elemental and Sr isotope composition of Himalayan weathering fluxes: insights from the carbonate geochemistry of stream waters. *Geochimica et Cosmochimica Acta* 66/19, 3417–3429.

JACOBSON, A. D., J. D. BLUM, C. P. CHAMBERLAIN, D. CRAW, P. O. KOONS, 2003: Climatic and tectonic controls on chemical weathering in the New Zealand Southern Alps. *Geochimica et Cosmochimica Acta* 67/1, 29–46.

JELÍNEK, V., 1973: Precision A.C. bridge set for measuring magnetic susceptibility and its anisotropy. *Studia Geophysica et Geodaetica* 17/1, 36–48.

JELÍNEK, V., 1996:. A high sensitivity spinner magnetometer. *Studia Geophysica et Geodaetica* 40/1, 58–78.

JIN, Z., J. PENG (Eds.), 1998: *Vegetation of Kunming*, Yunnan Science and Technology Press, Kunming, 431–434, 457–466, 471–484.

KIRSCHVINK, J. L., 1980: The least-squares line and plane and the analysis of palaeomagnetic data. *Geophysical Journal of the Royal Astronomic Society* 62/3, 699–718.

KLIMCHOUK, A., 2000: Dissolution and Conversion of Gypsum and Anhydrite. In: Klimchouk, A., D. C. Ford, A. N. Palmer, W. Dreybrodt (Eds.), *Speleogenesis. Evolution of Karst Aquifers*, National Speleological Society, Huntsville, Alabama, 160–168.

KNEZ, M., 1997: Prvi rezultati raziskav kamnine v treh lunanskih kamnitih gozdovih (Yunnan, Kitajska). *Acta Carsologica* 26/2, 431–439.

KNEZ, M., 1998: Lithologic Properties of the Three Lunan Stone Forests (Shilin, Naigu and Lao Hei Gin). In: *Chen et al.*, 1998, 30–43.

KNEZ, M., T. SLABE, 2001a: Oblika in skalni relief stebrov v Naigu kamnitem gozdu (JZ Kitajska). *Acta Carsologica* 30/1, 13–24.

KNEZ, M., T. SLABE, 2001b: The lithology, shape and rock relief of the pillars in the Pu Chao Chun stone forest (Lunan stone forests, SW China). *Acta Carsologica* 30/2, 129–139.

KNEZ, M., T. SLABE, 2002: Lithologic and morphological properties and rock relief of the Lunan stone forests. In: Gabrovšek, F. (Ed.), *Evolution of karst: from Prekarst to Cessation*, Publishing ZRC, Ljubljana, 259–266.

KNEZ, M., T. SLABE, 2006: Lithological characteristics, form, and rock relief of the Lunan Stone Forests (South China karst). *Geografski vestnik* 78/1, 9–24.

KNEZ, M., T. SLABE, 2007: Shilin, the Formation of Stone Forest in Various Rock Types (Lunan, Yunnan, China). *Acta Geologica Sinica (Engl. Ed.)* 81/1, 148–157.

KNEZ, M., T. SLABE, 2010: Karren of Mushroom Mountain (Junzi Shan) in the Eastern Yunnan Ridge, Yunnan, China: Karstological and Tourist Attraction. *Acta Geologica Sinica (Engl. Ed.)* 84/2, 424–431.

KNEZ, M., J. KOGOVŠEK, A. KRANJC, H. LIU, M. PETRIČ, T. SLABE, 2009: The Shuilian cave in the upper region of the Chang river (karst of NW Yunnan, China). *Acta Carsologica* 38, 97–106.

KOGOVŠEK, J., 1984: Vertikalno prenikanje vode v Škocjanskih jamah in Dimnicah. *Acta Carsologica* 12/3, 49–65.

KOGOVŠEK, J., 1998: Physical and chemical characteristics of groundwater of Tianshengan area (The wider area of the tracing experiments). In: *Chen et al.*, *1998*, 91–98.

KOGOVŠEK, J., 2007: Rainwater percolation dynamics assessment through the vadose karst zone on the basis of discharge measurements. *Acta Carsologica* 36/2, 245–254.

KOGOVŠEK, J., H. LIU, 1999: Water tracing test in the Tianshengan region, China, at low water level in November 1998. *Acta Carsologica* 28/2, 241–253.

KOGOVŠEK, J., H. LIU, 2000: Water tracing test in the Tianshengan region, Yunnan–China, at high water level. *Acta Carsologica* 29/2, 249–259.

KOGOVŠEK, J., M. PETRIČ, 2002: Podzemno raztekanje vode iz ponora Tržiščice (JV Slovenija) / Underground water flow from the Tržiščica sinking stream (SE Slovenia). *Acta Carsologica* 31/2, 75–91.

KOGOVŠEK, J., M. PETRIČ, 2006: Tracer test on the Mala gora landfill near Ribnica in south-eastern Slovenia. *Acta Carsologica* 35/2, 91–101.

KOGOVŠEK, J., S. ŠEBELA, 2004: Water tracing through the vadose zone above Postojnska jama, Slovenia. *Environmental Geology* 45/7, 992–1001.

KOGOVŠEK, J., H. LIU, M. PETRIČ, 1997: Properties of underground water flow in karst area near Lunan in Yunnan Province, China. In: A. Kranjc (Ed.), *Tracer Hydrology 97*, *Proceedings of the 7th International Symposium on Water Tracing (Portorož/Slovenia, 26–31 May 1997)*, A. A. Balkema, Rotterdam, 255–261.

KOGOVŠEK, J., H. LIU, M. PETRIČ, W. WU, 1998: Tracing test in the Tianshengan area. In: *Chen et al., 1998*, 99–112.

KOGOVŠEK, J., A. KRANJC, T. SLABE, S. ŠEBELA, 1999: South China Karst 1999, Preliminary research in Yunnan. *Acta Carsologica* 28/2, 225–240.

KRANJC, A., H. LIU, 2001: Lunan Shilin (stone forest), human impact and protection of (eventual) world heritage site (Yunnan, China). *Acta Carsologica* 30/1, 25–38.

LATELLA, L., C. HU, 2008: Biological investigation of the Museo Civico di Storia Naturale of Verona in South China caves. In: Latella, L., R. Zorzin (Eds.), *Research in South China Karst*, Memorie del Museo Civico di Storia Naturale di Verona, 2. Serie. Memorie Naturalistiche 3, 65–88.

LELOUP, P. H., R. LACASSIN, P. TAPPONIER, U. SCHÄRER, D. ZHONG, X. LIU, L. ZHANG, S. JI, P. T. TRINH, 1995: The Ailao Shan-Red River shear zone (Yunnan, China), Tertiary transform boundary of Indochina. *Tectonophysics* 251, 3–84.

LI, H., 1988: The Aquatic Vegetation and Flora in Changhu Lake, *Journal of Yunnan University (Natural Sciences Edition)* 10, suppl., 119–123.

LI, J., J. ZHANG, 2002: The weathering function of basin and global climate change. *Advance in Earth Sciences* 17/3, 411–419 (in Chinese with English abstract).

LIANG, F., 2000: *Genesis of Lunan Stone Forest Landscape and Subsoil Dissolution*. Master's degree thesis in physical geography. Institute of Geographic Sciences and Natural Resources Research, Chinese Academy of Sciences, Beijing.

LIN, J., 1997a: Genesis of Lunan stone forest and its geomorphological significance. In: *Song et al.*, 1997, 30–33.

LIN, J., 1997b: Formation of Lunan Stone Forest and environmental change. *Carsologica Sinica* 16/4, 346–350.

LIU, H., W. WU, 1998: A study on recent karst denudation rate of karst in Lunan Stone Forest. *Yunnan Geographic Environment Research* 10 (suppl.), 114–121.

LIU, H., Y. ZHOU, 2003: The characteristic of cave development in Shilin. *Advance in Earth Sciences* 18/6, 891–898.

LIU, T., M. TAN, X. QIN, S. ZHAO, T. LI, J. LA, D. ZHANG, 1997 : Discovery of microbedding in speleothems in China and its significance in the study of global change. *Quaternary Sciences* 1, 41–51.

LIU, Y., X. PENG, Z. HUANG, 1988: A deformational study after the Tonghai earthquake. *Journal of Seismological Research* 4, 369–376.

LOWE, D. J., T. WALTHAM, 1995: *A Dictionary of Karst and Caves*. Cave Studies Series 6, British Cave Research Association, London, 40 p.

LUO, G., C. YAN, X. LI, J. JIANG, J. MA, 2003: Exploration of water resource and multiple model for water resource development in karst areas with the Preferred Plane Theory. *Acta Geologica Sinica (Engl. Ed.)* 77/1, 129–135.

LUO, J., Y. YANG, Z. ZHAO, J. CHEN, J. YANG, 1994: Evolution of Tethys in western Yunnan and mineralization for main metal deposits. *Geological Memoirs* 4/45, 47–48 (in Chinese with English abstract).

MA, X., 1936: Preliminary investigation on the Lunan stone forest, Yunnan, from the geomorphological view. *Theoretical Review* 1/1.

MA, X. (Ed.), 1990: *Lithospheric Dynamics Atlas of China*. China Cartographic Publishing House, Beijing, 68 p.

MAIRE, R., S. ZHANG, S. SONG, 1991: Genèse des karsts subtropicaux de Chine du Sud (Guizhou, Sichuan, Hubei). Grottes et karsts tropicaux de Chine Meridionale, *Karstologia mémoires* 4, 162–186.

MEYBECK, M., 1987: Global chemical weathering of surficial rocks estimated from river dissolved loads. *American Journal of Science* 287, 401–428.

MICHEL, G. W., M. BECKER, D. ANGERMANN, C. REIGBER, E. REINHART, 2000: Crustal motion in E- and SE-Asia from GPS measurements. *Earth Planets Space* 52, 713–720.

MIHEVC, A., T. SLABE, S. ŠEBELA, 1998: Denuded caves – an inherited element in the karst morphology: the case from Kras. *Acta Carsologica* 27/1, 165–174.

MOLDOVAN, O. T., T. PIPAN, S. IEPURE, A. MIHEVC, J. MULEC, 2007: Biodiversity and ecology of fauna in percolating water in selected Slovenian and Romanian caves. *Acta Carsologica* 36/3, 493–501.

OARGA, A., 2008: Species richness from pools and drips in selected Romanian caves. *16th International Karstological School Classical Karst*, Postojna, Slovenia (CD).

OU, P., 1988: The Phytocaenosium features of the vegetation of around Yuehu Lake in Lunan. *Journal of Yunnan University (Natural Sciences Edition)* 10, suppl., 124–140.

PALMER, A. N., 2007: *Cave geology*. Cave Books, Dayton, Ohio, 454 p.

PAN, J., S. JI, 1997: Criteria of world natural heritage sites with respect to Lunan Shilin. In: *Song et al.*, 1997, 34–36.

PENG, J., 1988: A Study on the Vegetation surrounding Changhu Lake in Lunan. *Journal of Yunnan University (Natural Sciences Edition)* 10, suppl., 107–117.

PENTECOST, A., Z. ZHANG, 2001: A review of Chinese travertines. *Cave and Karst Science* 28/1, 15–28.

PESCE, G. L., D. P. GALASSI, 1986: Taxonomic and phylogenetic value of the armature of coxa and antenna in stygobiont cyclopoid copepods. *Bollettino di Zoologia* 53, 5.

PETRIČ, M., 2002: *Characteristics of recharge-discharge relations in karst aquifer*. Publishing ZRC, Postojna–Ljubljana, 154 p.

PIPAN, T., 2005: *Epikarst – a promising habitat. Copepod fauna, its diversity and ecology: a case study from Slovenia (Europe)*. Publishing ZRC, Postojna–Ljubljana, 101 p.

234

PIPAN, T., D. C. CULVER, 2005: Estimating biodiversity in the epikarstic zone of a West Virginia cave. *Journal of Cave and Karst Studies* 67/2, 103–109.

PIPAN, T., A. BLEJEC, A. BRANCELJ, 2006a: Multivariate Analysis of Copepod Assemblages in Epikarstic Waters of Some Slovenian Caves. *Hydrobiologia* 559/1, 213–223.

PIPAN, T., M. C. CHRISTMAN, D. C. CULVER, 2006b: Dynamics of epikarst communities: microgeographic pattern and environmental determinants of epikarst copepods in Organ Cave, West Virginia. *American Midland Naturalist* 156, 75–87.

PIPAN, T., V. NAVODNIK, F. JANŽEKOVIČ, T. NOVAK, 2008: Studies of the fauna of percolation water of Huda luknja, a cave in isolated karst in northeast Slovenia. *Acta Carsologica* 37/1, 141–151.

PLAN OF PROTECTION, 2001: *Plan of Protection and Development Action in Northwest of Yunnan*, The Joint Office of Protected and Development Projects in Northwest of Yunnan, 1.8.2001.

RAVBAR, N., 2002: Chinese karst terminology (examples from tropical and subtropical karst). *Acta Carsologica* 31/2, 189–208.

RAYMO, M. E., W. F. RUDDIMAN, 1992: Tectonic forcing of late Cenozoic climate. *Nature* 359, 117–122.

ROUCH, R., 1977 : Considérations sur l'écosystème karstique. *Comptes Rendus de l'Académie des Sciences* 284, 1101–1103.

SALOMON, J.-N., 1997: Comparaison entre les "Stone Forests" du Lunan (Yunnan-Chine) et les Karsts a "Tsingy" de Madagascar. In: *Song et al.*, 1997, 124–136.

SARIN, M. M., 2001: Biogeochemistry of Himalayan rivers as an agent of climate change. *Current Science* 81/11, 1446–1450.

SARIN, M. M., S. KRISHNASWAMI, K. DILLI, B. L. K. SOMAYAJULU, W. S. MOORE, 1989: Major ion chemistry of the Ganga-Brahmaputra river system: Weathering processes and fluxes to the Bay of Bengal. *Geochimica et Cosmochimica Acta* 53/5, 997–1009.

SIMON, K. S., T. PIPAN, D. C. CULVER, 2007: A conceptual model of the flow and distribution of organic carbon in caves. *Journal of Cave and Karst Studies* 69/2, 279–284.

SLABE, T., 1995: *Cave Rocky Relief and its Speleogenetical Significance*. Zbirka ZRC 10, ZRC Publishing, Ljubljana, 128 p.

SLABE, T., 1998: Rock Relief of Pillars in the Lunan Stone Forests. In: *Chen et al.*, 1998, 51–67.

SLABE, T., 1999: Subcutaneous rock forms. *Acta Carsologica* 28/2, 255–271.

SLABE, T., 2005: Two experimental modelings of karst rock relief in plaster: subcutaneous "rock teeth" and "rock peaks" exposed to rain. *Zeitschrift für Geomorphologie* 49/1, 107–119.

SLABE, T., M. KNEZ, 2004: Karst subsoil rock forms. *Annales* 14/2, 259–266.

SONG, L. H., 1986: Origination of Stone Forest in China. *International Journal of Speleology* 15/1–4, 3–13.

SONG, L., 1995: *The stone forest landscape and its tourist value*. Institute for Geography of the Chinese Academy of Sciences, Beijing.

SONG, L., Y. LI, 1997: Definition of shilin and its evolution in Lunan County, Yunnan, China. In: *Song et al.*, 1997, 37–45.

SONG, L., F. LIANG, 2001: Distribution of $CO_2$ in soil air affected by vegetation in the Shilin National Park. *Acta Geologica Sinica (Engl. Ed.)* 75/3, 288–293.

SONG, L., F. LIANG, 2009: Two important evolution models of Lunan shilin karst. *Karst Rock Features. Karren Sculpturing*, Carsologica 9, ZRC Publishing, Ljubljana, 453–459.

SONG, L. H., H. LIU, 1992: Control of geological structures over development of cockpit karst in south Yunnan, China. *Tübingen Geographische Studien* 109, 57–70.

SONG, L., F. WANG, 1997: Lunan Shilin Landscape in China. *Proceedings of the 12th International Congress of Speleology*, *Symposium* 8/1, 433–435.

SONG, L., Y. HE, Y. FENG, 1993: Ground water tracing in Wulichong surface drainage system, Mengzi county, Yunnan province. *Proceedings of the 11th International Congress of Speleology*, Beijing, 227–229.

SONG, L., T. WALTHAM, N. CAO, F. WANG, 1997: *Stone Forest – a Treasure of Natural Heritage*. Proceedings of International Symposium for Lunan Shilin to Apply for World Natural Heritage Status. China Environmental Science Press, Beijing, 136 p.

SONG, Q., Z. ZHANG, 1999: *The Basis of Geology*. High Education Publishing House, Beijing (in Chinese).

STANDARD METHODS, 1992: *Standard methods for the examination of water and wastewater, 18th Edition*. American Public Health Association.

SWEETING, M. M., 1995: *Karst in China. Its Geomorphology and Environment*. Springer Verlag, Berlin, Heidelberg, New York, 265 p.

ŠEBELA, S., 1996: Results of tectonic measurements in the Lunan Stone Forest, China. *Acta Carsologica* 25, 438–455.

ŠEBELA, S., 1998: *Tectonic structure of Postojnska Jama Cave System.* Zbirka ZRC 18, ZRC Publishing, Ljubljana, 112 p.

ŠEBELA, S., J. KOGOVŠEK, 2006: Hydrochemic characteristics and tectonic situation of selected springs in central and NW Yunnan province, China. *Acta Carsologica* 35/1, 23–33.

ŠEBELA, S., R. C. ORNDORFF, D. J. WEARY, 1999: Geological controls in the development of caves in the south-central Ozarks of Missouri, USA. *Acta Carsologica* 28/2, 273–291.

ŠEBELA, S., T. SLABE, J. KOGOVŠEK, H. LIU, P. PRUNER, 2001: Baiyun Cave in Naigu Shilin, Yunnan Karst, China. *Acta Geologica Sinica (Engl. Ed.)* 75/3, 279–287.

ŠEBELA, S., T. SLABE, H. LIU, P. PRUNER, 2004: Speleogenesis of selected caves beneath the Lunan Shilin and caves of fenglin karst in Qiubei, Yunnan. *Acta Geologica Sinica (Engl. Ed.)* 78/6, 1289–1298.

TAN, M., H. CHENG, R. L. EDWARDS, J. HOU, T. LIU, 2000: TIMS-230Th dating for very young annual laminated stalagmites. *Quaternary Sciences* 20/4, 391.

TAPPONIER, P., P. MOLNAR, 1977: Active faulting and tectonics of China. *Journal Geophysical Research* 82, 2905–2930.

TAPPONNIER, P., G. PELTZER, A. Y. LE DAIN, R. ARMIJO, P. COBBOLD, 1982: Propagating extrusion tectonics in Asia: new insights from simple experiments with plasticine. *Geology* 10/12, 611–616.

THOMAS, A. D., 2006: Seasonality of bedrock weathering chemistry and $CO_2$ consumption in a small watershed, the White River, Vermont. *Chemical Geology* 231/3, 236–251.

TIAN, Y., J. ZHANG, L. SONG, H. BAO, 2003: A Study on aerial algae communities on the surface of carbonate rock of the Yunnan Stone Forest. *Carsologica Sinica* 22/3, 203–211.

TRČEK, B., 2003: *Epikarst zone and the karst aquifer behavior. A case study of the Hubelj catchment, Slovenia.* Geological Survey of Slovenia, Ljubljana, 100 p.

TRIMMEL, H., 1997: Karst forms comparable to stone forests within the Mediterranean Basin. In: *Song et al.*, 1997, 46–51.

TYTG, 1995: *Taoni Yangguihua Tourism Geograqphy*, Yunnan University Press.

UNESCO, 2007: Sites. [Online]. Available from: *http://whc.unesco.org/sites/1083-loc.htm/* (accessed 21st August 2007).

URUSHIBARA-YOSHINO, K., F. D. MIOTKE, RESEARCH GROUP OF SOLUTION RATES IN JAPAN, 1999: Solution Rate of Limestone in Japan. *Physics and Chemistry of the Earth A* 24/10, 899–903.

VELBEL, M. A., 1993: Temperature dependence of silicate weathering in nature: How strong a negative feedback on long term accumulation of atmospheric $CO_2$ and global greenhouse warming? *Geology* 21, 1059–1062.

WALTHAM, A. C., 1996: Limestone karst geomorphology in the Himalayas of Nepal and Tibet. *Zeitschrift für Geomorphologie,* N. F., 40/1, 1–22.

WALTHAM, T., 1997: Pinnacle karst of Gunung Api, Mulu, Sarawak. In: *Song et al.*, 1997, 52–55.

WANG, E., B. C. BURCHFIEL, 2000: Late Cenozoic to Holocene deformation in southwestern Sichuan and adjacent Yunnan, China, and its role in formation of the southeastern part of the Tibetan Plateau. *Geological Society of America Bulletin* 112/3, 413–423.

WANG, E., B. C. BURCHFIEL, L. H. ROYDEN, L. CHEN, J. CHEN, J. W. LI, Z. CHEN, 1998: *The late Cenozoic Xianshuihe-Xiaojiang, Red River, and Dali fault systems of southwestern Sichuan and Central Yunnan, China.* Geological Society of America Special Paper 327, 108 p.

WANG, F., Z. LI, B. LI, H. TAO, H. GENG, 1994: Brief review of exploiting history of Stone Forest in Lunan, Yunnan. *Study of Karst and Cave Scenic Tourist Resources*, Seismology Publisher, 219–222.

WANG, M., B. SHOU, 1989: Objective Analysis on the Climatic Types of Yunnan, *Weather over Lown Latitude Plateau* 2/2, 83–89.

WANG, W., D. QIU, J. WU, H. YE, 1996: *The soils of Yunnan*. Yunnan Science and Technology Press, Kunming (in Chinese).

WANG, X., 1985: Analysis of the microfeatures on the quartz sand grain surface in Lunan Stone Forest. In: *Karst Geomorphology and Speleology*, Science Press, Beijing, 87–95 (in Chinese).

WHITE, A. D., A. E. BLUM, 1995: Effects of climate on chemical weathering in watersheds. *Geochimica et Cosmochimica Acta* 59/9, 1729–1747.

WU, Z., S. WU, 1998: A Proposal for a New Floristic Kingdom (Realm) – the E. Asiatic Kingdom, its Delineation and Characteristics. In: Zhang A., S. Wu (Eds.), *Floristic Characteristics and Diversity of East Asian Plants*, CHEP Beijing, Springer Verlag, Berlin, 1–42.

WU, Z., Y. ZHU (Eds.), 1987: *Vegetation of Yunnan*. Science Press, Beijing, 29–44, 763–765 (in Chinese).

YANG, Y., 1991: *Integrated Physical Regionalization of Yunnan Province, China*. Higher Education Press, Beijing, 16–18.

YU, Y., B. YANG, 1997: Palaeo-environments during formation of Lunan Stone Forest. In: *Song et al.*, 1997, 63–67.

YU, J., X. WANG, Z. WANG, 1985: Lunan stone forest of Yunnan province – its morphological characteristics and paleogeographical environment. *Chinese Science Bulletin* 30/2, 219–223.

YUAN, D. (Ed.), 1988: *Glossary of Karst Geology*. Geological Publishing House, Beijing, 55 p (in Chinese, with English abstract).

YUAN, D., 1991: *Karst of China*. Geological Publishing House, Beijing, 224 p.

YUAN, D., 1997: A global perspective of Lunan Stone forest. In: *Song et al.*, 1997, 68–70.

YUNNAN BUREAU OF GEOLOGY, 1985: *Investigation Report on Region Geology*. Bureau of Geology and Mineral Resources of Yunnan Province, Chengdu.

YUNNAN GARDENING BUREAU, 1999: *Yunnan Province gardening bureau arranges Scenic spots in Yunnan*. Yunnan Art Press.

ZHANG, C., M. DAY, 2002: A web-based Spatial Decision Support System for conservation of Lunan Stone Forest Landscape. *International Conference on Computer Graphics and Spatial Information Systems*, China Meteorological Press, Beijing, 653–661.

ZHANG, C., M. DAY, W. LI, 2003: Landuse and land cover change in the Lunan Stone Forest, China. *Acta Carsologica* 32/2, 161–174.

ZHANG, C., W. LI, M. DAY, 2005: Towards establishing effective protective boundaries for the Lunan Stone Forest using an online spatial decision support system. *Acta Carsologica* 34/1, 151–167.

ZHANG, F., F. WANG, H. WANG, 1997: Lunan Stone forest landscape and its protection and conservation. In: *Song et al.*, 1997, 71–77.

ZHANG, F., H. GENG, Y. LI, Y. LIANG, Y. YANG, J. REN, F. WANG, H. TAO, Z. LI, 1997: *Study on the Lunan stone forest karst, China*. Yunnan Science and Technology Press, Kunming, 155 p (Chinese, English content and summary).

ZHANG, J., 1996: *The control of basin weathering function on river* (in Chinese with English abstract). Ocean Publishing House, 12–304.

ZHANG, S., 1984: The development and evolution of Lunan Stone Forest. *Carsologica Sinica* 3/2, 78–87.

ZHANG, S., 1997: Stone Forest in China and pinnacle karst in Madagascar. In: *Song et al.*, *1997*, 78–80.

ZU, D., 1990: *A Dictionary of Modern Geography*. Trade Press, Beijing, 863 p.

ZUPAN HAJNA, N., 1997: Kamniti gozdovi na krasu in njihova geološka pogojenost. *Geološki zbornik* 13, 144–151.

ZUPAN HAJNA, N., 1998: Clastic Sediments from Karst of Southeast Yunnan and Northwest Guizhou. In: *Chen et al.*, *1998*, 213–223.
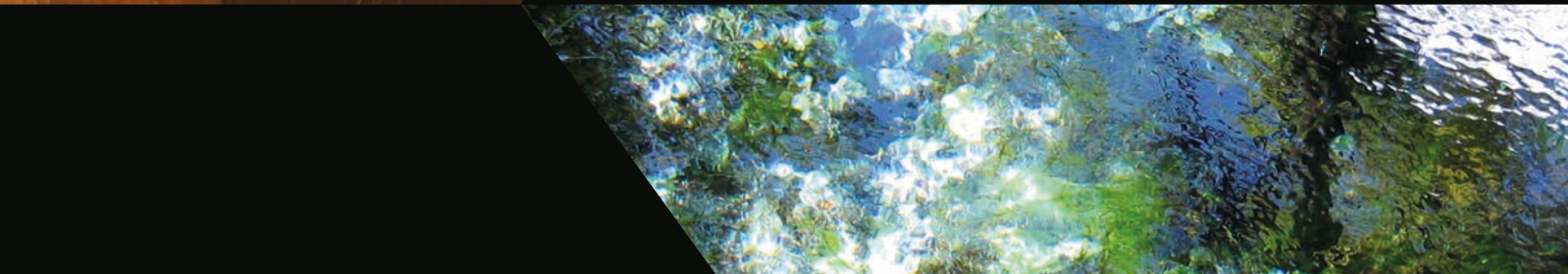
Binggui Cai

Lawrence J. Flynn

Chuxing Huang

Nina G. Jablonski

Xueping Ji

Martin Knez

Janja Kogovšek

Andrej Kranjc

Guan Li

Zheng Li

Zhicai Li

Deshen Liu

Hong Liu

Yu Liu

Janez Mulec

Andreea Oarga

Metka Petrič

Tanja Pipan

Petr Pruner

Licheng Shen

Tadej Slabe

Stanka Šebela

Paul S. C. Taçon

Guoan Wang

Ping Wang

Shiyu Yang

Yan Zhou